NASA TECHNICAL MEMORANDUM

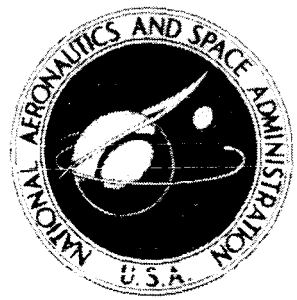

NASA TM X-2511

NASA TM X-2511

WIND-TUNNEL INVESTIGATION OF THE AERODYNAMIC CHARACTERISTICS OF THE M2-F2 LIFTING-BODY ENTRY CONFIGURATION AT TRANSONIC AND SUPERSONIC MACH NUMBERS

by Earl R. Keener and Jack J. Brownson

Ames Research Center
Moffett Field, Calif. 94035

NATIONAL AERONAUTICS AND SPACE ADMINISTRATION • WASHINGTON, D. C. • APRIL 1972

1. Report No.	2. Government Accession No.	3. Recipient's Catalog No.
NASA TM X-2511		

4. Title and Subtitle	5. Report Date
WIND-TUNNEL INVESTIGATION OF THE AERODYNAMIC CHARACTERISTICS OF THE M2-F2 LIFTING-BODY ENTRY CONFIGURATION AT TRANSONIC AND SUPERSONIC MACH NUMBERS	April 1972
	6. Performing Organization Code
7. Author(s)	8. Performing Organization Report No.
Earl R. Keener and Jack J. Brownson	A-4131
	10. Work Unit No.
9. Performing Organization Name and Address	124-07-11-06-00-21
NASA Ames Research Center Moffett Field, Calif., 94035	11. Contract or Grant No.
	13. Type of Report and Period Covered
12. Sponsoring Agency Name and Address	Technical Memorandum
National Aeronautics and Space Administration Washington, D. C. 20546	14. Sponsoring Agency Code

15. Supplementary Notes

16. Abstract

Results are presented for a 1/12-scale model for a Mach number range of 0.6 to 2 at Reynolds numbers from 4 to 13 million. Angles of attack and sideslip were varied from -8° to +20° and -4° to +6°, respectively. A brief history of the development of the configuration is included.

17. Key Words (Suggested by Author(s))	18. Distribution Statement
Aerodynamic stability and control Lifting body entry vehicle Transonic and supersonic Mach numbers Wind Tunnel model	Unclassified - Unlimited

19. Security Classif. (of this report)	20. Security Classif. (of this page)	21. No. of Pages	22. Price*
Unclassified	Unclassified	135	$3.00

*For sale by the National Technical Information Service, Springfield, Virginia 22151

NOTATION

The longitudinal force and moment coefficients are referred to the stability system of axes, and the lateral-directional characteristics are referred to the body system of axes. The moment center is located at 55 percent of the body reference length from the nose (49.6 percent of the actual length) and 7 percent of the length below the cone axis. Zero angle on all control surfaces is defined as the position where the control surface is tangent with the model surface at the control hinge line. The coefficients and symbols used are defined as follows:

b	reference span, 24.2 cm
C_D	drag coefficient, $\frac{\text{drag}}{qS}$
C_L	lift coefficient, $\frac{\text{lift}}{qS}$
C_l	rolling-moment coefficient, $\frac{\text{rolling moment}}{qSb}$
C_m	pitching-moment coefficient at body station $0.55l$ (0.496 X total length), $\frac{\text{pitching moment}}{qSl}$
C_n	yawing-moment coefficient, $\frac{\text{yawing moment}}{qSb}$
C_{p_b}	base-pressure coefficient
C_Y	side-force coefficient, $\frac{\text{side force}}{qS}$
l	reference length (length before addition of final boattail, used throughout configuration development) 50.8 cm
$\frac{L}{D}$	lift-drag ratio
M	free-stream Mach number
q	free-stream dynamic pressure
R	Reynolds number, based on reference length (l)
S	reference planform area (area before addition of final boattail, used throughout configuration development) 896 cm^2

α	angle of attack, referenced to the cone axis (which is parallel to the flat portion of the upper surface)
β	angle of sideslip
δ_a	differential deflection angle of upper flaps for aileron control ($\delta_{u_L} - \delta_{u_R}$), positive for right roll
δ_l	deflection angle of lower flap, trailing edge down is positive
δ_r	differential deflection angle of rudders ($\delta_{r_L} + \delta_{r_R}$)
δ_{rf}	rudder-flare deflection angle $0.5(\delta_{r_L} - \delta_{r_R} - \lvert\delta_r\rvert)$
$\delta_{r_R}, \delta_{r_L}$	deflection angle of right or left rudder (each rudder deflects only outward): δ_{r_L} is always zero or positive; δ_{r_R} is always zero or negative
δ_u	average deflection angle of upper flaps, $\frac{\delta_{u_R} + \delta_{u_L}}{2}$
$\delta_{u_R}, \delta_{u_L}$	deflection angle of right or left upper flap segment, trailing edge down is positive
$\Delta(\ )$	incremental value

Subscripts

α	derivative with respect to α, per deg
β	derivative with respect to β, per deg
δ	derivative with respect to control deflection, per deg

WIND–TUNNEL INVESTIGATION OF THE AERODYNAMIC CHARACTERISTICS OF THE M2–F2 LIFTING–BODY ENTRY CONFIGURATION AT TRANSONIC AND SUPERSONIC MACH NUMBERS

Earl R. Keener and Jack J. Brownson

Ames Research Center

SUMMARY

The results of a wind-tunnel investigation of the aerodynamic characteristics of a 1/12-scale model of the M2–F2 lifting-body entry configuration are presented for a Mach number range of 0.6 to 2.0 at Reynolds numbers from 4 to 13 million. Angles of attack and sideslip were varied over a range from -8° to +20° and -4° to +6°, respectively.

The results show that the configuration has satisfactory longitudinal and lateral-directional stability and control characteristics throughout the Mach number range investigated, provided that the upper and lower flaps are deflected at least -15° and +25°, respectively. Flap and rudder control effectiveness are more than adequate; aileron-control effectiveness provided by the upper flaps is adequate at subsonic speeds and marginal at supersonic speeds. Two control cross-coupling effects occur at subsonic speeds for the M2–F2 configuration: a small adverse roll due to rudder deflection and a large adverse yaw due to aileron deflection. The latter problem is essentially eliminated by a center vertical fin.

INTRODUCTION

A series of investigations was conducted to determine the aerodynamic characteristics of lifting bodies in the form of blunt half-cones to evaluate their suitability as entry vehicles (refs. 1-26). The investigations led to the design and construction of a piloted flight research vehicle, the M2–F2 (fig. 1), designed for transonic and supersonic speeds. The configuration was developed from preliminary wind-tunnel tests and from previous experience with a low-speed flight research vehicle, the M2–F1 (fig. 2). Subsequently, a series of detailed wind-tunnel tests was conducted to confirm the adequacy of the configuration and to provide the aerodynamic characteristics for the design of the flight test vehicle.

The purpose of the present paper is to present the aerodynamic characteristics of a 1/12-scale model of the M2–F2 configuration for Mach numbers from 0.6 to 2. The data are primarily from the Ames 6- by 6-foot wind tunnel; however, data from the Ames 11- by 11-foot wind tunnel for Mach numbers from 0.6 to 1.3 are also presented. The appendix includes a brief history of the development of the configuration.

MODEL

The 1/12-scale model of the M2–F2 configuration is shown in figure 3, and the model dimensions are given in figure 4. The model had a fiberglass shell fitted to a steel plate that incorporated a mounting for a six-component strain-gage balance. All controls were fixed with brackets, as shown in figure 3(b). The lower flap was flat and not curved at the edges to fit the body contour. All control hinge lines were always sealed. Figure 3(c) shows the center vertical fin installed on the model.

The control system of the M2–F2 configuration consists of a lower surface flap, a pair of upper surface flaps, and a rudder on each of the vertical-tail surfaces (see figs. 3, 4, and 5). The lower surface flap provides longitudinal control over the entire speed range from entry to landing. The upper surface flaps are effective at subsonic and low supersonic speeds for additional longitudinal control and for lateral control. A split-flap-type rudder is located on the outboard trailing-edge surface of the vertical tails; the inboard half of the trailing edge is fixed to shield the upper flaps from the effects of rudder deflection. One surface at a time deflects outboard for directional control, and both surfaces simultaneously deflect outboard for rudder flare. Zero angle on all control surfaces is defined as that position where the control surface is tangent with the model surface at the control hinge line.

TESTS

The primary tests were conducted in the Ames 6- by 6-foot transonic wind tunnel at Mach numbers from 0.6 to 2.0. The Reynolds number was about 6 million at M = 0.6 to 0.9, decreasing to about 4 million at M = 2.0. Additional data were obtained in the Ames 11- by 11-foot transonic wind tunnel at Mach numbers from 0.6 to 1.3 and at Reynolds numbers of 6 and 13 million. Data were obtained at angles of attack from -8° to +20° at sideslip angles of 0° and 4° and at sideslip angles from -4° to +6° at an angle of attack of 6°.

Transition strips of grit particles were used for most of the tests to induce a turbulent boundary layer over most of the model. The strips, 1.2 cm wide, were located 10 cm from the nose (around the forebody) and on each side of the leading edge of the vertical tails (fig. 3). Tests were made with grit of two sizes (0.010 and 0.062 cm) and without grit; there was no noticeable effect on the results.

For most of the tests, data were recorded with increasing angle of attack, and repeat points were taken at $\alpha = 0°$. However, during several tests at selected Mach numbers, data were recorded with decreasing angle of attack to investigate a possible flow-hysteresis effect. There were no significant differences in the aerodynamic characteristics.

During the tests, transonic buffeting was indicated by: (1) the displayed force outputs of the model balance, and (2) the displayed position and hinge-moment outputs of the controls for tests (unreported) when remote controls were used. These displayed outputs were quite unsteady at Mach numbers from 0.9 to 1.0, and the unsteadiness increased with angle of attack.

ACCURACY

The model angles of attack and sideslip from the 6- by 6-foot wind tunnel were corrected for stream angle effects and for sting bending under load. No base pressure adjustments were made to the data.

The uncertainties in the test results, based on calibrations and the repeatability of the data, are estimated to be as follows:

Mach number	±0.01
Lift coefficient	±0.005
Drag and side-force coefficients	±0.003
Pitching-moment coefficient	±0.0025
Yawing-moment coefficient	±0.0005
Rolling-moment coefficient	±0.0008
Side-force coefficient	±0.003
Angles of attack and sideslip, deg	±0.1
Control angles, deg	±0.3

PRESENTATION OF RESULTS

Figures 6 through 9 present a comparison of data from two wind tunnels. Figures 10 through 18 present the longitudinal stability and control characteristics, and figures 18 through 35 present the lateral-directional stability characteristics. The following table summarizes the purpose of each figure.

Figure	Purpose
	Comparison of Data From Two Wind Tunnels
6	Longitudinal characteristics
7	Base pressure
8	Lateral-directional characteristics
9	Effect of Reynolds number
	Longitudinal Characteristics
Lift, drag, and stability:	
10	Selected δ_u
11 & 12	Selected δ_e
13	Selected δ_{rf}
14	Effect of vertical fins
15	Effect of canopy
16	Summary of figures 10 & 11 vs. M

Figure	Purpose
Flap effectiveness over Mach number range:	
17	$\delta_u = -20°, \delta_e = +35°$
18	Flap deflections for longitudinal trim

Lateral-Directional Characteristics

Stability:	
19	Variation with β (including body alone)
20	Variation with α
21	Summary of figure 19 vs. M
22	Effect of canopy
23	Effect of center fin
Effect of flap deflection:	
24	Lower flap
25	Upper flap
Effect of rudder deflection:	
26	Variation with β
27	Effect of rudder flare
28	Variation with α
29	Summary of rudder effectiveness vs. M
Effect of aileron deflection:	
30	Variation with β without center fin
31	Variation with β with center fin
32	Variation with α without center fin
33	Variation with α with center fin
34	Summary of aileron effectiveness vs. M with and without center fin
35	Aileron-rudder interconnect ratio for $C_{n_{\delta_a}} = 0$

DISCUSSION

Comparison of Data From Two Wind Tunnels

The 1/12-scale M2–F2 model was about the maximum size allowable for the Ames 6- by 6-foot transonic-supersonic wind tunnel, which has suction slots in the floor and ceiling to prevent choking of the transonic flow. Because transonic-flow and high angle-of-attack data might be subject to tunnel flow interference effects, the identical model was tested in the Ames 11- by 11-foot transonic wind tunnel at Mach numbers from 0.6 to 1.3 with controls fixed at angles identical to those for the 6-foot tunnel tests. The model was about half-maximum size for the 11-foot tunnel, which has transonic boundary-layer removal on all four walls. The longitudinal and

lateral-directional results from the two wind tunnels, presented in figures 6 and 8, agree closely except at a Mach number of 1.1 where small diffferences occur in C_{m_α} and C_{n_β} possibly because of the shock reflection from the walls of the 6-foot tunnel.

In the 11-foot tunnel the model was tested at two Reynolds numbers, 6.7 and 13.4 million, at Mach numbers of 0.80 and 0.95. The results in figure 9 show no effect of Reynolds number for the conditions tested. Similar results were obtained at Reynolds numbers as low as 4 million. This fact is somewhat surprising considering the possible local-flow separation over the boattail and also the upper surface vortex system that was shown in previous studies (ref. 4) to exist for the M2 configuration. Evidently, the vortex flow system over the upper surface is well established at the Reynolds numbers of the test because of the relatively sharp upper surface outer edge. Reference 6 showed a distinct Reynolds number effect at very low values of about 2 million, and reference 4 showed a distinct effect of edge radius for larger radii. It should not be concluded from these results that Reynolds number effects are not important for lifting bodies. Large-scale tests are necessary to explore the possibility of significant scale effects.

Longitudinal Stability Characteristics

Stability at transonic Mach numbers– The longitudinal lift, drag, and pitching-moment characteristics of the M2–F2 lifting-body configuration are documented in figures 10–16 for the 1/12-scale model at Mach numbers from 0.6 to 2.0. A primary problem in this Mach number range during the development of the M2–F2 configuration concerned the elimination of transonic longitudinal instabilities. Transonic longitudinal instability (positive dC_m/dC_L), similar to that reported in reference 6 for a previous configuration, is shown in the pitching-moment curves in figure 12(b) and (c) at M = 0.8 and 0.95 and $C_L < 0.3$ for the condition of low flap-deflection angles. However, the configuration is stable (negative dC_m/dC_L) for $C_L > 0.1$, when the lower flap is deflected at least 15°. Furthermore, the low lift instability is removed completely when the upper flap is also deflected (figs. 10 and 11). Flap deflections in excess of $\delta_U = -15°$ and $\delta_l = 25°$ are required for trim at Mach numbers from 0.6 to 2.0. The deflected flaps and the attendant increase in drag are not detrimental to the flight plan at transonic and supersonic speeds, since the landing-site approach is primarily a problem of energy management. At landing speeds (ref. 20) the configuration is stable for much lower flap deflections ($\delta_U = 0$ and $\delta_l = 10°$), which are required to reduce the drag and increase the L/D during the final landing approach.

In figures 10 to 12 transonic instability is also apparent at high lift at Mach numbers near 0.80. The decrease in stability begins at $\alpha \simeq 8°$, becoming neutrally stable at $\alpha \simeq 13°$, and is not affected by flap deflection (figs. 10(b) and 11(b)). At M = 0.90 the instability is essentially gone. At M = 0.60 the onset of the instability is delayed to $\alpha \simeq 12°$. It is likely that the region of instability is outside the required flight regime.

Effect of rudder flare– Rudder flare (symmetrical deflection of the rudders for speed control) produces a large drag increment and an increase in the longitudinal stability, as shown in figure 13. At M = 0.6 and 0.8 the rudder flare causes a negative shift in C_{m_o}, but at $M > 0.9$ the shift becomes positive. Two different and opposite effects from rudder flare are affecting the C_{m_o}. The larger, one, subsonically, is an increase in the pressure on the lower aft corners of the model causing a negative C_{m_o} shift. This same pressure increase would also contribute adverse roll with rudder

deflection. As the Mach number increases, the drag increment from the rudder area located above the moment center becomes the larger effect to give a positive C_{m_o} shift.

Effect of the vertical fins– Adding vertical fins to the basic body (fig. 14) at $M < 1$ increases the lift on the afterbody and decreases the pitching moment. At supersonic Mach numbers the effect of the vertical fins is much smaller. It should be noted that the upper and lower flaps are undeflected, giving the adverse pitching-moment characteristics.

Effect of the canopy– Whether the canopy is on, off, or located forward has no effect on the longitudinal characteristics (fig. 15). The forward location would be advantageous for visibility.

Variation of longitudinal characteristics with Mach number– The longitudinal aerodynamic characteristics as a function of Mach number are presented in figure 16. The characteristics are presented for control deflections of $\delta_u = -20°$, $\delta_l = 35°$, $\delta_{rf} = 0°$ and for trimmed control deflections, where appropriate. The experimental curve for $M = 0.6$ to 2 was obtained from figures 10 and 11 for the 1/12-scale model in the 6- by 6-foot wind tunnel. Additional results are included for the full-scale model at $M = 0.25$ in the 40- by 80-foot wind tunnel (ref. 20), and for the 1/20-scale model at $M = 10.4$ in the 3.5-foot-hypersonic wind tunnel (ref. 22).

Flap effectiveness– The effectiveness in pitching moment ($dC_m/d\delta$) of the upper and lower flaps is shown in figure 17 for two conditions: upper flap effectiveness at $\delta_u = -20°$ and lower flap effectiveness at $\delta_l = 35°$. At subsonic speeds the upper flap effectiveness is approximately linear with flap deflection (figs. 10 and 11). The effectiveness shown of about 0.003 per degree represents a change in trim lift coefficient of about 0.1 per degree of upper flap deflection. The upper flap is about 50 percent more effective than the lower flap. At supersonic speeds the effectiveness of both flaps is nonlinear (figs. 10 and 11) and the magnitude decreases to about one-half the transonic value; however, the flap control is adequate for trim capability over the lift range measured. Surprisingly, the upper flap is about as effective at $M = 2$ as the lower flap; however, it is expected that the upper flap effectiveness would decrease to zero at $M > 2$. At $M > 10.4$ (ref. 22) the lower flap is effective from zero to maximum lift. In summary, the longitudinal controls are very effective at subsonic speeds and adequate at supersonic speeds.

Flap trim angles– Approximate flap angles for trim (interpolated from figs. 10 and 11) at $C_L = 0$, 0.2, and 0.4 are shown in figure 18 for two conditions: $\delta_l = 35°$ with variable upper flap and $\delta_u = -20°$ with variable lower flap. (Transonic stability requires $\delta_u < -15°$ and $\delta_l > 25°$, as shown by shaded area.) Upper flap angles range from -27° to -10° for Mach numbers from 0.6 to 2.0 for $C_L = 0$ and 0.2. Lower flap angles range from 25° to 55° and 25° to 37° for the same conditions of $C_L = 0$ and 0.2. For Mach numbers up to 0.9, the high effectiveness of the flaps is apparent by the small change in deflection for trim. Increasing Mach number is seen to require a much larger range of flap angles for the same lift range.

Lateral-Directional Stability Characteristics

Lateral-directional characteristics of basic configuration– The basic configuration is directionally stable (positive C_{n_β}) and has positive effective dihedral (negative C_{l_β}) as may be seen in figures 19, 20, and 21. It is evident from figure 20 that the incremental change in yawing-moment coefficient, ΔC_n, with angle of sideslip, β, varies markedly with angle of attack, and the manner of this variation changes with Mach number.

Effects of configuration on lateral-directional characteristics– The basic body has neutral directional stability at supersonic Mach numbers, is unstable at subsonic Mach numbers, and has positive effective dihedral at all Mach numbers. The vertical fins provide all the directional stability, as may be seen in figure 19. The fins also add to the effective dihedral to a smaller extent. Removing the lower flap has serious effects on the lateral-directional characteristics at transonic Mach numbers of 0.8 and 0.9 (see fig. 19). As previously noted, deterioration of the longitudinal characteristics also occurs at these Mach numbers with inadequate lower flap deflection (see fig. 12). An earlier configuration without a lower flap, reported in reference 8, exhibited similar deficiencies. The lateral-directional characteristics of the configuration are relatively insensitive to the presence of the canopy or to its location (see fig. 22). A center fin as shown in figure 4(c) located between the upper flaps adds only slightly to the directional stability and has little to no effect on the effective dihedral as may be seen in figure 23.

Effect of control deflection on lateral-directional stability– Varying the deflection of the lower flap from 15° to 35° has little to no effect on the lateral-directional characteristics (see fig. 24), but complete withdrawal or removal of the flap has serious effects (see fig. 19). As may be seen in figure 25, the upper flap has small effects on the lateral-directional characteristics, except at $M = 0.9$, where there is some loss in directional stability with lower flap deflection. Rudder deflection produces the desired yawing moments without altering the lateral-directional stability (see fig. 26). Large rudder flaring (symmetrical deflection of the rudders) increases the directional stability without affecting the lateral characteristics (fig. 27). (Of course, there is considerable increase in drag associated with large rudder flare angles (fig. 13).) There are no effects of aileron deflection on lateral-directional stability either with or without the center fin (see figs. 30 and 31).

Lateral-directional control characteristics– As may be observed in figures 26, 28, and 29, directional control with the rudders is more than adequate. For example, figure 26 shows that 10° of rudder deflection will trim out yawing moments due to as much as 5° of sideslip angle at $M \leqslant 1.3$ and to about 3° at $M = 2.0$. There is a small adverse rolling moment associated with rudder deflection (positive $C_{l_{\delta_r}}$) which decreases to zero at $M = 2.0$ (fig. 29). The adverse rolling moment is believed to result both from the location of the rudders above the roll axis and from the effect of the rudders on the lower body pressures.

Figure 34 shows that roll control ($C_{l_{\delta_a}}$) is adequate at subsonic Mach numbers but deteriorates as the Mach number increases, which is to be expected for upper surface controls. The loss of roll control at the higher Mach number can be overcome by use of the rudder for roll control by way of sideslip and the resulting C_{l_β}. This method is intended for use at the higher Mach numbers, and is not usable at low altitudes and Mach numbers because of the slow response time (i.e. the vehicle could not roll until sideslip had developed). Associated with aileron deflection is a large adverse yawing moment, about equal in magnitude to the rolling moment (figs. 32 and 34(b)). To counteract this yawing moment, an interconnect to the rudders would be required. The interconnect ratio required for $C_n = 0$, as seen in figure 35, varies with Mach number. However, a center fin (see fig. 4(c)), located between the upper flaps is effective in reducing the adverse yaw with aileron deflection, as may be seen in figures 33 and 34(b). The center fin would possibly remove the necessity for aileron-rudder interconnect, as shown in figure 35.

SUMMARY OF RESULTS

Detailed wind-tunnel tests with a 1/12-scale model of the M2–F2 flight research vehicle were conducted to document the aerodynamic characteristics of this lifting-body entry configuration at transonic and supersonic speeds. The results can be summarized as follows:

1. Upper and lower surface flap deflections counteract both a tendency of the basic configuration toward zero-lift neutral longitudinal stability throughout the Mach range from 0.6 to 2.0 and a moderate-lift unstable break in pitching moment at Mach numbers of 0.9 to 1.

2. High-lift longitudinal instability at Mach 0.6 to 0.85 was not eliminated; however, it is considered to be out of the normal flight range of the vehicle.

3. The longitudinal controls are very effective at subsonic speeds and adequate at supersonic speeds.

4. Rudder flare (symmetrical deflection of the rudders) produces a large drag which is available for speed control.

5. The configuration with control surfaces properly deflected is directionally stable and has positive effective dihedral throughout the angle of attack and Mach number ranges investigated.

6. The aerodynamic characteristics are essentially unaffected by the presence of the canopy or its location.

7. Directional control is more than adequate.

8. A small adverse roll due to rudder deflection occurs at subsonic speeds.

9. Using the upper flaps as ailerons provides adequate roll control at subsonic speeds but not at supersonic speeds.

10. Aileron deflection causes a large adverse yawing moment that may be reduced or eliminated by addition of a center fin.

Ames Research Center
National Aeronautics and Space Administration
Moffett Field, Calif., 94035, October 19, 1971

APPENDIX

DEVELOPMENT OF AMES M2 LIFTING–BODY CONFIGURATION

The Ames Research Center has engaged in a research program to study the aerodynamic characteristics of lifting bodies to determine their suitability for entry vehicles. The investigation included the study of several aerodynamic lifting shapes, such as circular discs; however, the primary configurations studied were blunt half cones. It was felt that while retaining some of the inherent stability of the parent cone shapes at supersonic speeds, these shapes would be easily adaptable to rocket boosters and easily protected from heating by the use of ablative materials. Preliminary tests (ref. 1) demonstrated that a blunt 30° half-cone has a hypersonic lift-drag ratio of about 0.5 and would have a lateral range from satellite orbit in the order of 200 nautical miles; however, the high drag resulting from the large blunt base limits the lift-drag ratio to only 0.9 at landing speeds (ref. 2). Hence, final landing would have to be by parachute, parawing. inflatable afterbody, or other auxiliary device.

Research on blunt half-cone lifting bodies was extended to include more slender bodies, which have higher hypersonic lift-drag ratios and can land horizontally. A lateral range potential of 1000 nautical miles was used as a criterion, which requires a hypersonic lift-drag ratio of about 1.4. Following an analytical study of the hypersonic characteristics of blunt half-cones, a 13° half-cone angle was selected for a detailed experimental investigation. Reference 3 describes the considerations that led to the selection of the 13° configuration and presents the results of wind-tunnel tests showing that the blunt 13° half-cone had a lift-drag ratio of 1.4 at supersonic speeds. Reference 4 shows the maximum lift-drag ratio at subsonic speeds to be 1.7, which is considerably below the minimum lift-drag ratio of 2.5 suggested in reference 5 to be required for a conventional horizontal landing.

The configuration was further developed to provide a conventional horizontal landing potential and still retain the good supersonic performance of the basic half-cone. The resulting 13° half-cone configuration was designated the M2 (fig. 5) to distinguish it from the blunt 30° half-cone configuration designated the M1. The configuration development is recorded in reference 4 and is reviewed in reference 6. The aerodynamic characteristics of the resulting landable configuration are documented in detail in references 7 to 12. An analytical study of the entry performance is discussed in reference 13. The use of deployable lifting surfaces was also investigated (ref. 14).

The development of a landable configuration subsequently led to a low-speed flight version of the M2, designated M2–F1 (figs. 2 and 5). Full-scale wind-tunnel test results are reported in reference 15. The M2–F1 was flown successfully on over 100 flights at the NASA Flight Research Center. The flight-research program is discussed in reference 16, and flight results are reported in references 17 and 18.

Subsequently, a joint NASA–Air Force flight research program was undertaken to determine the adequacy at subsonic and supersonic speeds of several existing lifting-body configurations, using the aerial-launch technique. This was to be a part of the general manned lifting-entry research program, described in reference 19. Preliminary wind-tunnel studies determined the proper modifications to the M2–F1 low-speed configuration required to achieve satisfactory characteristics

at transonic and supersonic speeds and to be compatible with the requirements for hypersonic entry. A detailed wind-tunnel test program documented the aerodynamic characteristics of the resulting M2–F2 configuration. The test program included full-scale low-speed tests (ref. 20), model tests of the aerial launch characteristics (ref. 21), hypersonic tests (refs. 22 and 23), and the transonic-supersonic tests reported herein.

The changes in the M2–F1 configuration that led to the M2–F2 configuration are as follows (fig. 5): The afterbody was changed by increasing the boattail length in order to reduce low speed base drag (ref. 20). The control surfaces were changed by eliminating the low-speed elevons and by adding a lower surface flap for improved transonic stability (refs. 6 and 7) and hypersonic longitudinal control (ref. 12). The canopy was moved forward for better visibility in an attempt to eliminate the necessity for a transparent nose window (although the flight vehicle retained the nose window for the flight research program).

A piloted version of the M2–F2 (fig. 1) was built, tested in the Ames large-scale wind tunnel (ref. 24), and flown at the Flight Research Center. Preliminary test results are reported in references 25 and 26. A comprehensive review of the development of the M2–F2 and of the flight test program is given in reference 27.

Following an accident with the M2–F2, the vehicle was rebuilt with several modifications and designated the M2–F3 (fig. 36). The primary modification to the configuration was a center fin to improve the low speed lateral-directional control characteristics.

REFERENCES

1. Eggers, Alfred J., Jr.; and Wong, Thomas J.: Re-entry and Recovery of Near-Earth Satellites, With Particular Attention to a Manned Vehicle. NASA MEMO 10-2-58A, 1958.

2. Savage, Howard F.; and Tinling, Bruce E.: Subsonic Aerodynamic Characteristics of Several Blunt, Lifting, Atmospheric-Entry Shapes. NASA MEMO 12-24-58A, 1958.

3. Rakich, John V.: Supersonic Aerodynamic Performance and Static-Stability Characteristics of Two Blunt-Nosed Modified 13° Half-Cone Configurations. NASA TM X-375, 1960.

4. Kenyon, George C.; and Edwards, George G.: A Preliminary Investigation of Modified Blunt 13° Half-Cone Re-entry Configurations at Subsonic Speeds. NASA TM X-501, 1961.

5. Weil, Joseph; and Matranga, Gene J.: Review of Techniques Applicable to the Recovery of Lifting Hypervelocity Vehicles. NASA TM X–334, 1960.

6. Dennis, David H.; and Edwards, George G.: The Aerodynamic Characteristics of Some Lifting Bodies. NASA TM X-376, 1960.

7. Kenyon, George C.; and Sutton, Fred B.: The Longitudinal Aerodynamic Characteristics of a Re-entry Configuration Based on a Blunt 13° Half-Cone at Mach Numbers to 0.92. NASA TM X-571, 1961.

8. Kenyon, George C.: The Lateral and Directional Aerodynamic Characteristics of a Re-entry Configuration Based on a Blunt 13° Half-Cone at Mach Numbers to 0.90. NASA TM X-583, 1961.

9. Rakich, John V.: Aerodynamic Performance and Static Stability of a Blunt-Nosed Boattailed 13° Half-Cone at Mach Numbers of 0.60 to 5.0. NASA TM X-570, 1961.

10. Hassell, James L., Jr.; and Ware, George M.: Investigation of the Low-Subsonic Stability and Control Characteristics of a 0.34-Scale Free-Flying Model of a Modified Half-Cone Reentry Vehicle. NASA TM X-665, 1962.

11. Axelson, J. A.: Pressure Distributions for the M-2 Lifting Entry Vehicle at Mach Numbers of 0.23, 5.2, 7.4, and 10.4. NASA TM X-997, 1964.

12. Axelson, John A.: Hypersonic Aerodynamic Characteristics of the Ames M2 Lifting Entry Configuration. NASA TM X-1301, 1966.

13. Syvertson, Clarence A.; Swenson, Byron L.; Anderson, Joseph L.; and Kenyon, George C.: Some Considerations of the Performance of a Maneuverable, Lifting-Body Entry Vehicle. Advances in the Astronautical Sciences, vol. 16, pt. 1, American Astronautical Society, 1963, pp. 898-918.

14. Spencer, Bernard, Jr.; and Phillips, W. Pelham: Low-Speed Aerodynamic Characteristics of a Modified Blunt 13° Half-Cone Lifting-Body Configuration Having Deployable Horizontal Tails With or Without Variable-Sweep Wings. NASA TM X-847, 1963.

15. Mort, Kenneth W.; and Gamse, Berl: Full-Scale Wind-Tunnel Investigation of the Longitudinal Aerodynamic Characteristics of the M2–F1 Lifting Body Flight Vehicle. NASA TN D-3330, 1966.

16. Horton, Victor W.; Layton, Garrison P., Jr.; and Thompson, Milton O.: Exploring New Manned Spacecraft Concepts. Astronautics and Aeronautics, vol. 2, May 1964, pp. 42-47.

17. Horton, Victor W.; Eldredge, Richard C.; and Klein, Richard E.: Flight-Determined Low-Speed Lift and Drag Characteristics of the Lightweight M2–F1 Lifting Body. NASA TN D-3021, 1965.

18. Smith, Harriet J.: Evaluation of the Lateral-Directional Stability and Control Characteristics of the Lightweight M2–F1 Lifting Body at Low Speeds. NASA TN D-3022, 1965.

19. Love, Eugene S.: Manned Lifting Entry. Astronautics and Aeronautics, vol. 4, May 1966, pp. 54-64.

20. Mort, Kenneth, W.; and Gamse, Berl: Low-Speed Wind-Tunnel Tests of a Full-Scale M2–F2 Lifting Body Model. NASA TM X-1347, 1967.

21. McKinney, Linwood W.; and Boyden, Richard P.: Predicted Characteristics of M2–F2 Lifting Body Launched From B-52 Airplane With Comparison of Flight Results. NASA TM X-1545, 1968.

22. Axelson, John A.; and Mellenthin, Jack A.: Hypersonic Aerodynamic Characteristics of the M2–F2 Lifting Entry Configuration. NASA TM X-1690, 1968.

23. Seegmiller, H. Lee: Convective Heat Transfer to the Ames M2 and M2–F2 Lifting Entry Vehicles. NASA TM X-1691, 1968.

24. Mort, Kenneth W.; and Gamse, Berl: Full-Scale Wind-Tunnel Investigation of the Aerodynamic Characteristics of the M2–F2 Lifting Body Flight Vehicle. NASA TM X-1588, 1968.

25. Holleman, Euclid C.: Stability and Control Characteristics of the M2–F2 Lifting Body Measured During 16 Glide Flights. NASA TM X-1593, 1968.

26. Flight Center Staff: Flight Test Results Pertaining to the Space Shuttlecraft. Symposium held at NASA Flight Research Center, June 30, 1970, NASA TM X-2101, 1970.

27. Syvertson, Clarence A.: Aircraft Without Wings. Science J., vol. 4, no. 12, Dec. 1968, pp. 46-51.

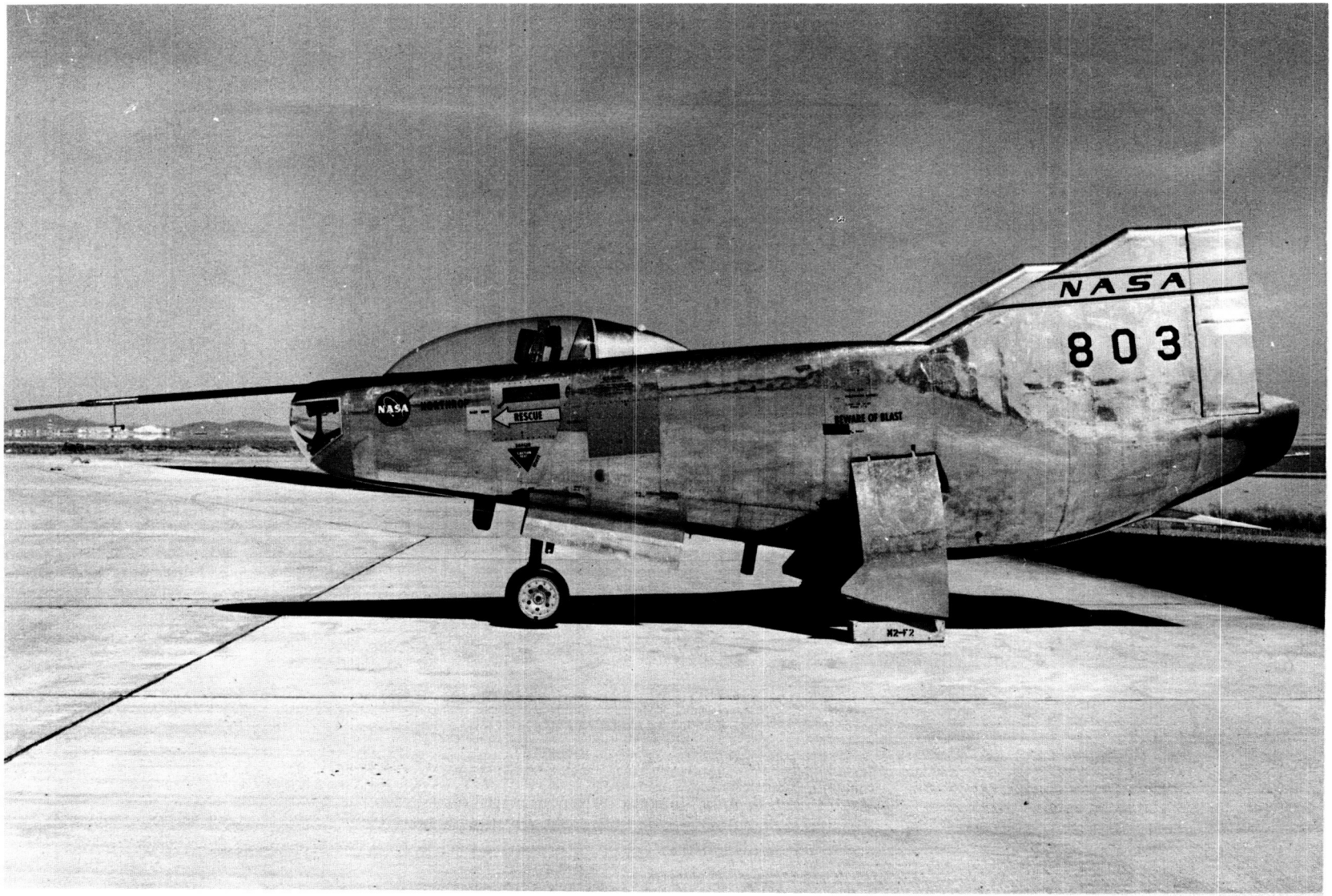

Figure 1.- M2-F2 flight research vehicle.

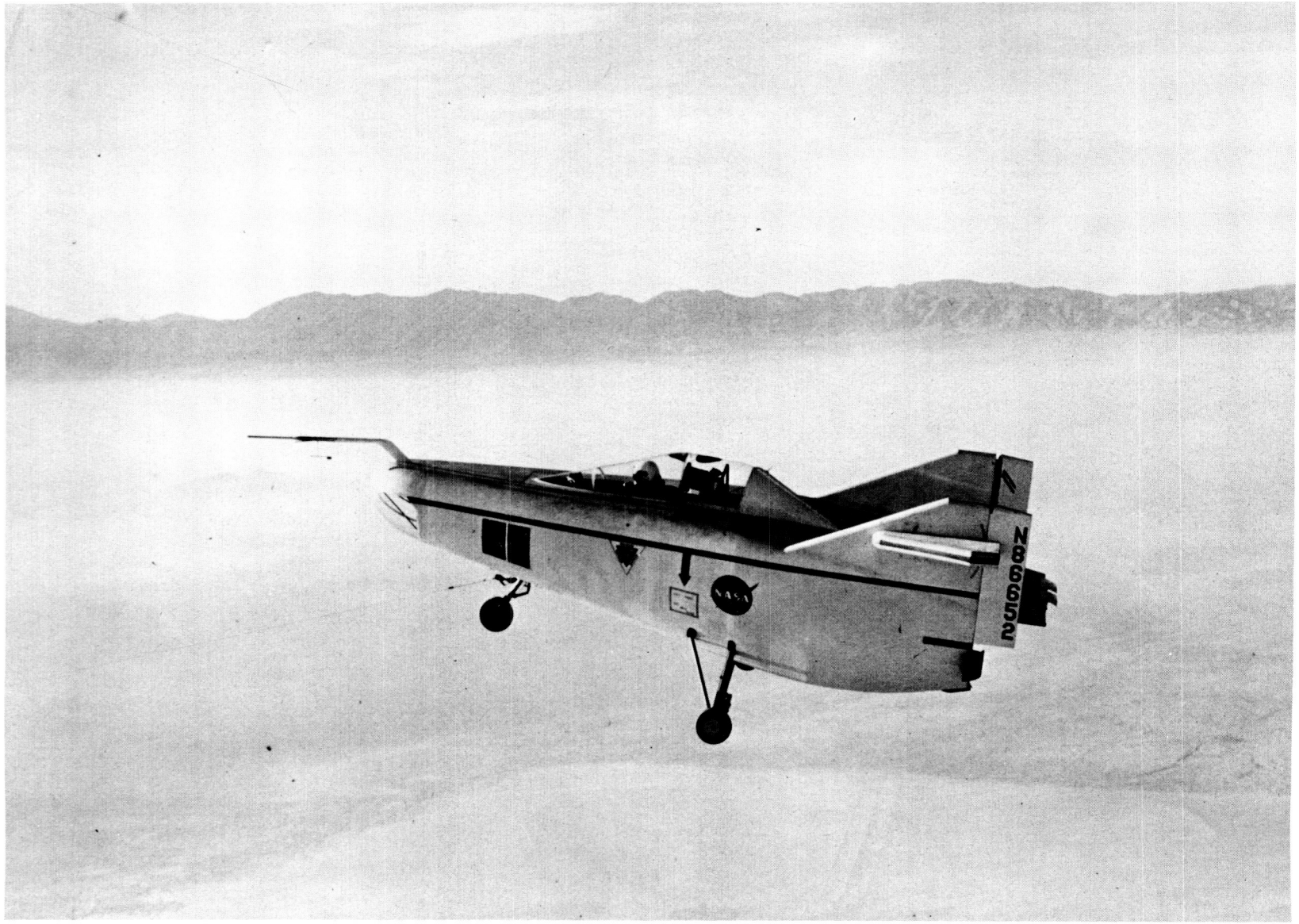

Figure 2.- M2-F1 flight research vehicle (predecessor of M2-F2).

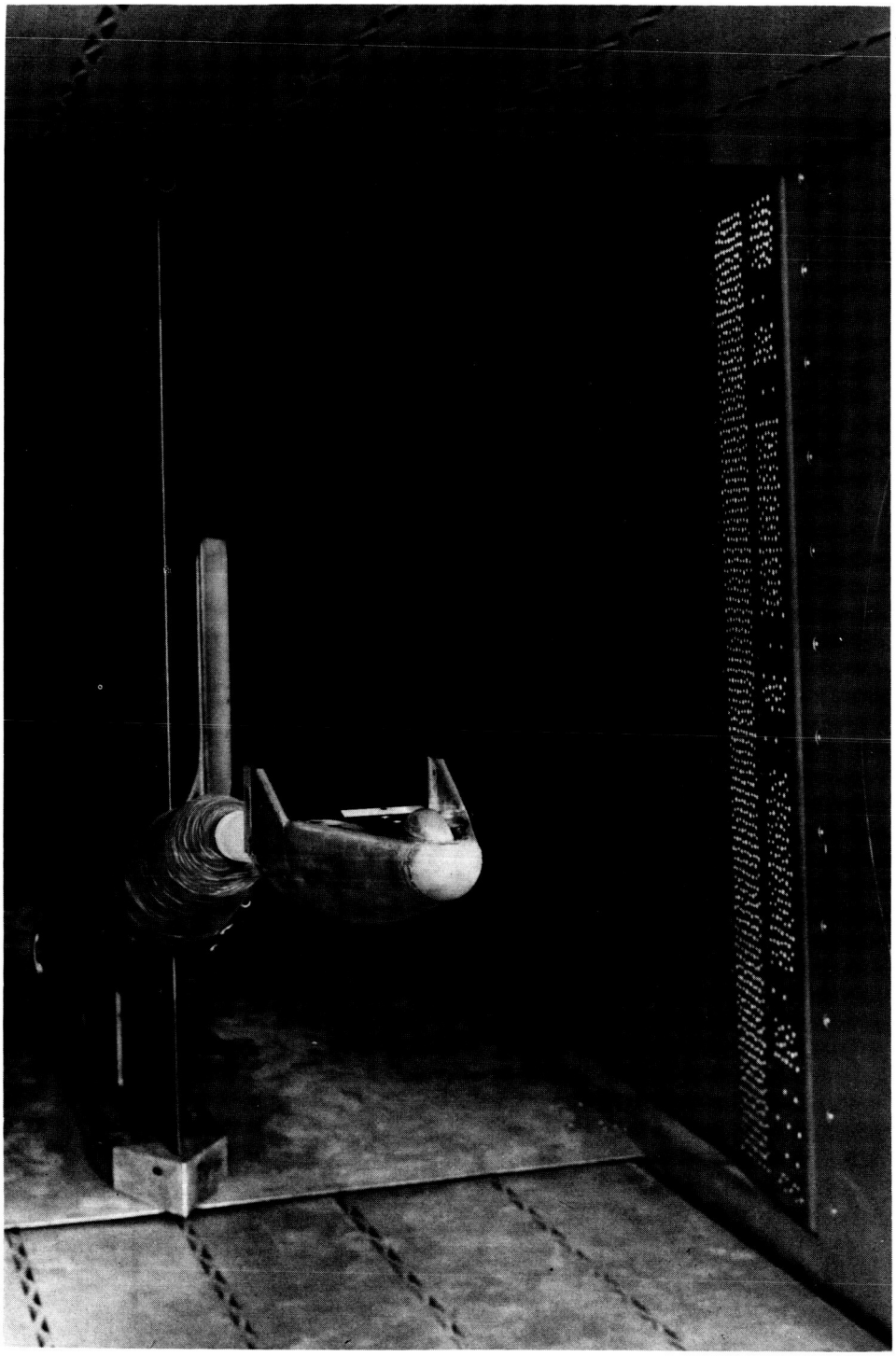

(a) Model in 6-by 6-Foot Wind Tunnel

Figure 3.- One-twelfth-scale model of M2-F2.

(b) Rear view

Figure 3.- Continued.

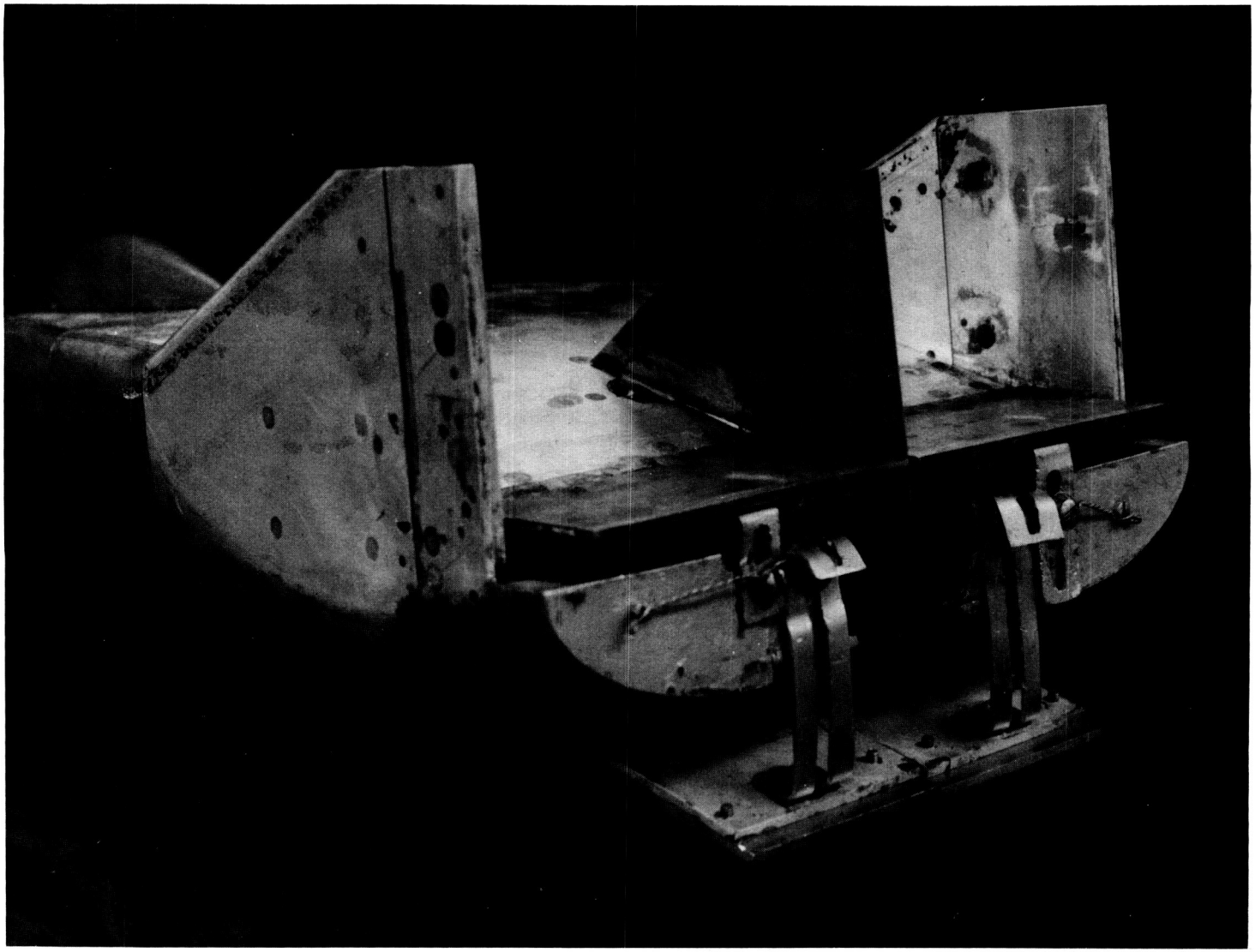

(c) Center fin installed on the model

Figure 3.- Concluded.

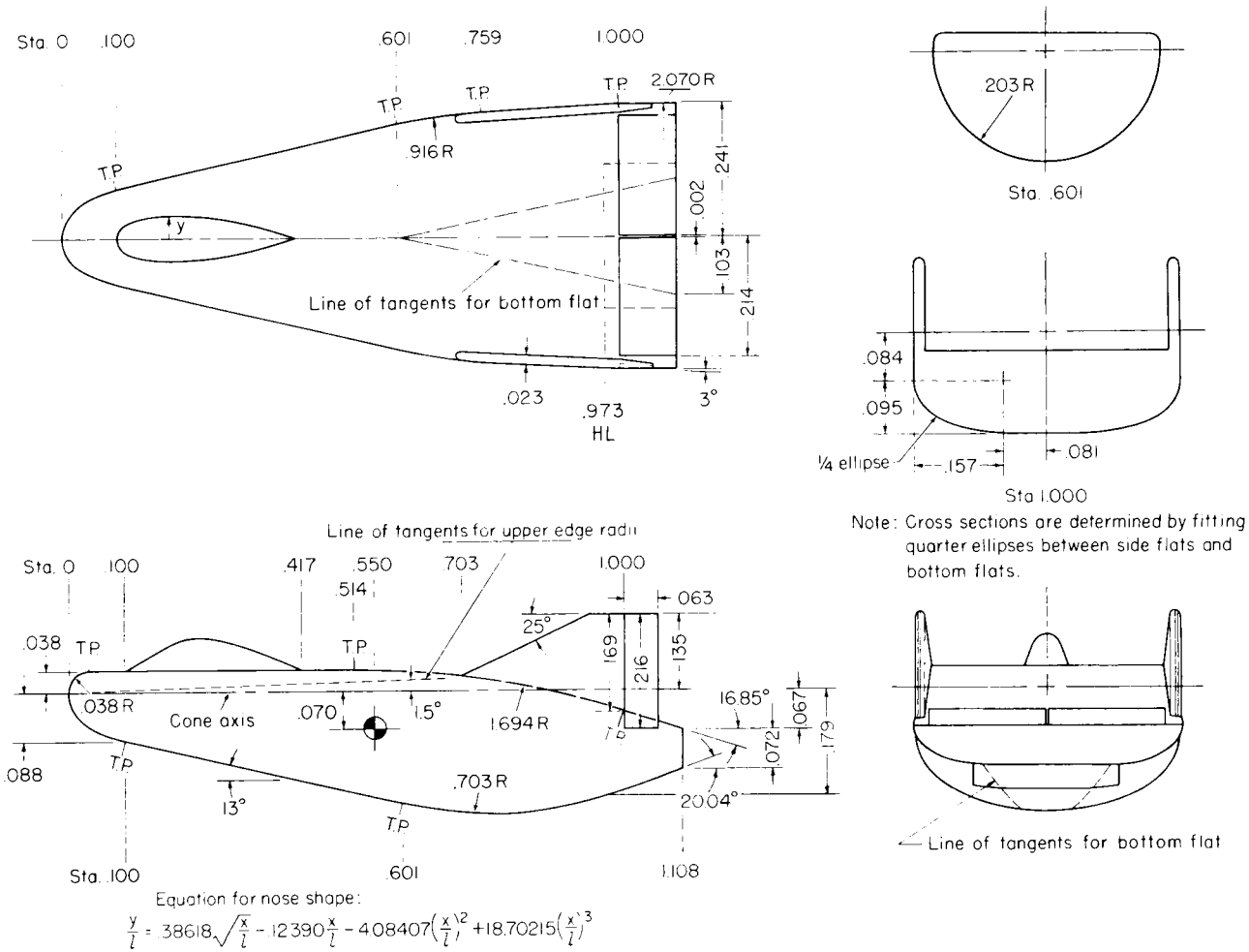

(a) Three-view drawing

Figure 4.- Model dimensions, given in fraction of model reference length (l = 50.8 cm).

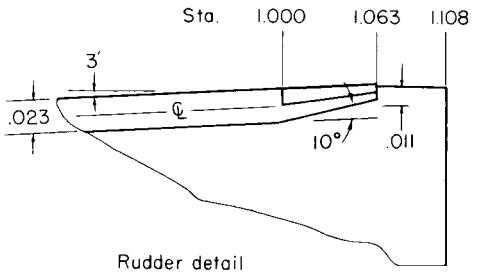

Rudder detail
Outer panel only deflects

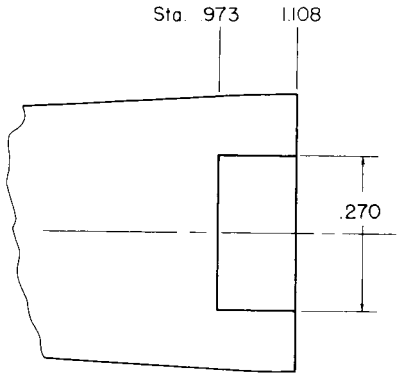

Lower flaps

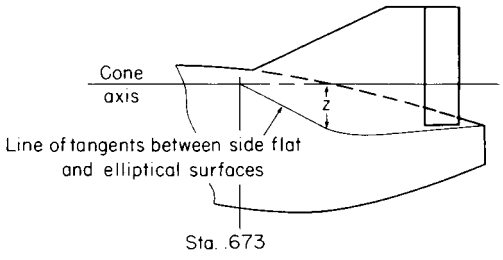

Control chord lengths

Rudder	.063
Upper flap	.103
Lower flap	.130

Line of tangents

Sta.	z
.673	0
.811	.069
.838	.081
.865	.088
.892	.092
.919	.092
.946	.091
.973	.088
1.108	.067

Canopy coordinates

Sta.	y	z
.100	0	0
.113	.024	–
.125	.030	–
.150	.035	–
.175	.038	.044
.200	.038	.053
.225	.038	.056
.250	.038	.055
.275	.035	.052
.300	.031	.045
.325	.026	.037
.350	.020	.028
.375	.014	.018
.400	.007	.008
.417	0	0

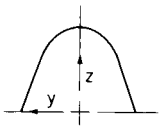

Sta. .225

Sta.	y	z
.225	.038	0
	.035	.010
	.031	.021
	.027	.031
	.023	.042
	.018	.048
	.011	.054
	0	.056

(b) Component details

Figure 4.- Continued.

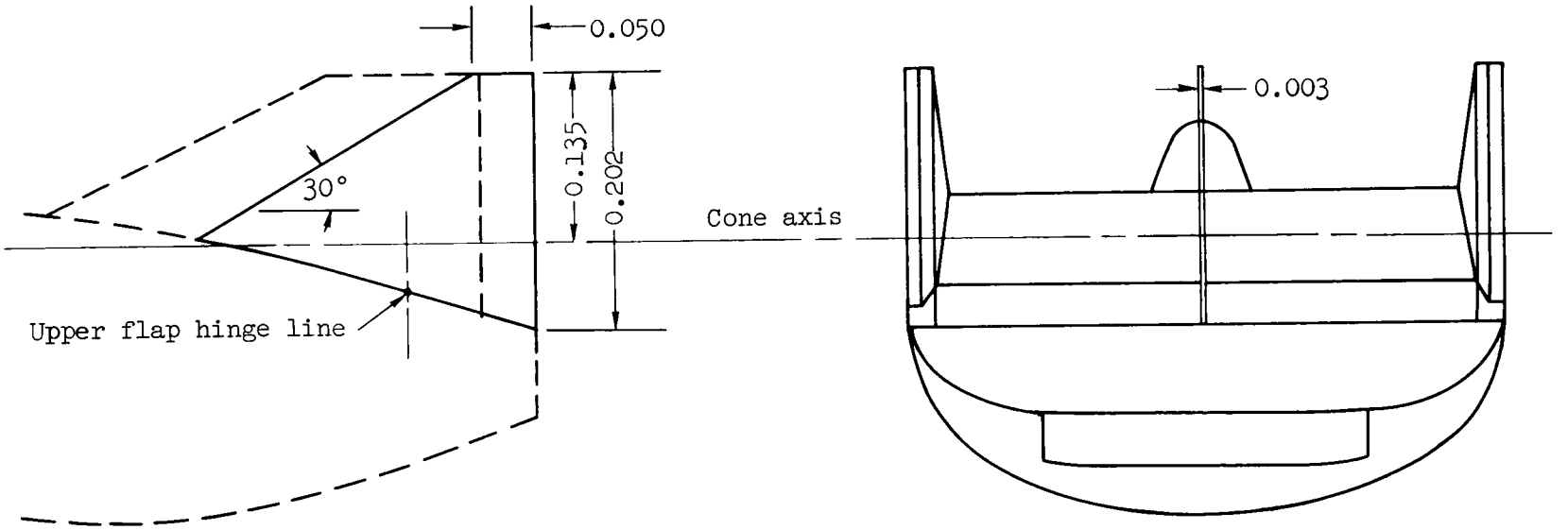

(c) Center fin

Figure 4.- Continued.

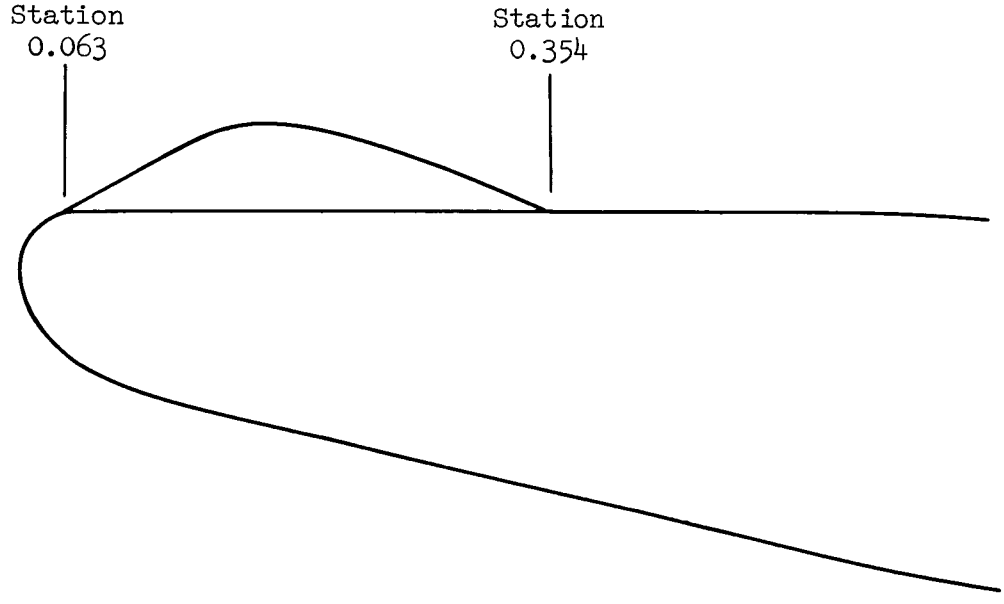

(d) Forward canopy location

Figure 4.- Concluded.

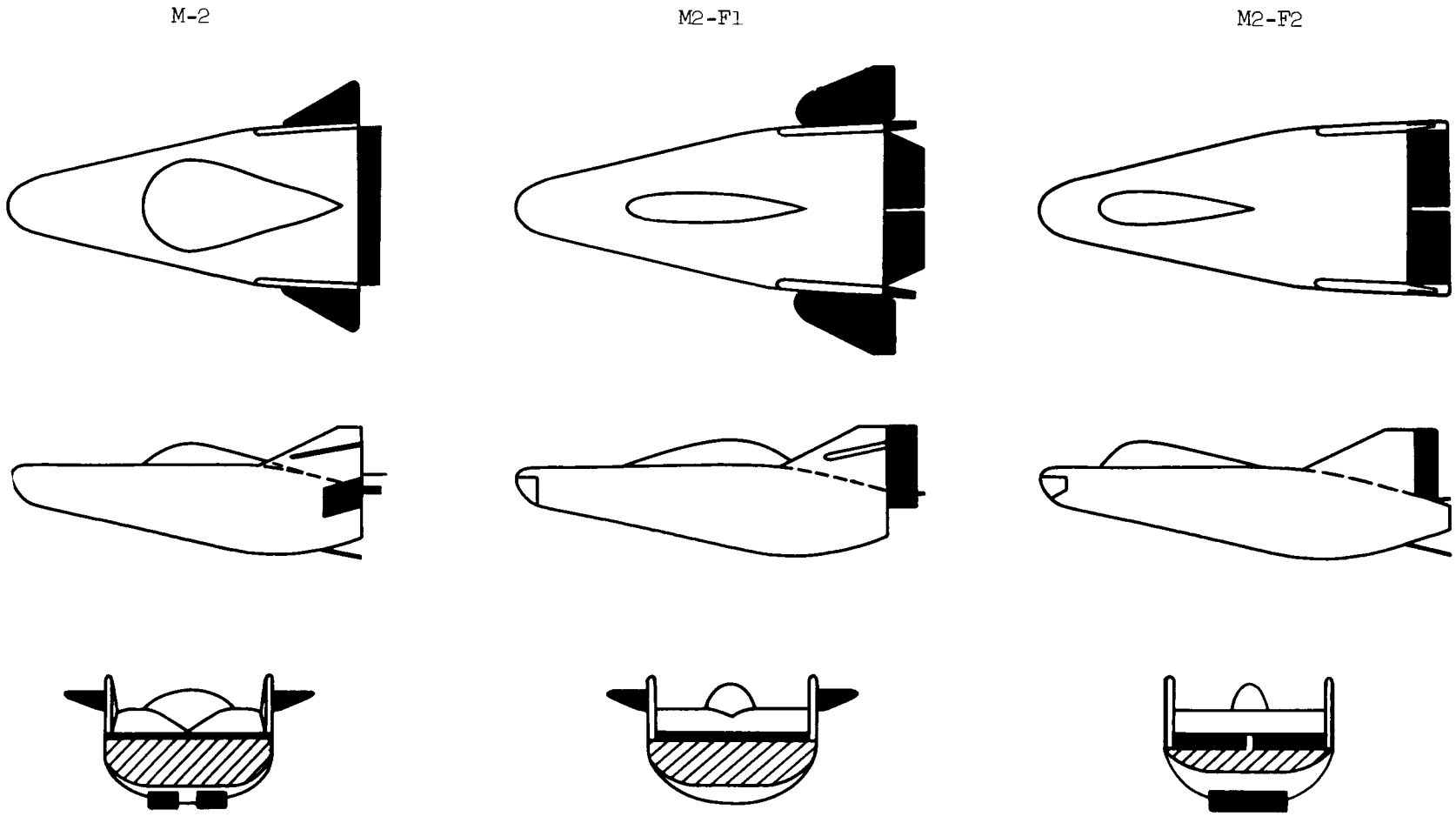

Figure 5.- Sketches of M-2, M2-F1 and M2-F2 configurations showing the controls.

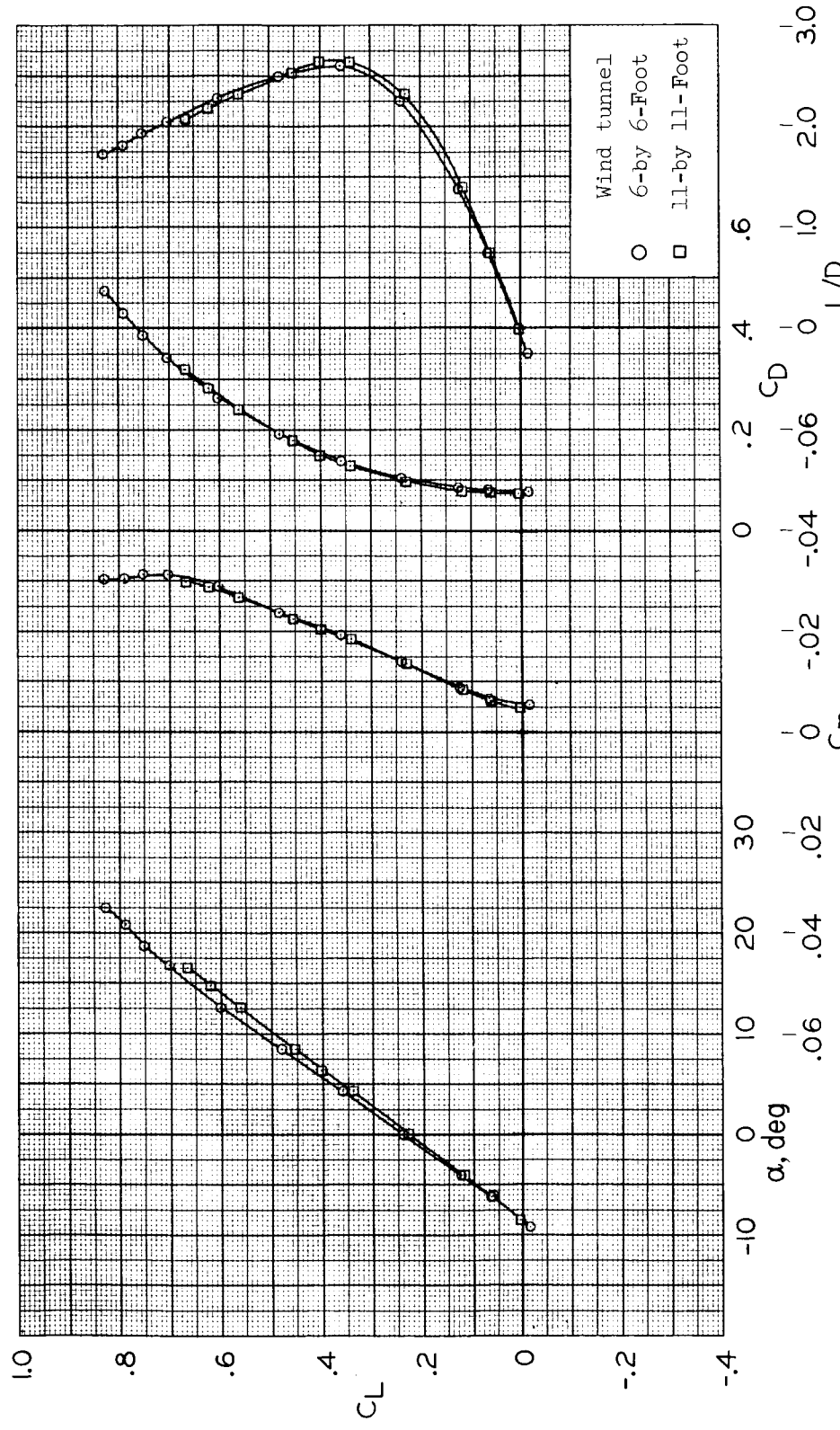

(a) M = 0.60

Figure 6.- Comparison of longitudinal characteristics obtained from 6-by 6-Foot and 11-by 11-Foot Wind Tunnels; R = 6×10^6; $\delta_u = -15°$, $\delta_l = 36°$, $\delta_{rf} = 5°$.

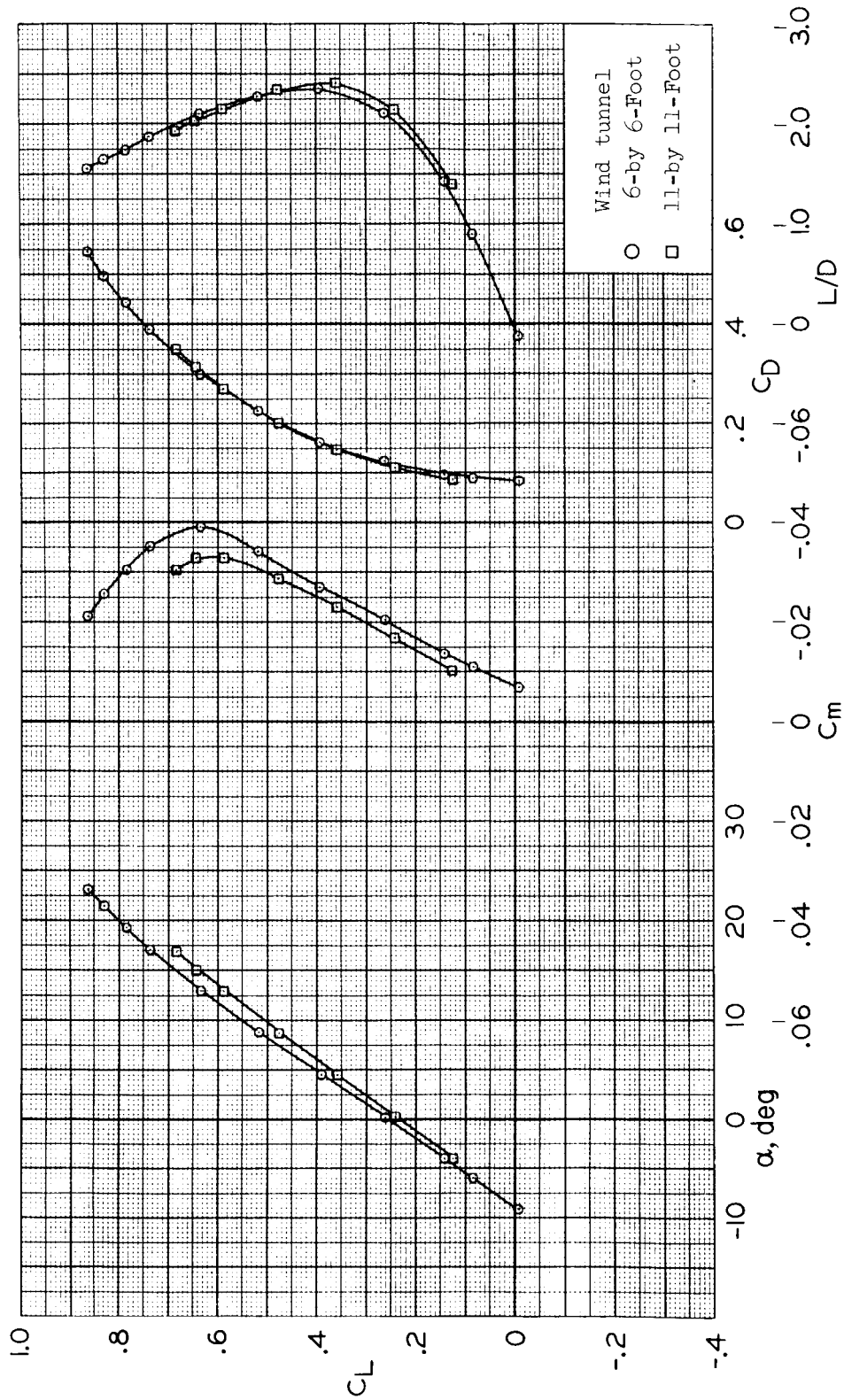

(b) M = 0.80

Figure 6.- Continued.

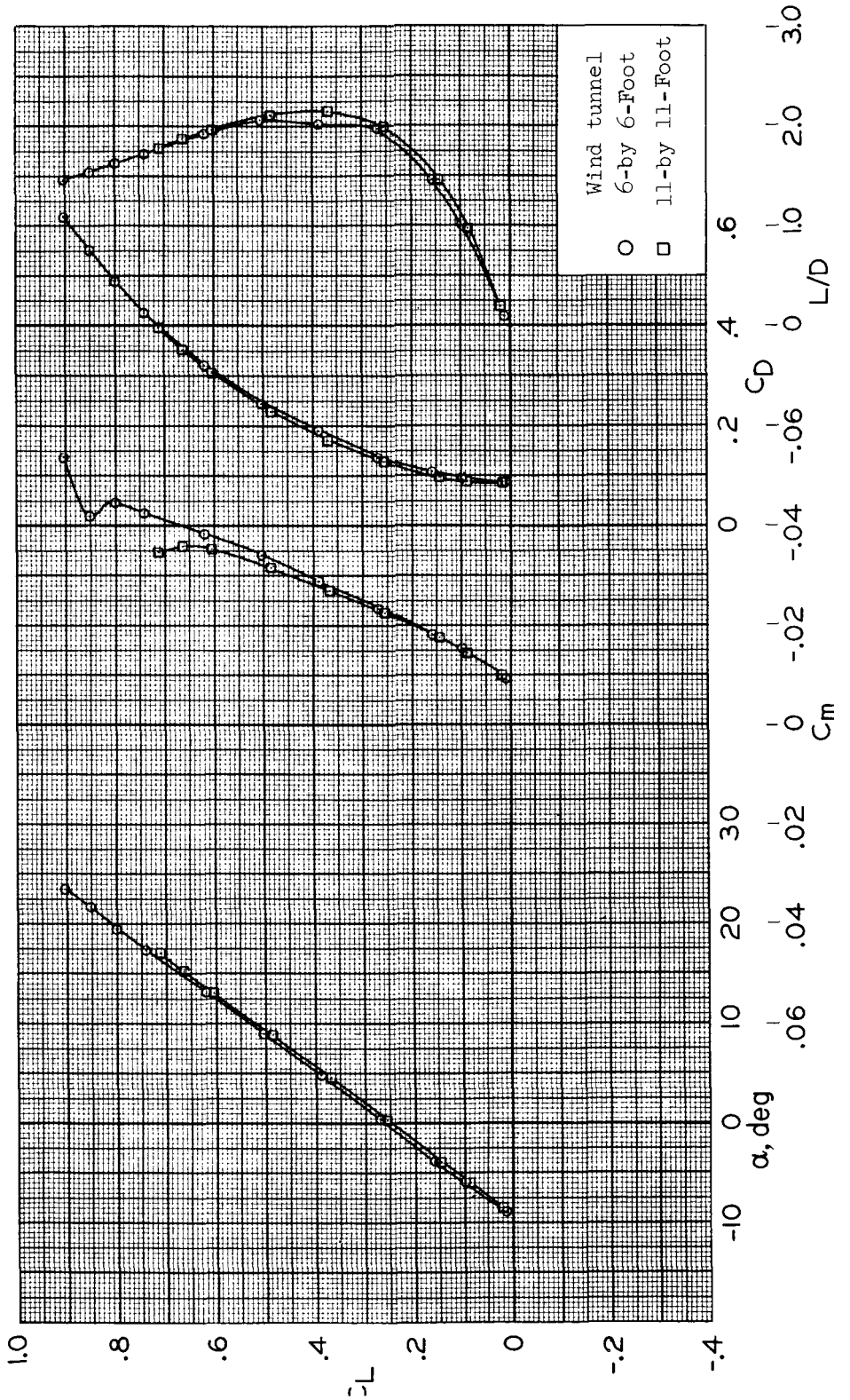

(c) M = 0.90

Figure 6.- Continued.

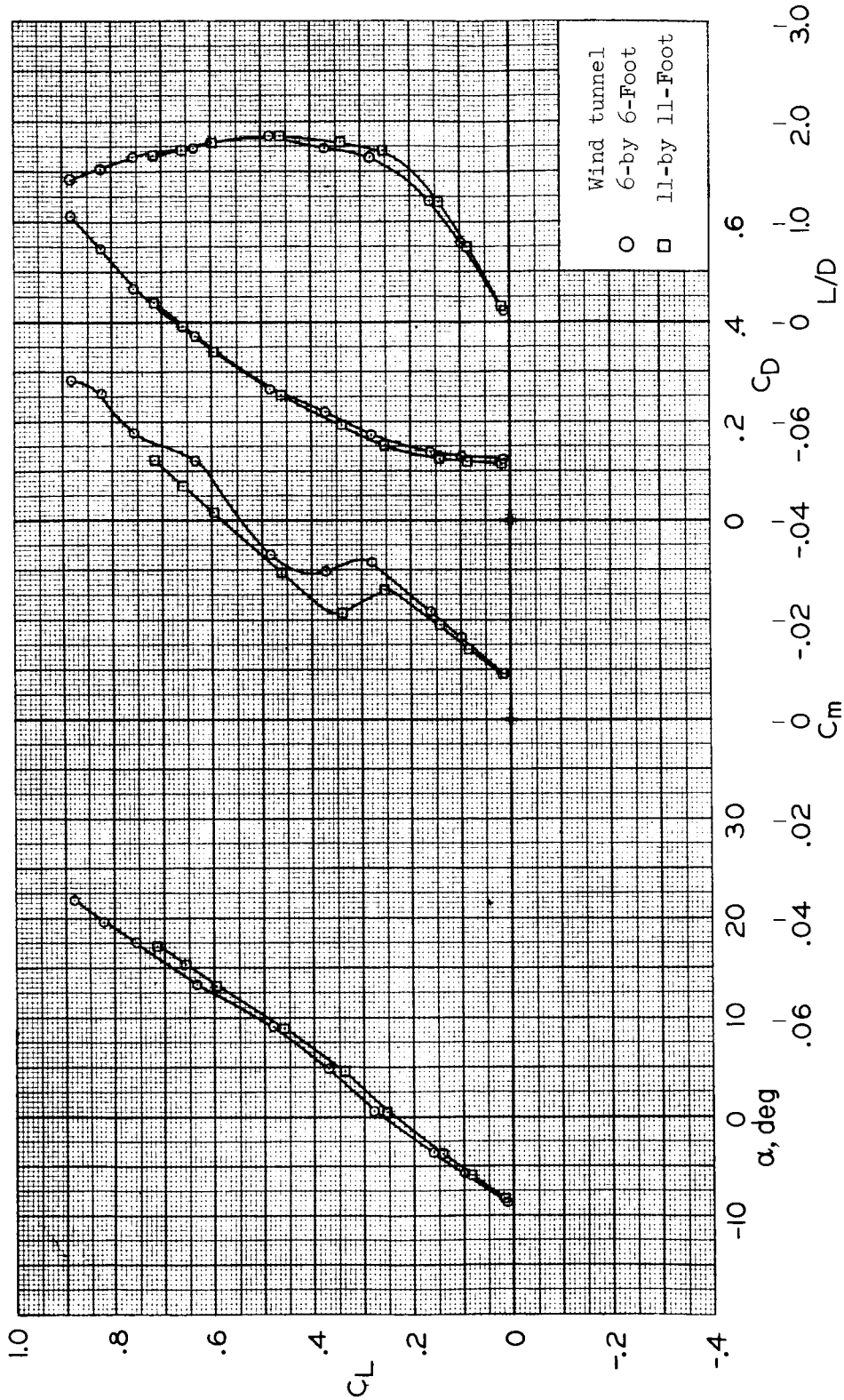

(d) M = 0.95

Figure 6.- Continued.

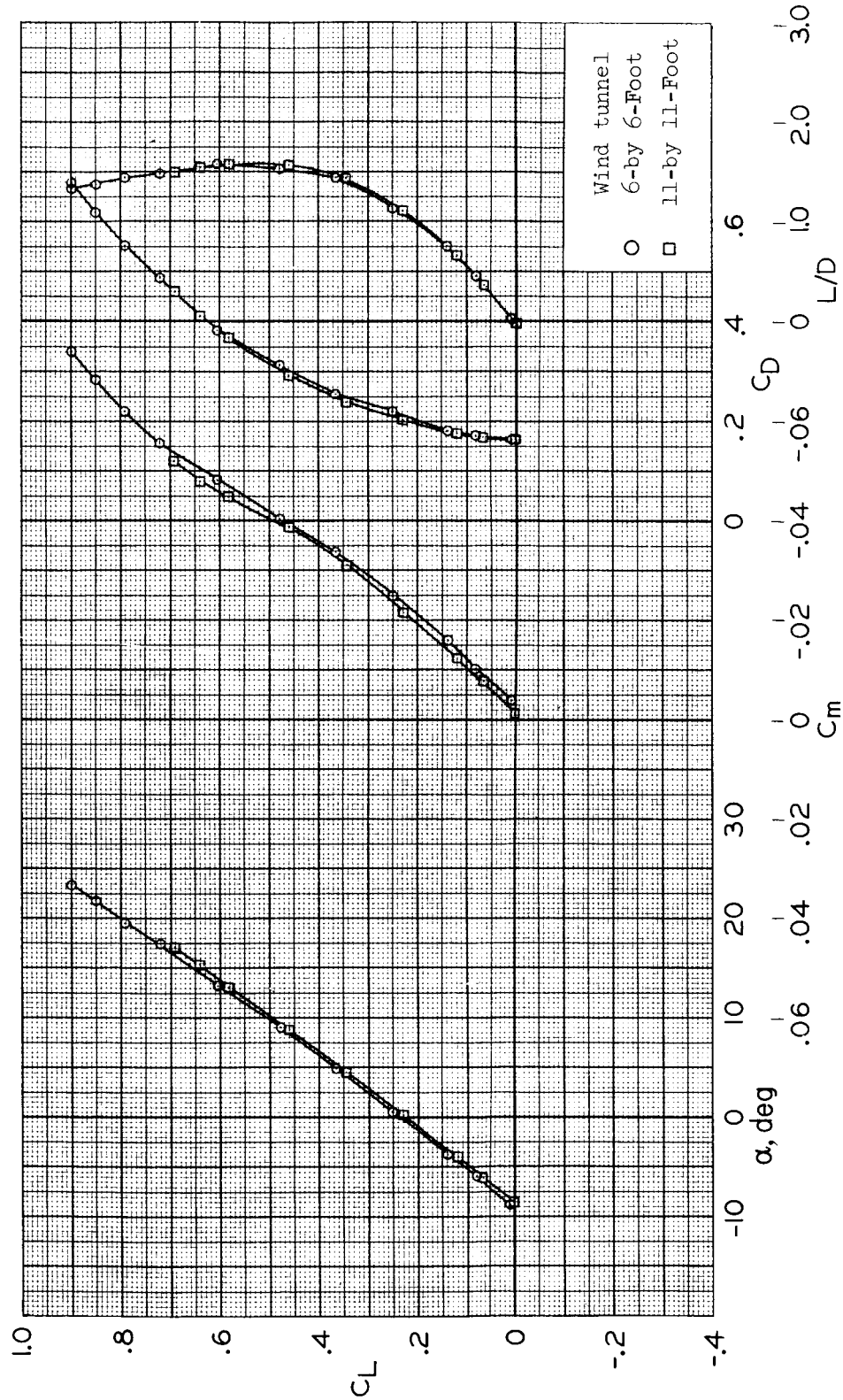

(e) M = 1.00

Figure 6.- Continued.

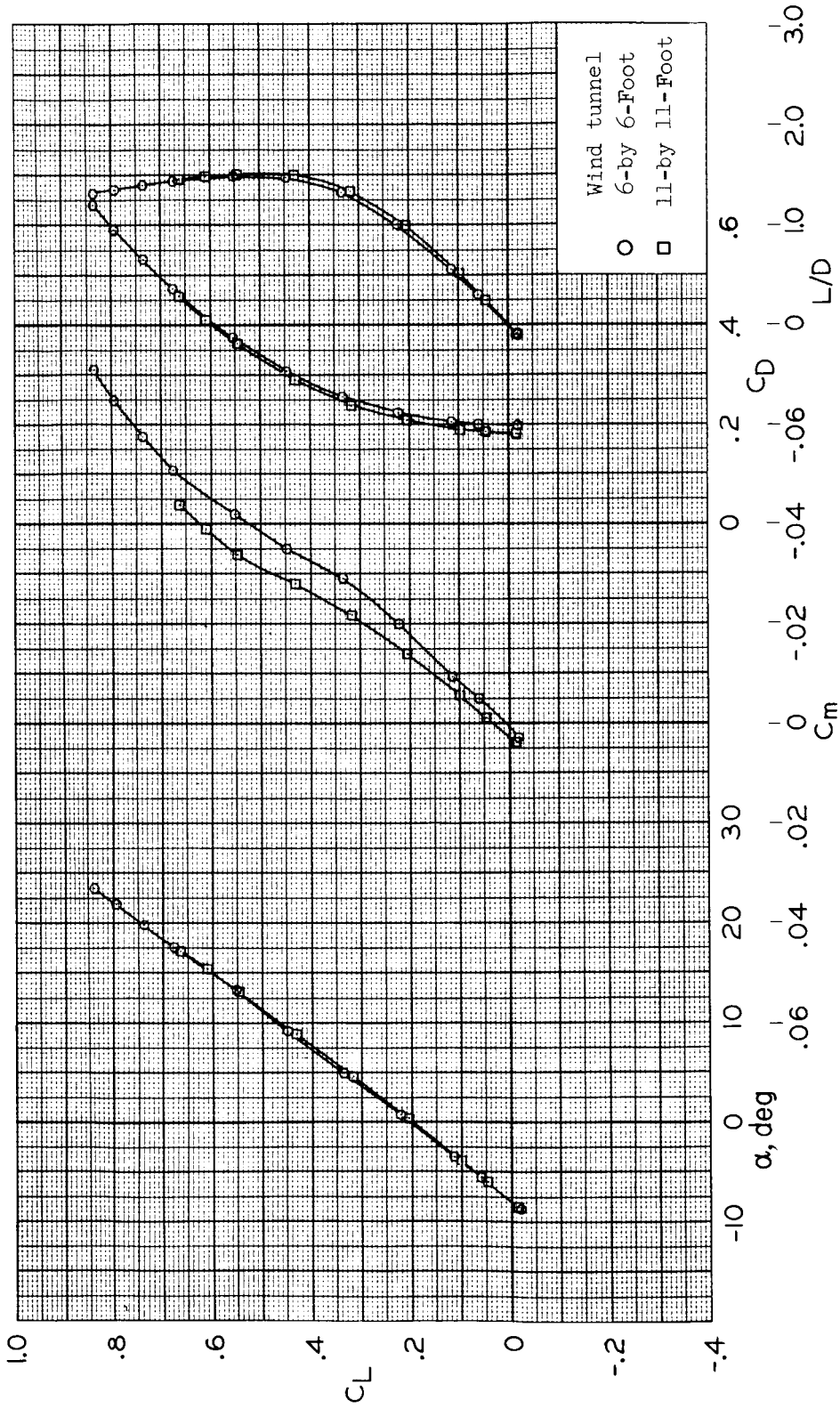

(f) M = 1.10

Figure 6.- Continued.

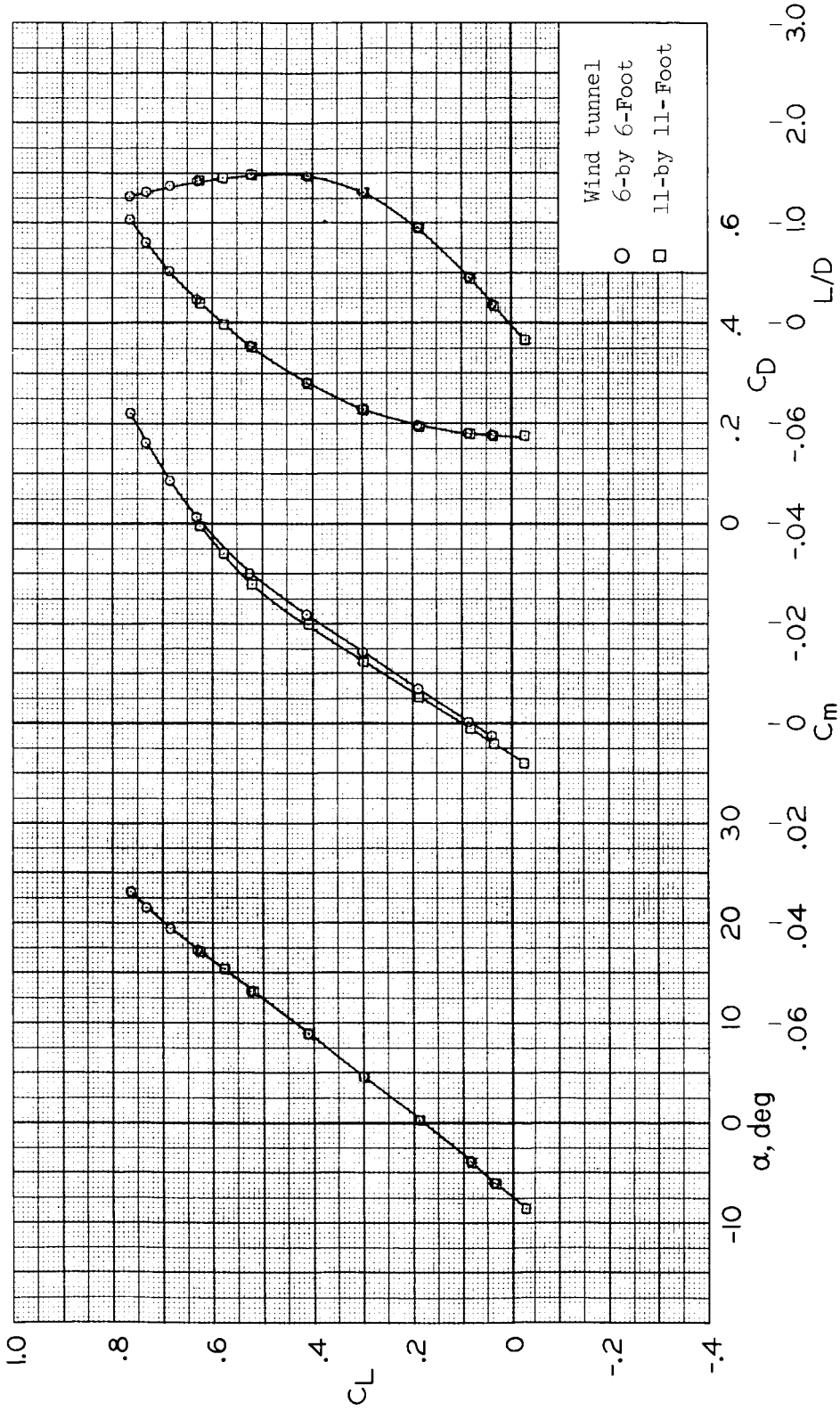

(g) M = 1.30

Figure 6.- Concluded.

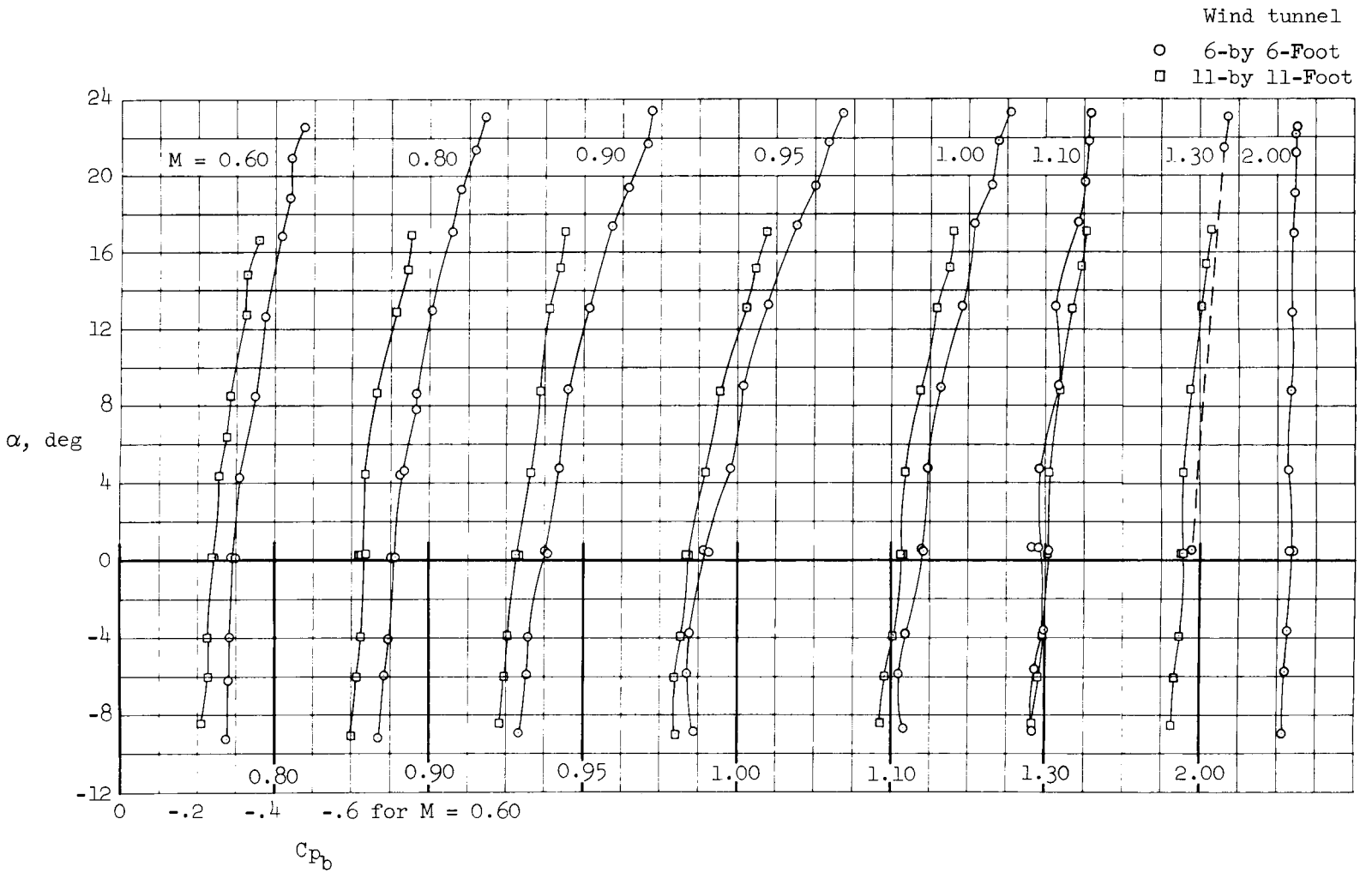

Figure 7.- Base pressure coefficient; R = 6×10^6; δ_u = -15°, δ_l = 36°, δ_{rf} = 5°.

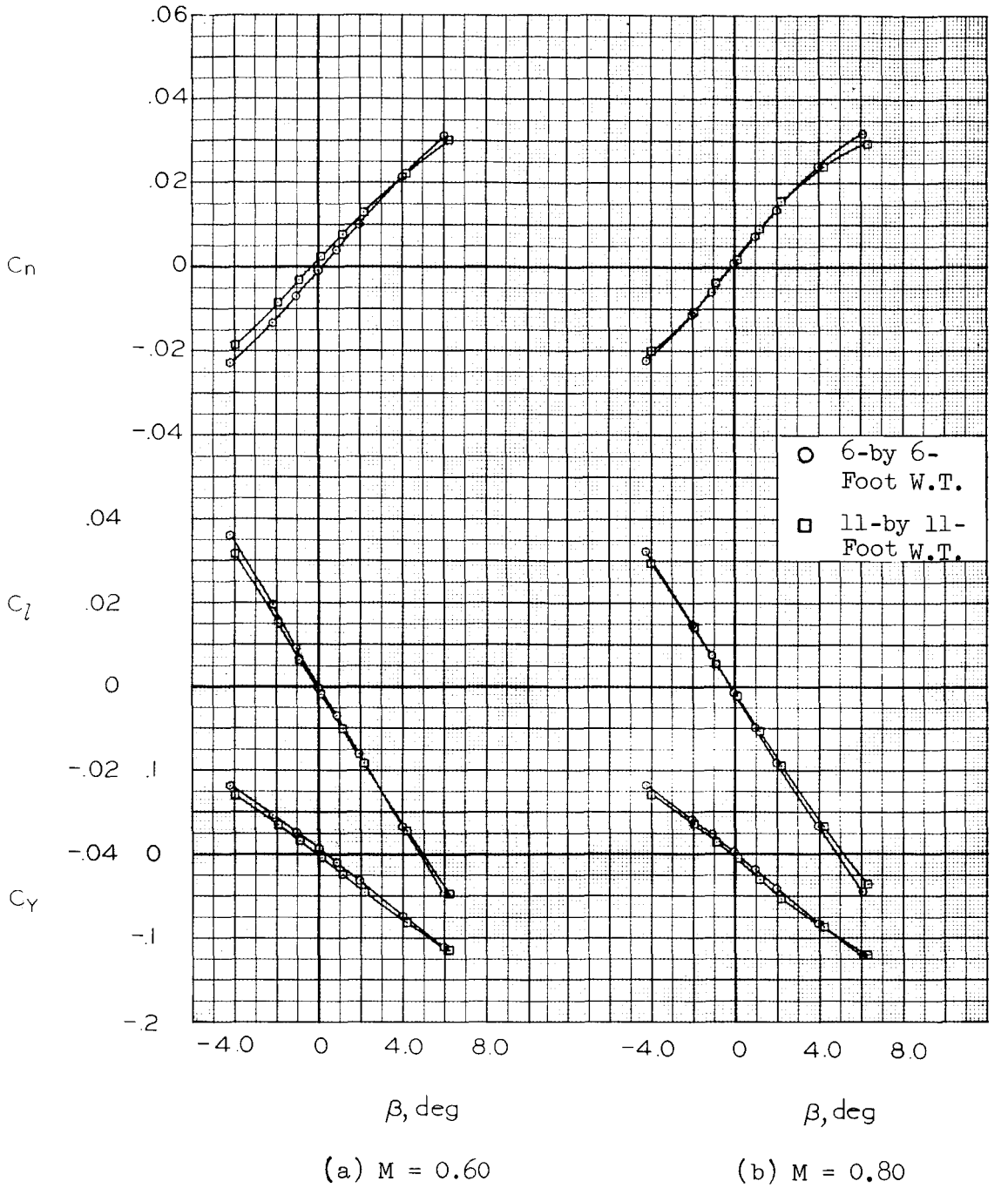

Figure 8.- Comparison of lateral-directional characteristics as measured in the 6-by 6-Foot and the 11-by 11-Foot Wind Tunnels; R = 6×10^6, $\alpha = 6°$, $\delta_u = -15°$, $\delta_l = 35°$, $\delta_{rf} = 5°$.

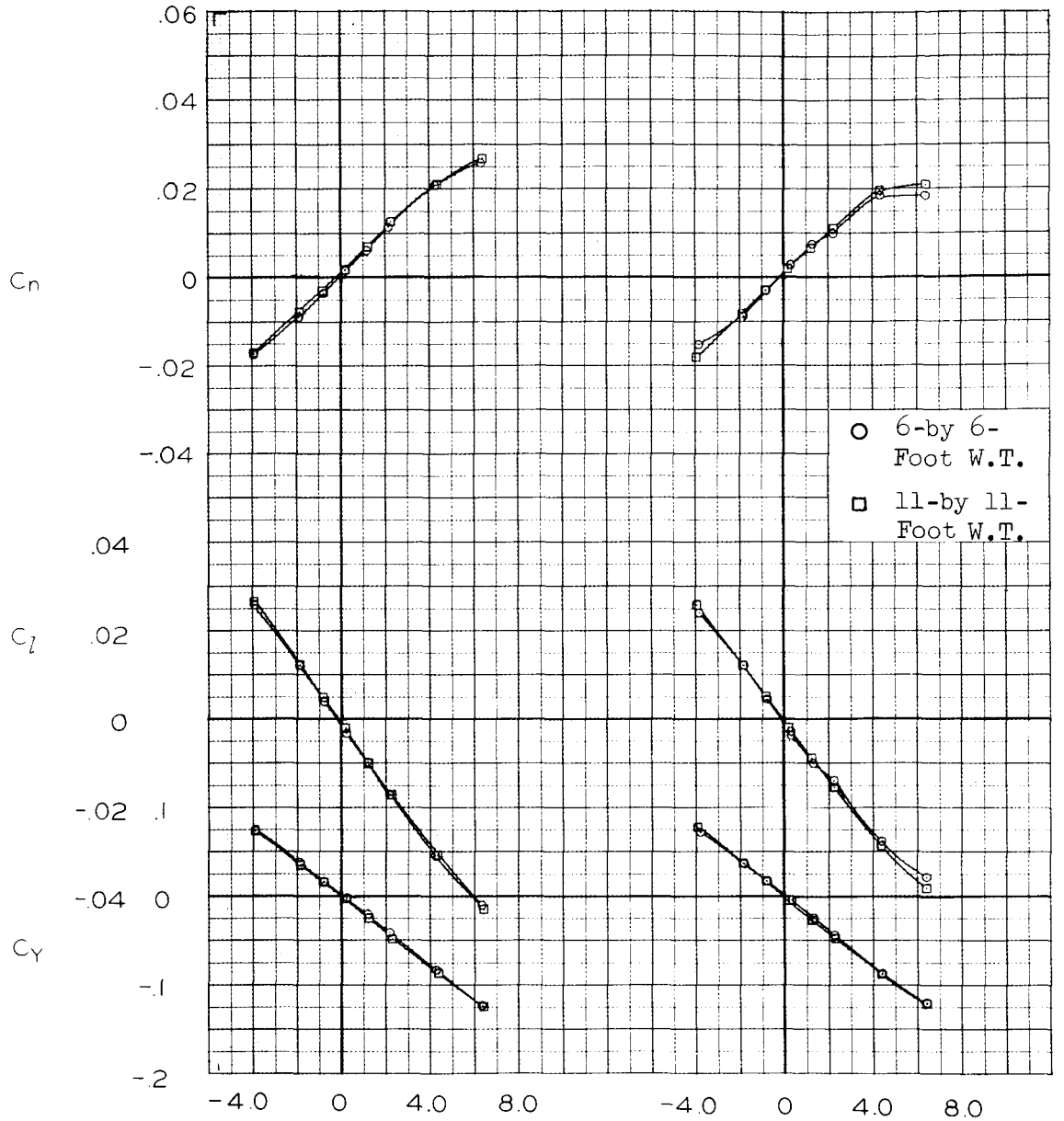

(c) M = 0.90 (d) M = 0.95

Figure 8.- Continued.

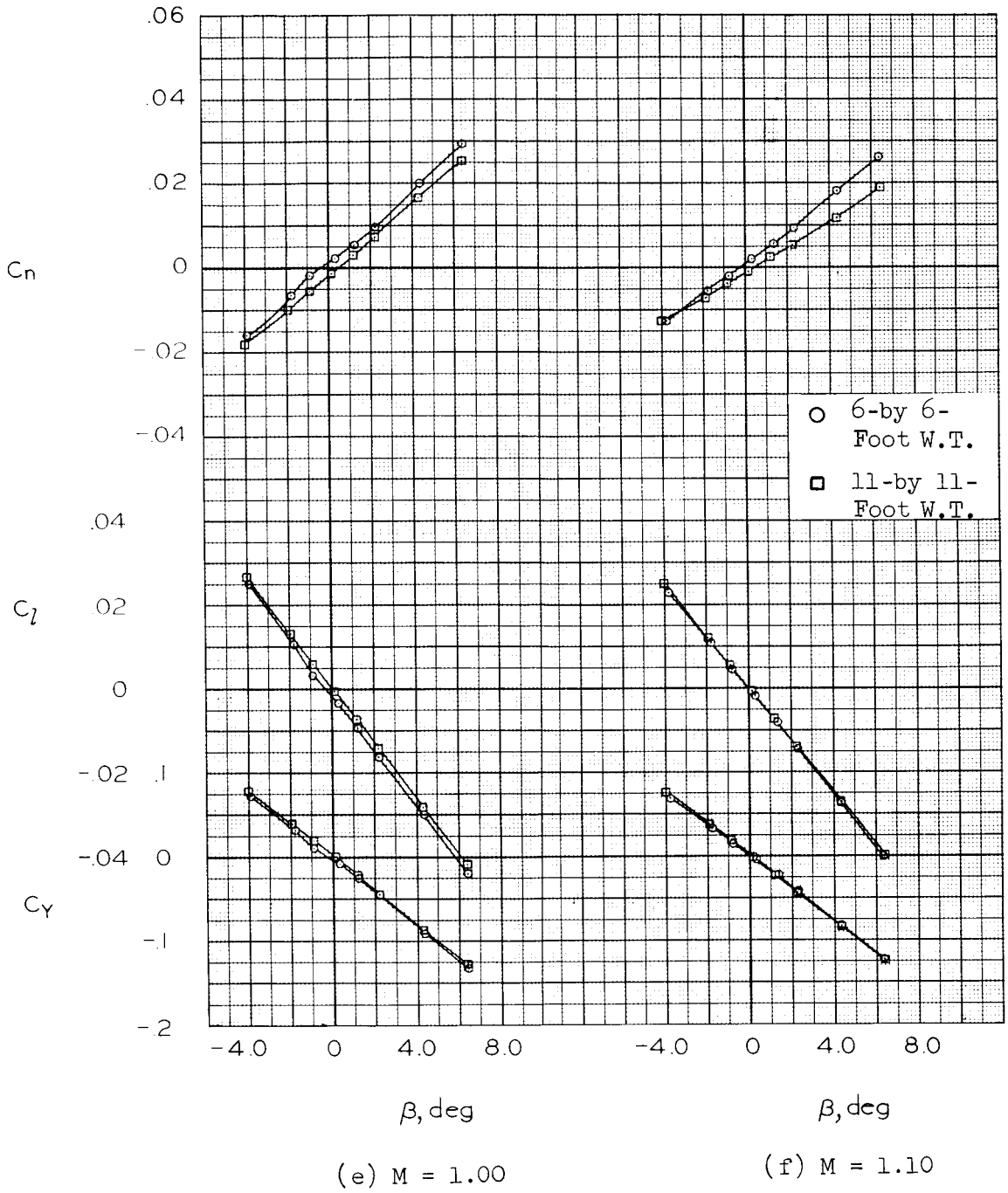

(e) M = 1.00

(f) M = 1.10

Figure 8.- Continued.

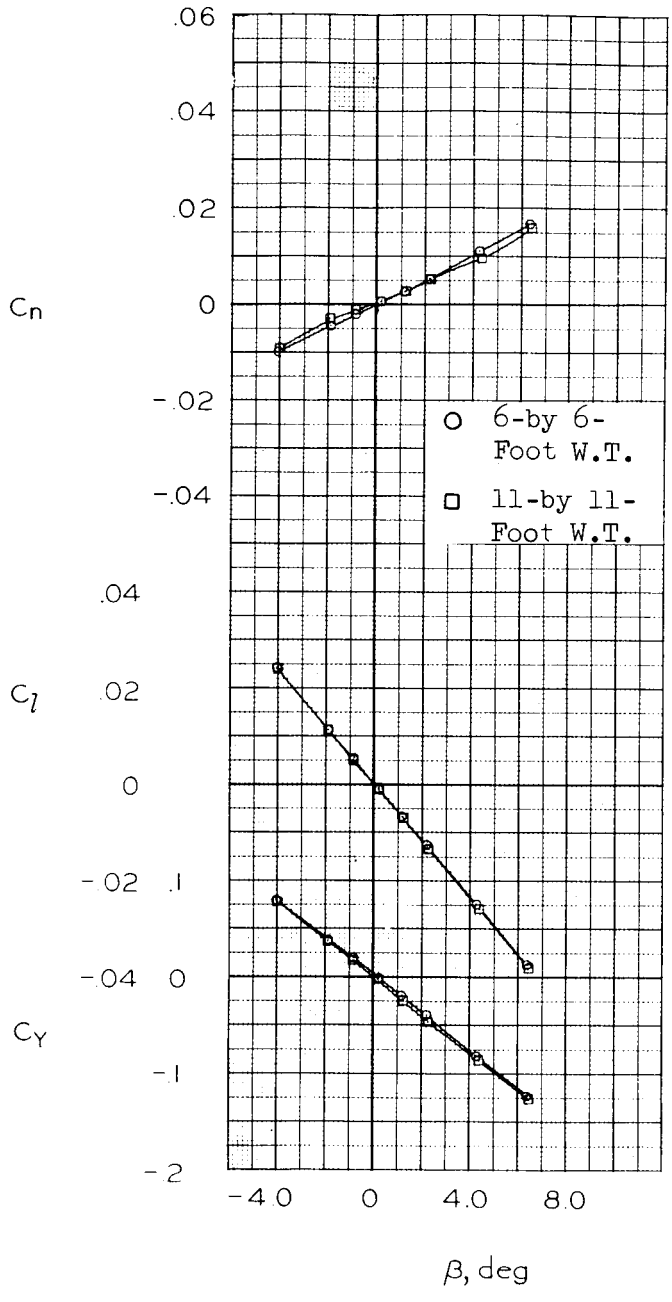

(g) M = 1.30

Figure 8.- Concluded.

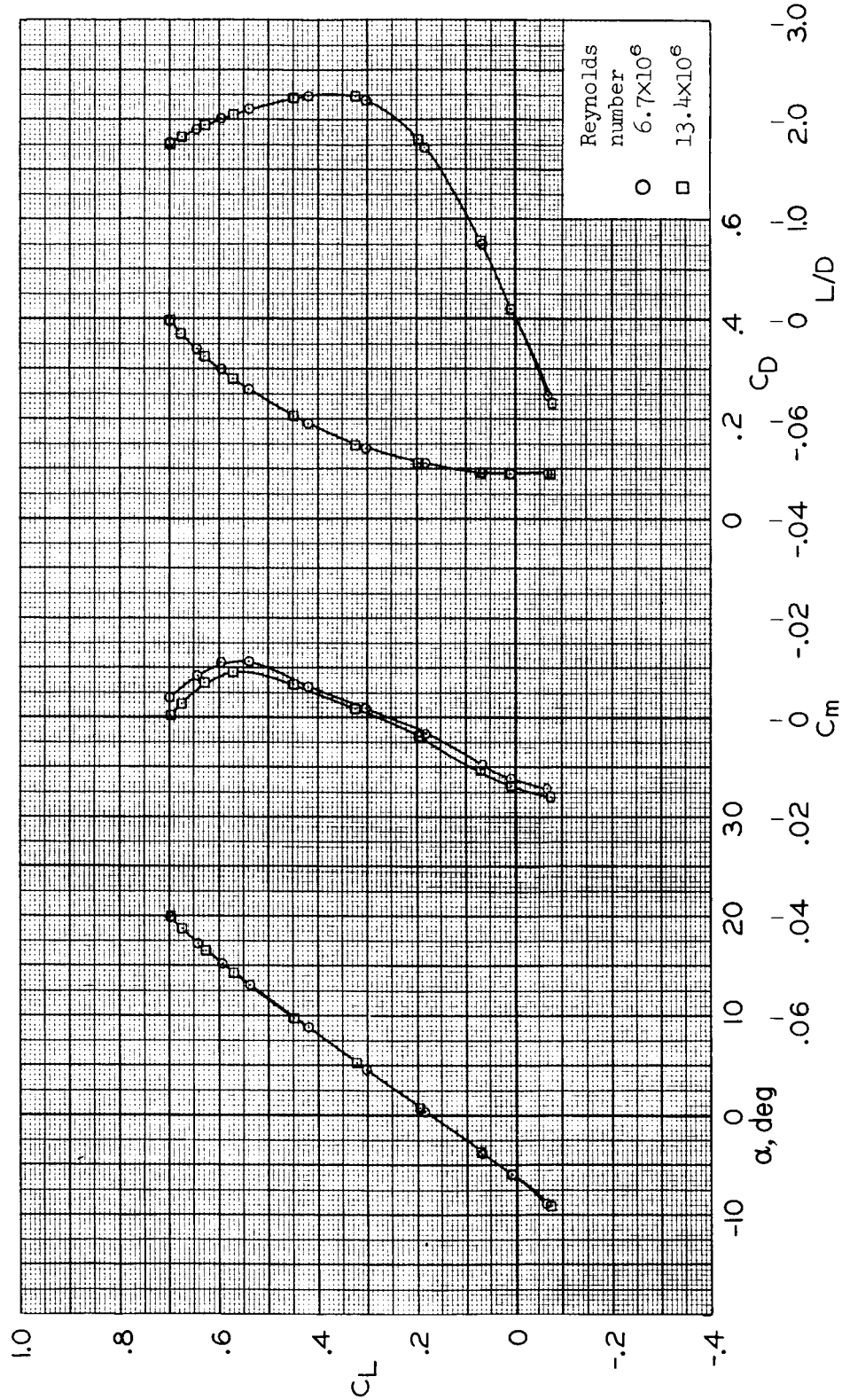

(a) M = 0.80

Figure 9.- Effect of Reynolds number on longitudinal characteristics; 11-by 11-Foot Wind Tunnel; $\delta_u = -20°$, $\delta_l = 36°$, $\delta_{rf} = 5°$.

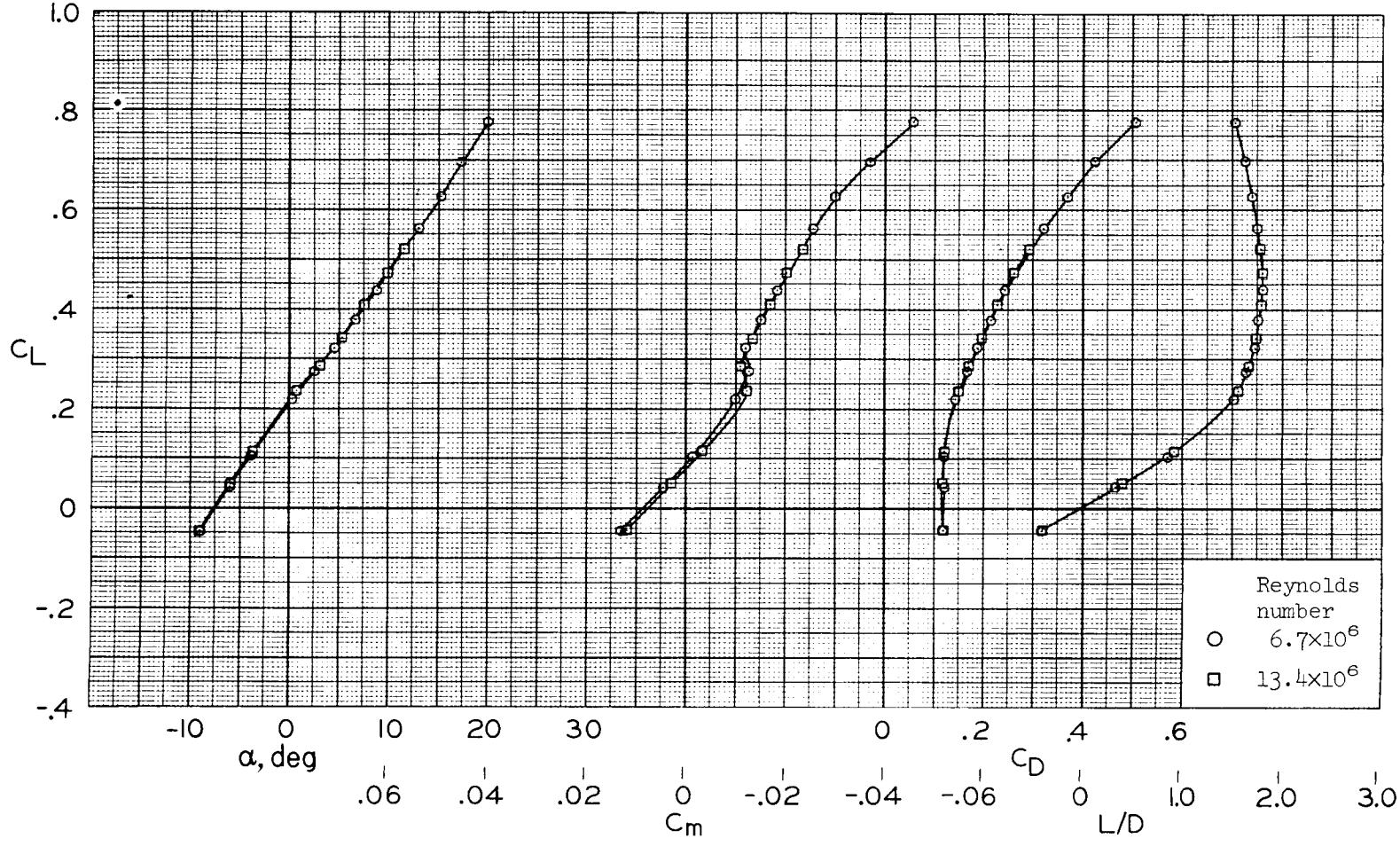

(b) M = 0.95

Figure 9.- Concluded.

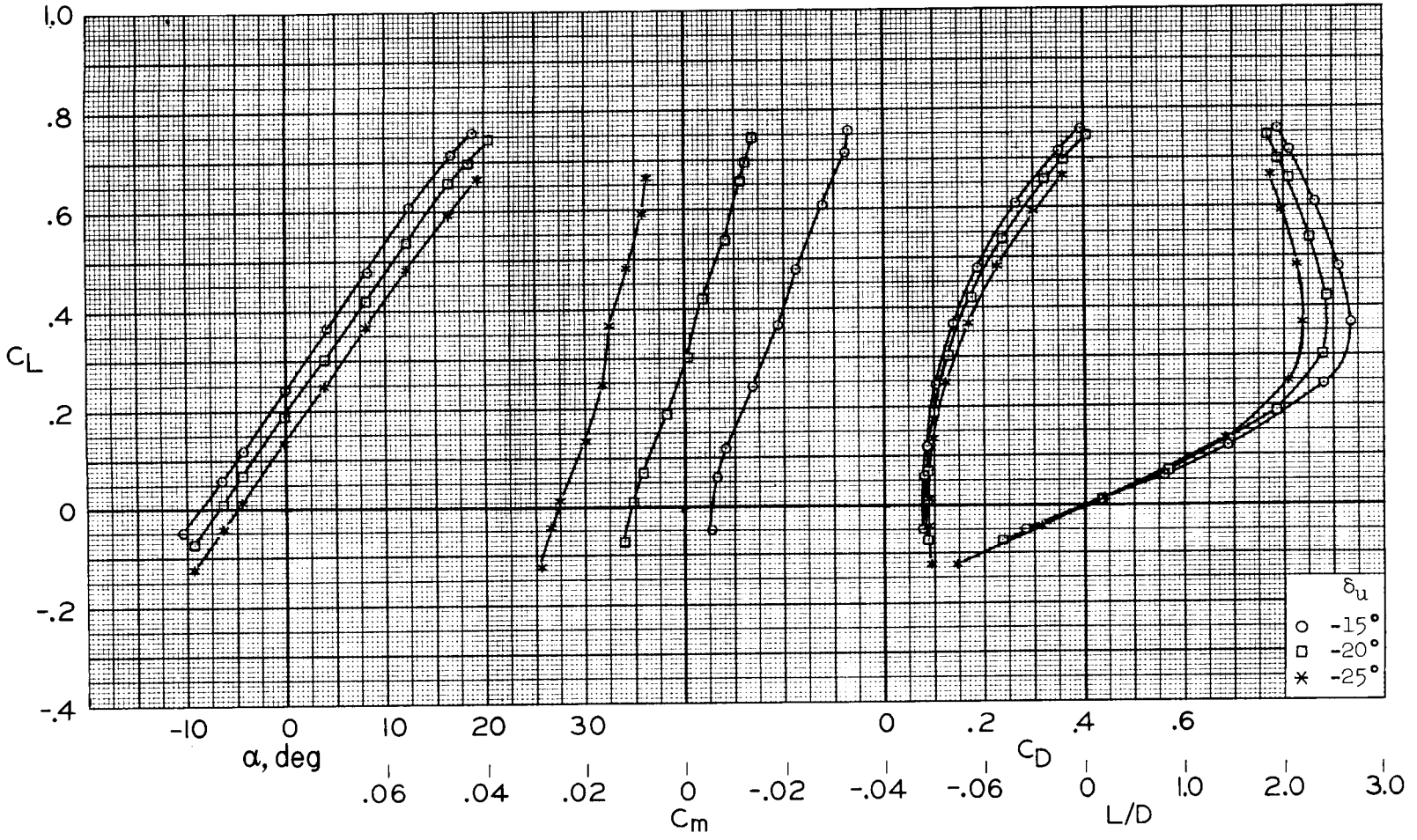

(a) M = 0.6, R = 5.7×10^6

Figure 10.- Longitudinal characteristics at selected upper flap deflections; $\delta_l = 35°$, $\delta_{rf} = 0°$.

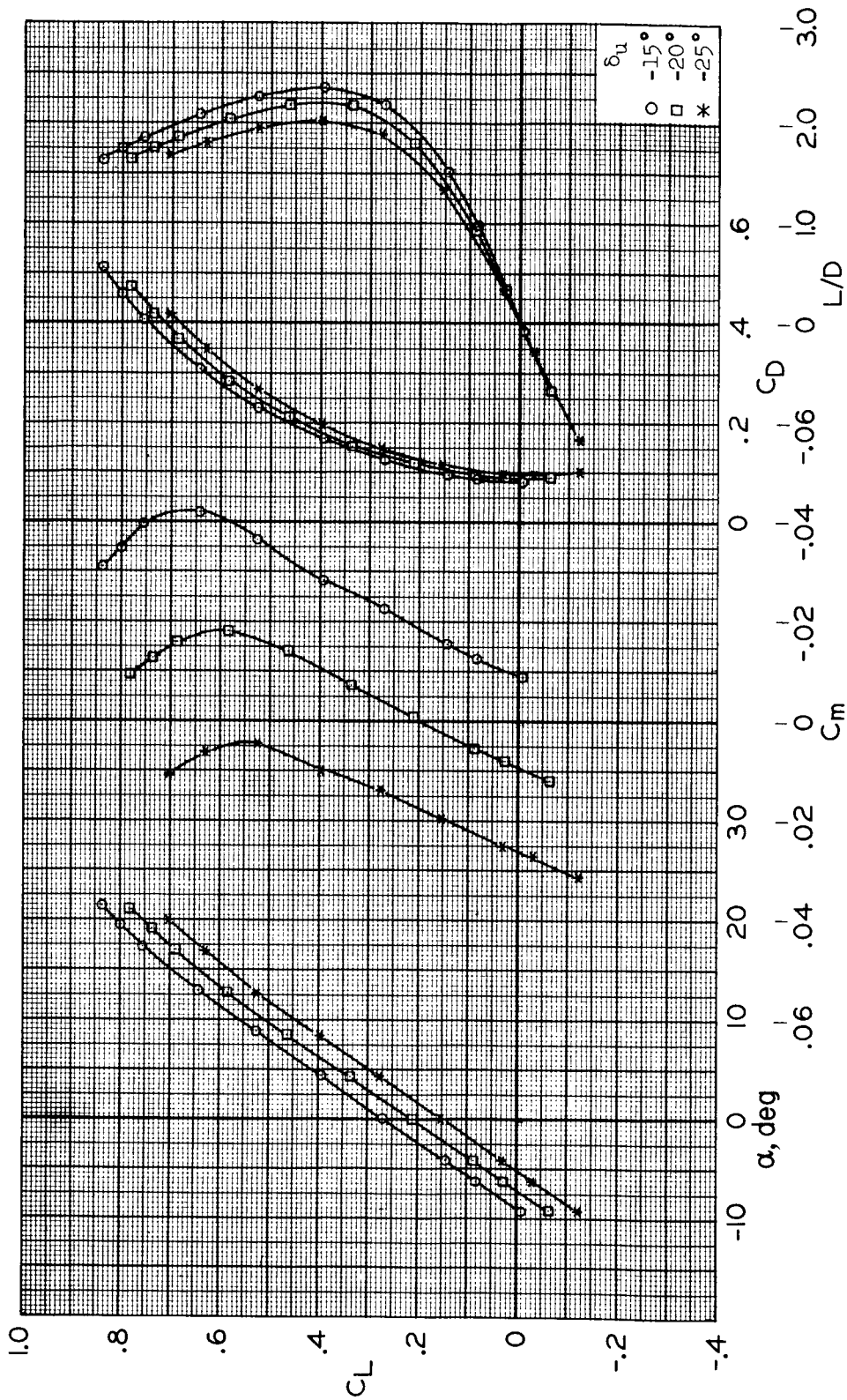

(b) M = 0.8, R = 6.4x10^6

Figure 10.- Continued.

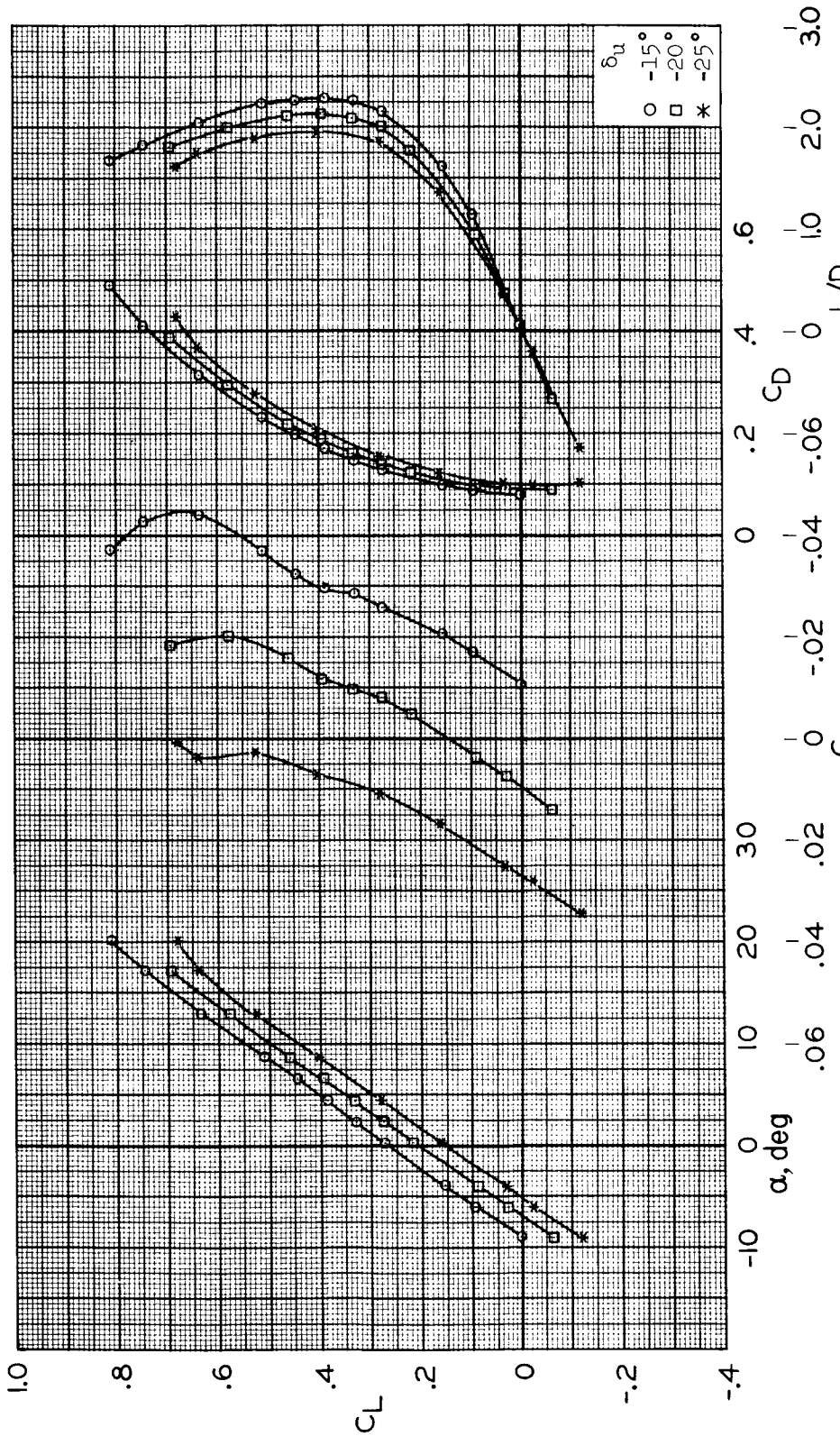

(c) M = 0.85, R = 6.4×10^6

Figure 10.- Continued.

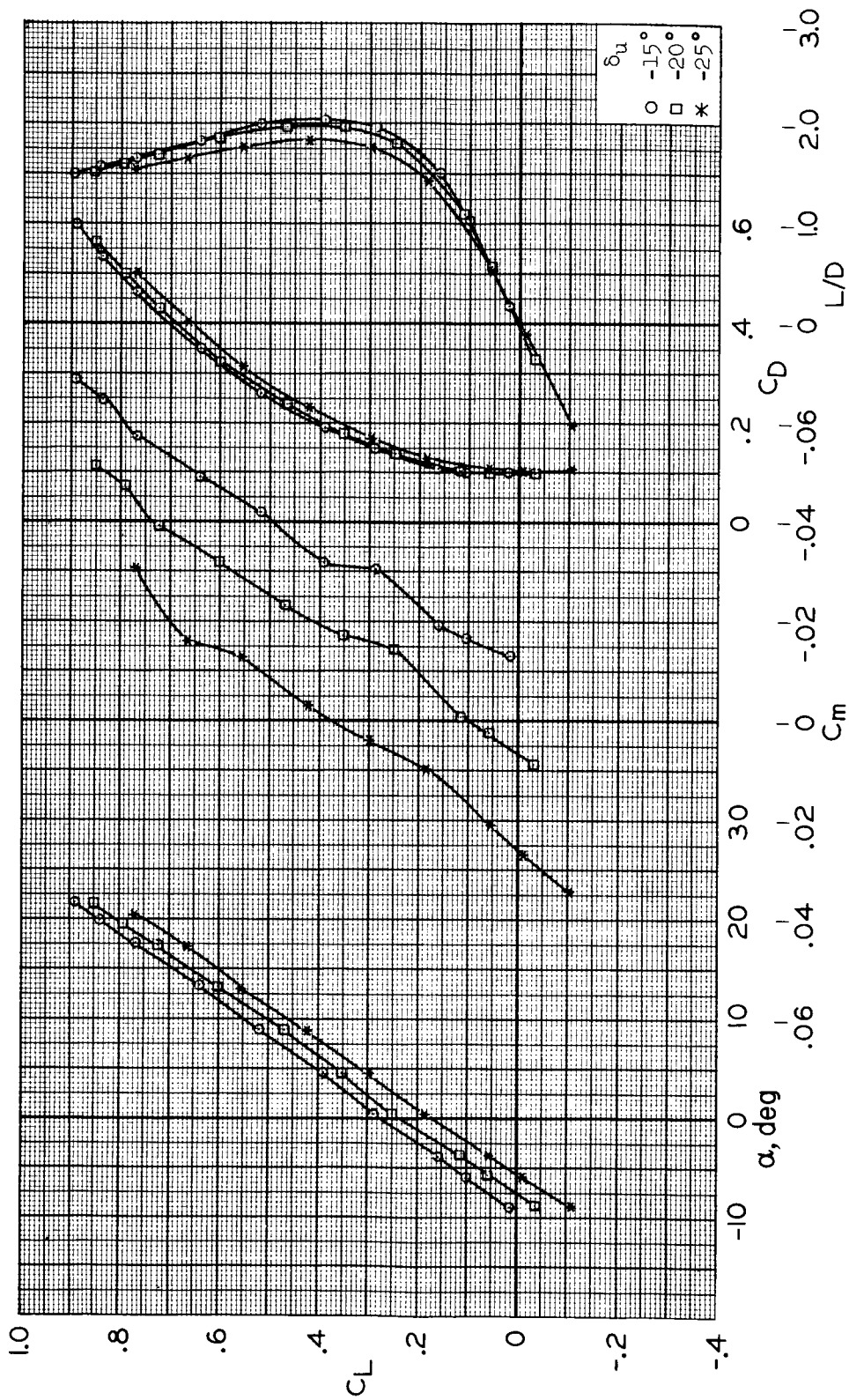

(d) M = 0.9, R = 6.4×10^6

Figure 10.- Continued.

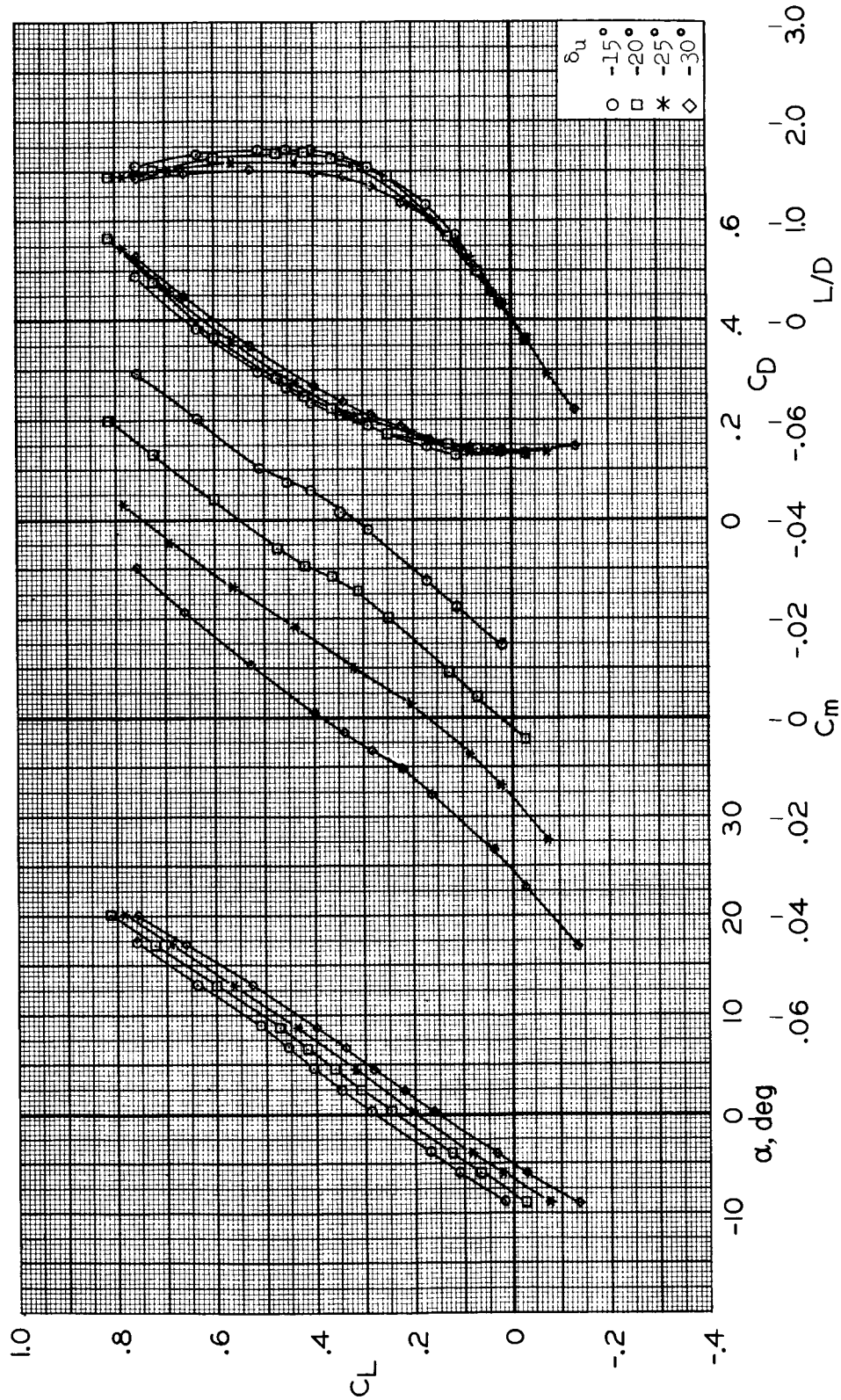

(e) M = 0.95, R = 5.6x10^6

Figure 10.- Contunued.

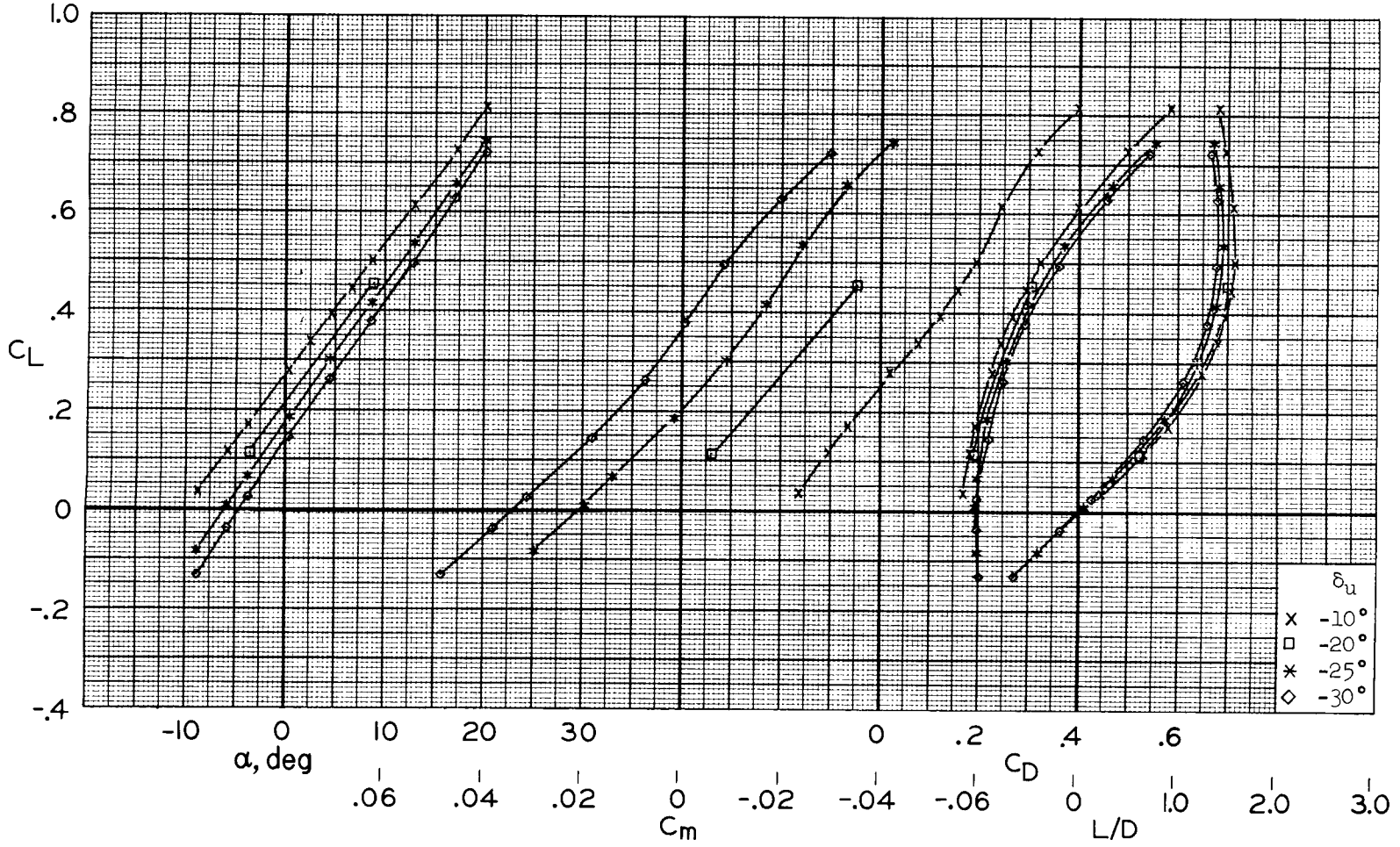

(f) M = 1.0, R = 4.8×10^6

Figure 10.- Continued.

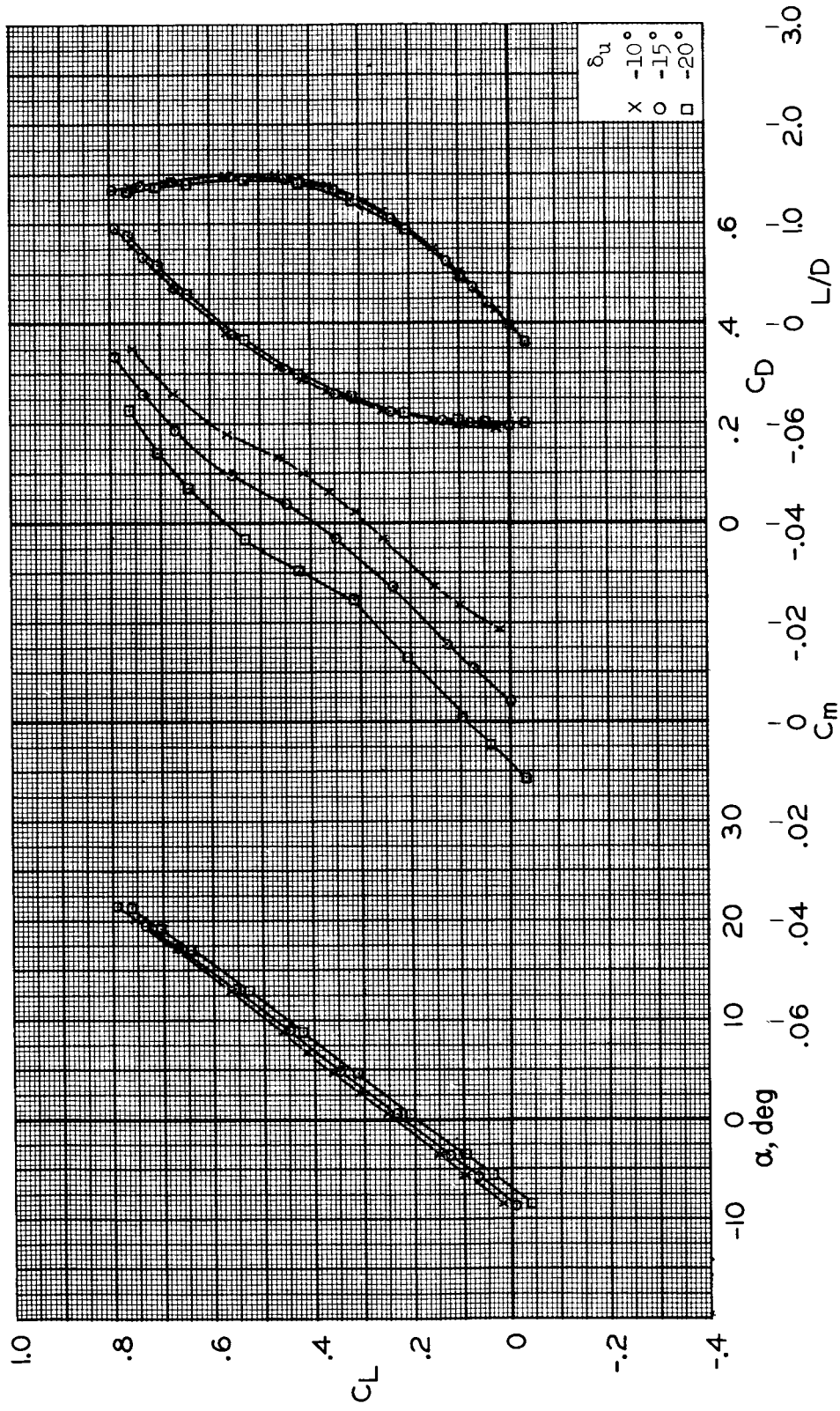

(g) M = 1.1, R = 4.1×10^6

Figure 10.- Continued.

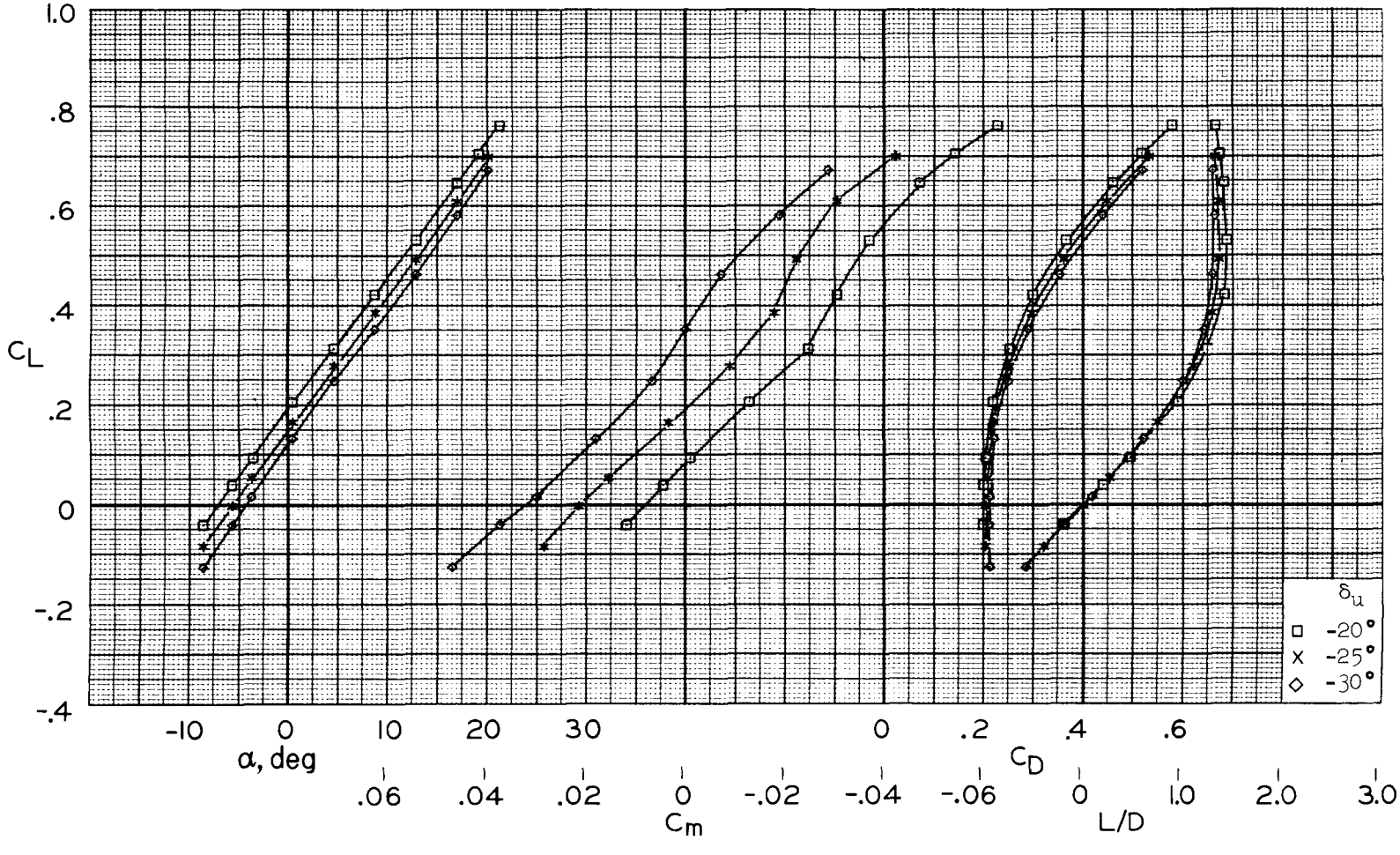

(h) M = 1.1, R = 4.1×10^6

Figure 10.- Continued.

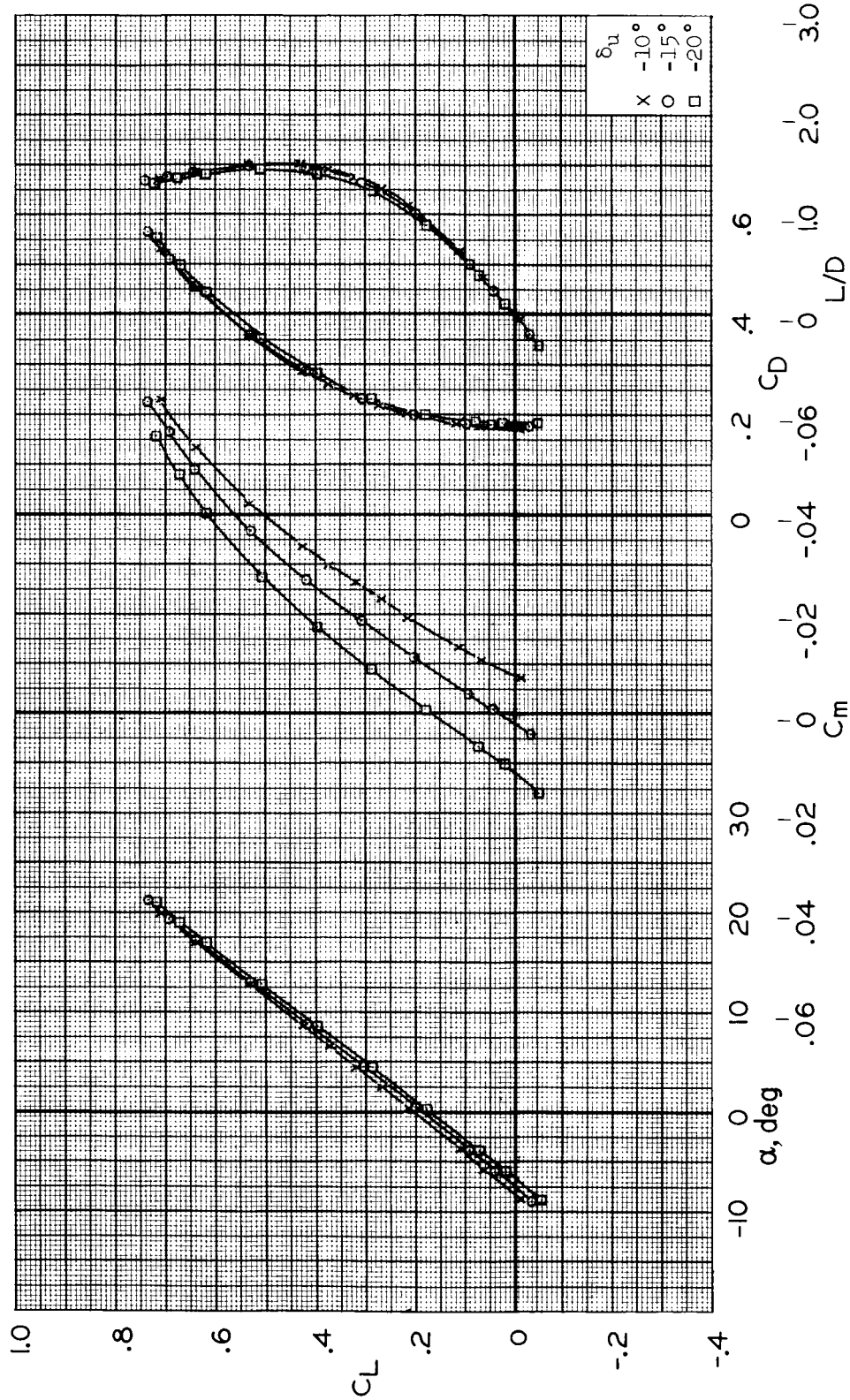

(i) M = 1.3, R = 4.1×10^6

Figure 10.- Continued.

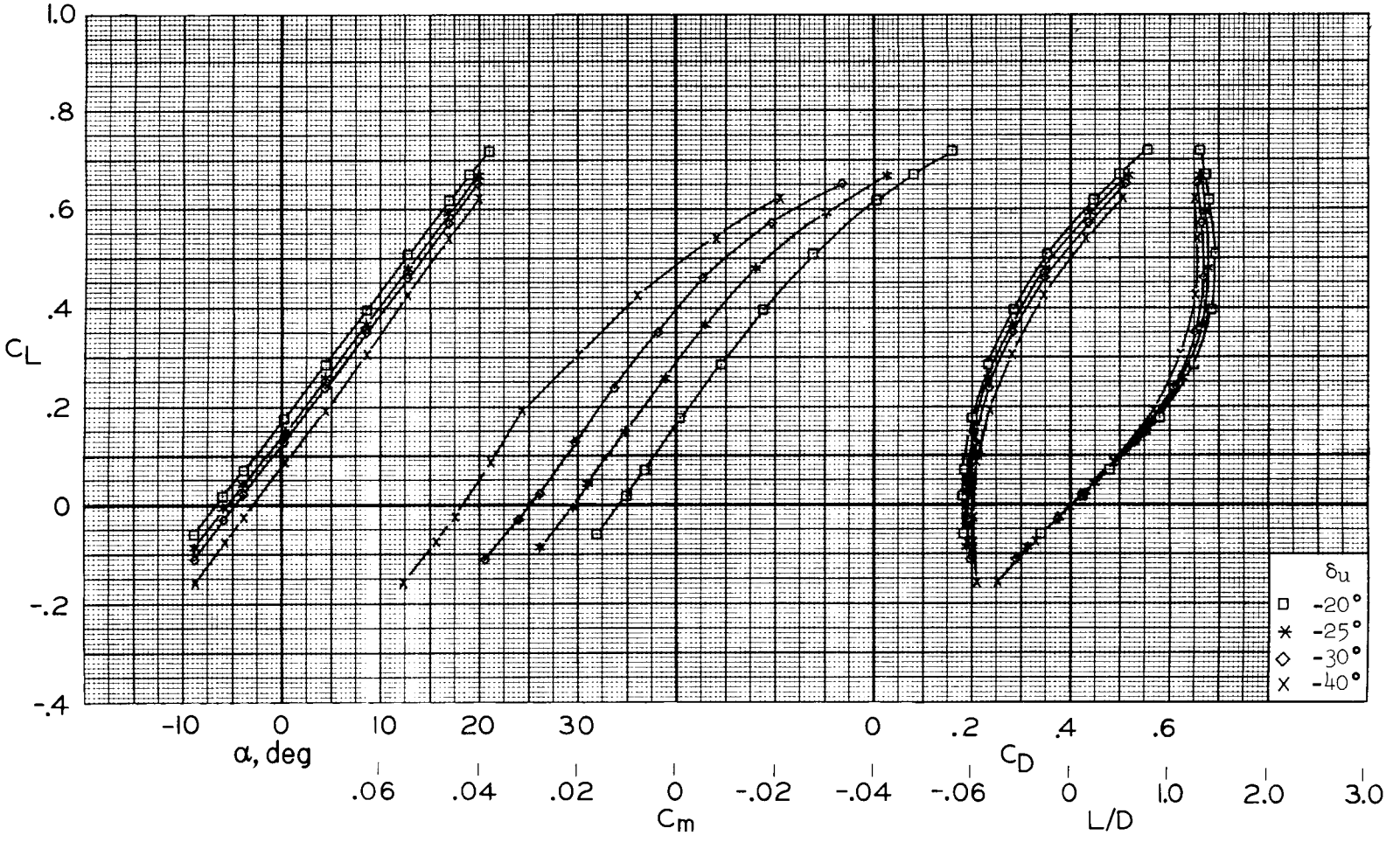

(j) M = 1.3, R = 4.1×10^6

Figure 10.- Continued.

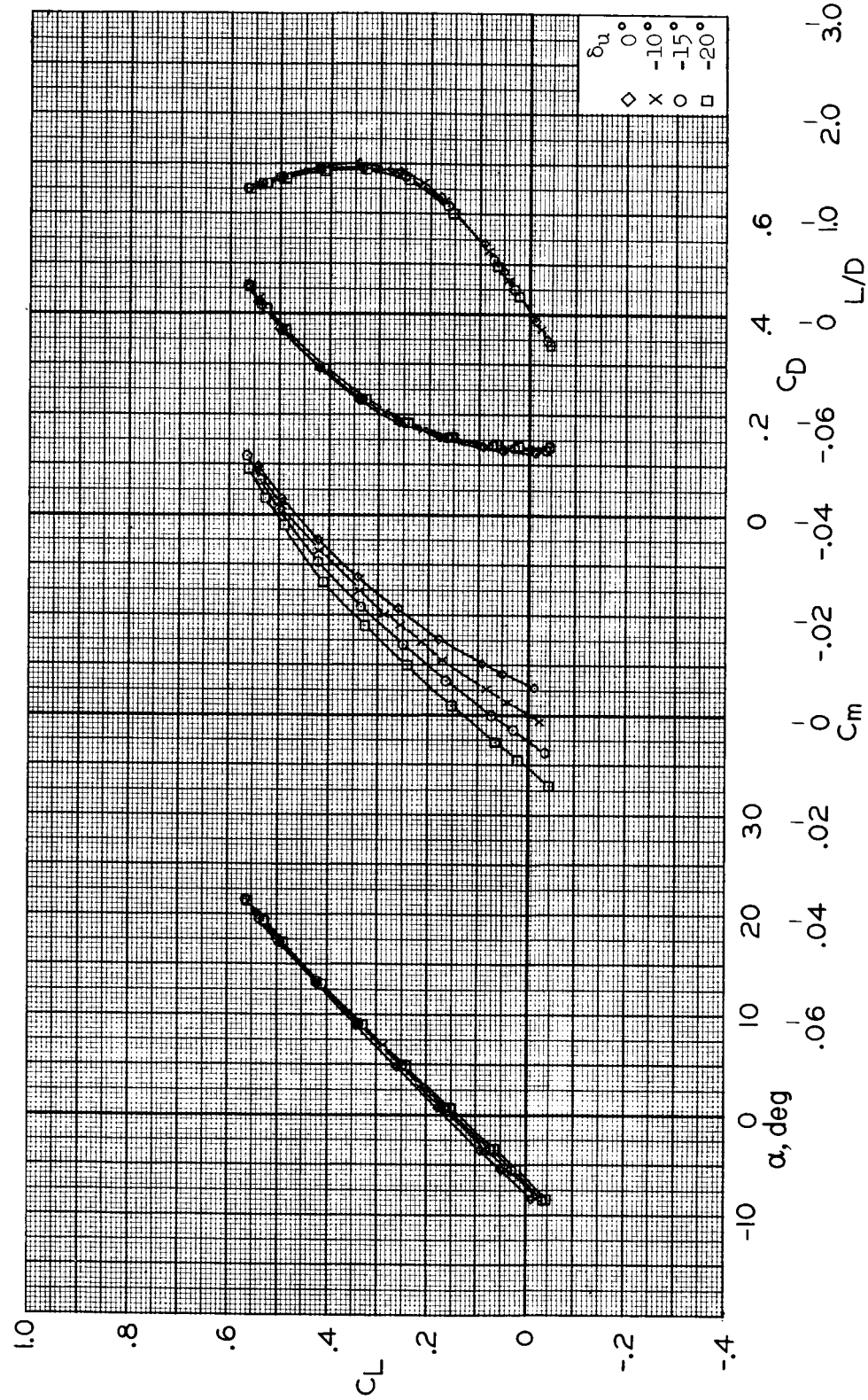

(k) M = 2.0, R = 4.1×10^6

Figure 10.- Continued.

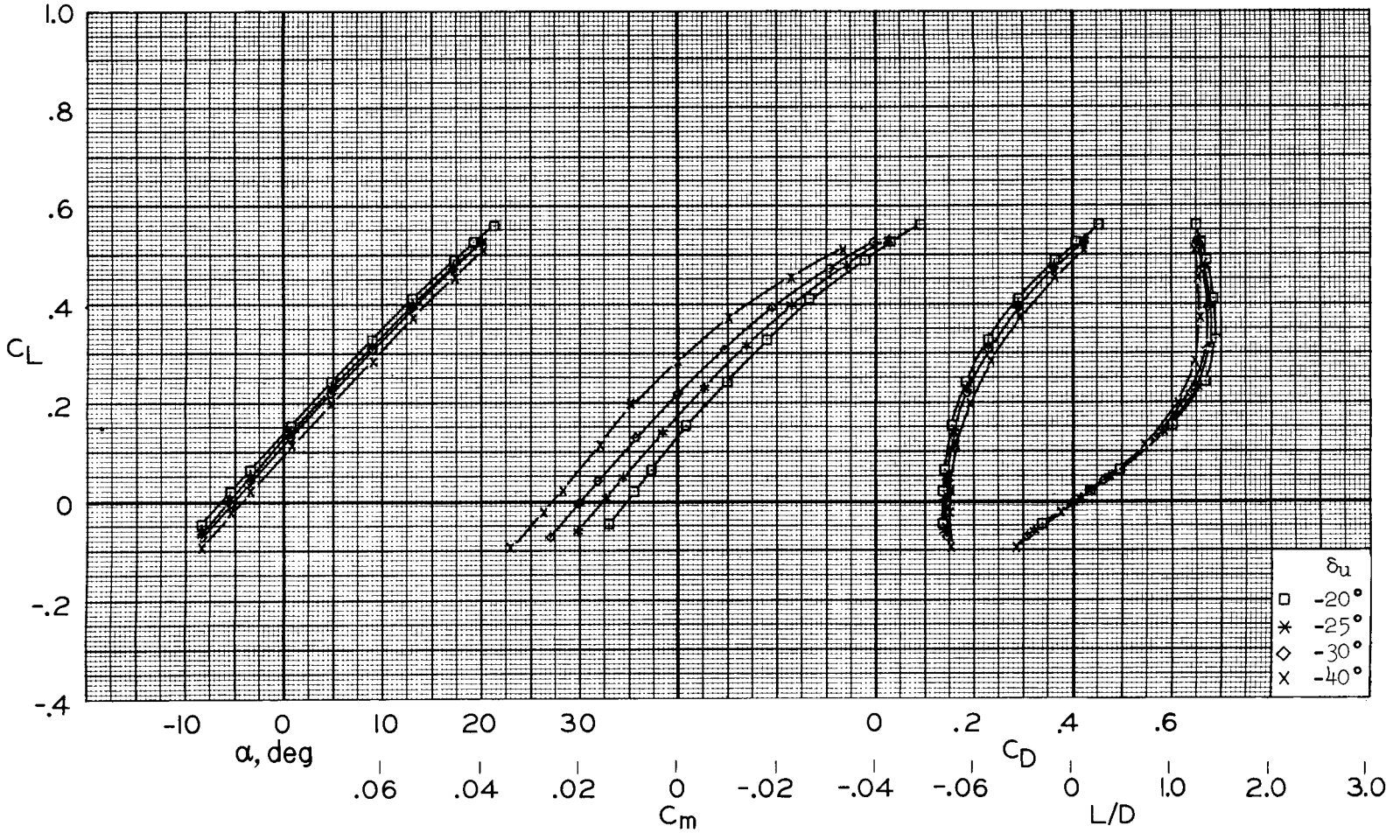

(1) M = 2.0, R = 4.1×10^6

Figure 10.- Concluded.

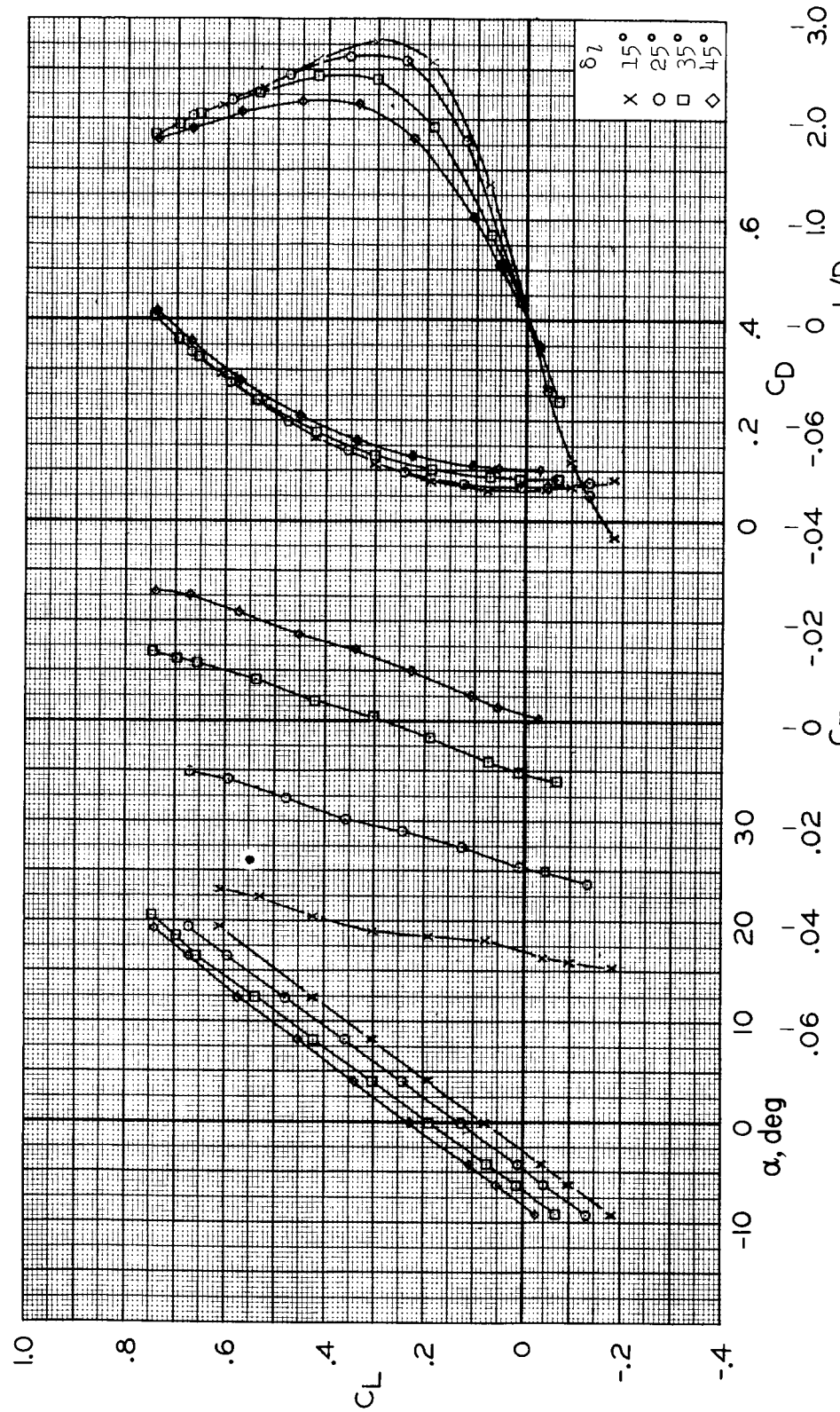

(a) M = 0.6, R = 5.7×10⁶

Figure 11.- Longitudinal characteristics at selected lower flap deflections; δ_u = -20°, δ_{rf} = 0°.

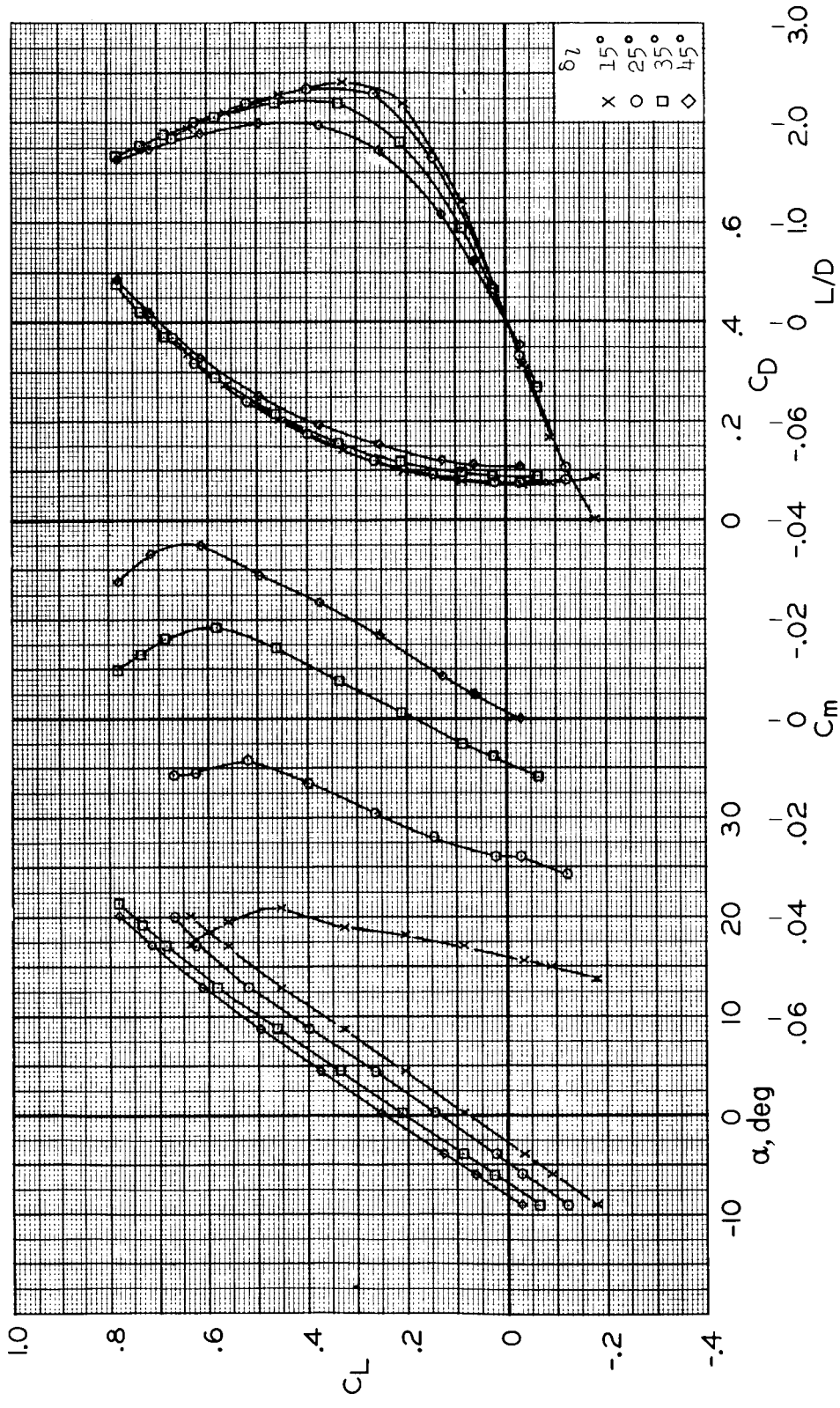

(b) M = 0.8, R = 6.4×10^6

Figure 11.- Continued.

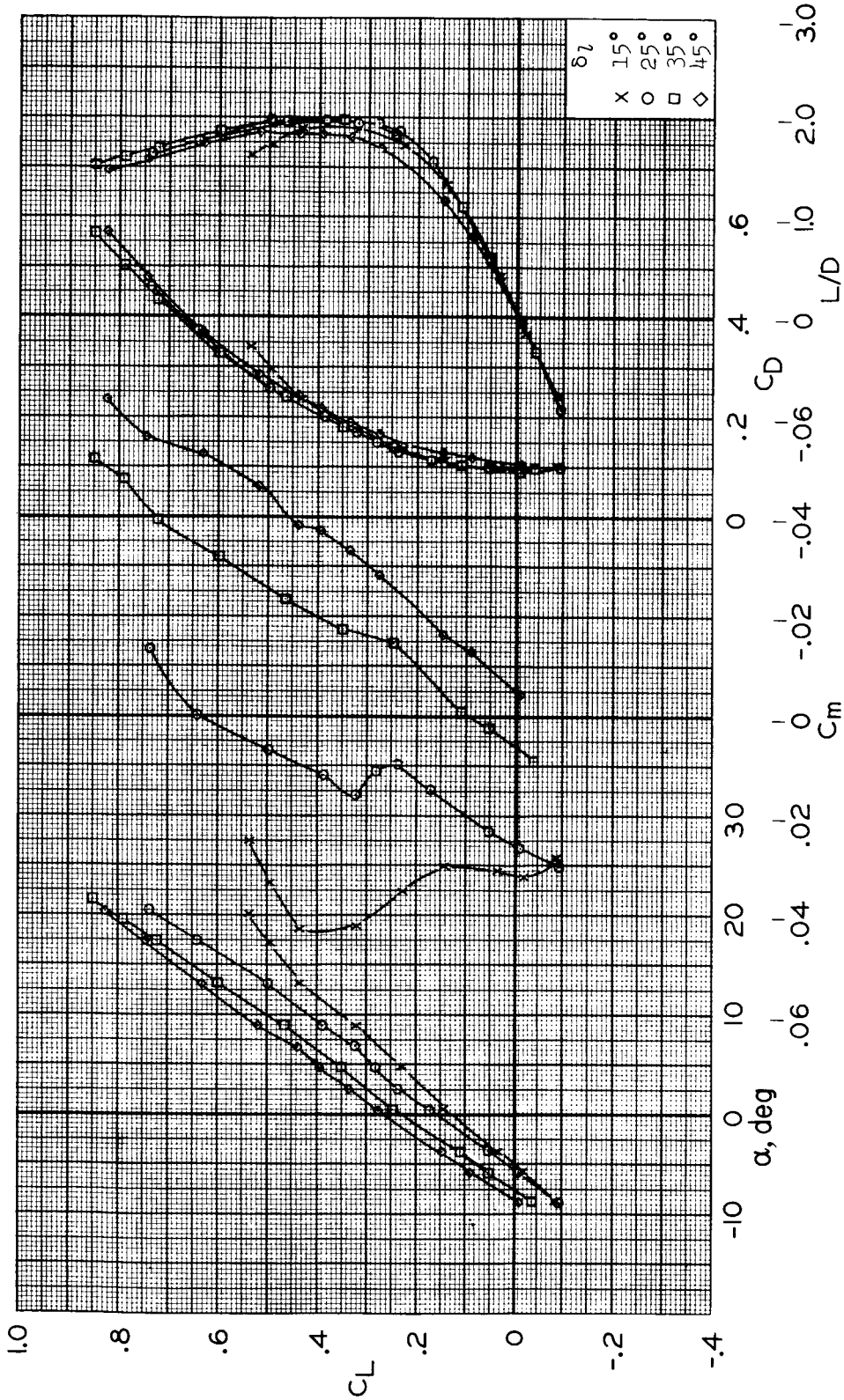

(c) M = 0.9, R = 6.4×10^6

Figure 11.- Continued.

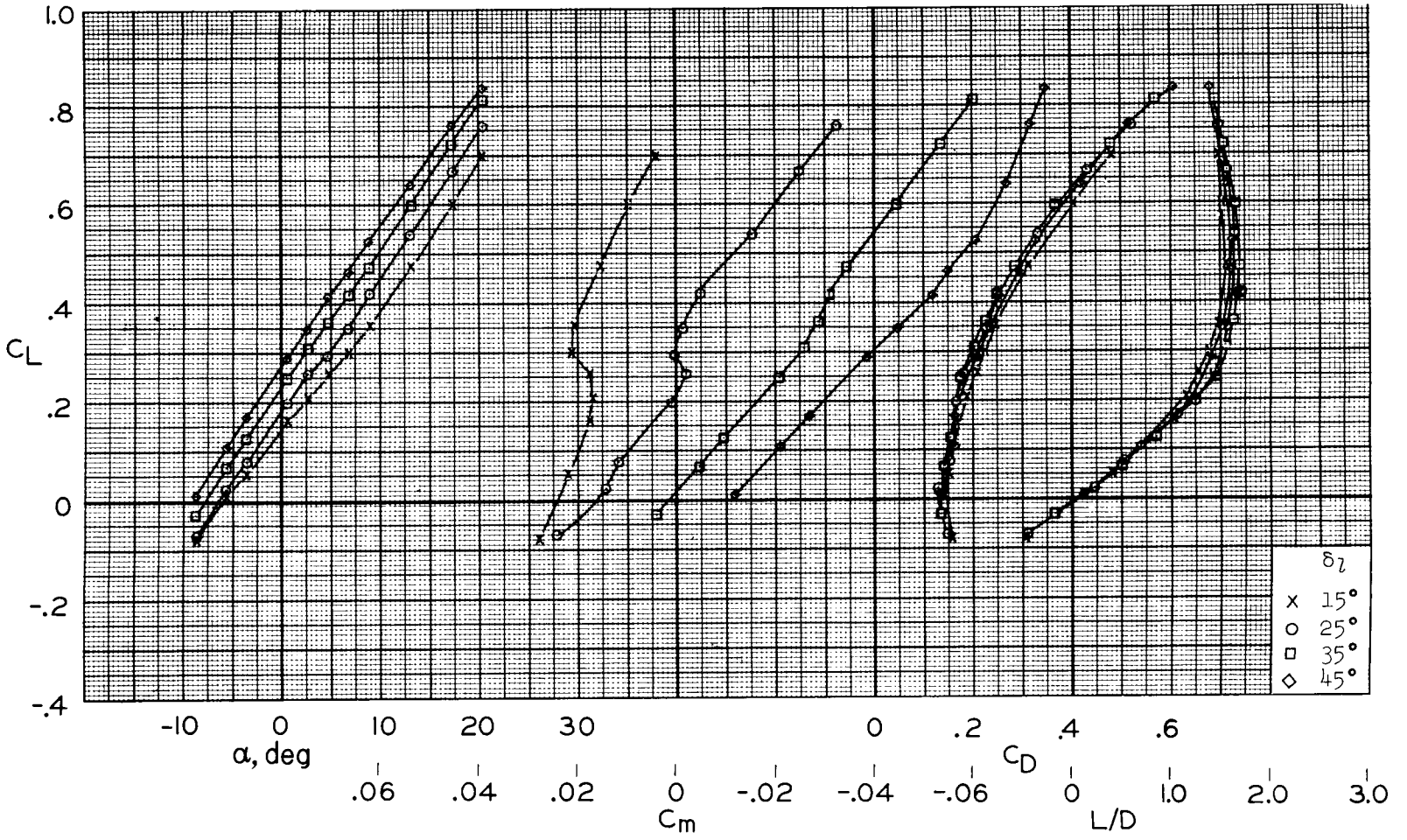

(d) M = 0.95, R = 5.6×10^6

Figure 11.- Continued.

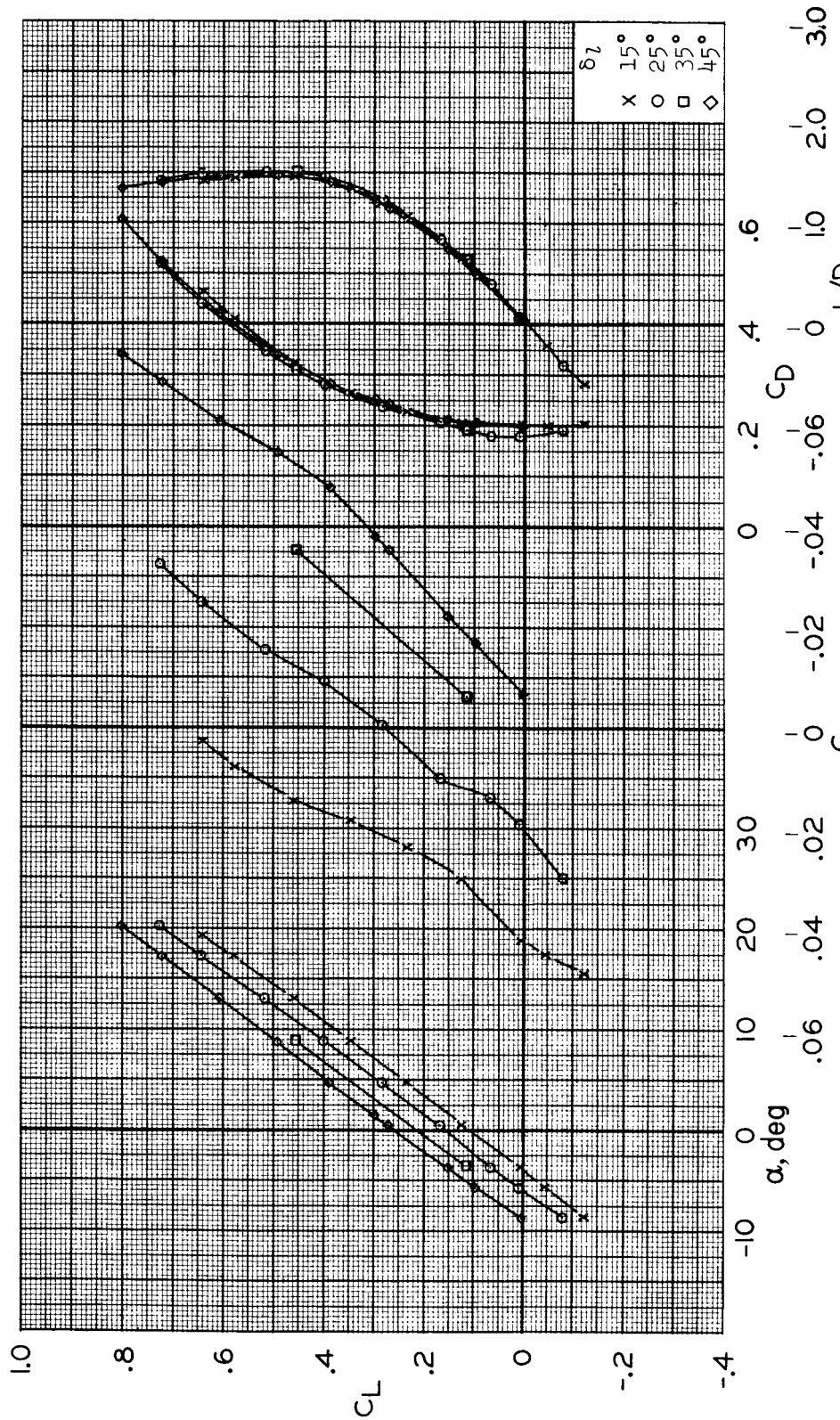

(e) M = 1.0, R = 4.8×10^6

Figure 11.- Continued.

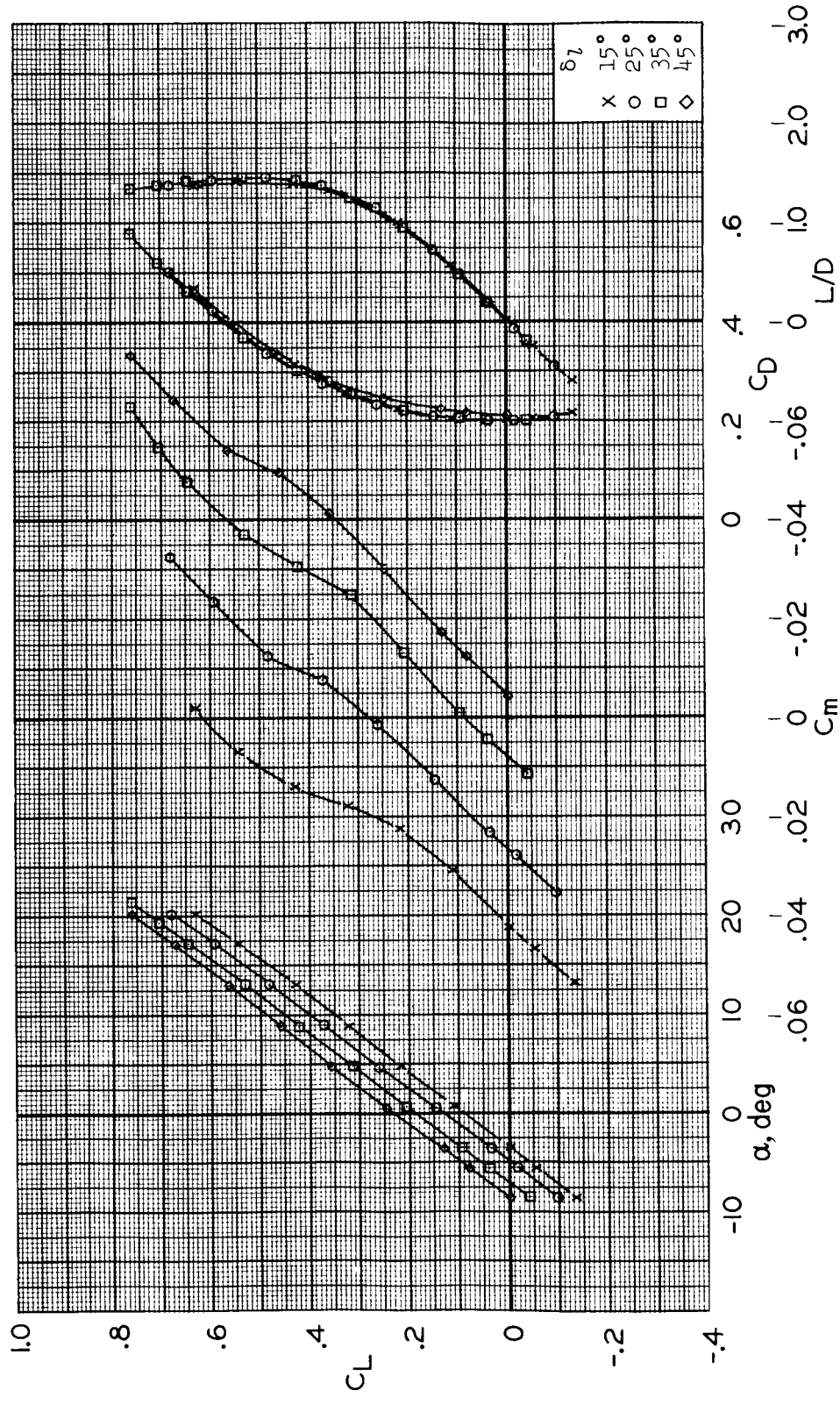

(f) M = 1.1, R = 4.1×10^6

Figure 11.- Continued.

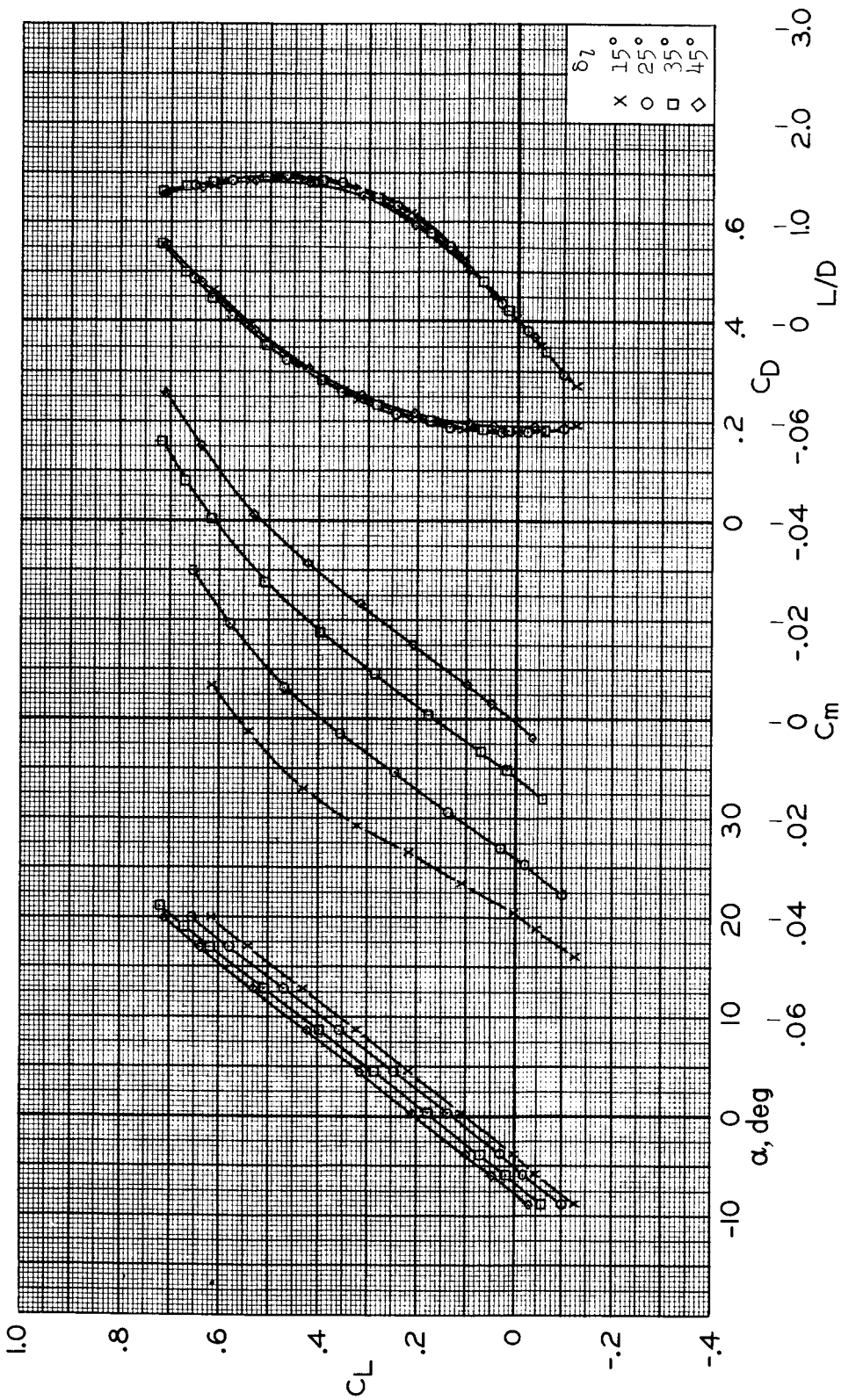

(g) M = 1.3, R = 4.1×10^6

Figure 11.- Continued.

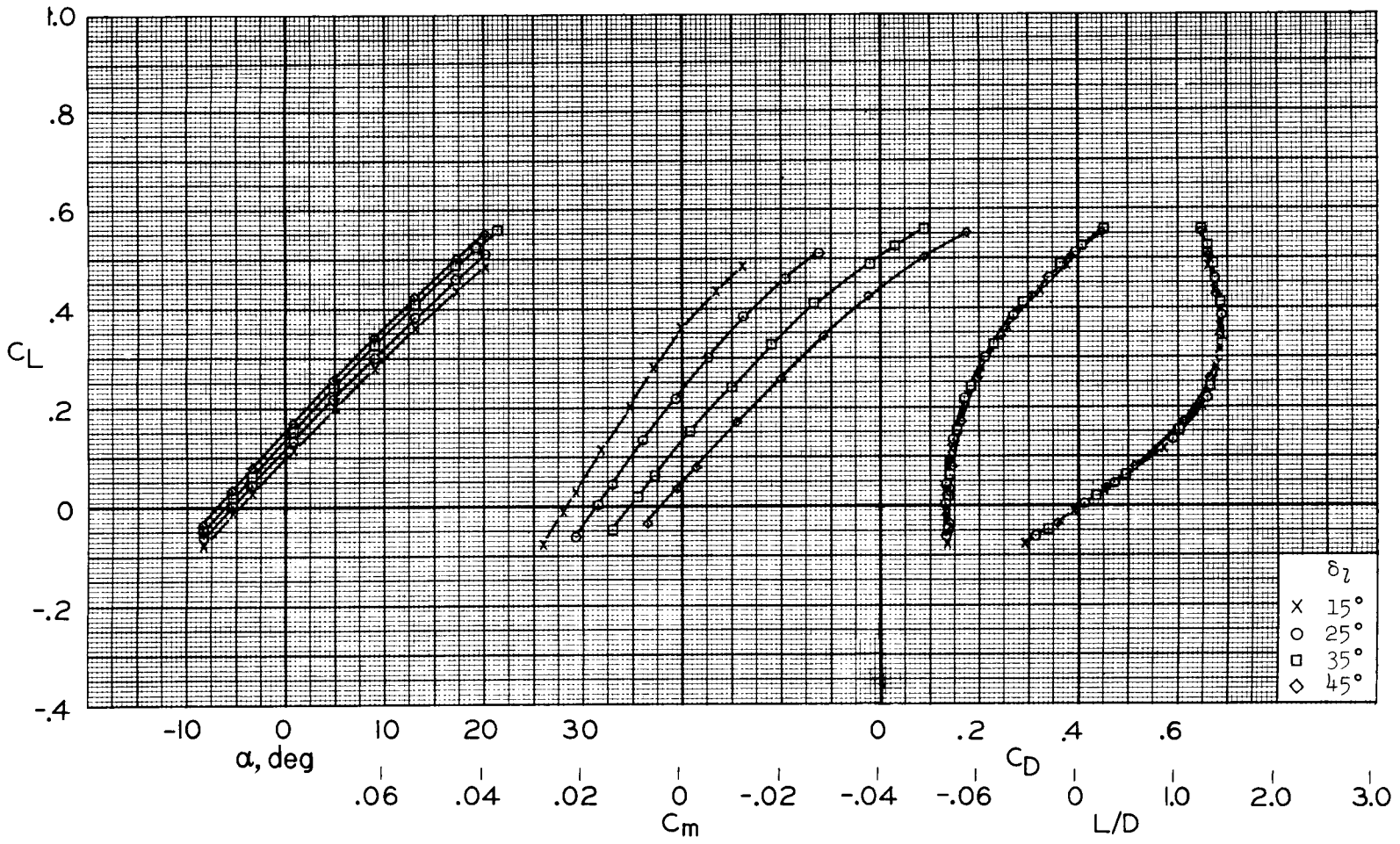

(h) M = 2.0, R = 4.1×10^6

Figure 11.- Concluded.

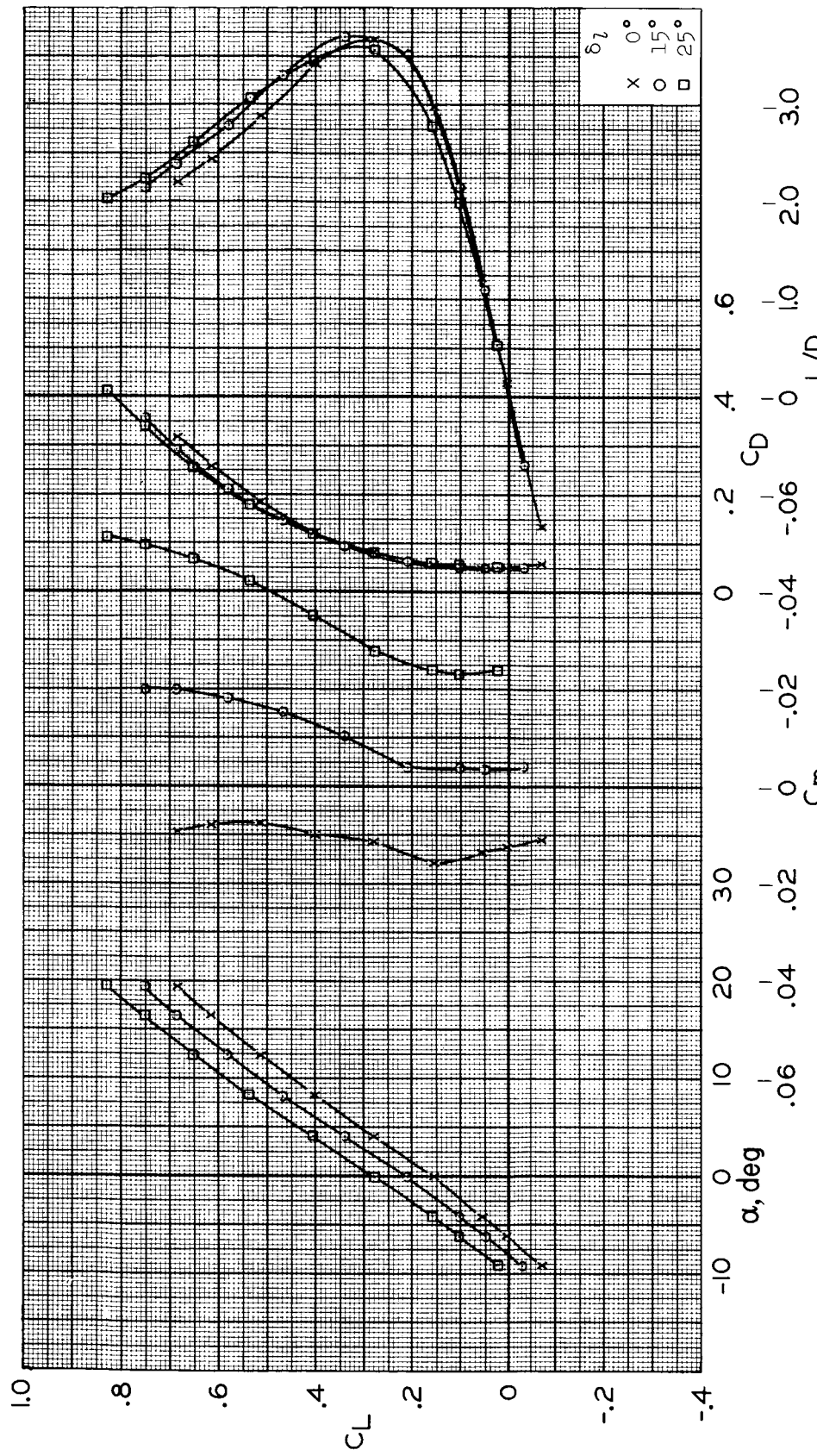

(a) M = 0.6, R = 5.7X10^6

Figure 12.- Longitudinal characteristics at selected lower flap deflections; δ_u = 0°, δ_{rf} = 0°.

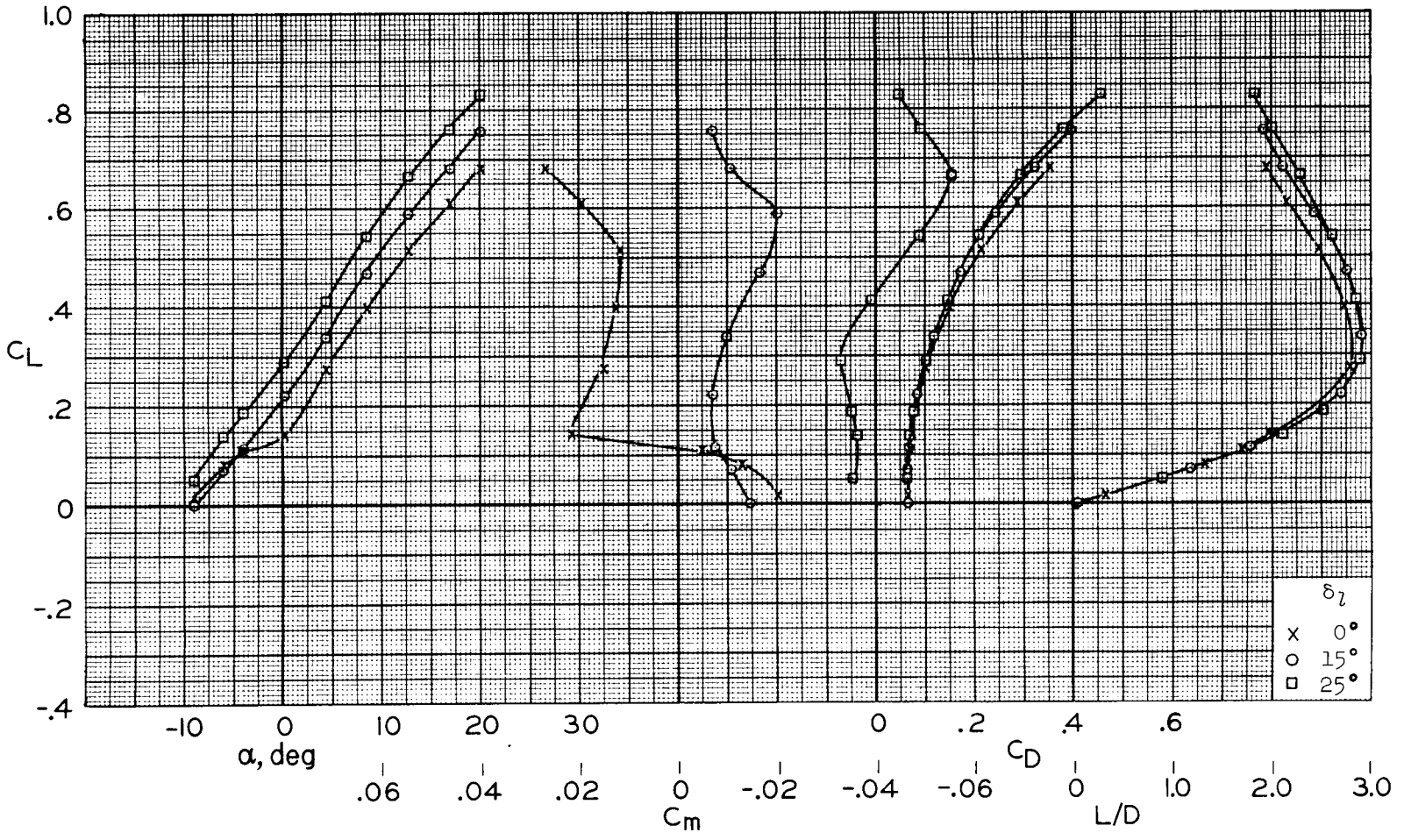

(b) M = 0.8, R = 6.4×10^6

Figure 12.- Continued.

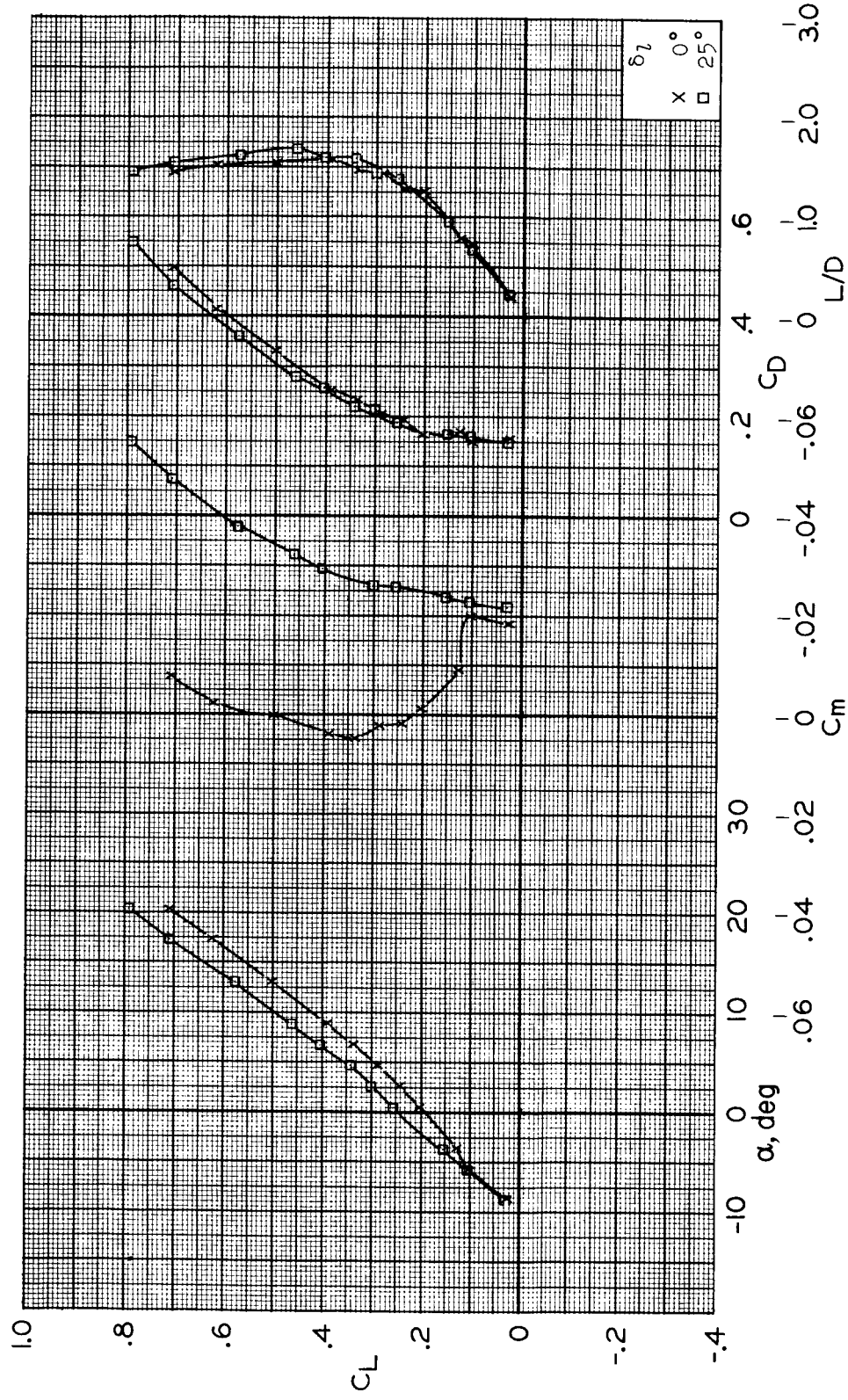

(c) M = 0.95, R = 5.6×10^6

Figure 12.- Continued.

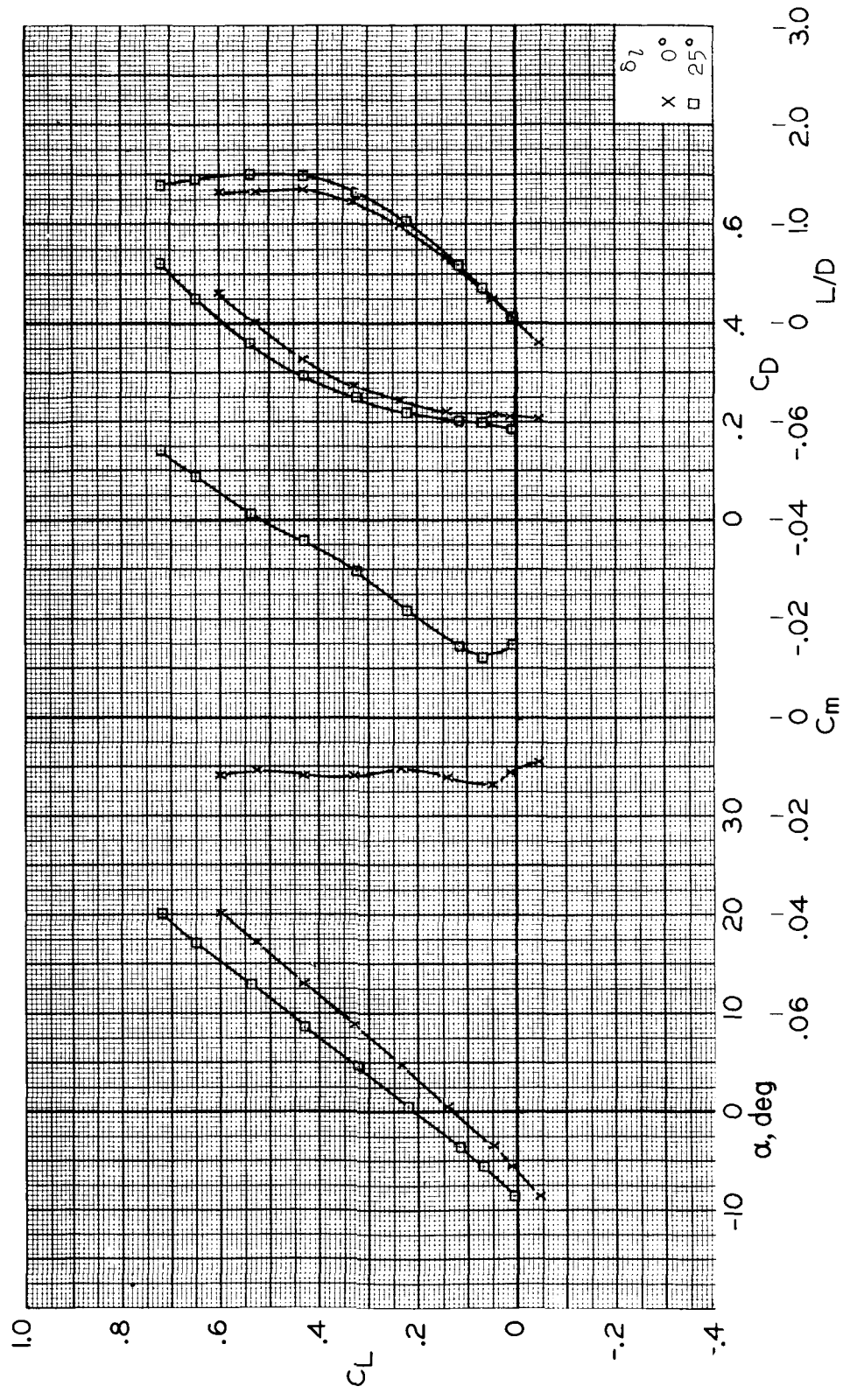

(d) M = 1.1, R = 4.1×10^6

Figure 12.- Continued.

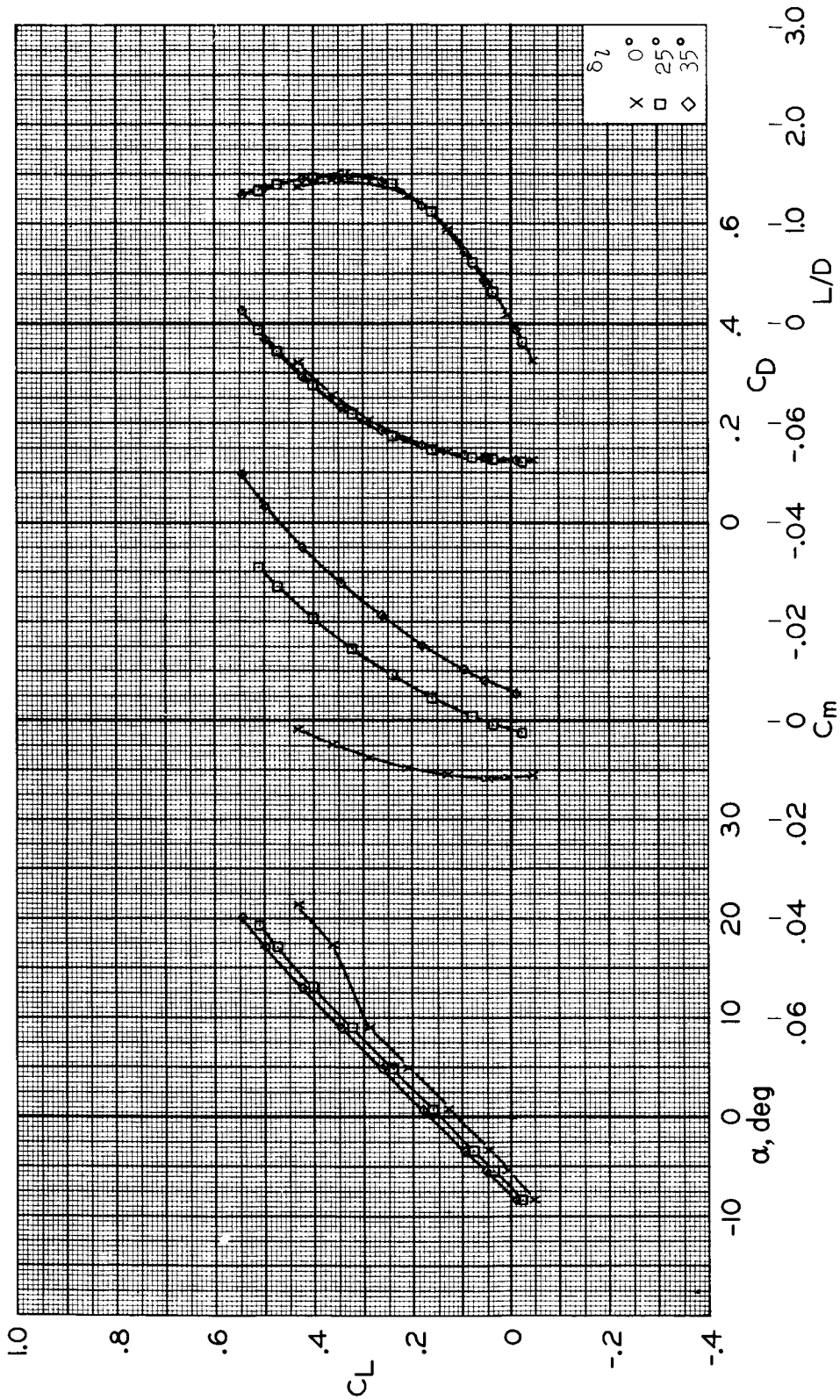

(e) M = 2.0, R = 4.1×10^6

Figure 12.- Concluded.

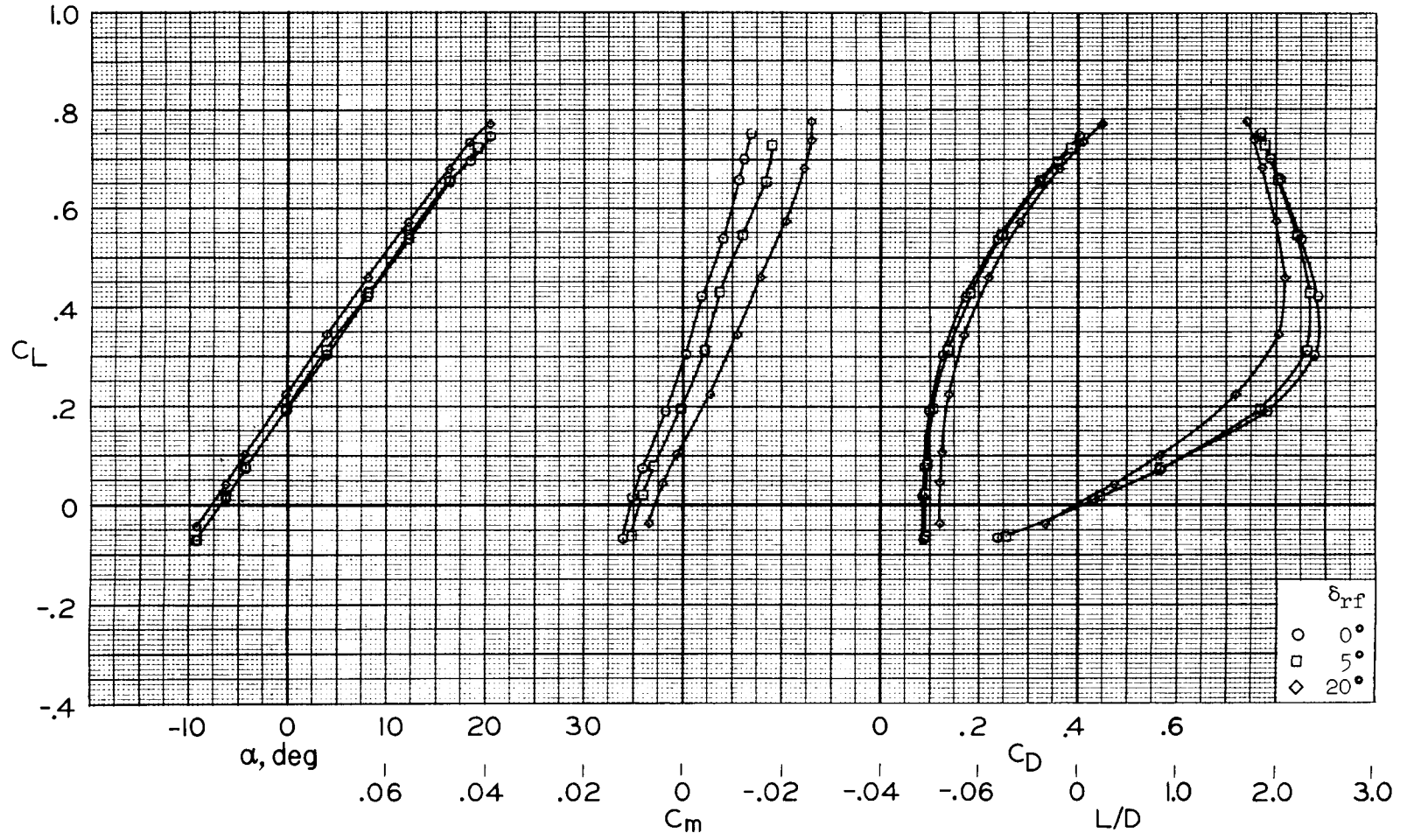

(a) M = 0.6, R = 5.7×10^6

Figure 13.- Effect of rudder flare deflection on longitudinal characteristics; $\delta_u = -20°$, $\delta_l = 35°$.

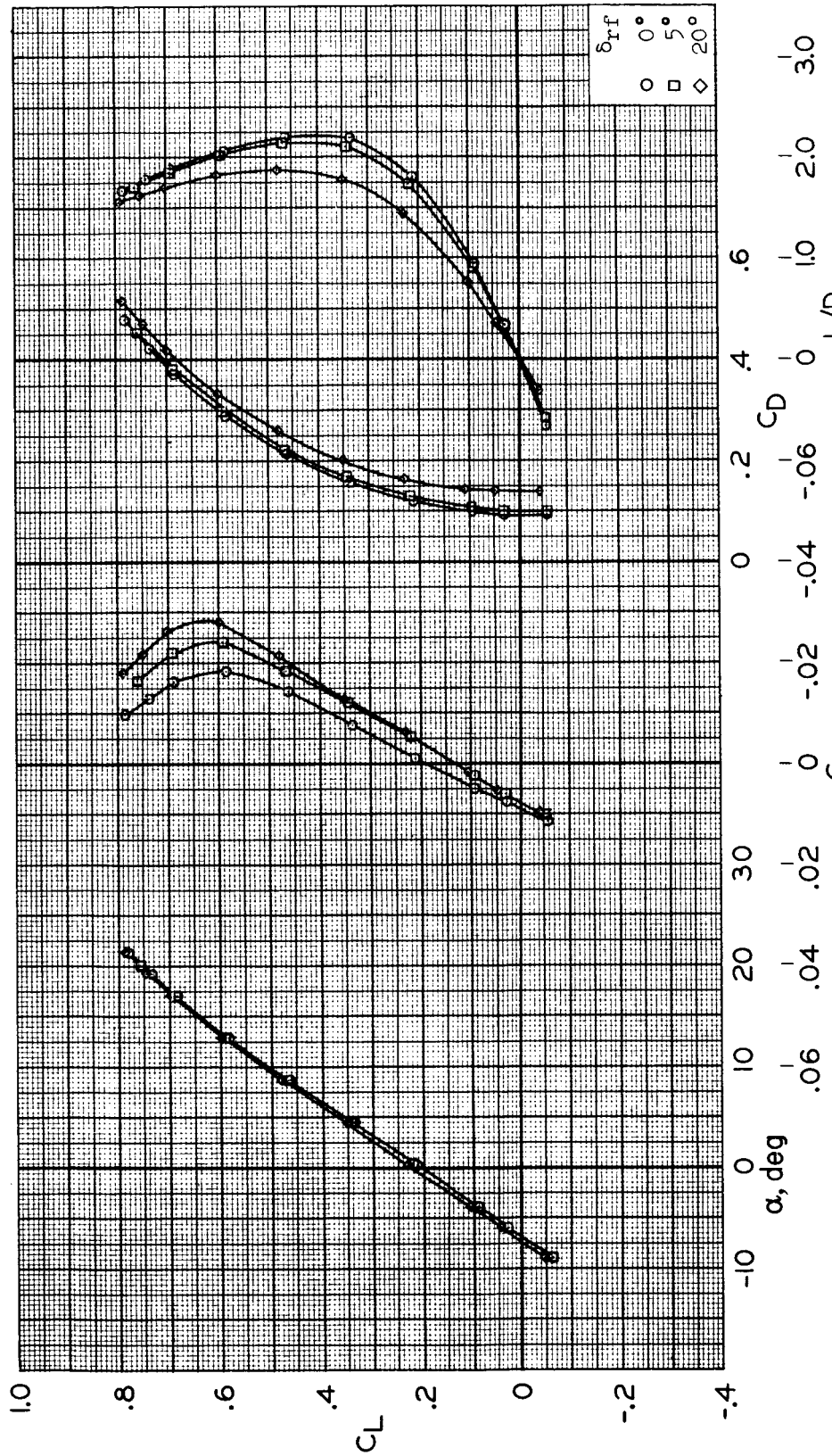

(b) M = 0.8, R = 6.4×10^6

Figure 13.- Continued.

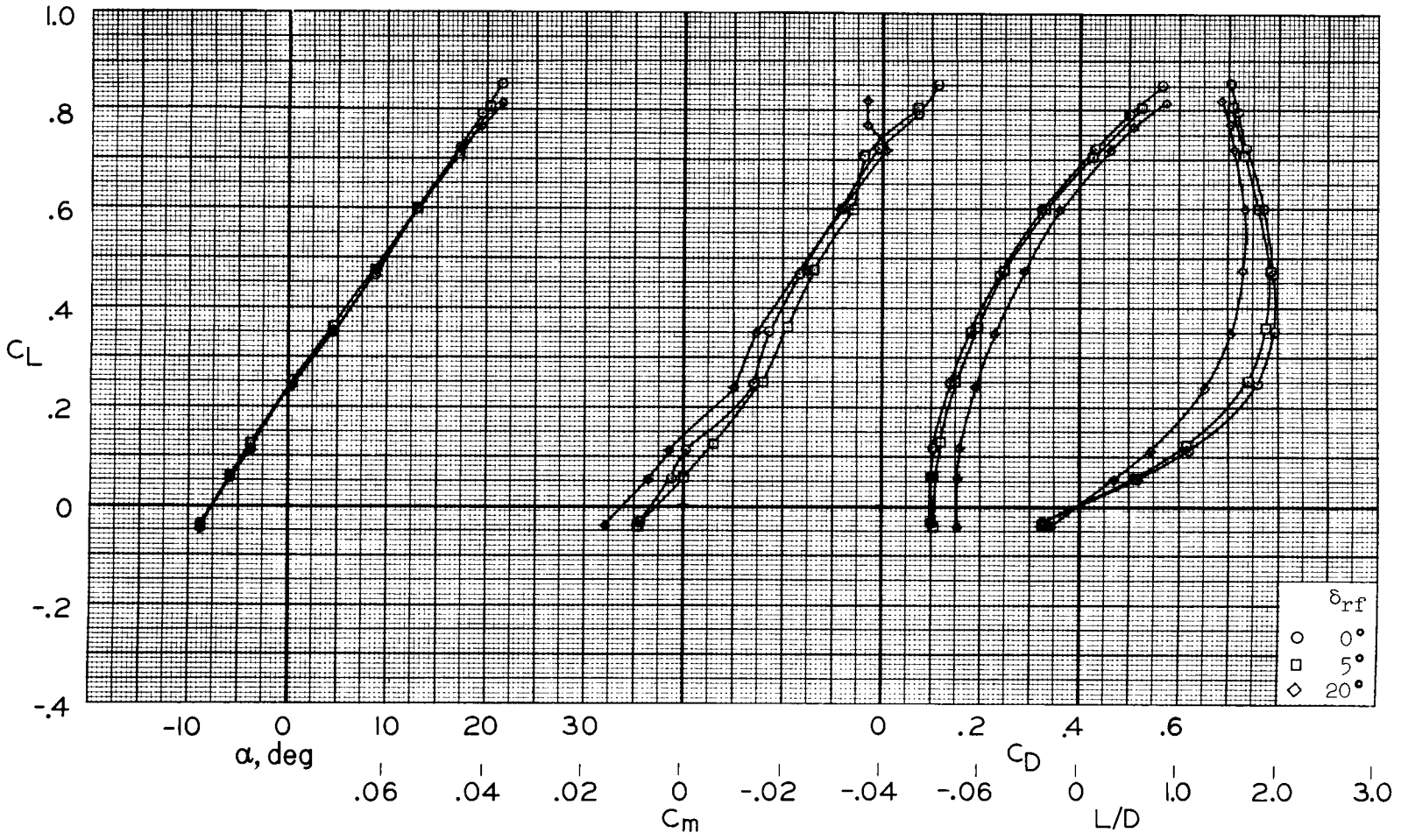

(c) M = 0.9, R = 6.4×10^6

Figure 13.- Continued.

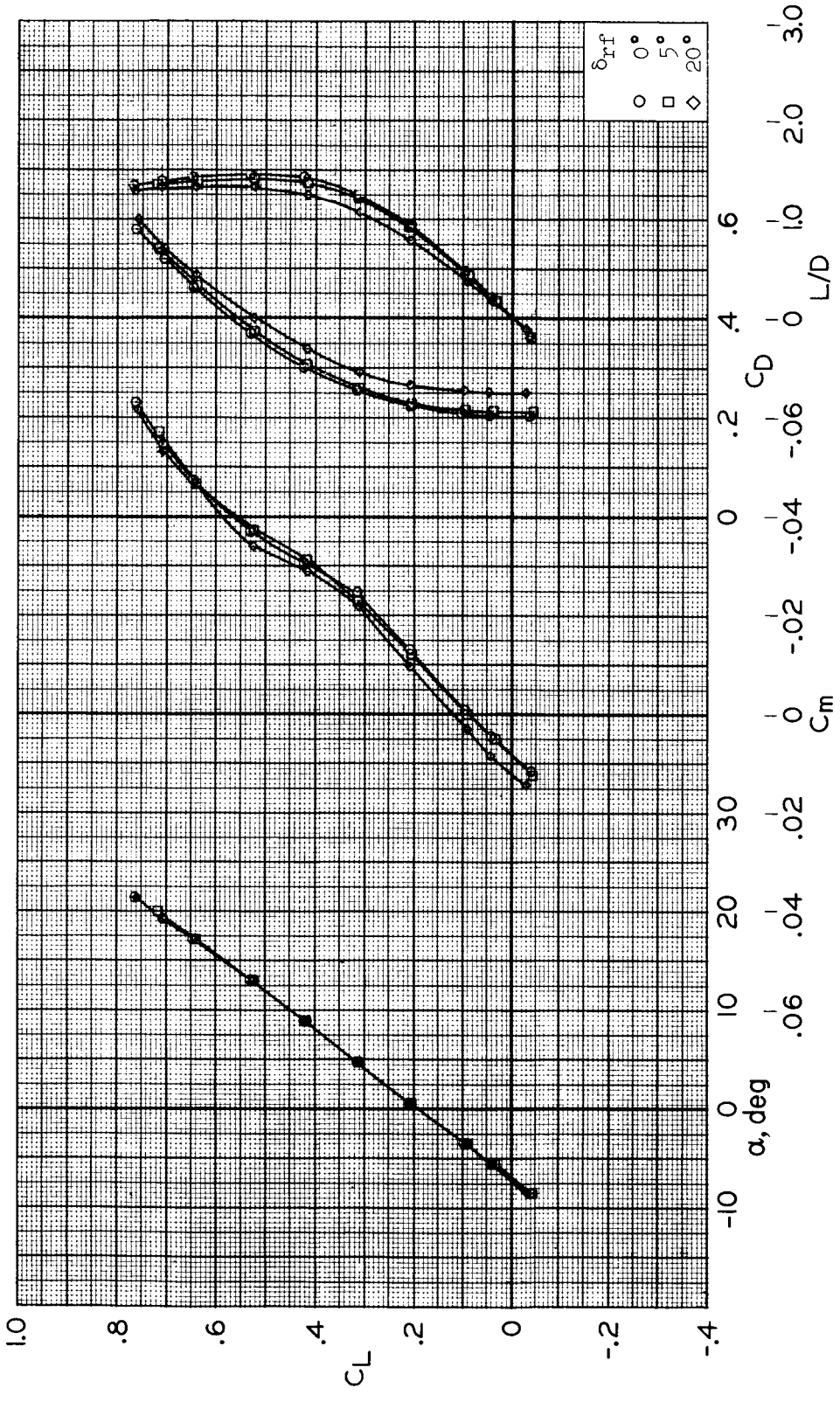

(d) M = 1.1, R = 4.1×10^6

Figure 13.- Continued.

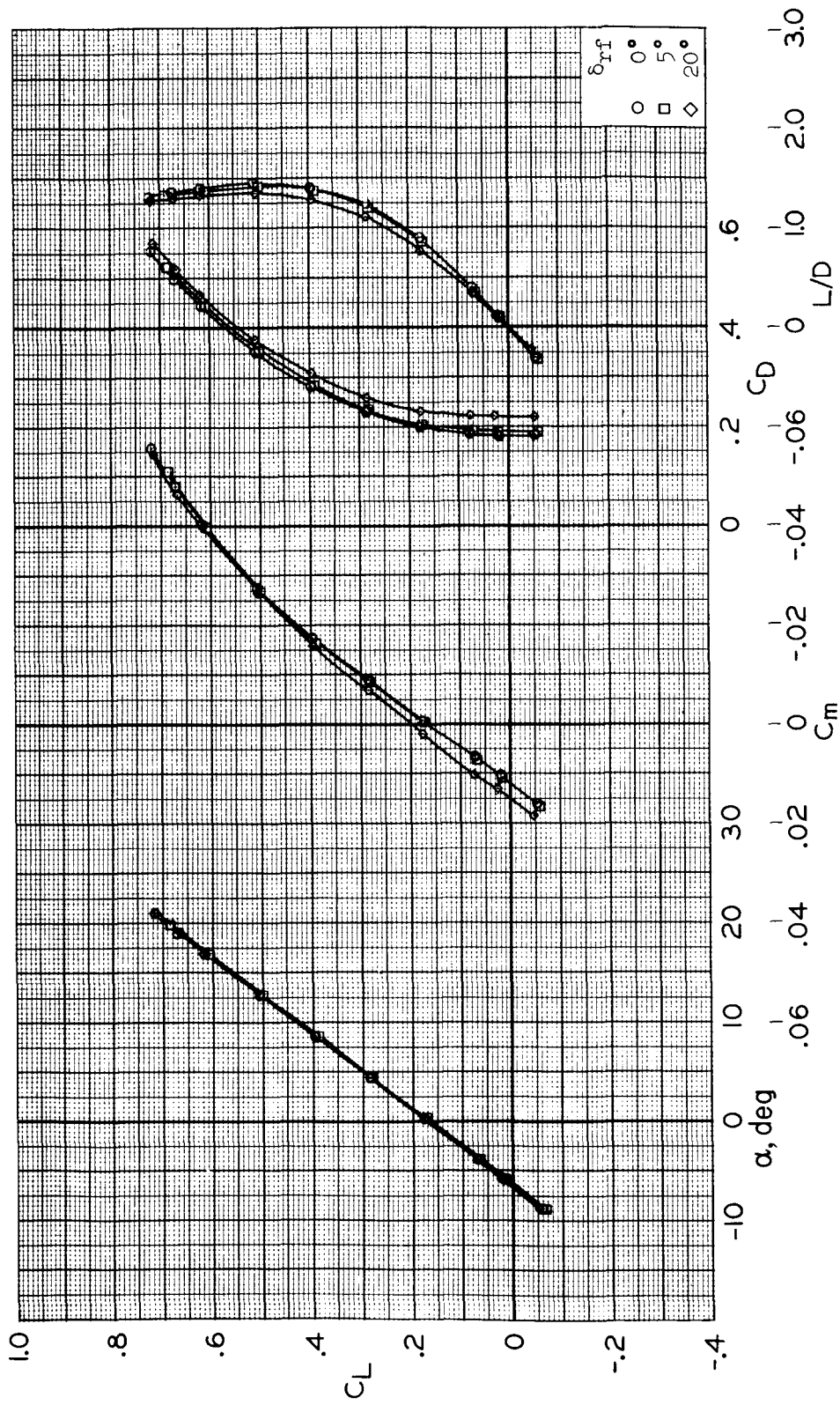

(e) M = 1.3, R = 4.1×10^6

Figure 13.- Continued.

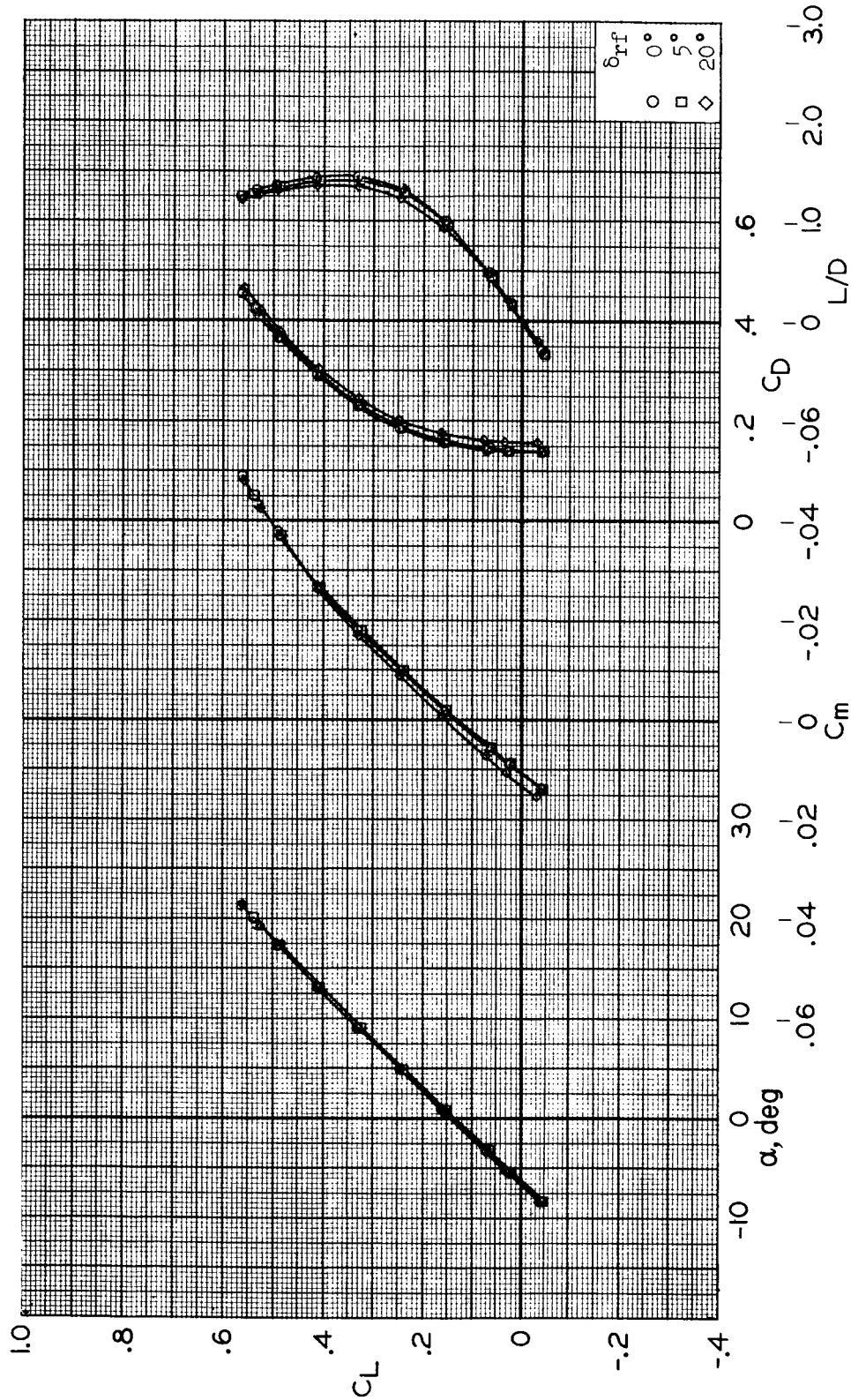

(f) M = 2.0, R = 4.1×10^6

Figure 13.- Concluded.

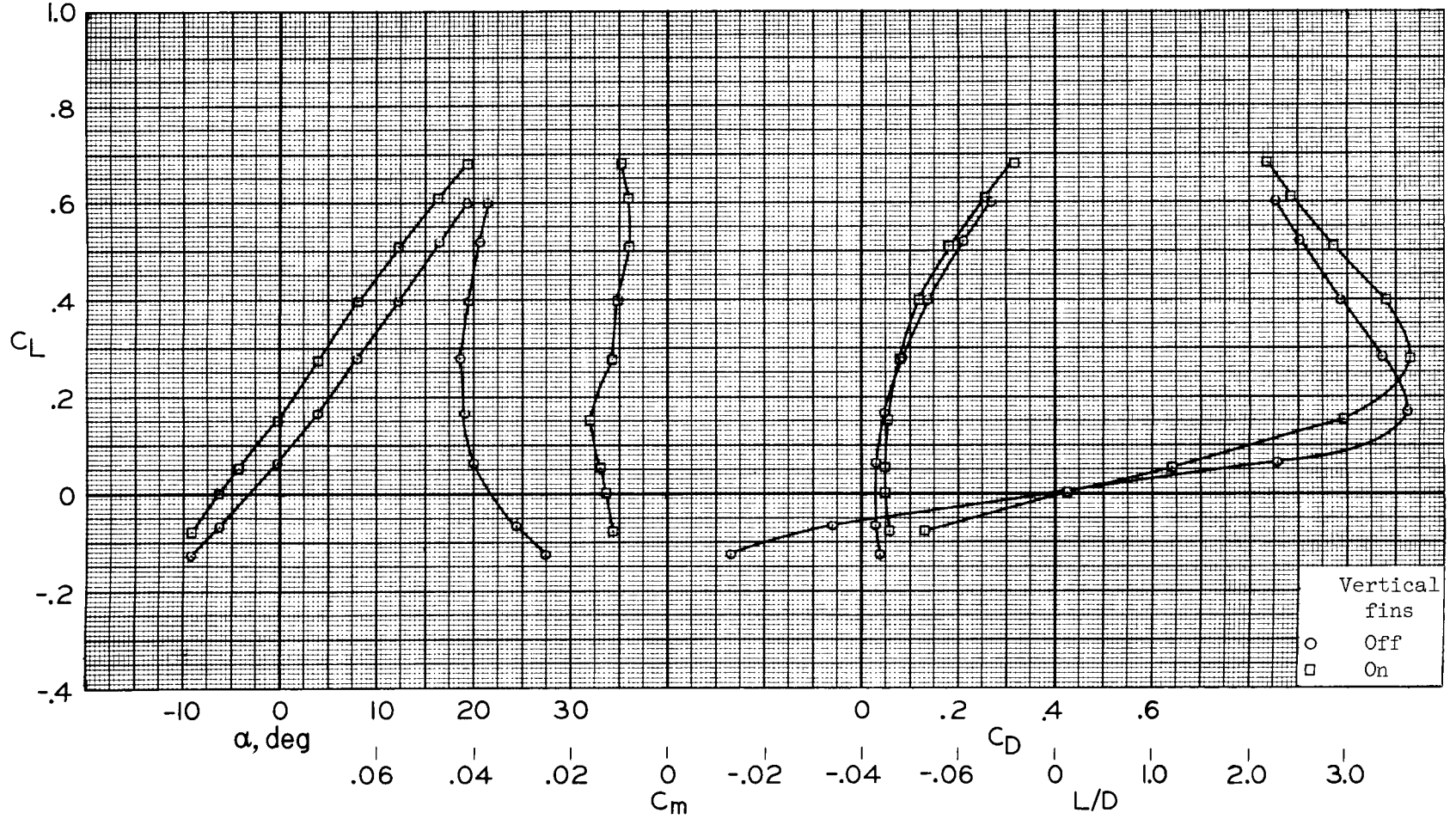

(a) M = 0.6, R = 5.7×10^6

Figure 14.- Effect of vertical fins on longitudinal characteristics; $\delta_u = 0°$, $\delta_l = 0°$.

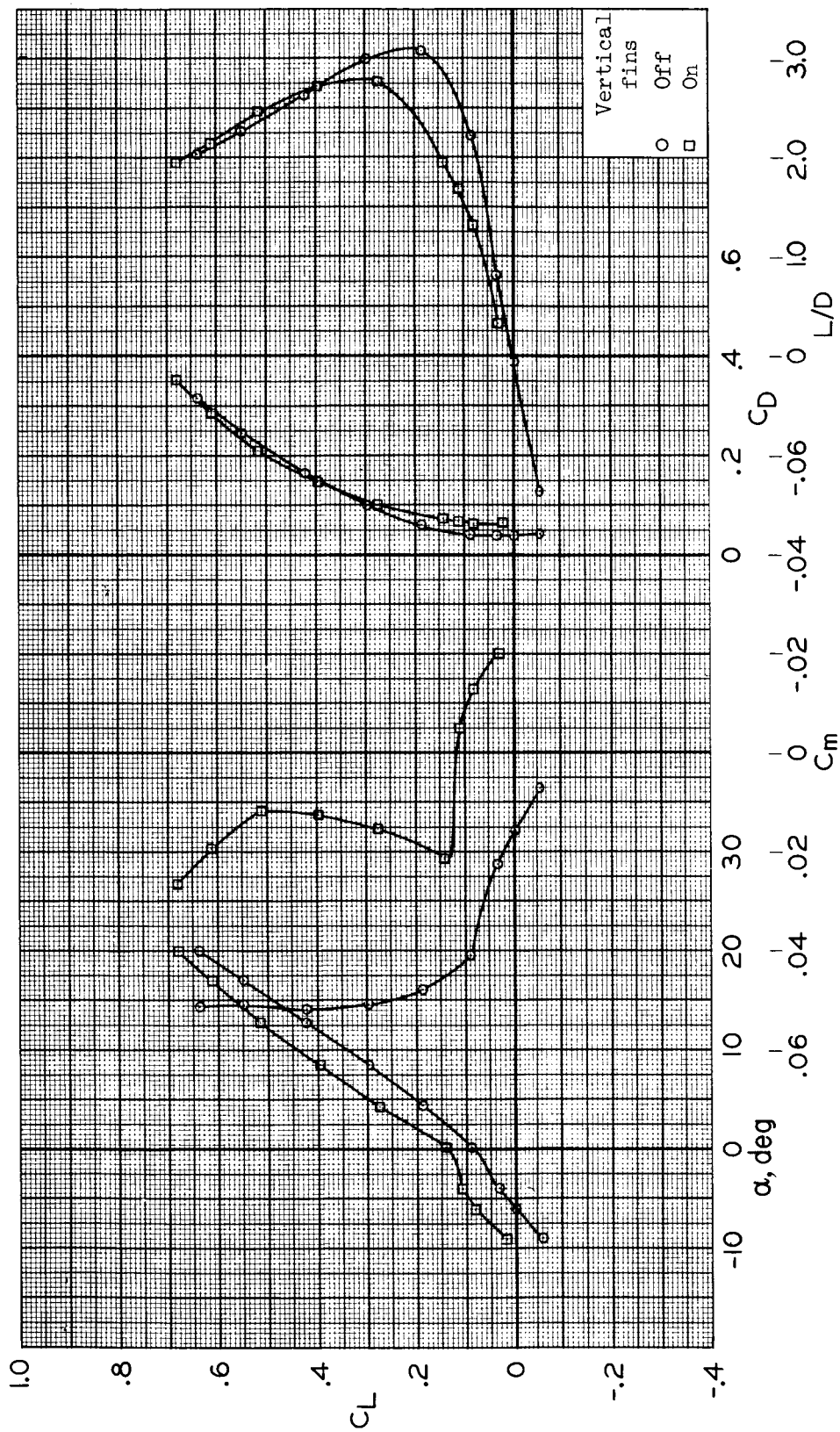

(b) M = 0.8, R = 6.4×10^6

Figure 14.- Continued.

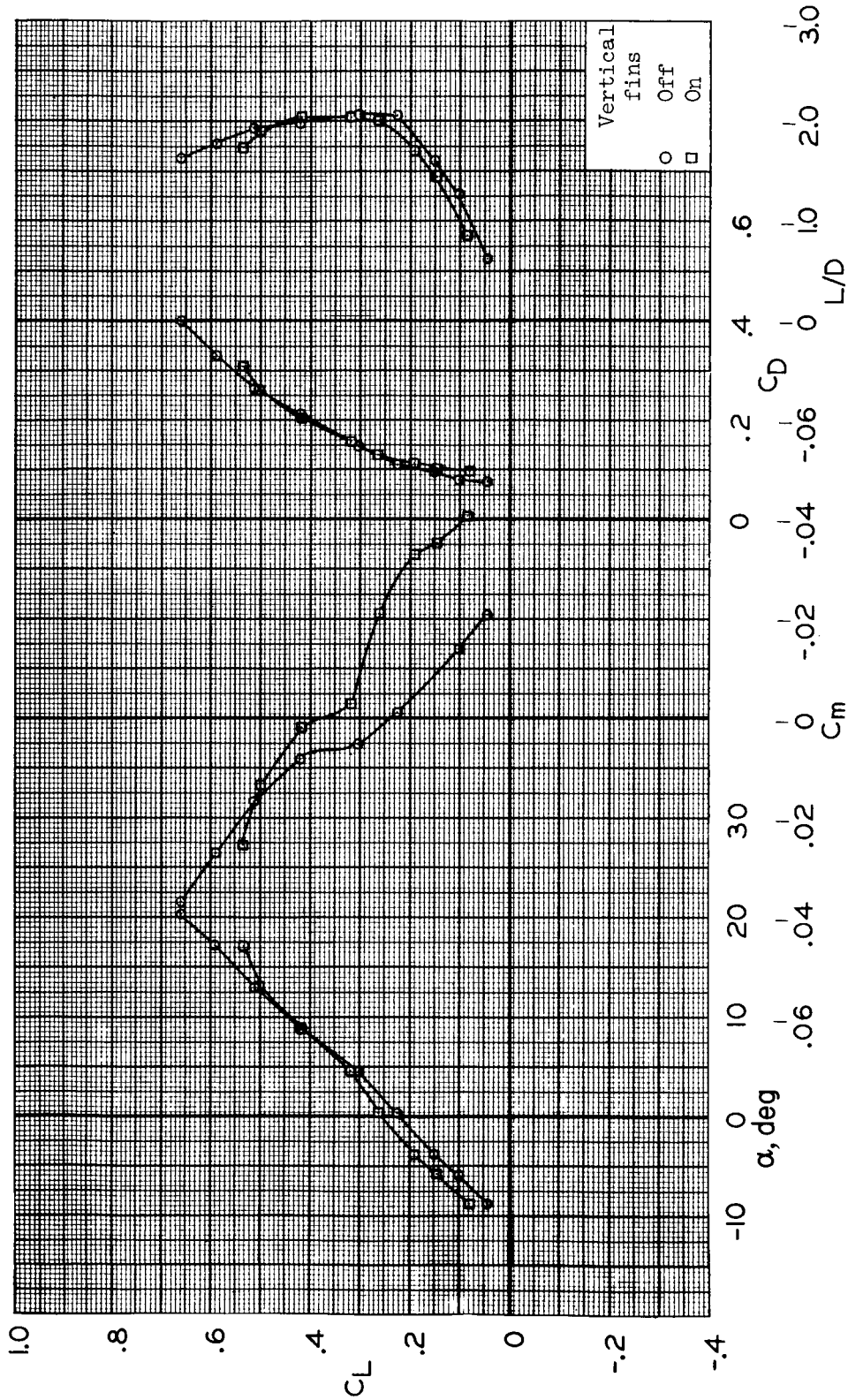

(c) M = 0.9, R = 6.4×10^6

Figure 14.- Continued.

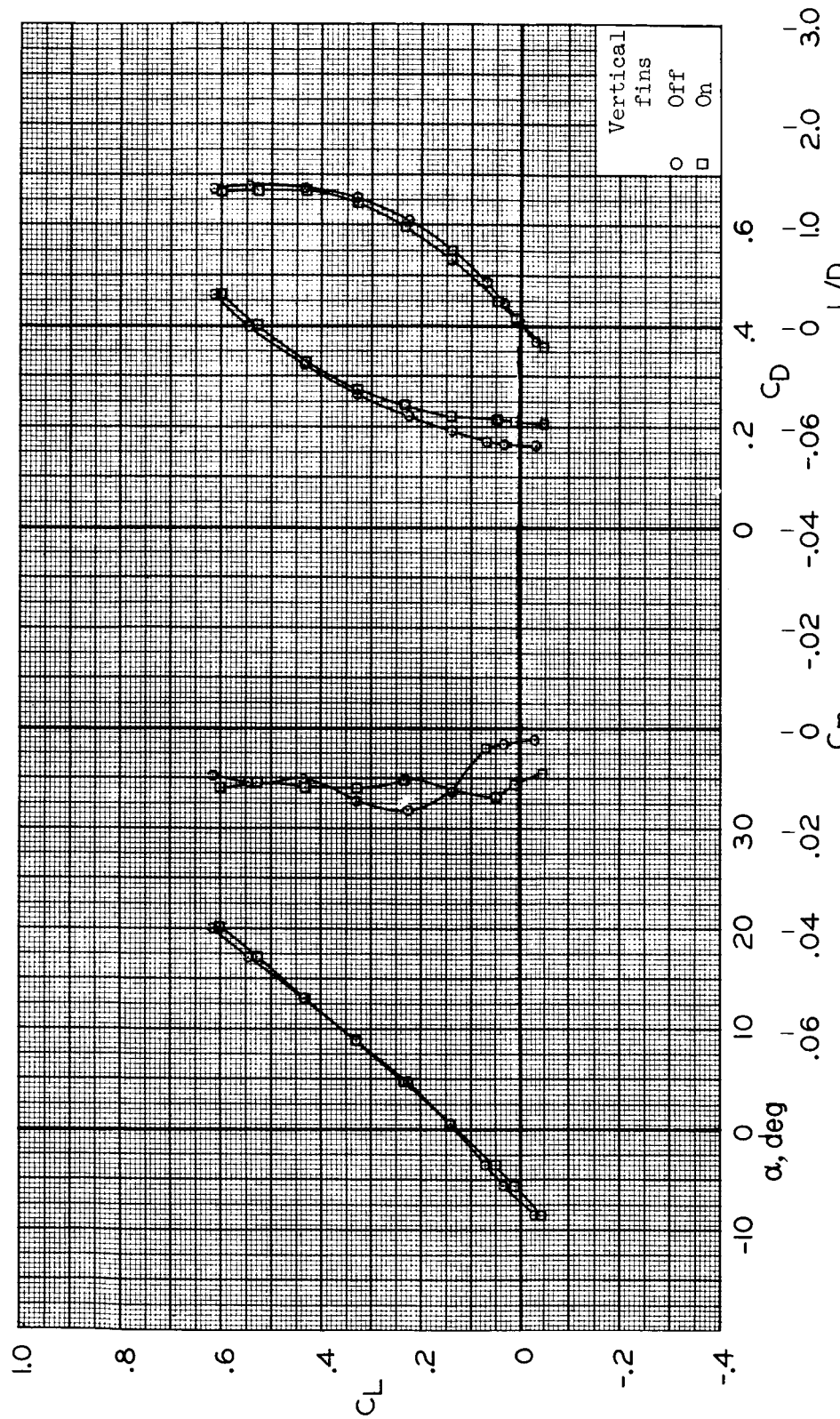

(d) M = 1.1, R = 4.1×10^6

Figure 14.- Continued.

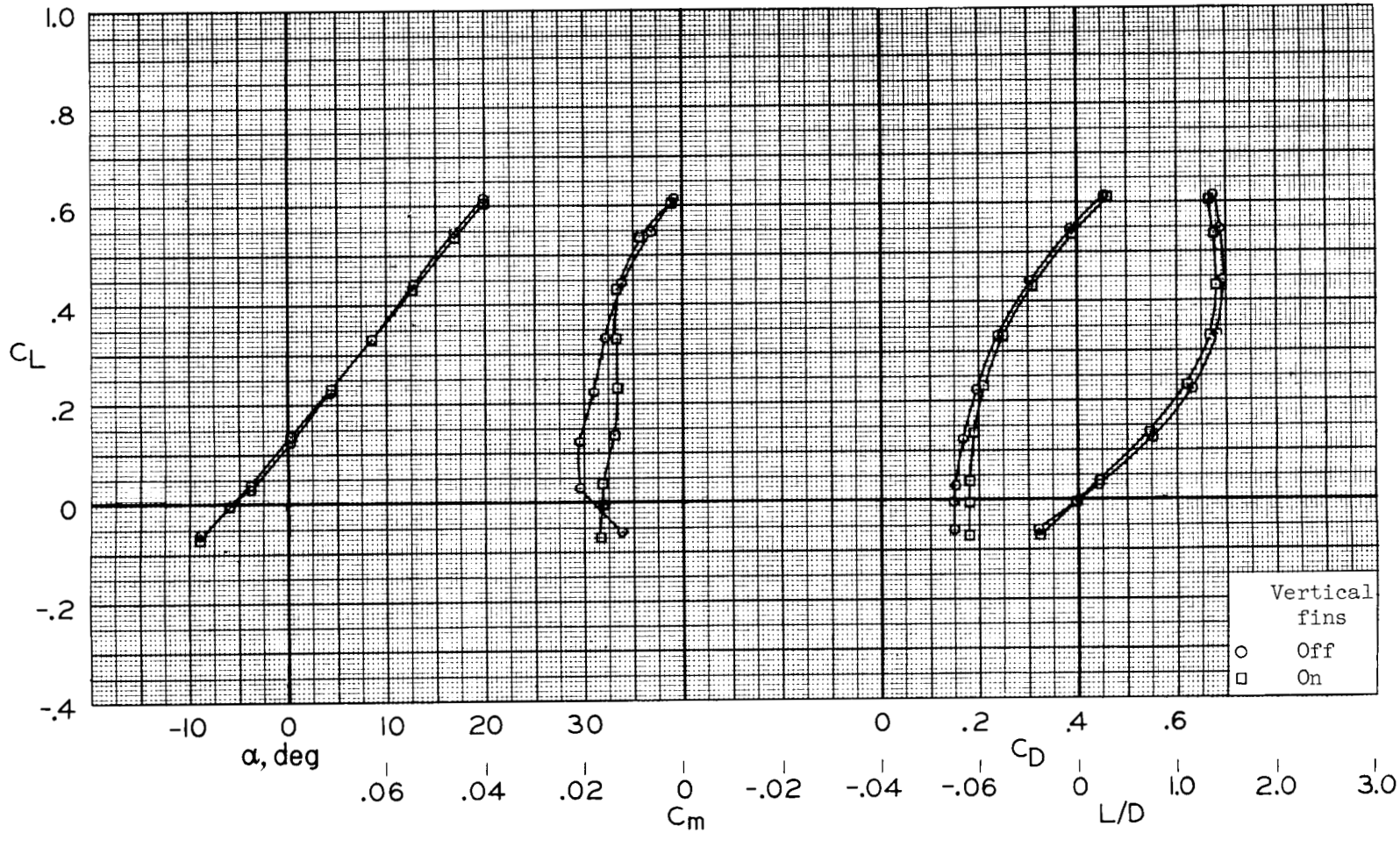

(e) M = 1.3, R = 4.1×10^6

Figure 14.- Continued.

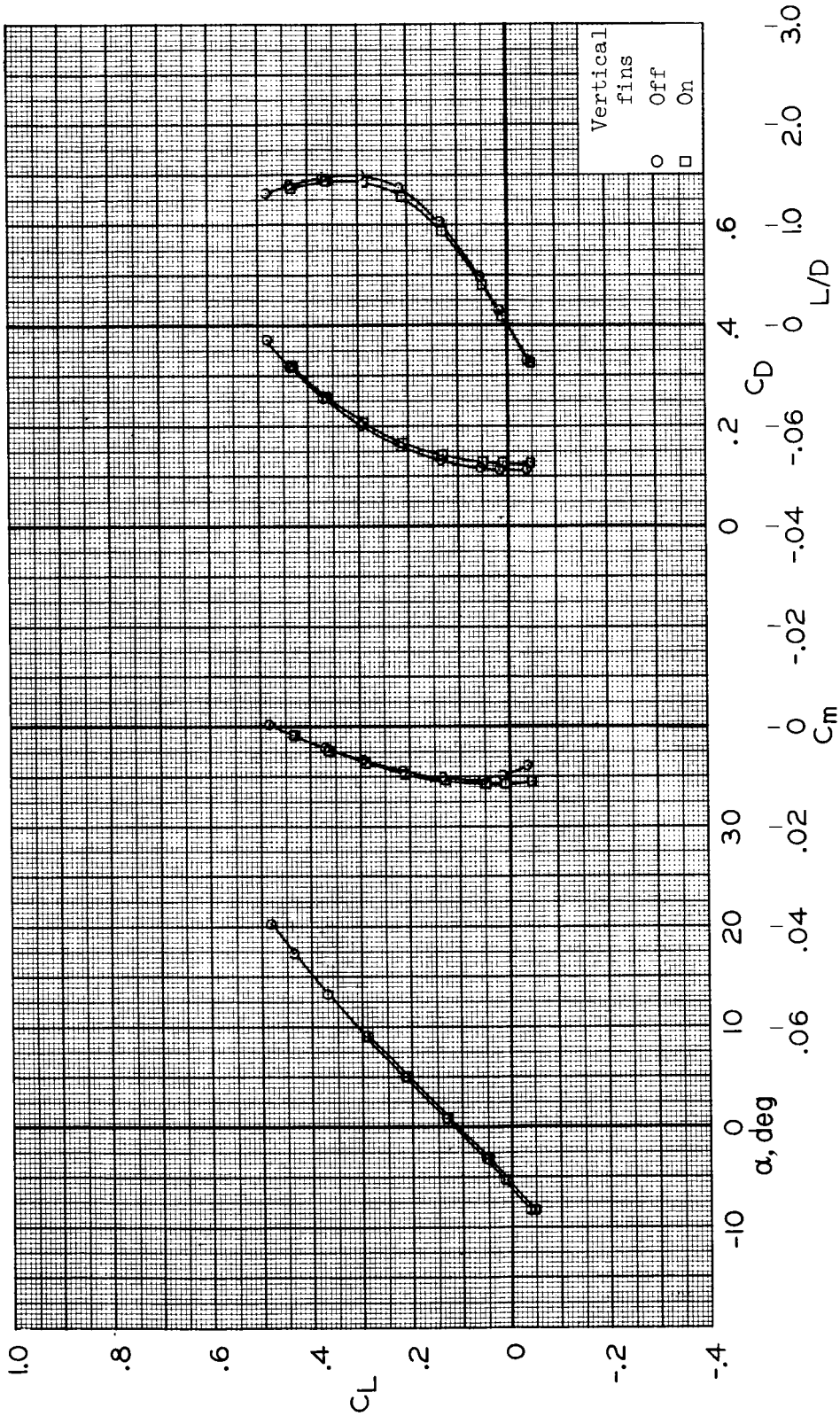

(f) M = 2.0, R = 4.1×10^6

Figure 14.- Concluded.

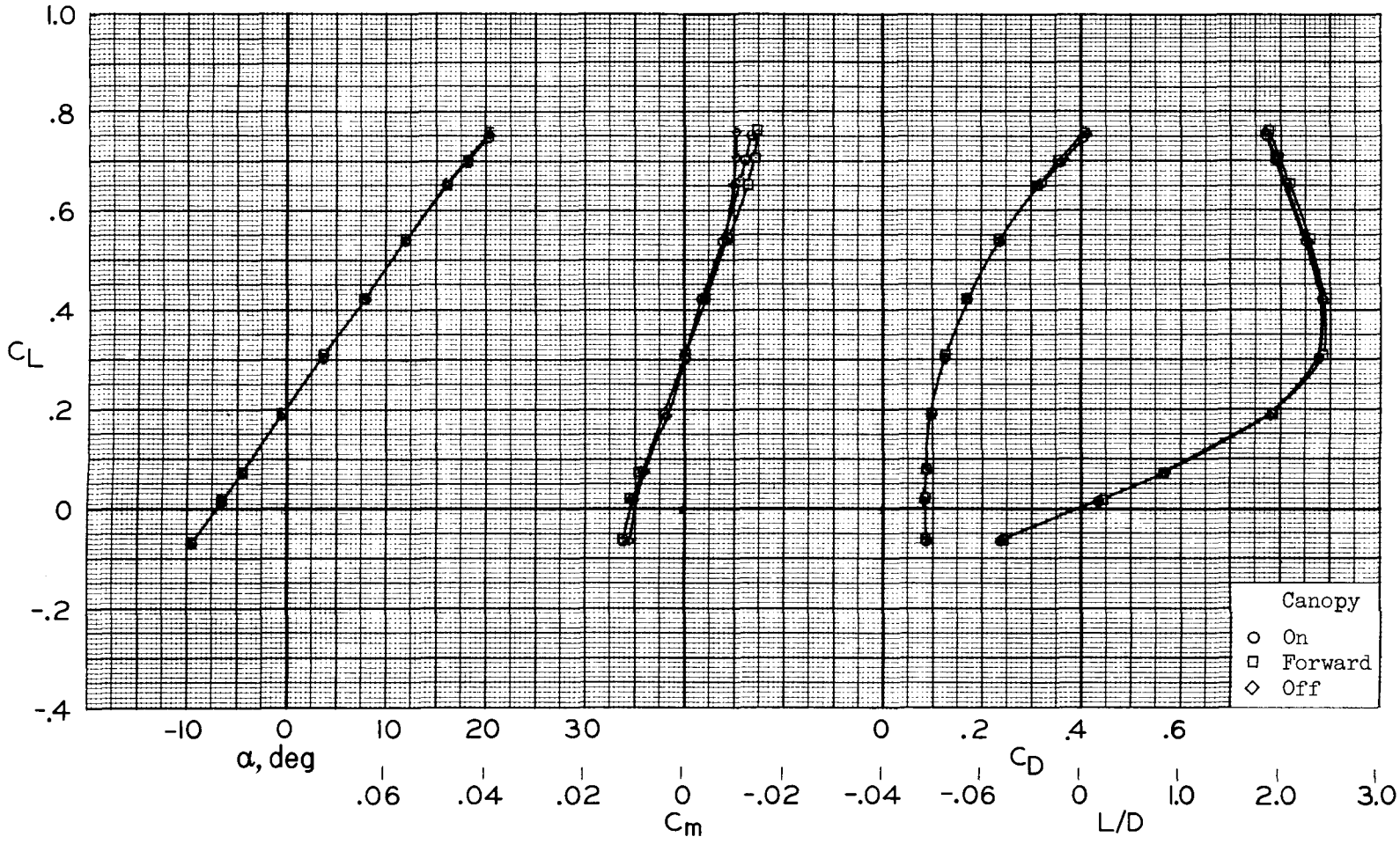

(a) M = 0.6, R = 5.8×10^6

Figure 15.- Effect of canopy on the longitudinal characteristics; $\delta_u = -20°$, $\delta_l = 35°$, $\delta_{rf} = 0°$.

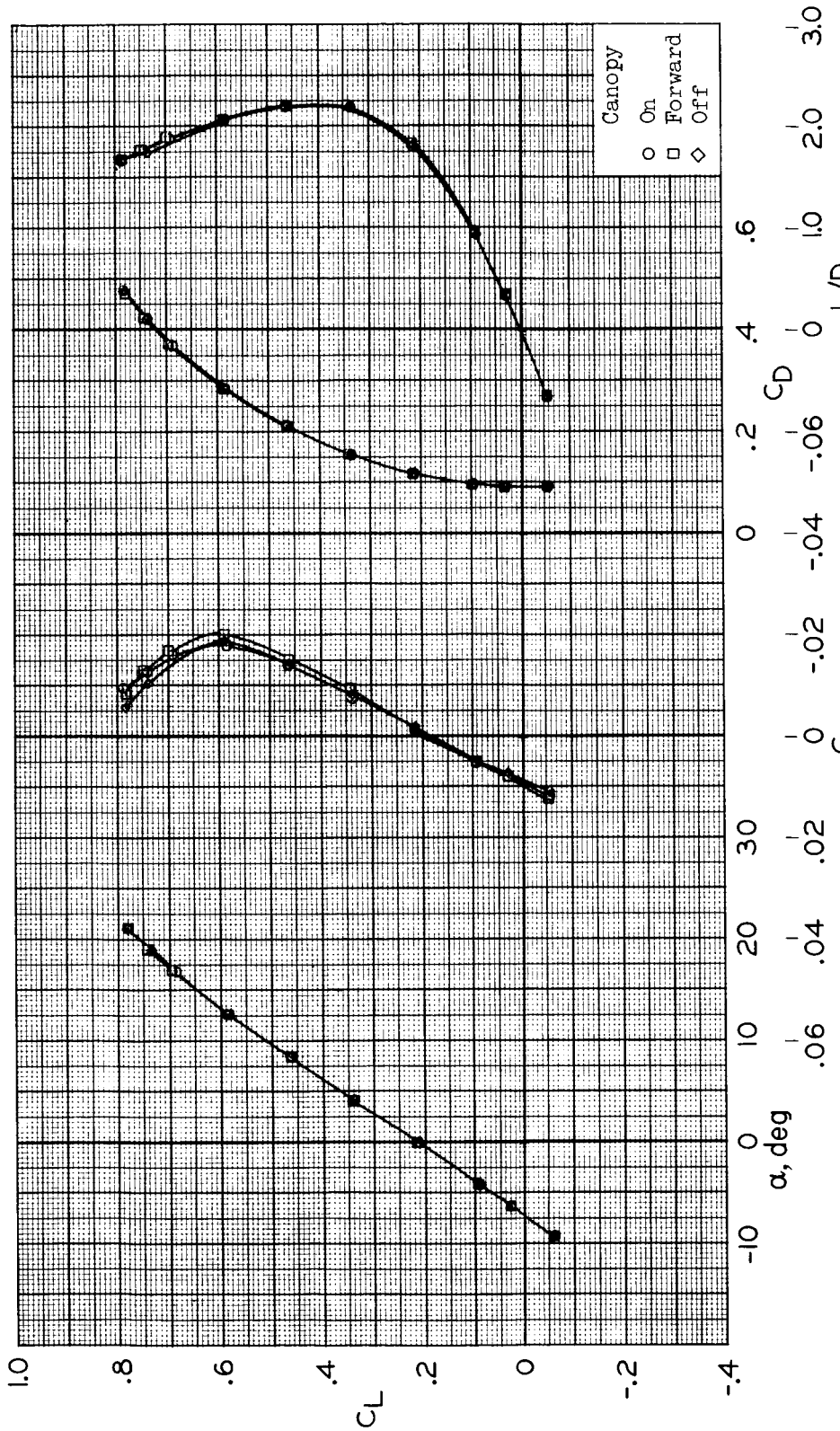

(b) M = 0.8, R = 6.6×10^6

Figure 15.- Continued.

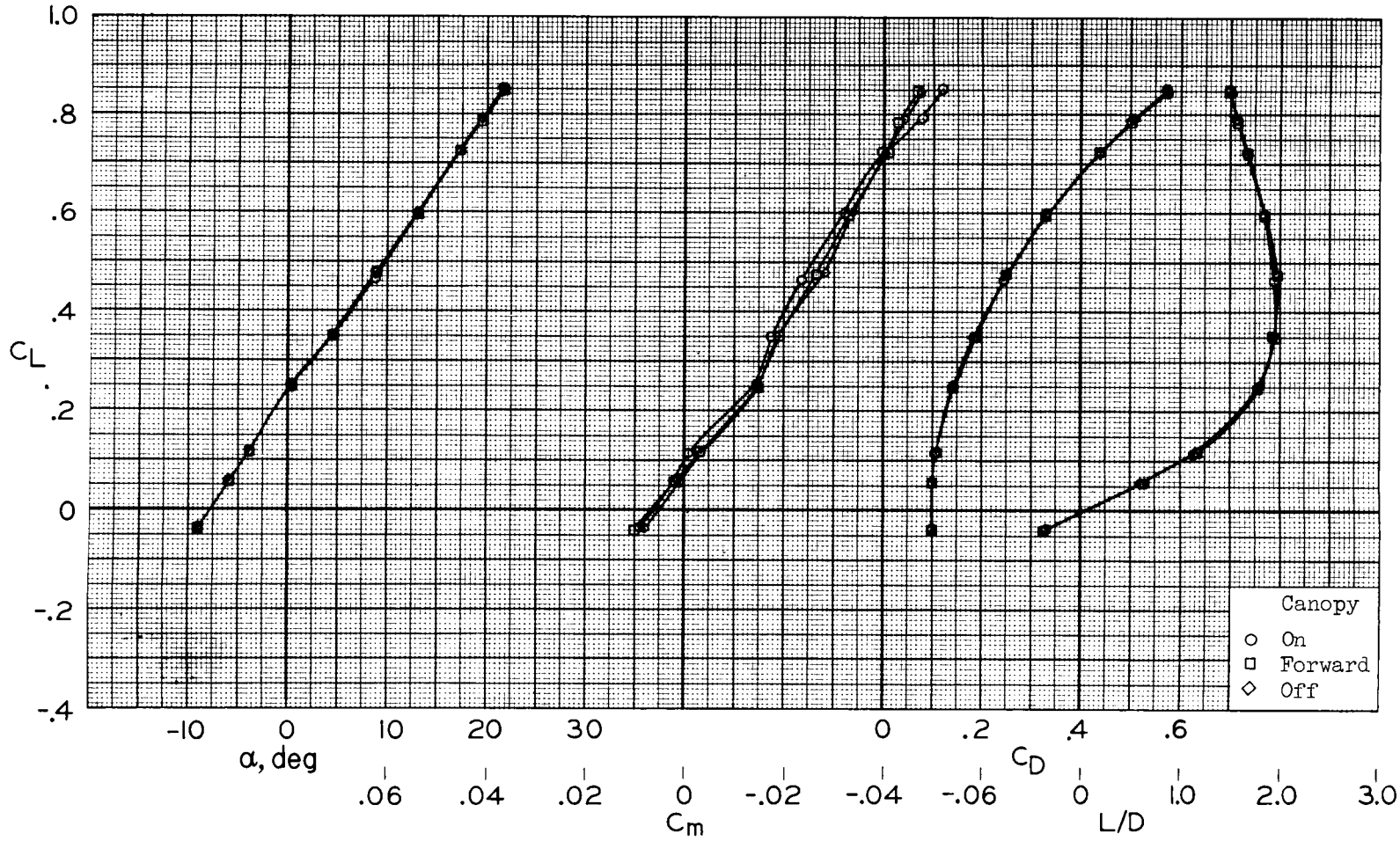

(c) M = 0.9, R = 6.5×10^6

Figure 15.- Continued.

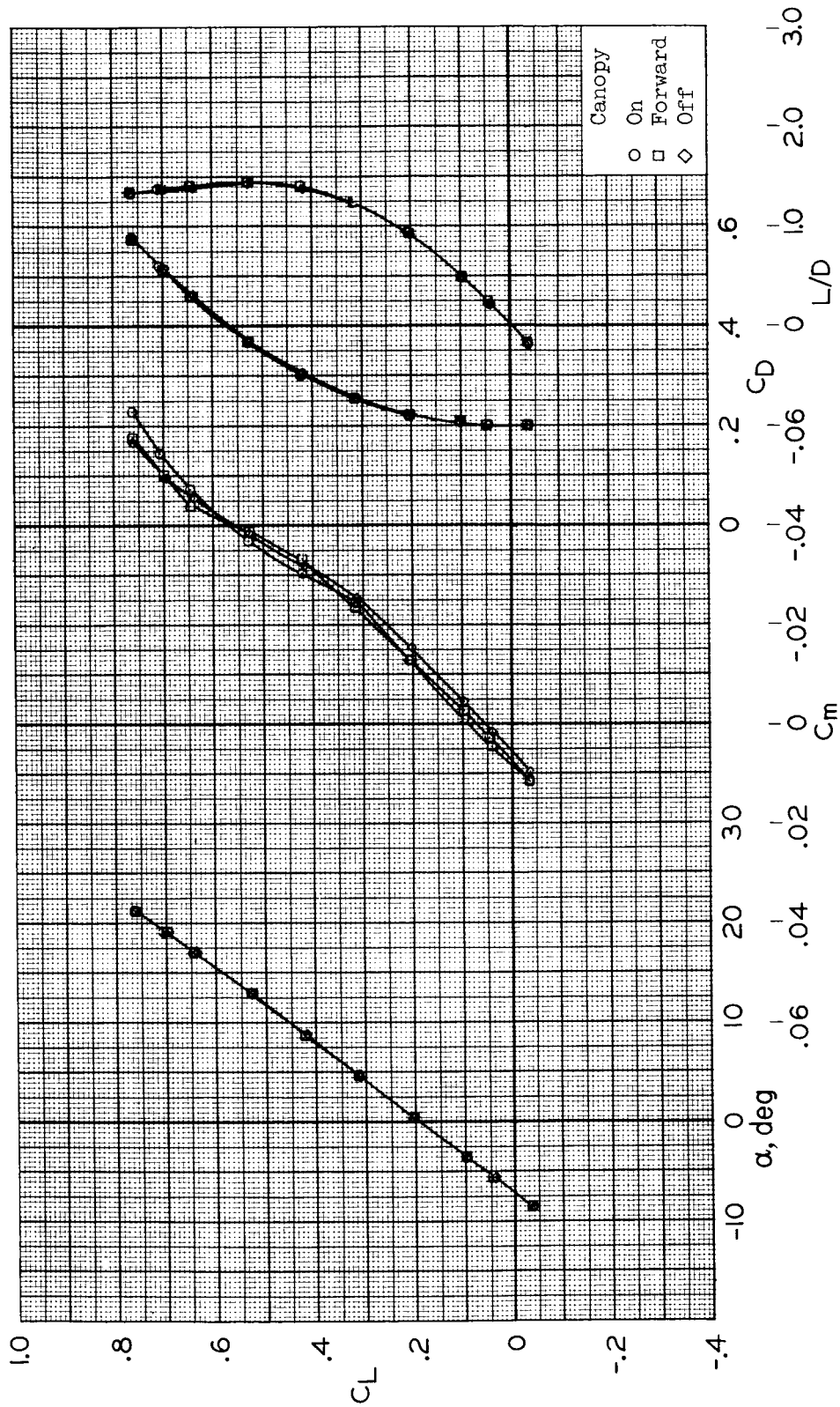

(d) M = 1.1, R = 4.2×10^6

Figure 15.- Continued.

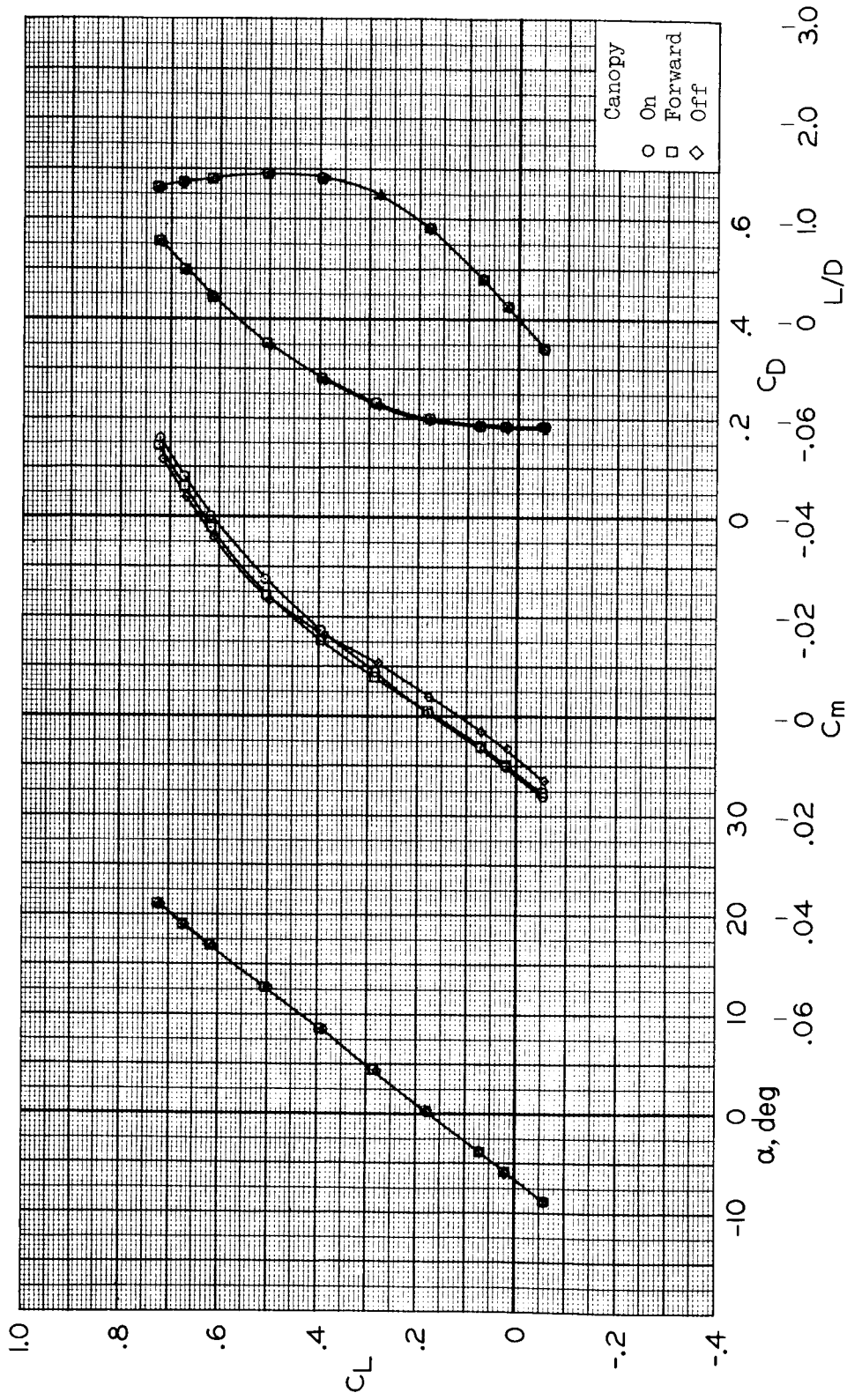

(e) M = 1.3, R = 4.2×10^6

Figure 15.- Continued.

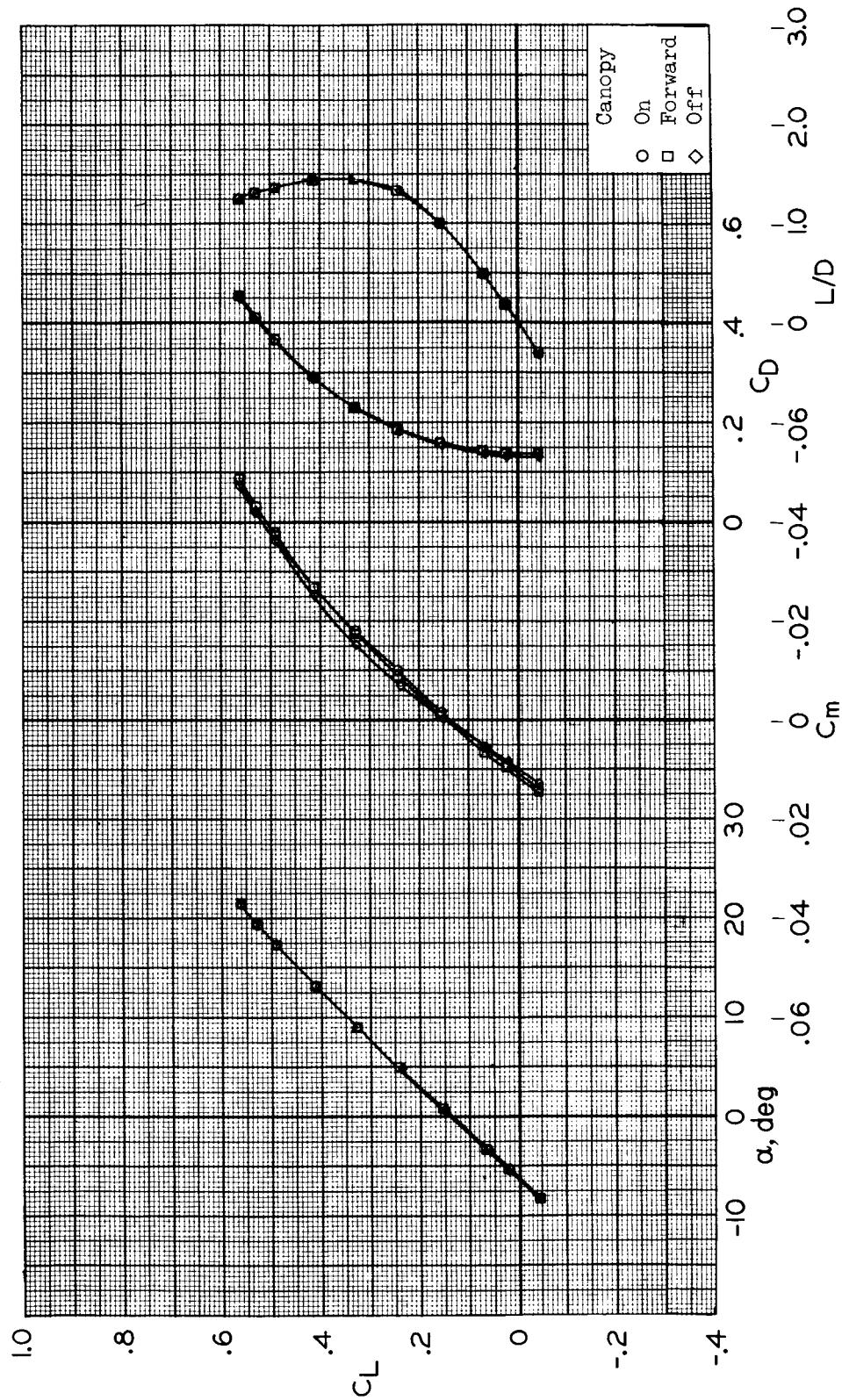

(f) M = 2.0, R = 4.2×10^6

Figure 15.- Concluded.

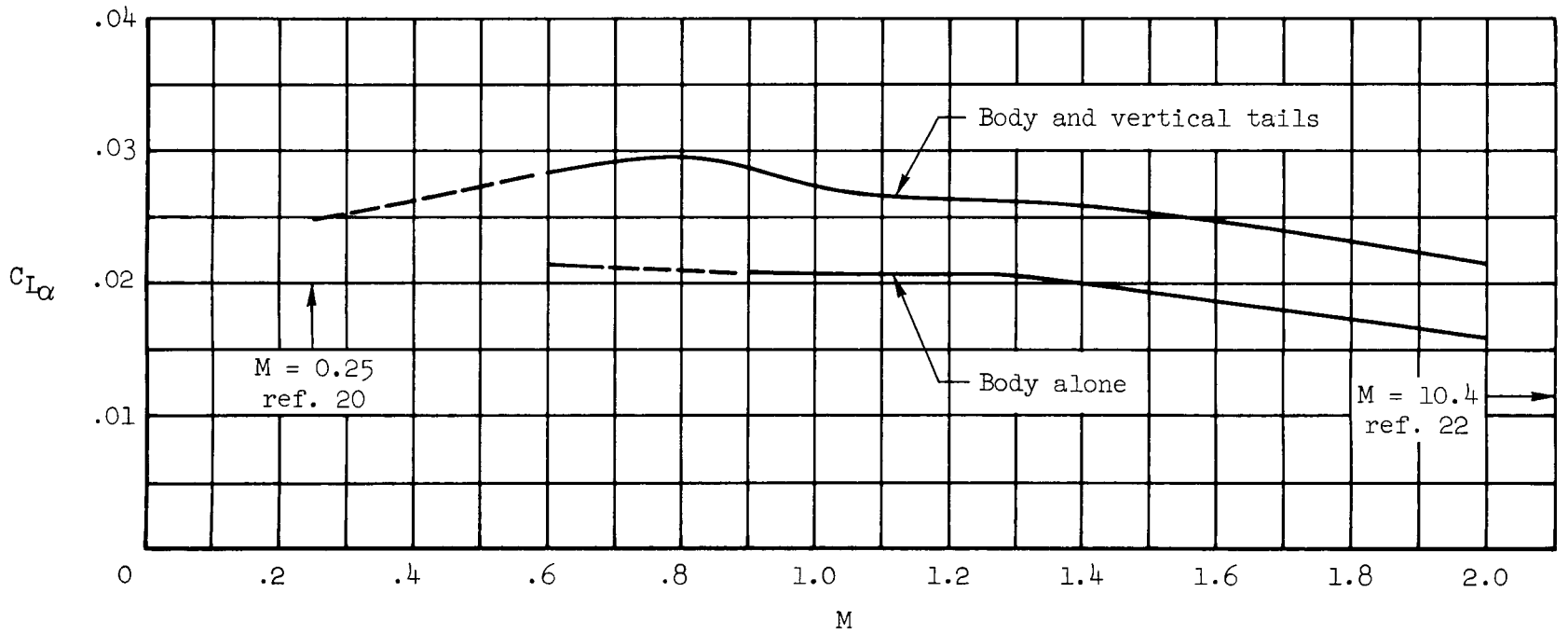

(a) Lift-curve slope; $C_L = 0$

Figure 16.- Variation of longitudinal characteristics with Mach number; $\delta_u = -20°$, $\delta_l = 35°$, $\delta_{rf} = 0°$.

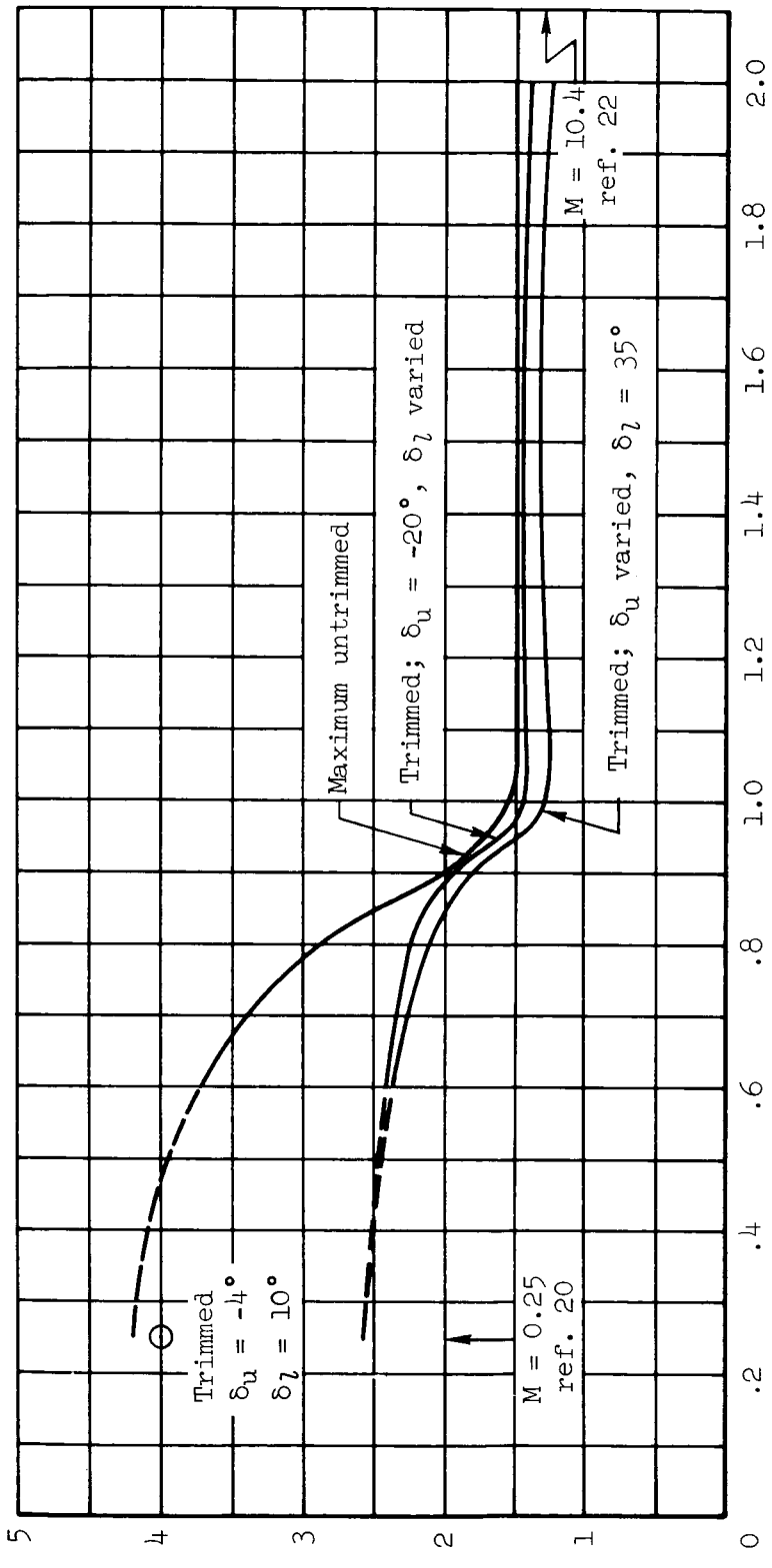

(b) Lift-drag ratio: untrimmed and trimmed

Figure 16.- Continued.

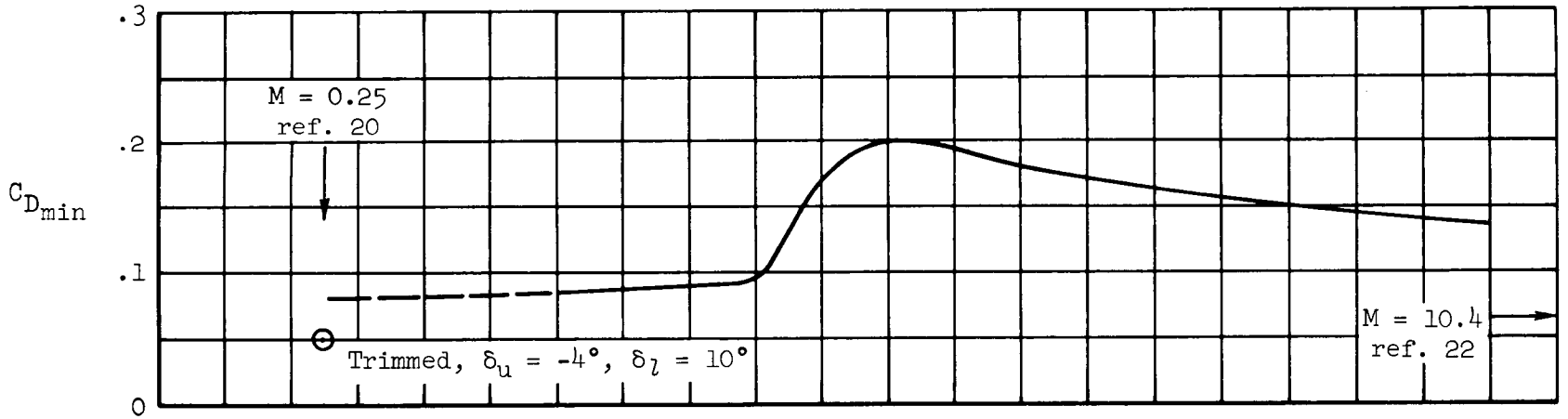

(c) Minimum drag

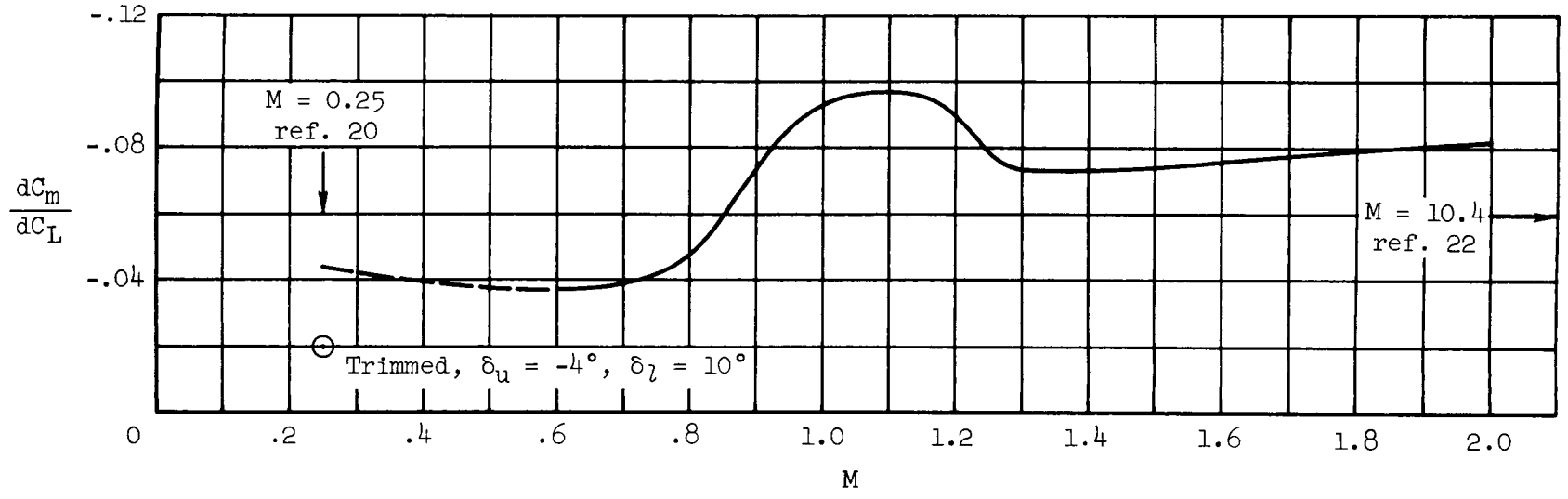

(d) Pitching-moment curve slope; $C_L \approx 0.1$

Figure 16.- Concluded.

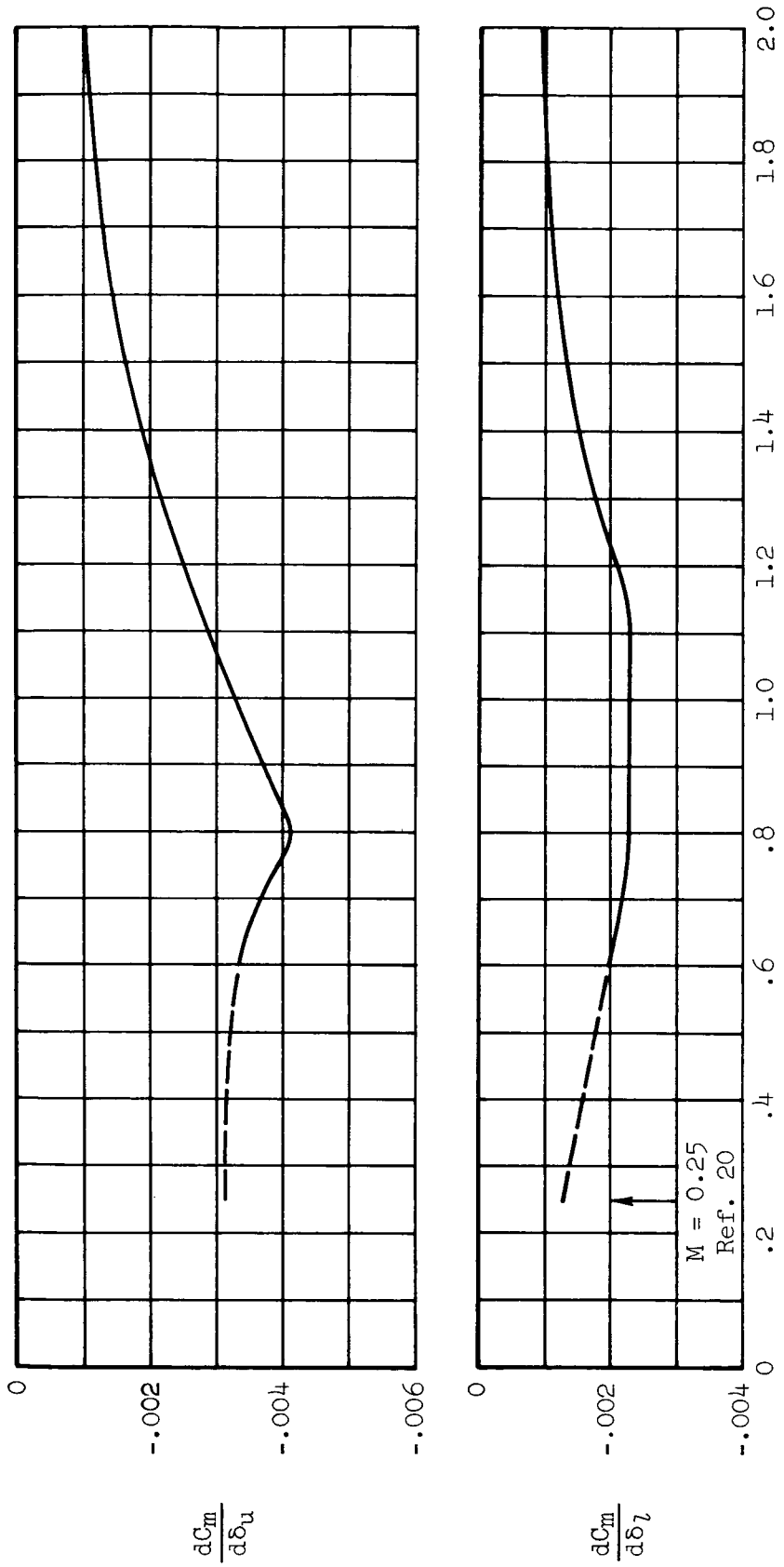

Figure 17.- Upper and lower flap effectiveness; $\delta_u = -20°$, $\delta_l = 35°$.

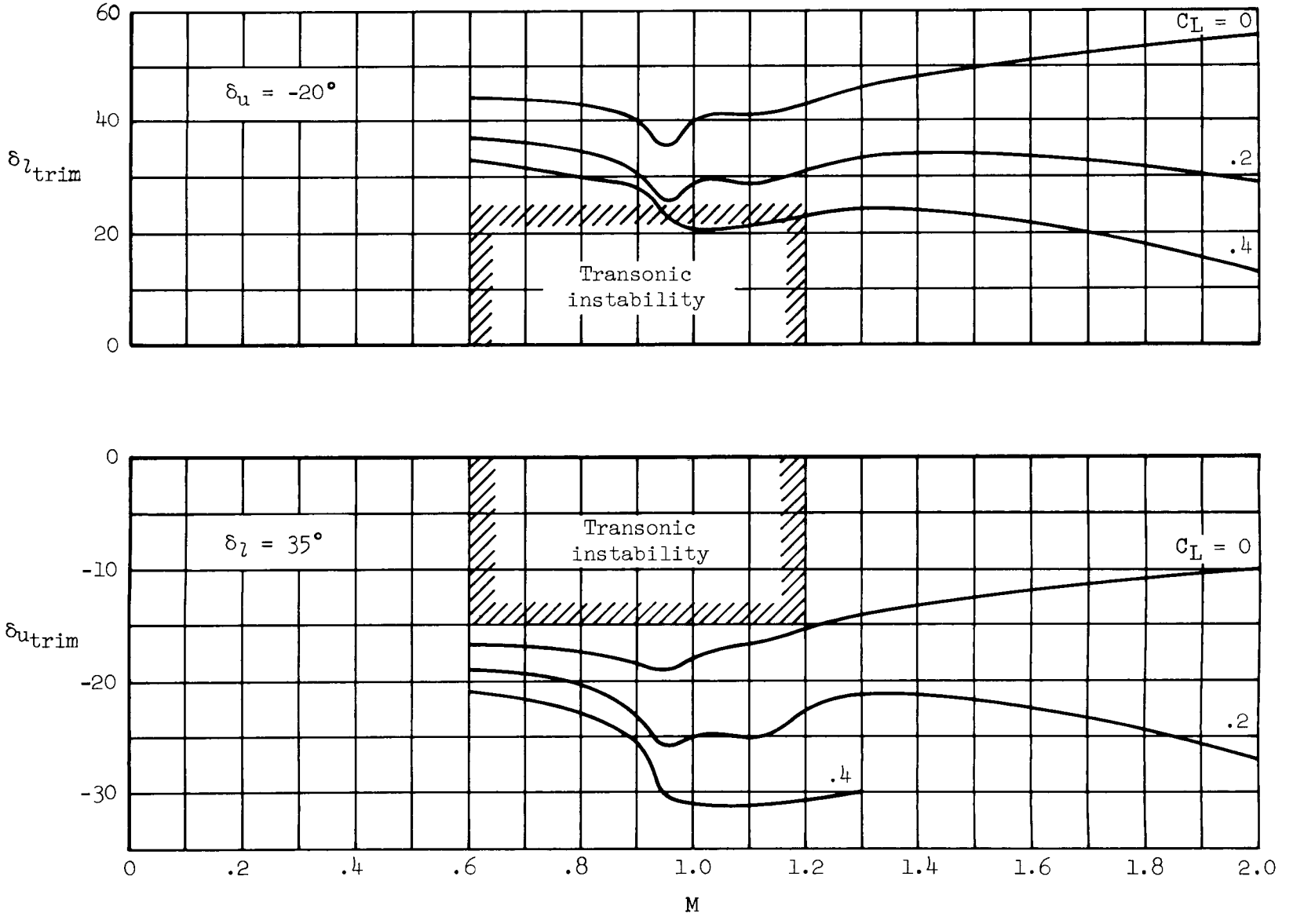

Figure 18.- Upper and lower flap deflections for trim.

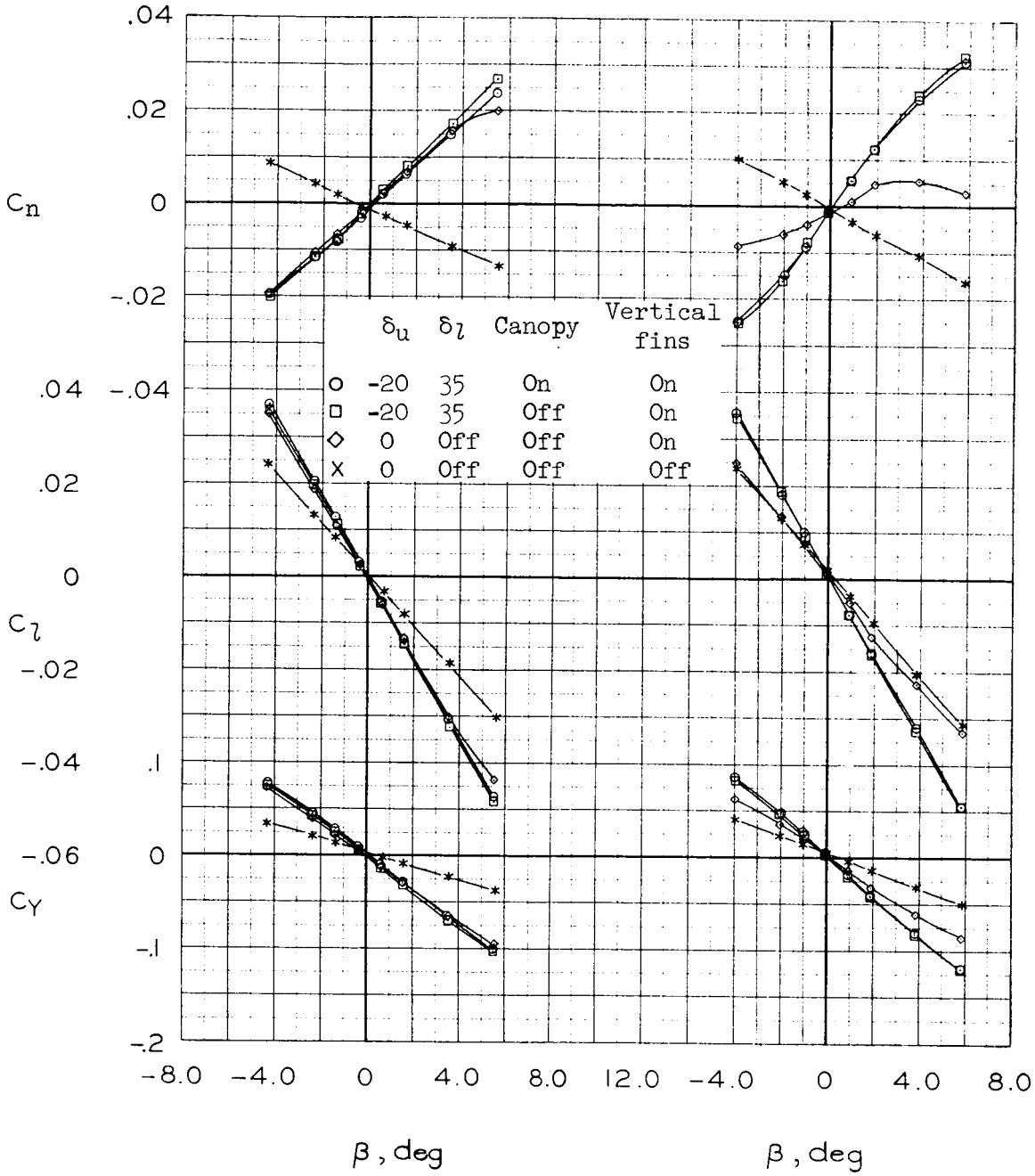

(a) M = 0.60, R = 5.8×10^6 (b) M = 0.80, R = 6.6×10^6

Figure 19.- Variation of lateral-directional characteristics with sideslip; $\alpha = 6°$.

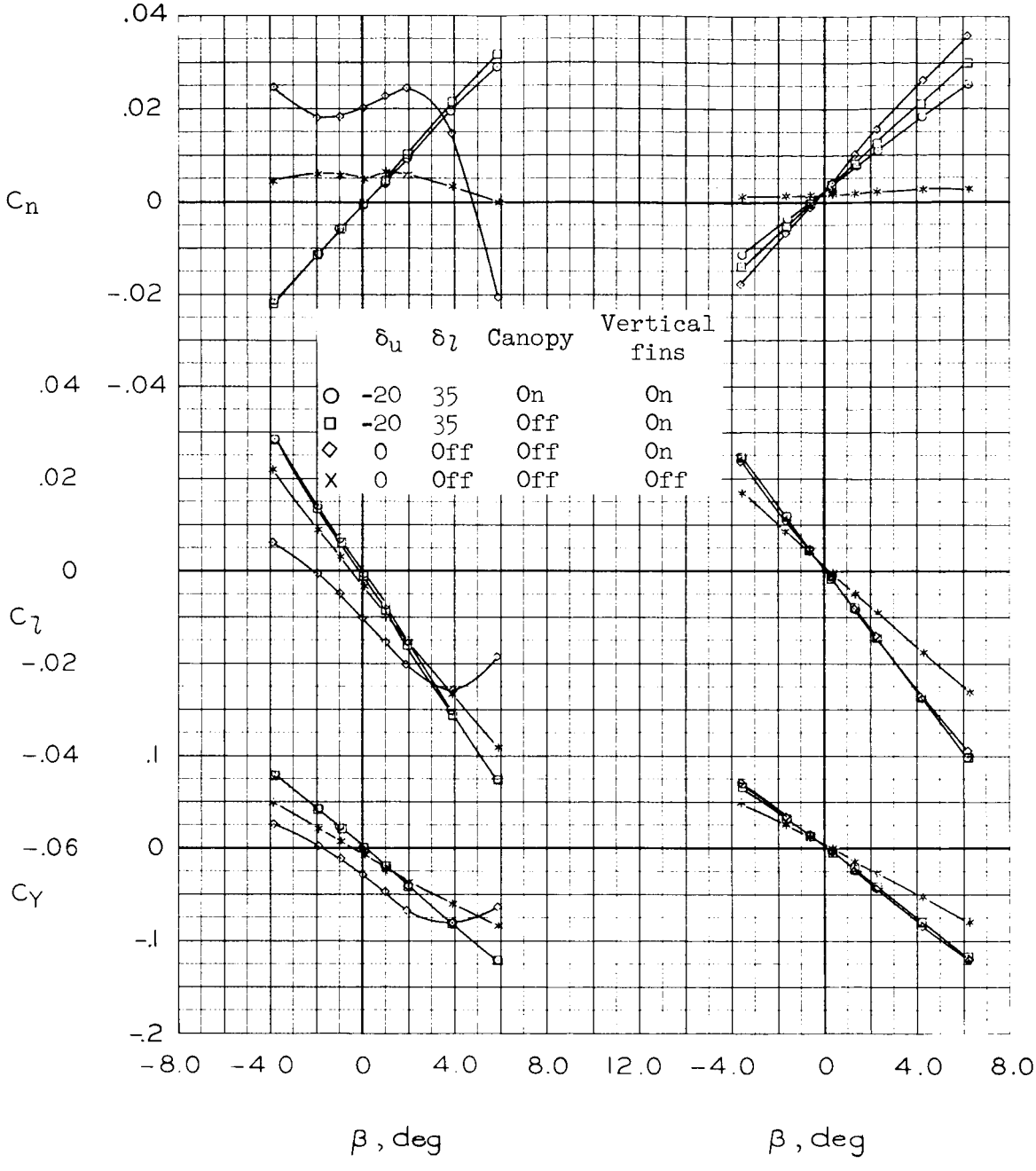

(c) M = 0.90, R = 6.5×10^6 (d) M = 1.10, R = 4.2×10^6

Figure 19.- Continued.

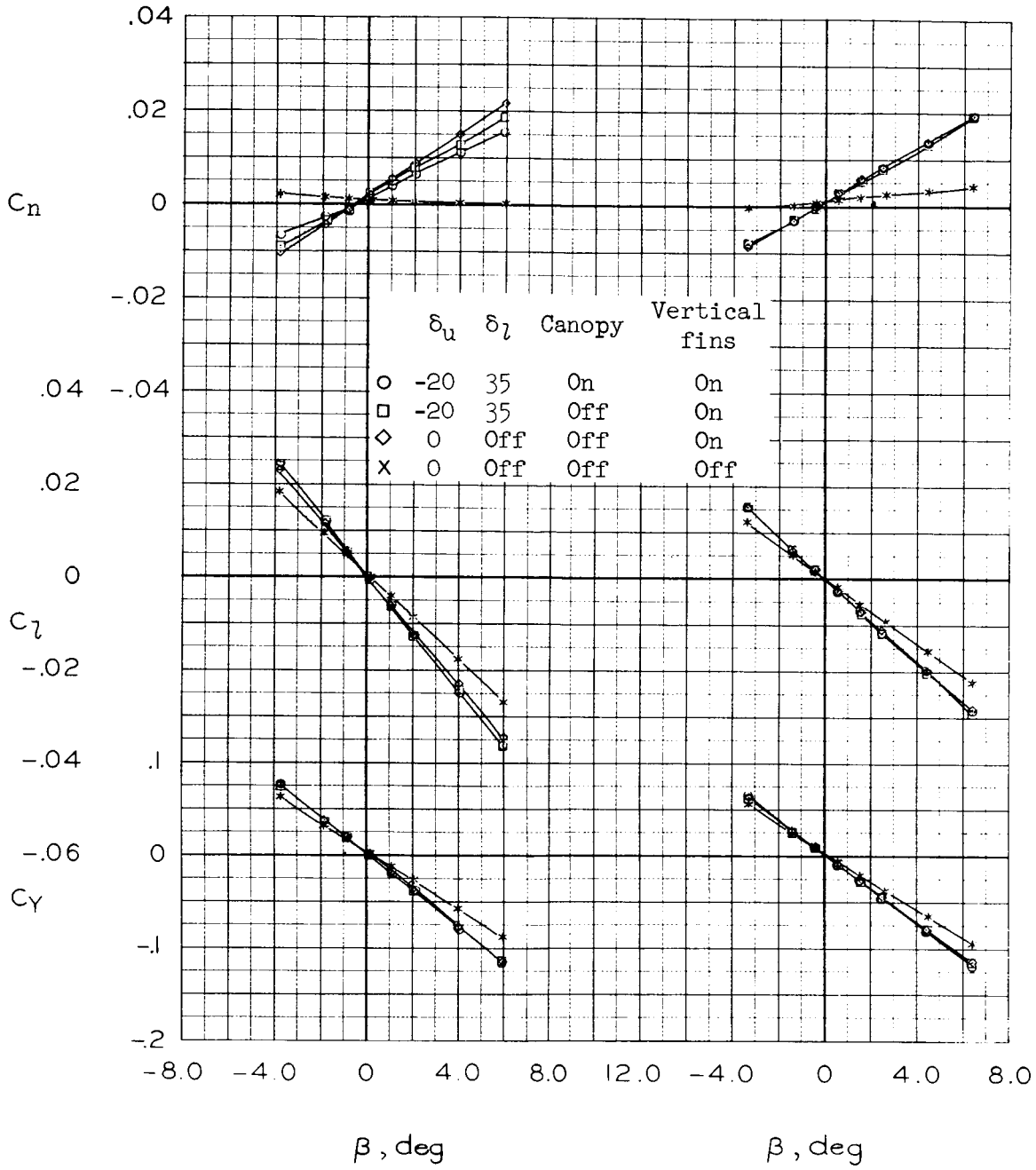

(e) M = 1.30, R = 4.2×10^6 (f) M = 2.00, R = 4.2×10^6

Figure 19.- Concluded.

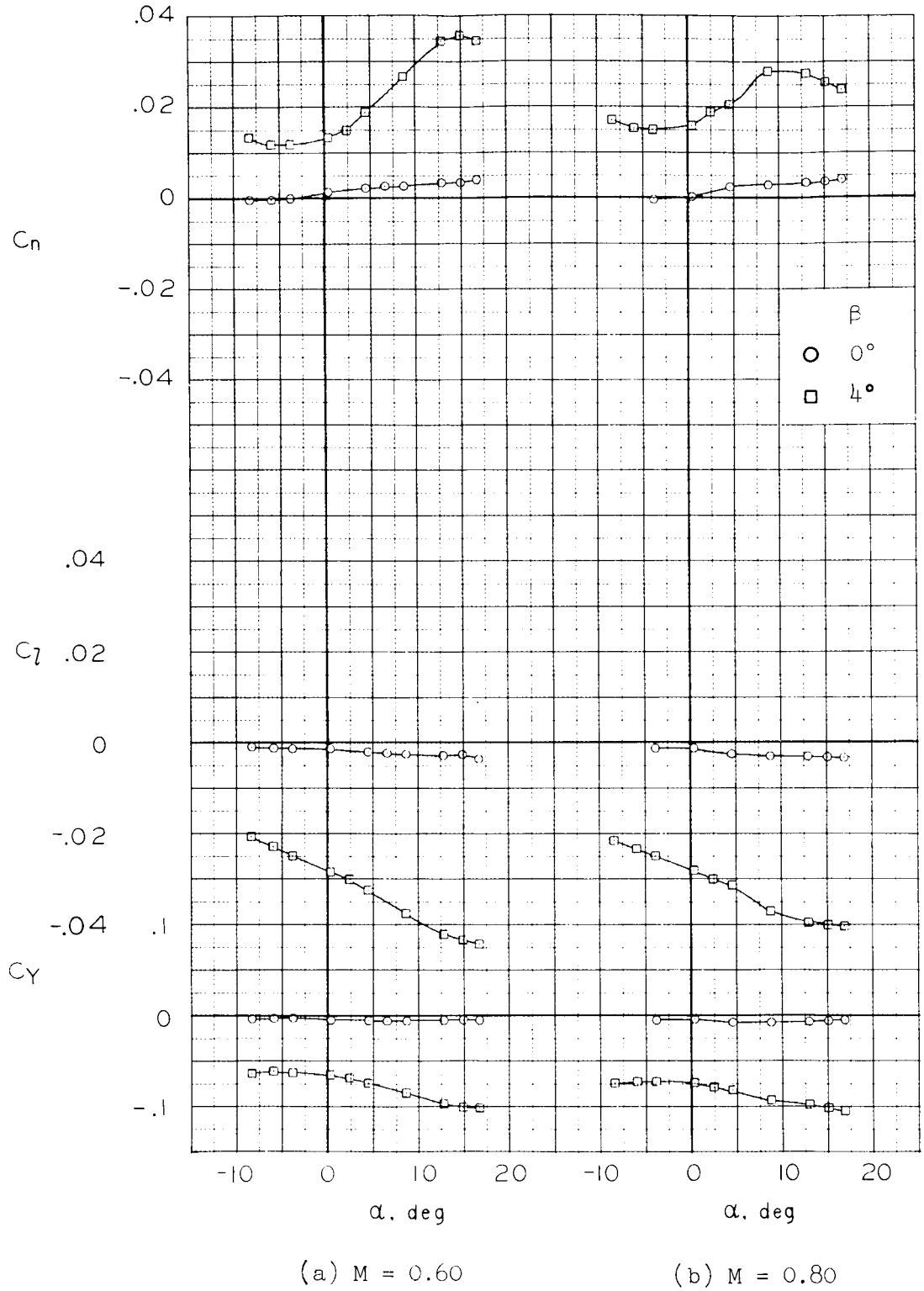

Figure 20.- Variation of lateral-directional characteristics with angle of attack; δ_u = -15°, δ_l = 35°, δ_{rf} = 5°, R = 6×10^6.

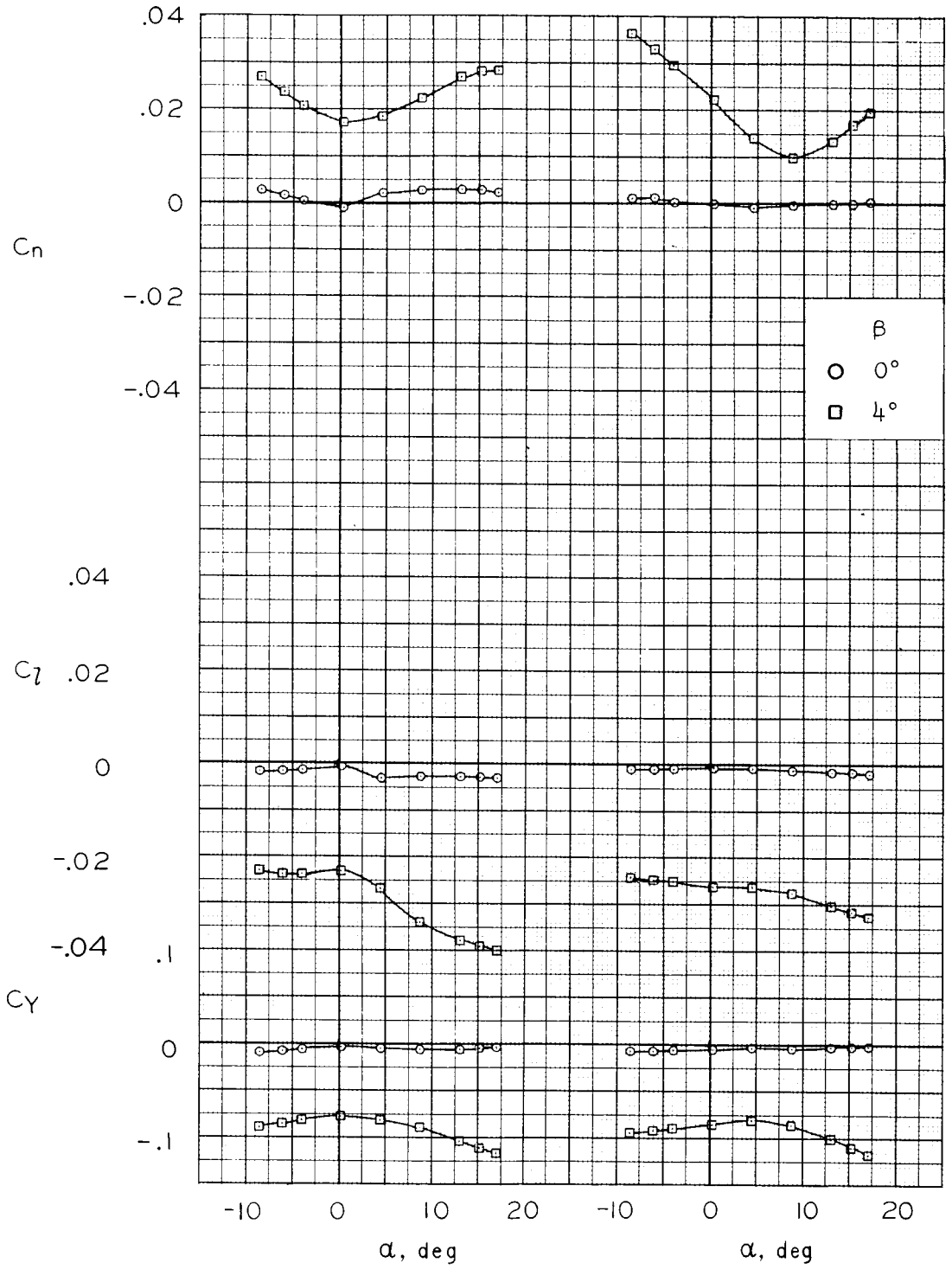

(c) M = 0.90 (d) M = 1.10

Figure 20.- Continued.

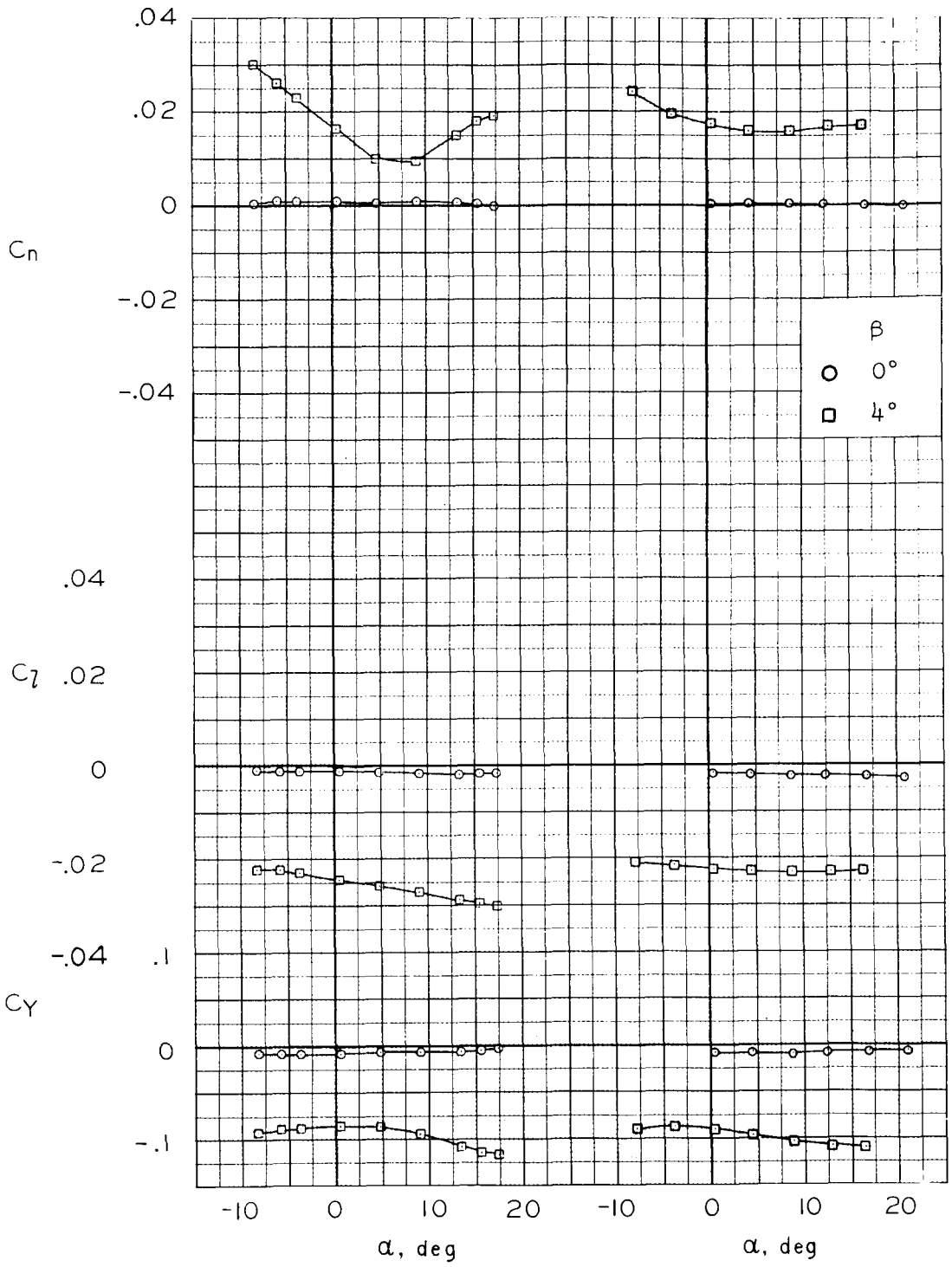

(e) M = 1.30 (f) M = 2.0, R = 4×10^6

Figure 20.- Concluded.

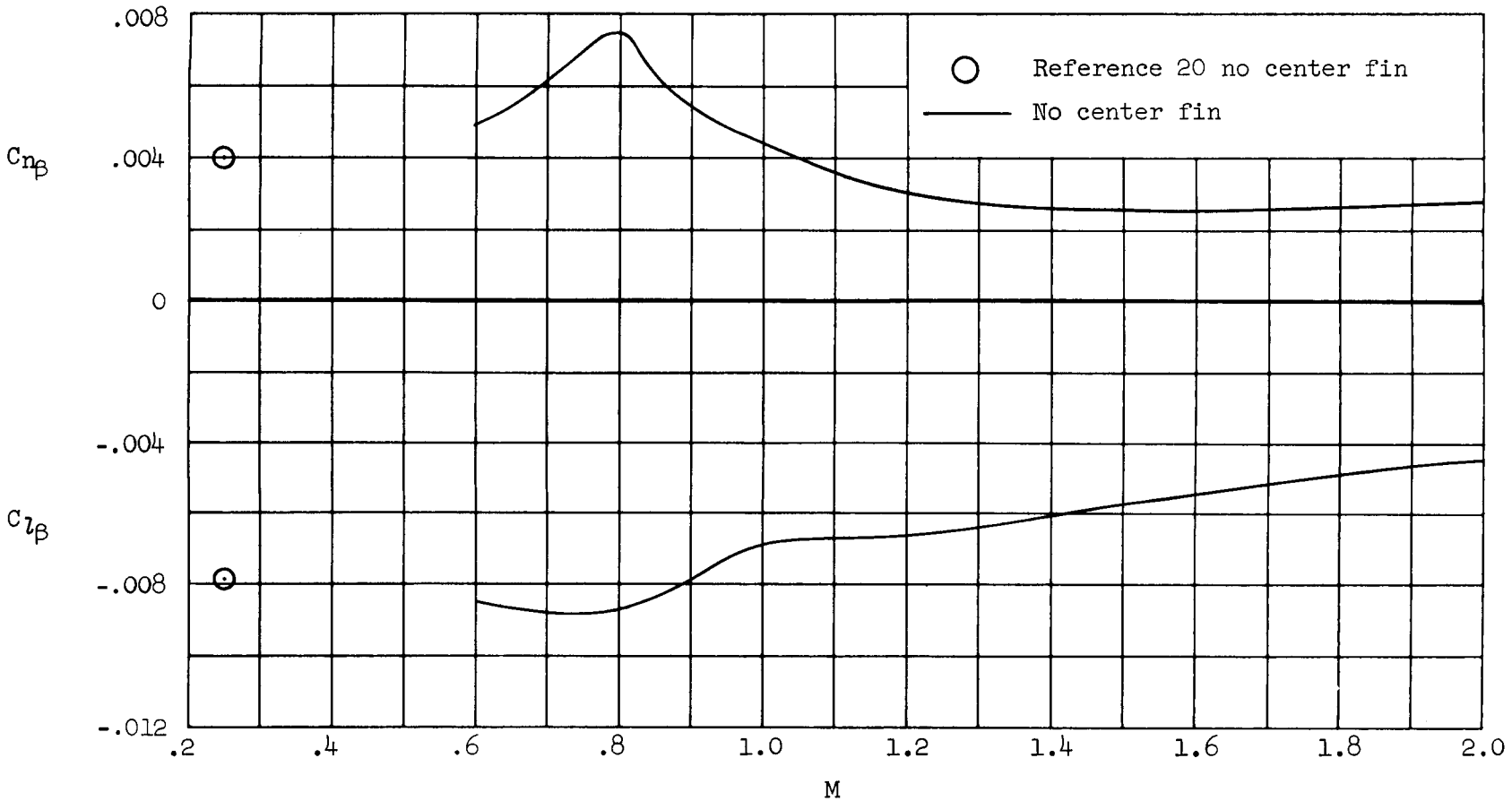

Figure 21.- Variation of lateral-directional sideslip derivatives with Mach number; $\alpha = 6°$, $\delta_u = -20°$, $\delta_l = 35°$, $\delta_{rf} = 0°$.

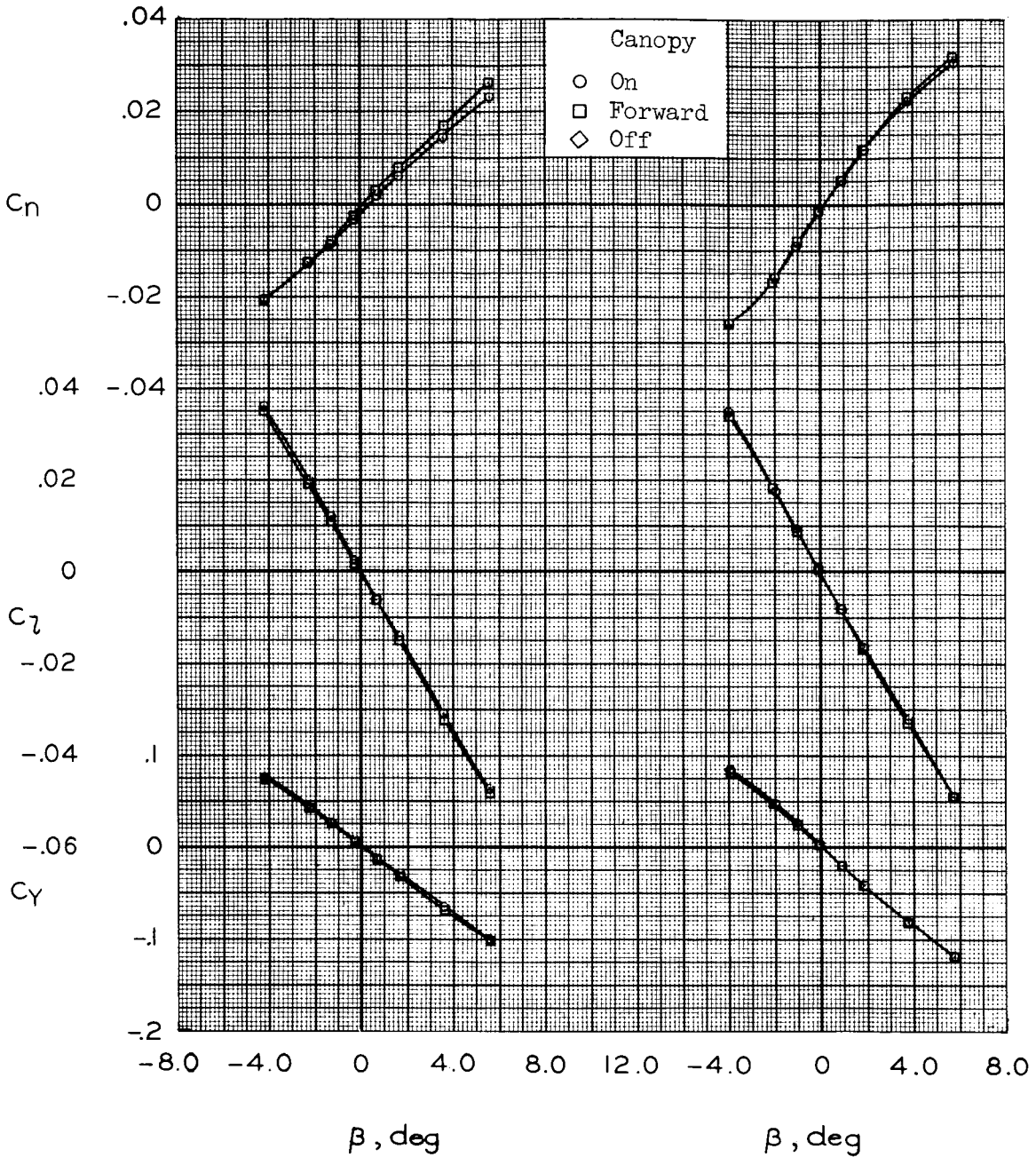

(a) M = 0.6, R = 5.8×10^6 (b) M = 0.80, R = 6.6×10^6

Figure 22.- Effect of canopy on lateral-directional characteristics with sideslip; $\alpha = 6°$, $\delta_u = -20°$, $\delta_l = 35°$, $\delta_{rf} = 0°$.

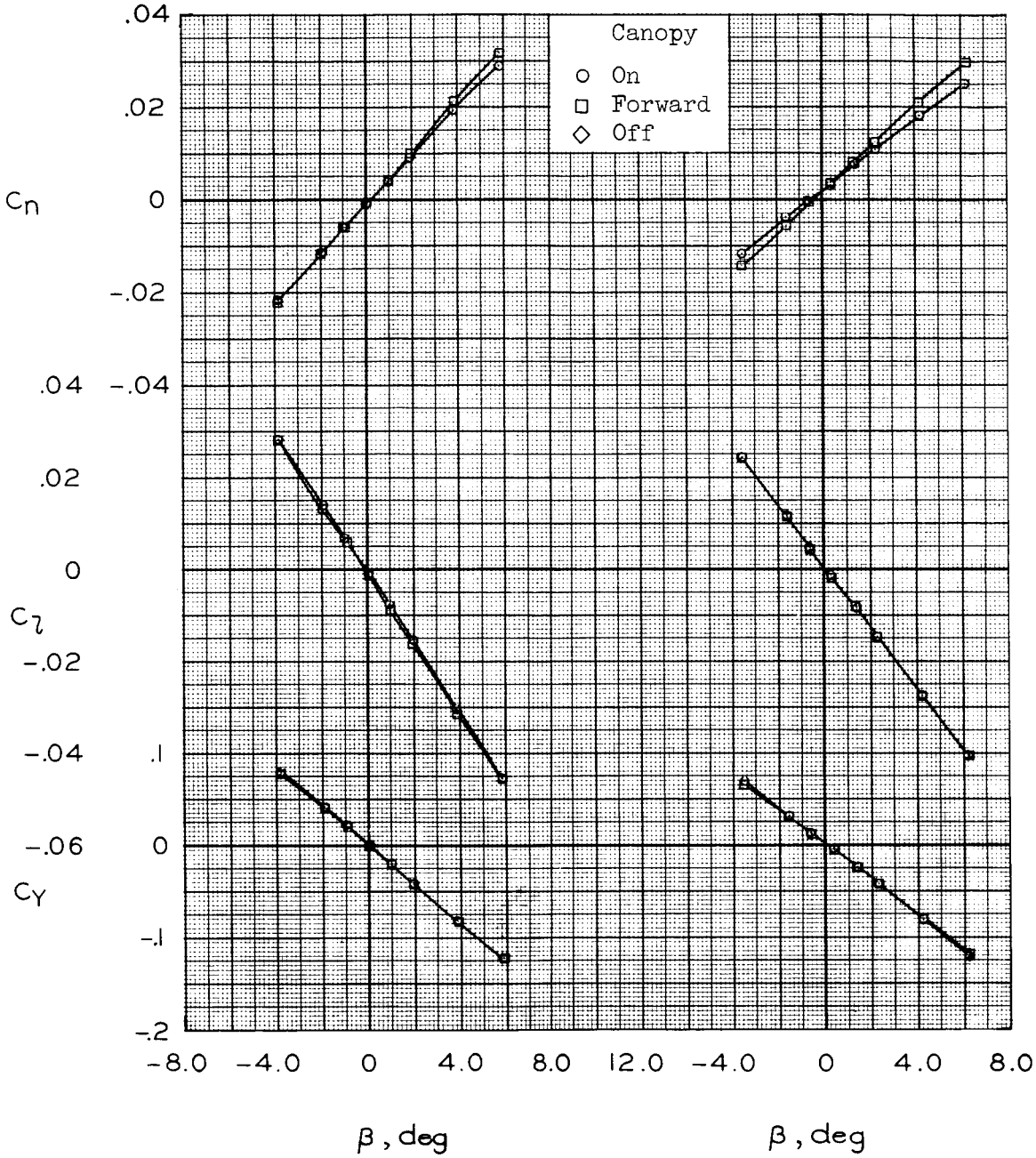

(c) M = 0.90, R = 6.5×10^6 (d) M = 1.10, R = 4.2×10^6

Figure 22.- Continued.

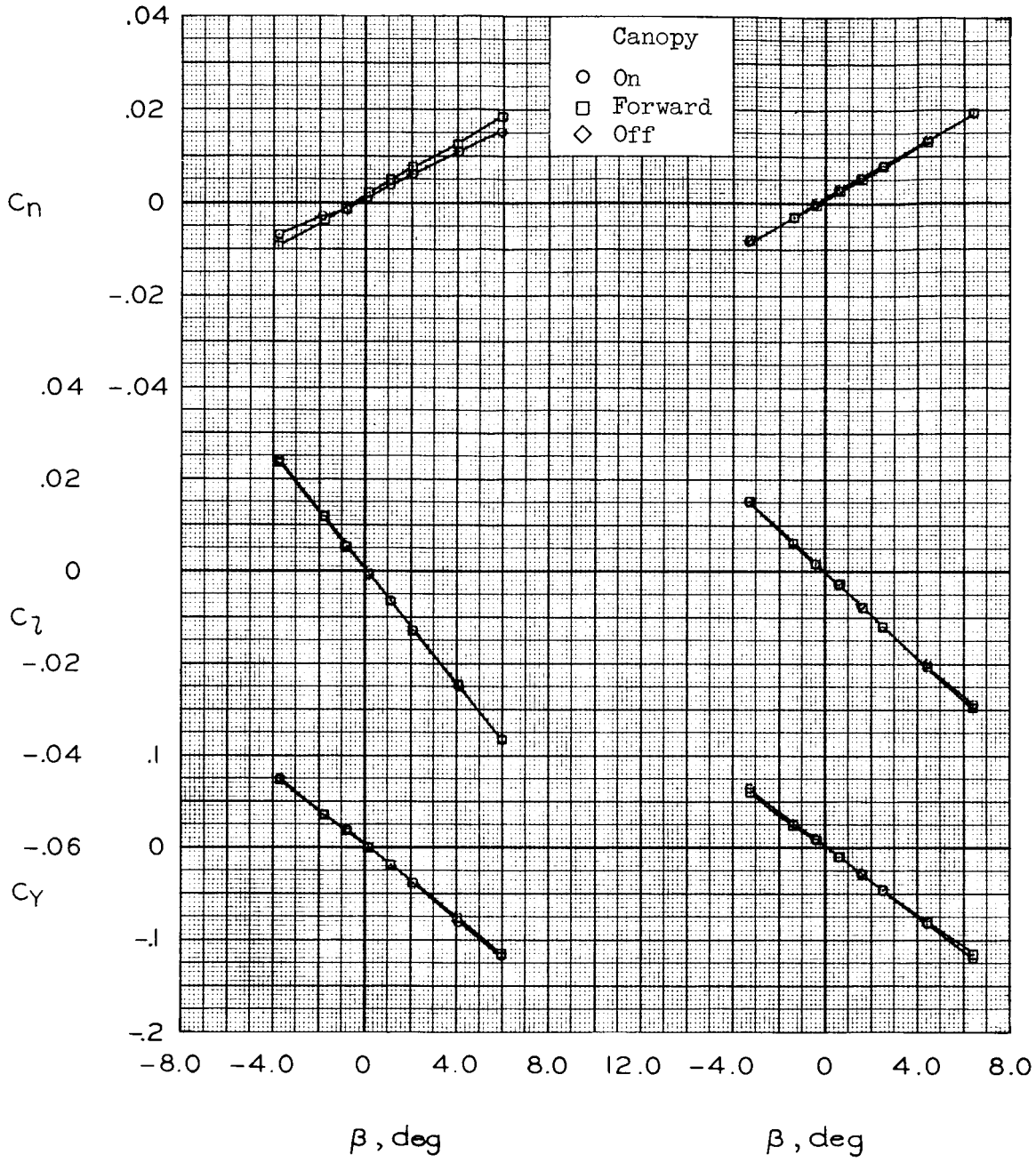

(e) M = 1.30, R = 4.2×10^6 (f) M = 2.00, R = 4.2×10^6

Figure 22.- Concluded.

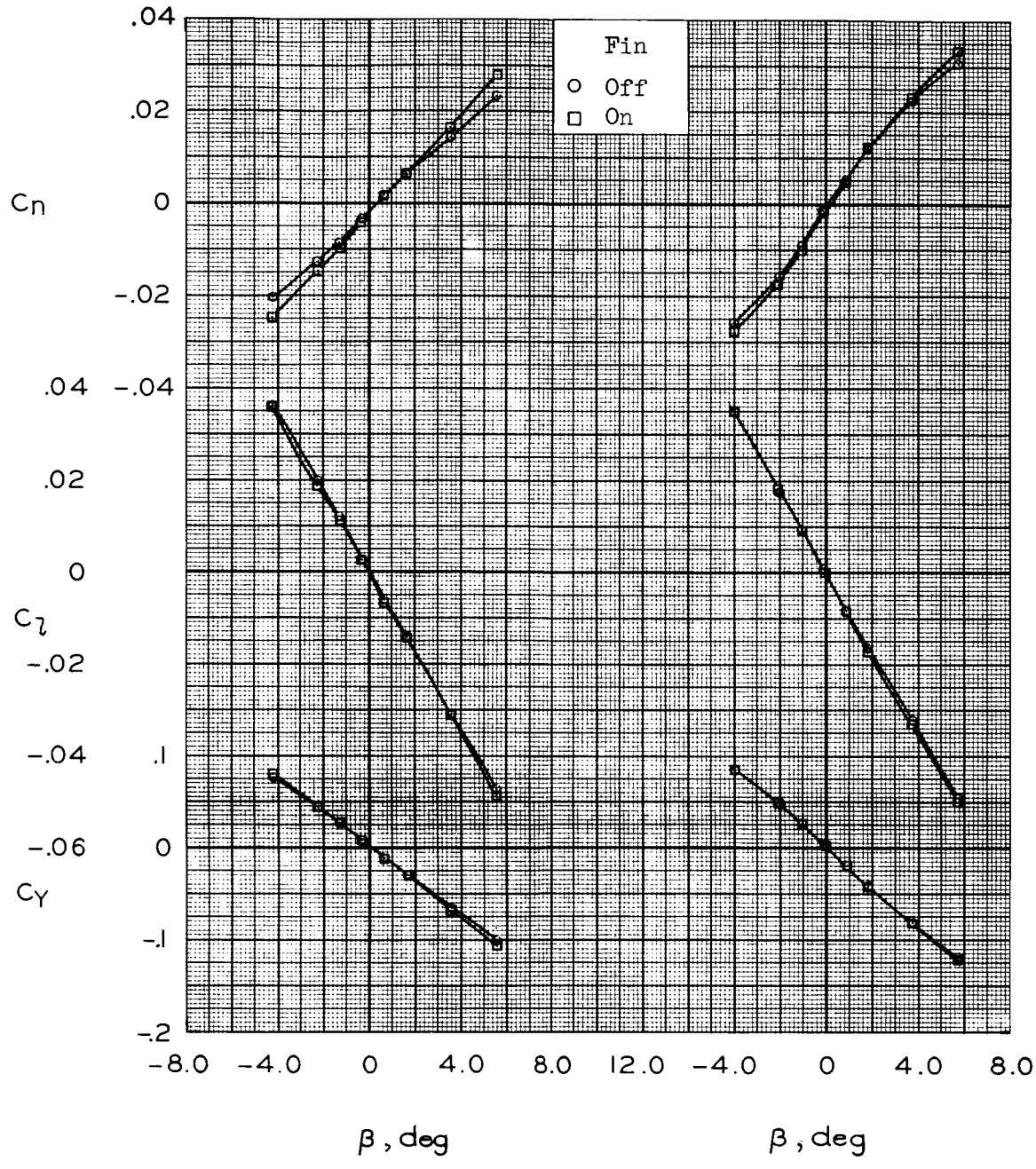

(a) M = 0.60, R = 5.8×10^6 (b) M = 0.80, R = 6.6×10^6

Figure 23.- Effect of center fin located between the upper flaps on lateral-directional characteristics; $\alpha = 6°$, $\delta_u = -20°$, $\delta_l = 35°$, $\delta_{rf} = 0°$.

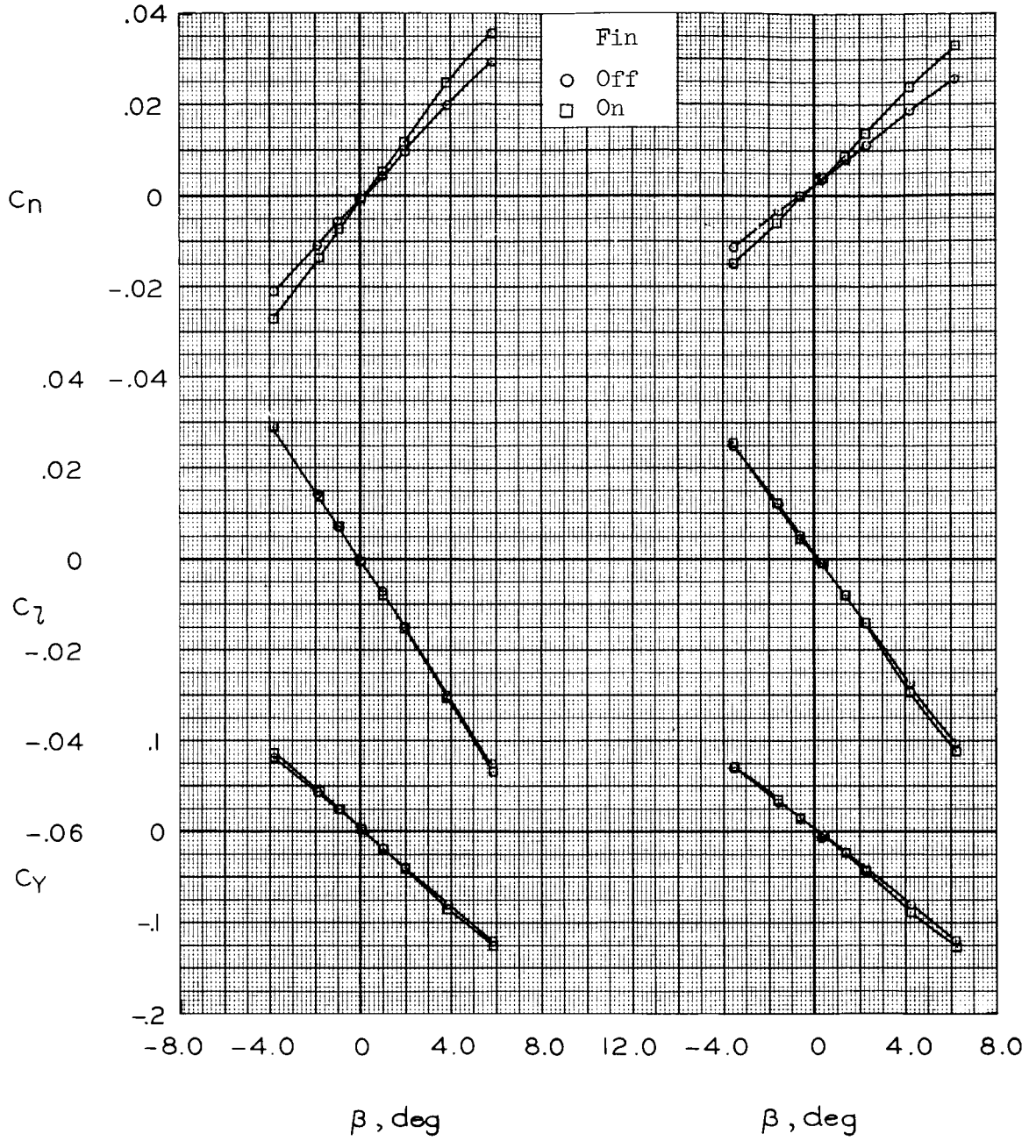

(c) M = 0.90, R = 6.5×10^6 (d) M = 1.10, R = 4.2×10^6

Figure 23.- Continued.

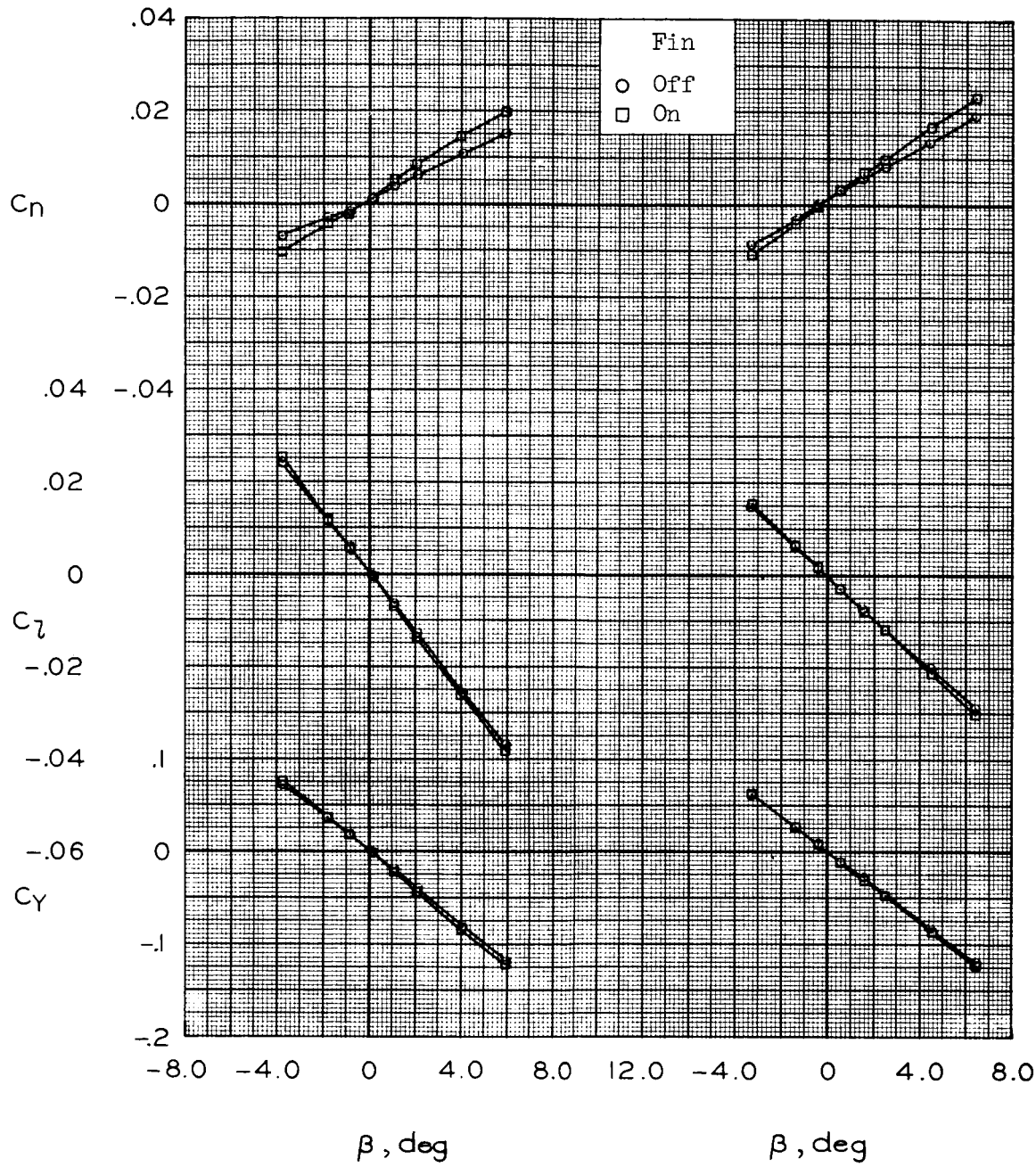

(e) M = 1.30, R = 4.2×10^6 (f) M = 2.00, R = 4.2×10^6

Figure 23.- Concluded.

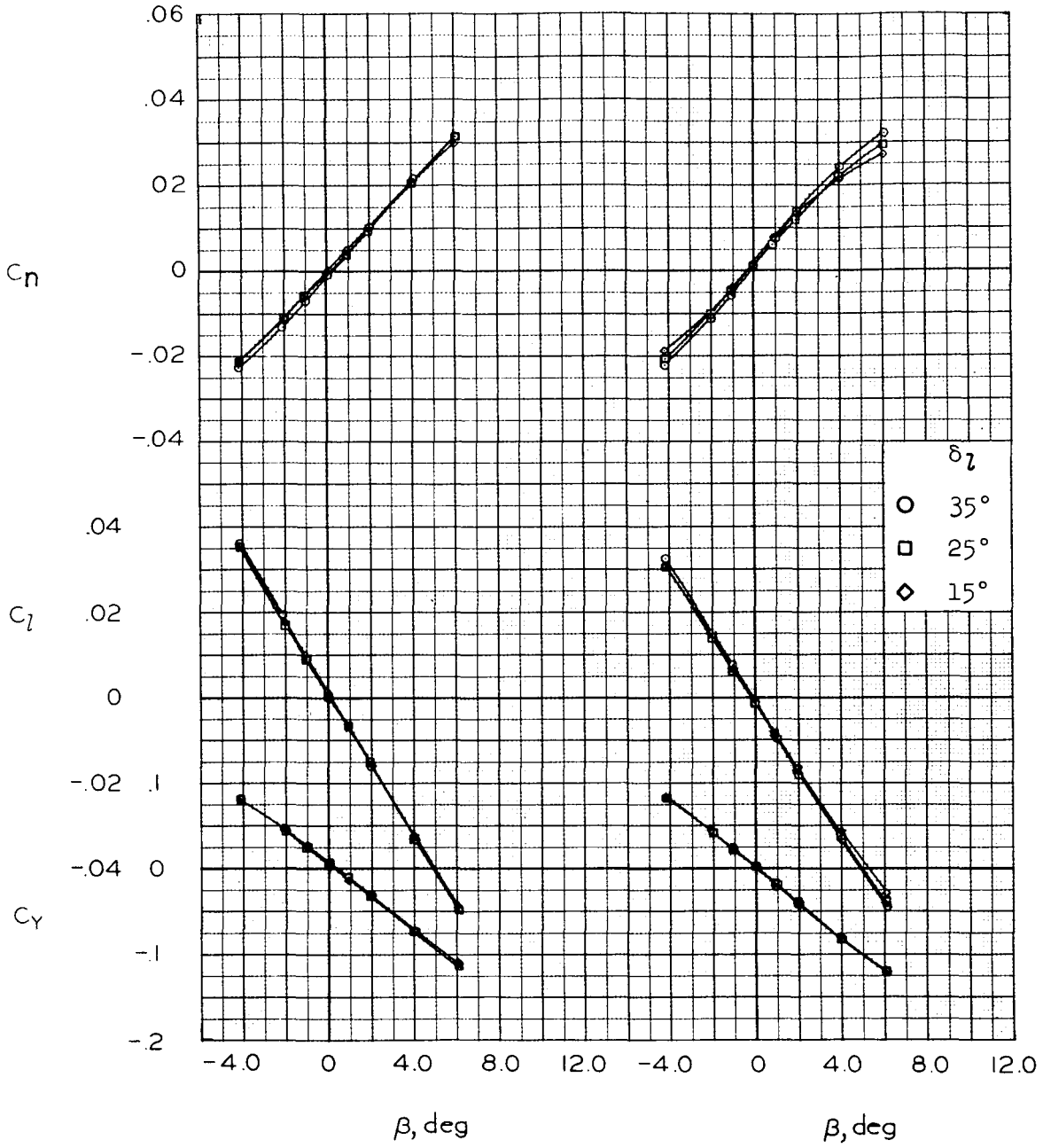

(a) M = 0.60, R = 5.6×10^6 (b) M = 0.80, R = 6.5×10^6

Figure 24.- Lateral-directional characteristics at selected lower-flap deflections; $\alpha = 6°$, $\delta_u = -15°$, $\delta_{rf} = 5°$.

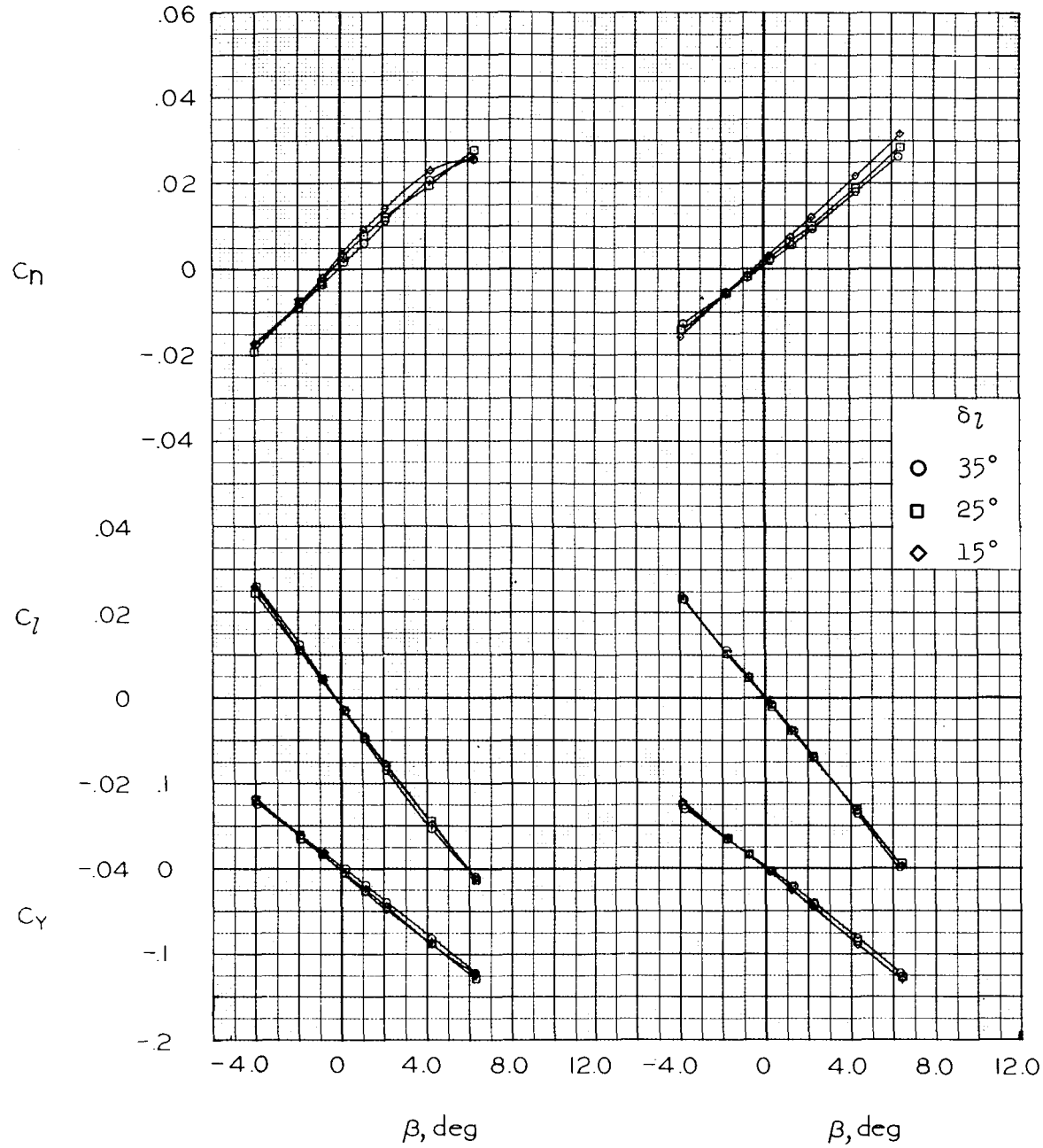

(c) M = 0.90, R = 6.5×10^6 (d) M = 1.10, R = 5.7×10^6

Figure 24.- Continued.

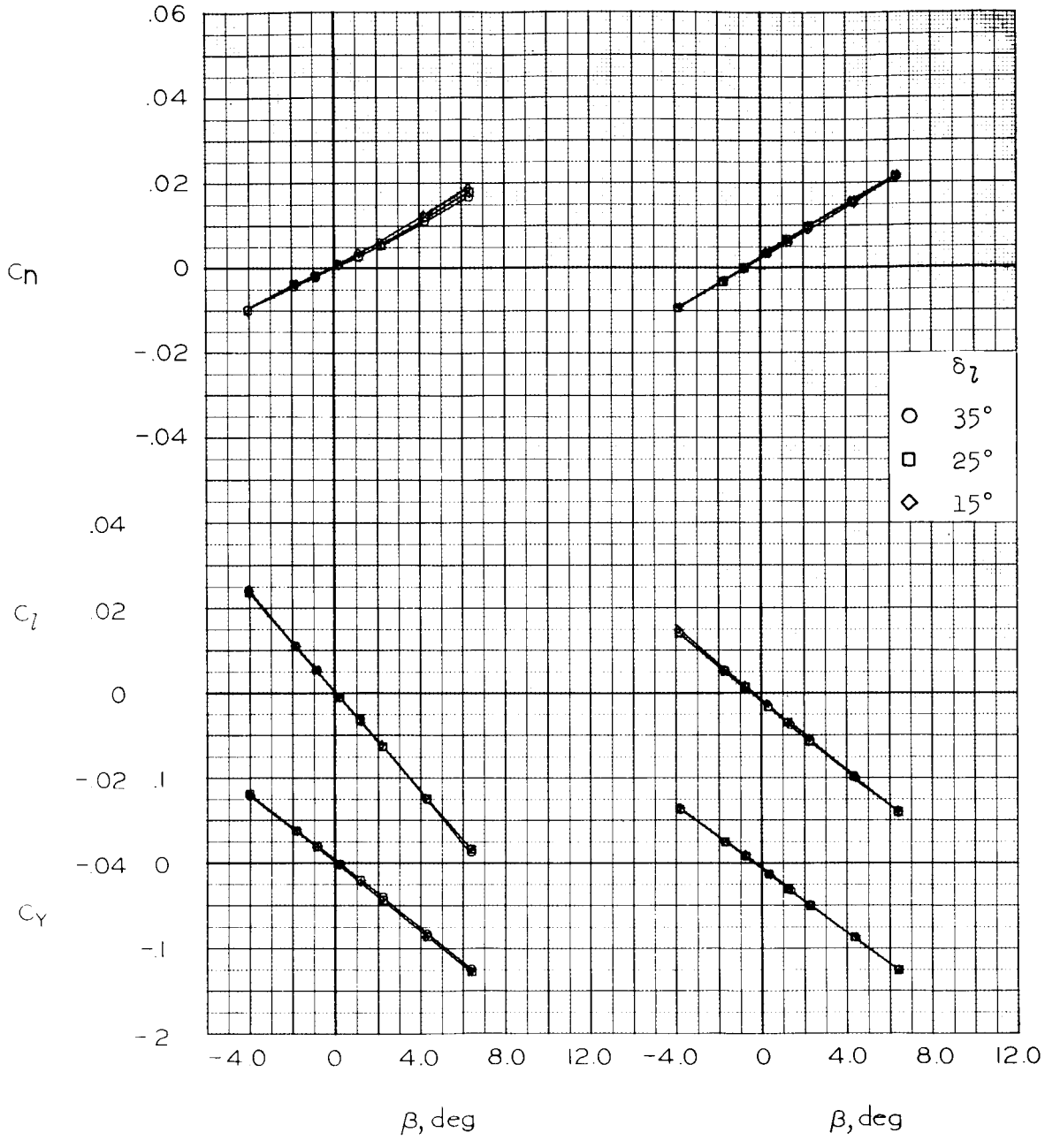

(e) M = 1.30, R = 5.7×10^6 (f) M = 2.00, R = 4.0×10^6

Figure 24.- Concluded.

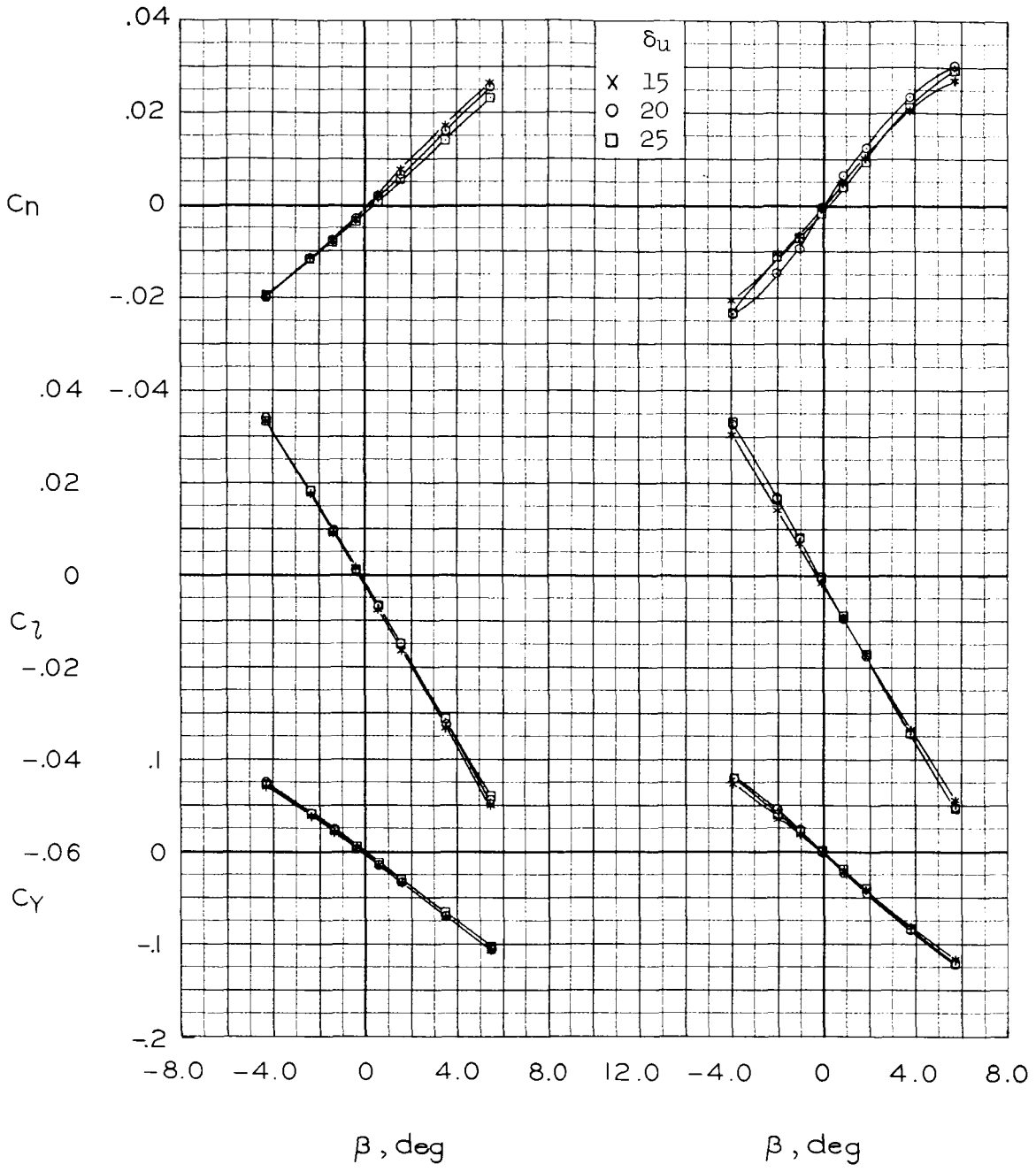

(a) M = 0.60, R = 5.6×10^6 (b) M = 0.80, R = 6.5×10^6

Figure 25.- Lateral-directional characteristics at selected upper-flap deflections; $\alpha = 6°$, $\delta_u = -15°$, $\delta_{rf} = 5°$.

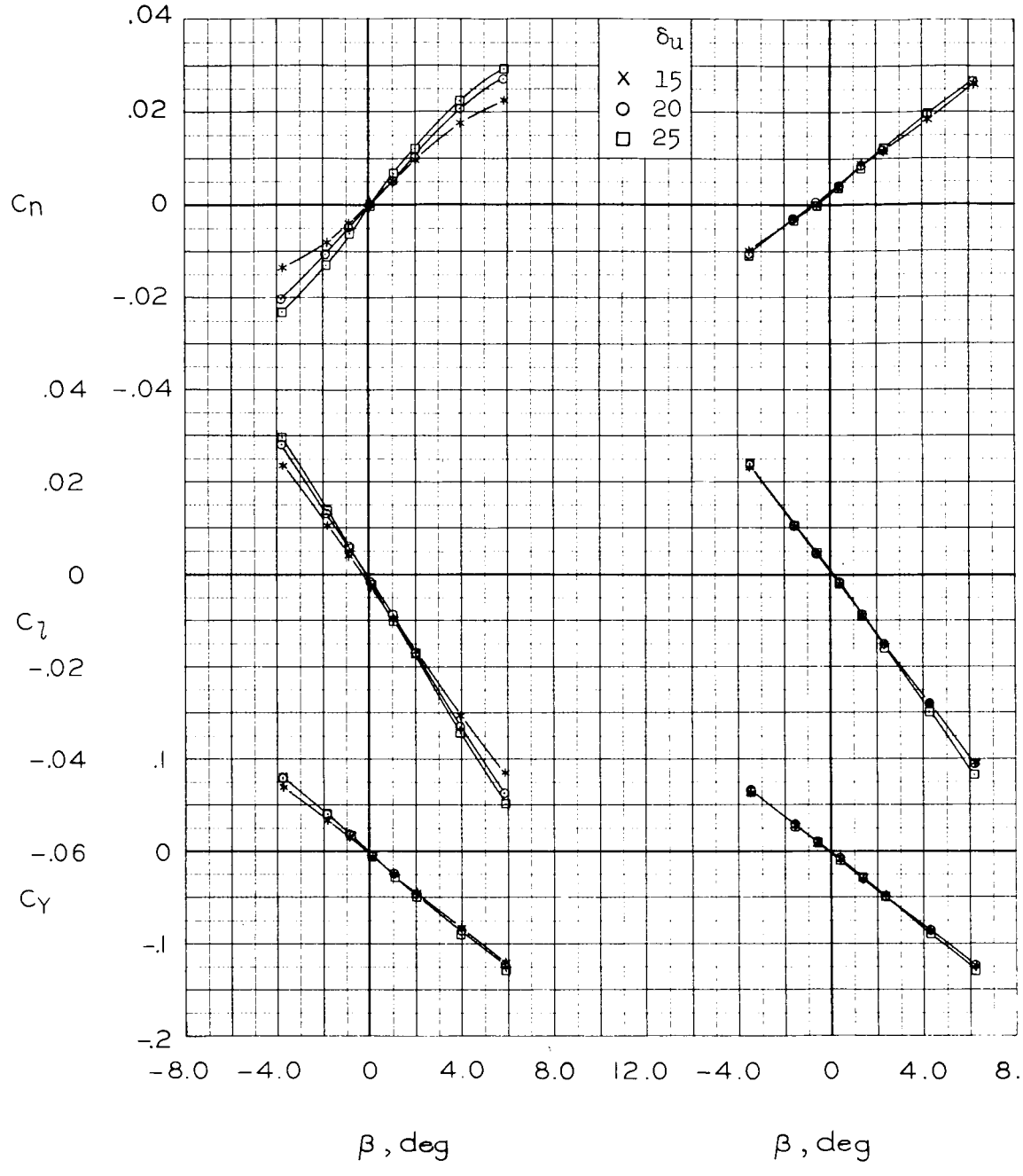

(c) M = 0.90, R = 6.5×10^6 (d) M = 1.10, R = 5.7×10^6

Figure 25.- Continued.

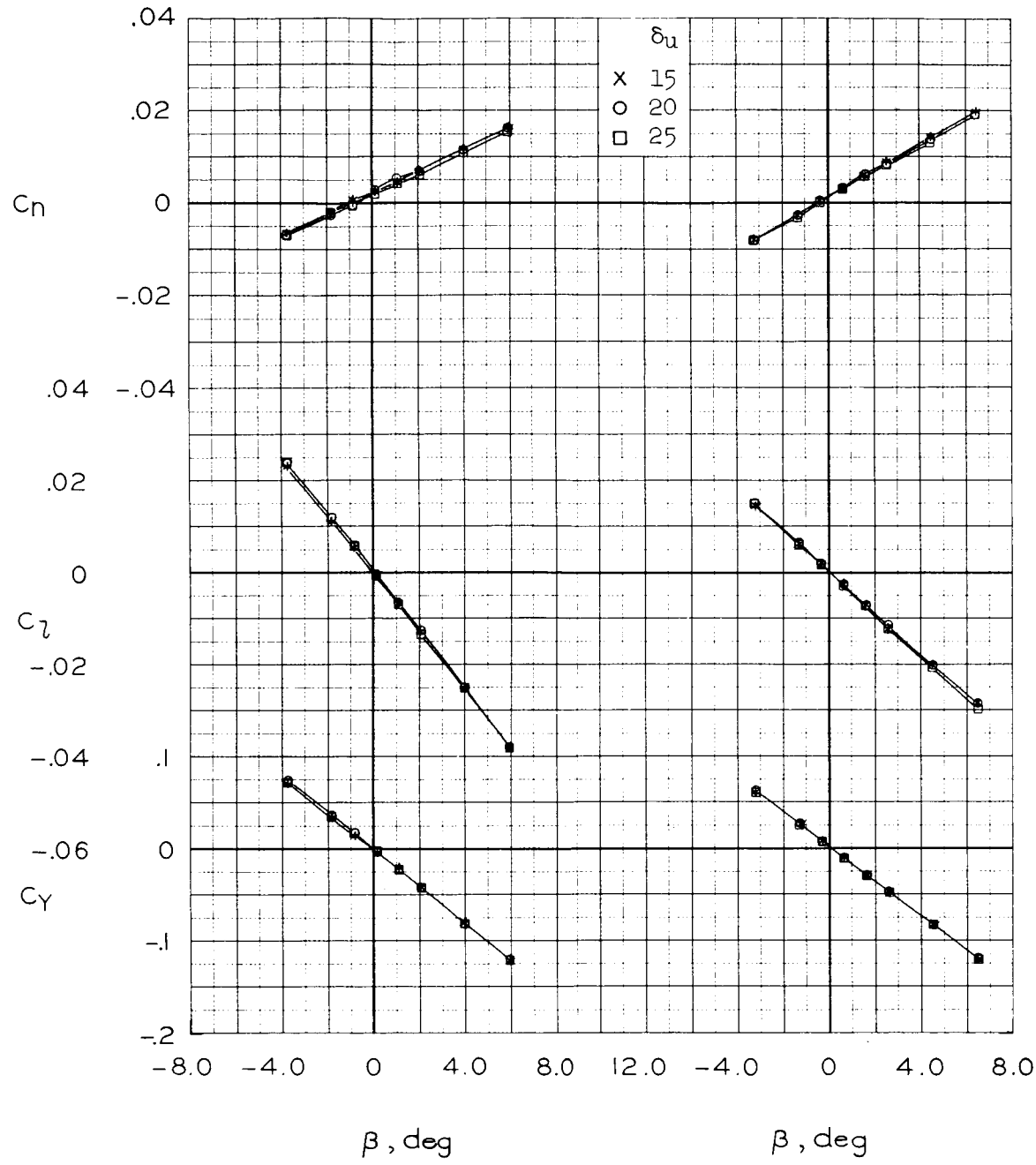

(e) M = 1.30, R = 5.7×10^6 (f) M = 2.00, R = 4.0×10^6

Figure 25.- Concluded.

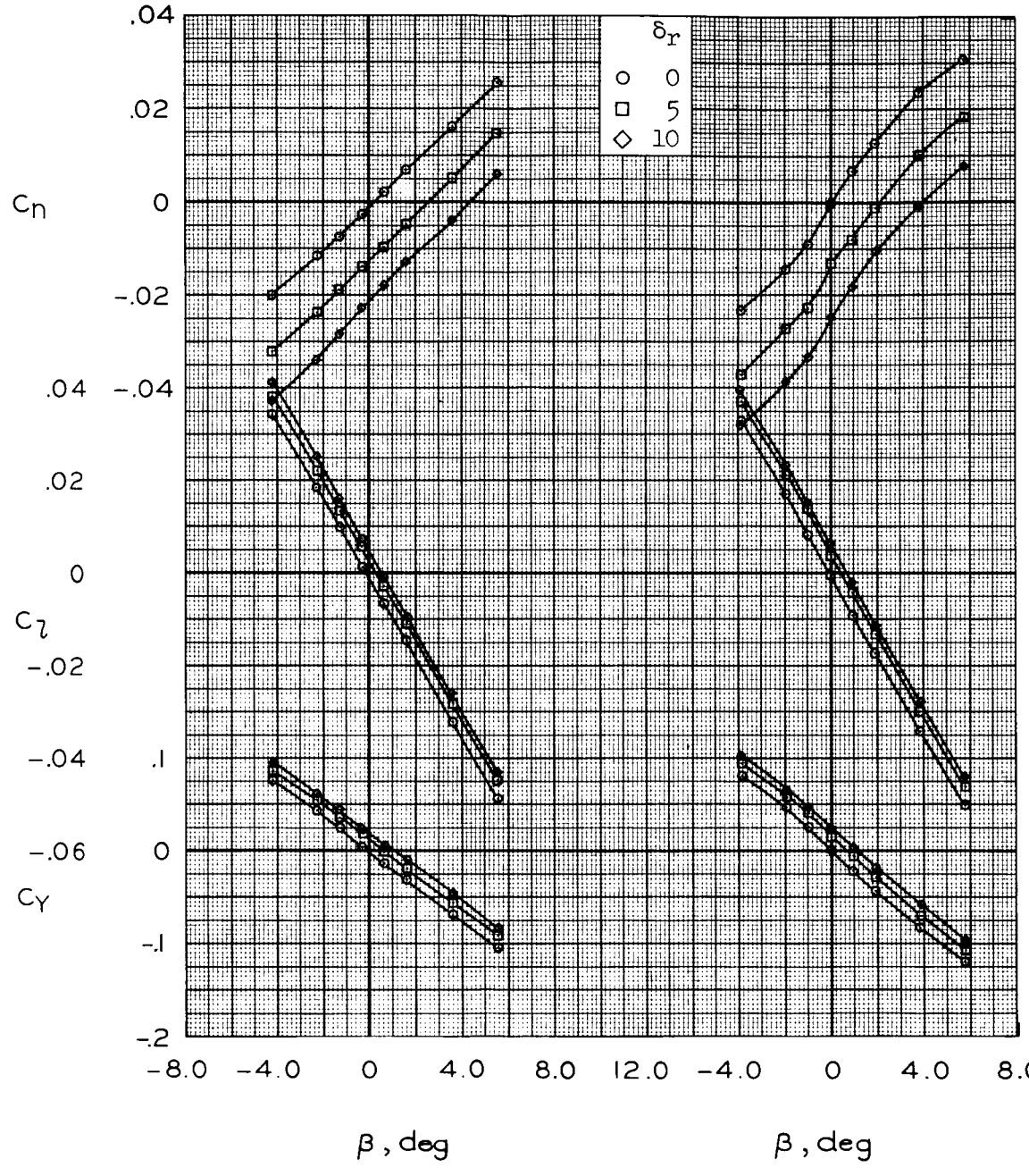

(a) M = 0.60, R = 5.8×10^6 (b) M = 0.80, R = 6.6×10^6

Figure 26.- Lateral-directional characteristics at selected rudder deflections; $\alpha = 6°$, $\delta_u = -20°$, $\delta_l = 35°$, $\delta_{rf} = 0°$.

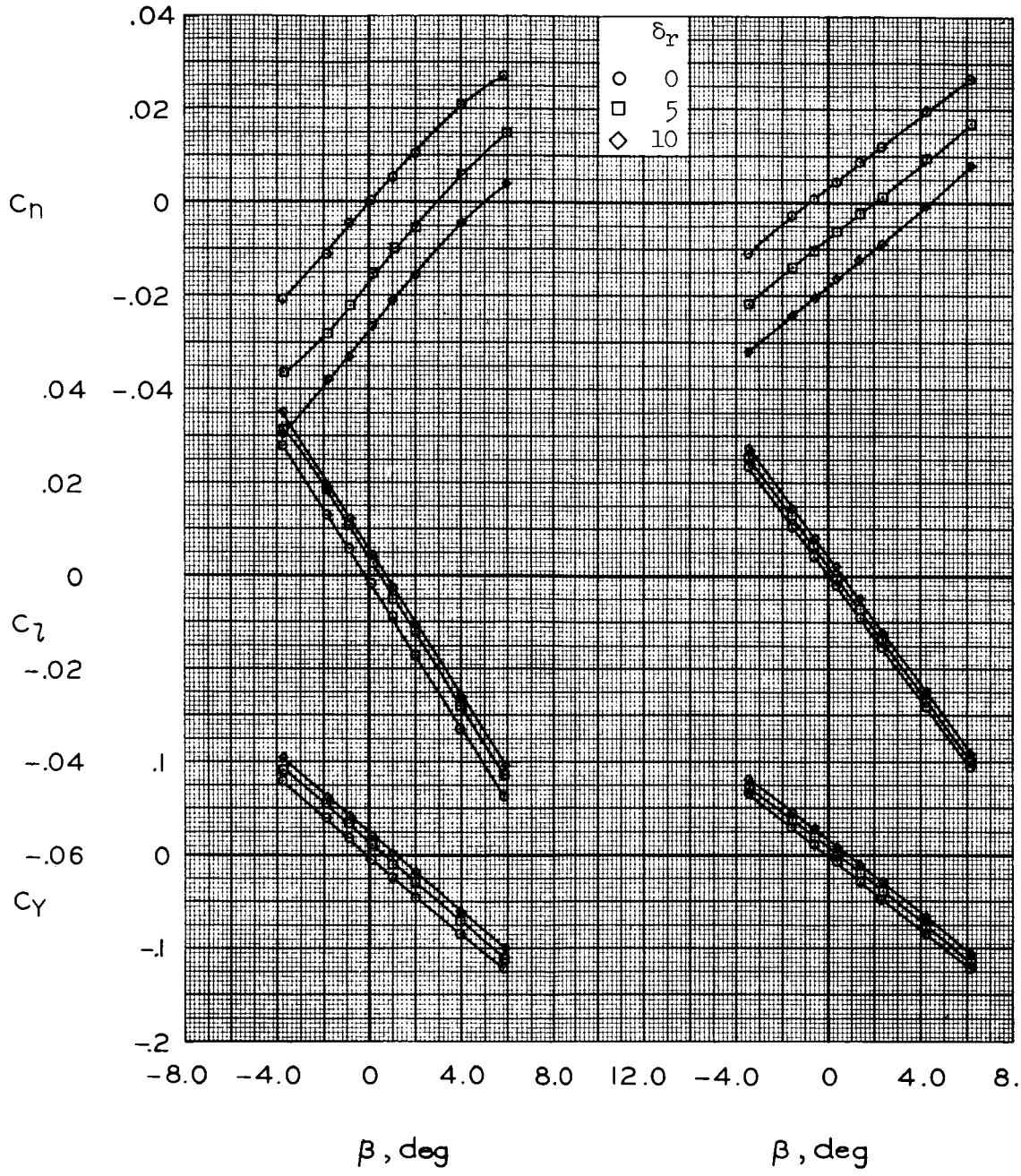

(c) M = 0.90, R = 6.5×10^6 (d) M = 1.10, R = 4.2×10^6

Figure 26.- Continued.

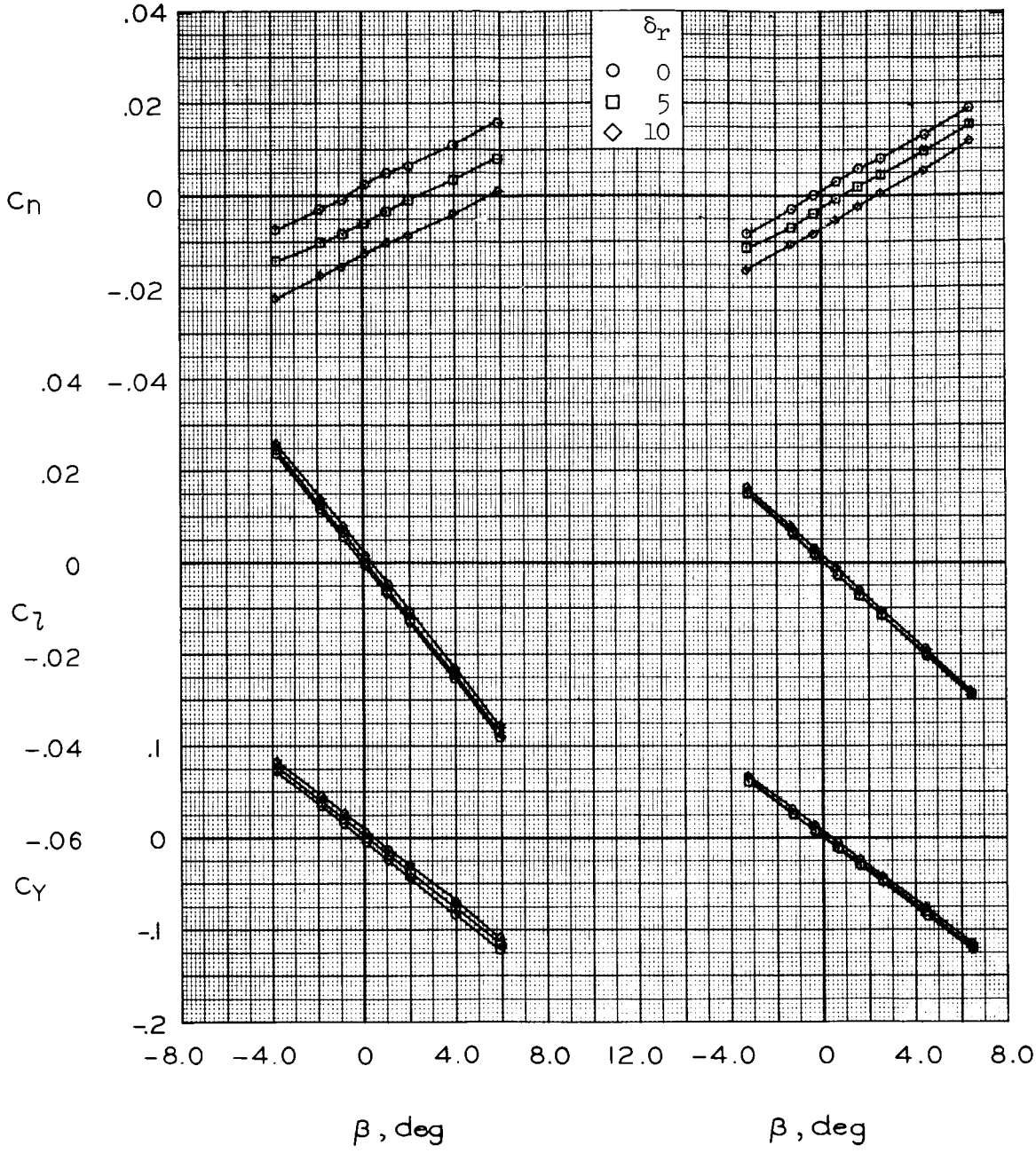

(e) M = 1.30, R = 4.2×10^6 (f) M = 2.00, R = 4.2×10^6

Figure 26.- Concluded.

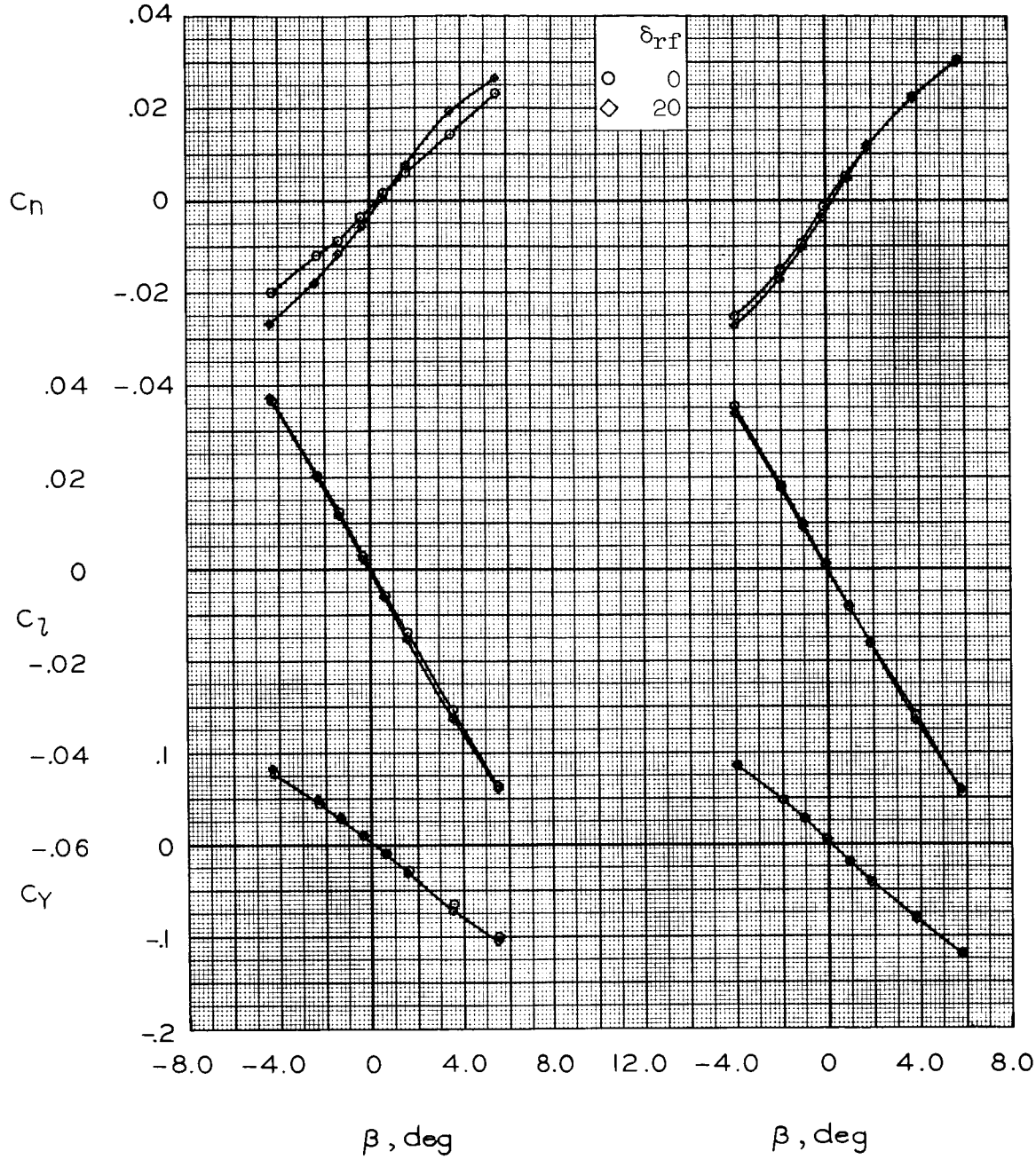

(a) M = 0.60, R = 5.8×10^6 (b) M = 0.80, R = 6.6×10^6

Figure 27.- Lateral-directional characteristics at two rudder-flare deflections; $\alpha = 6°$, $\delta_u = -20°$, $\delta_l = 35°$.

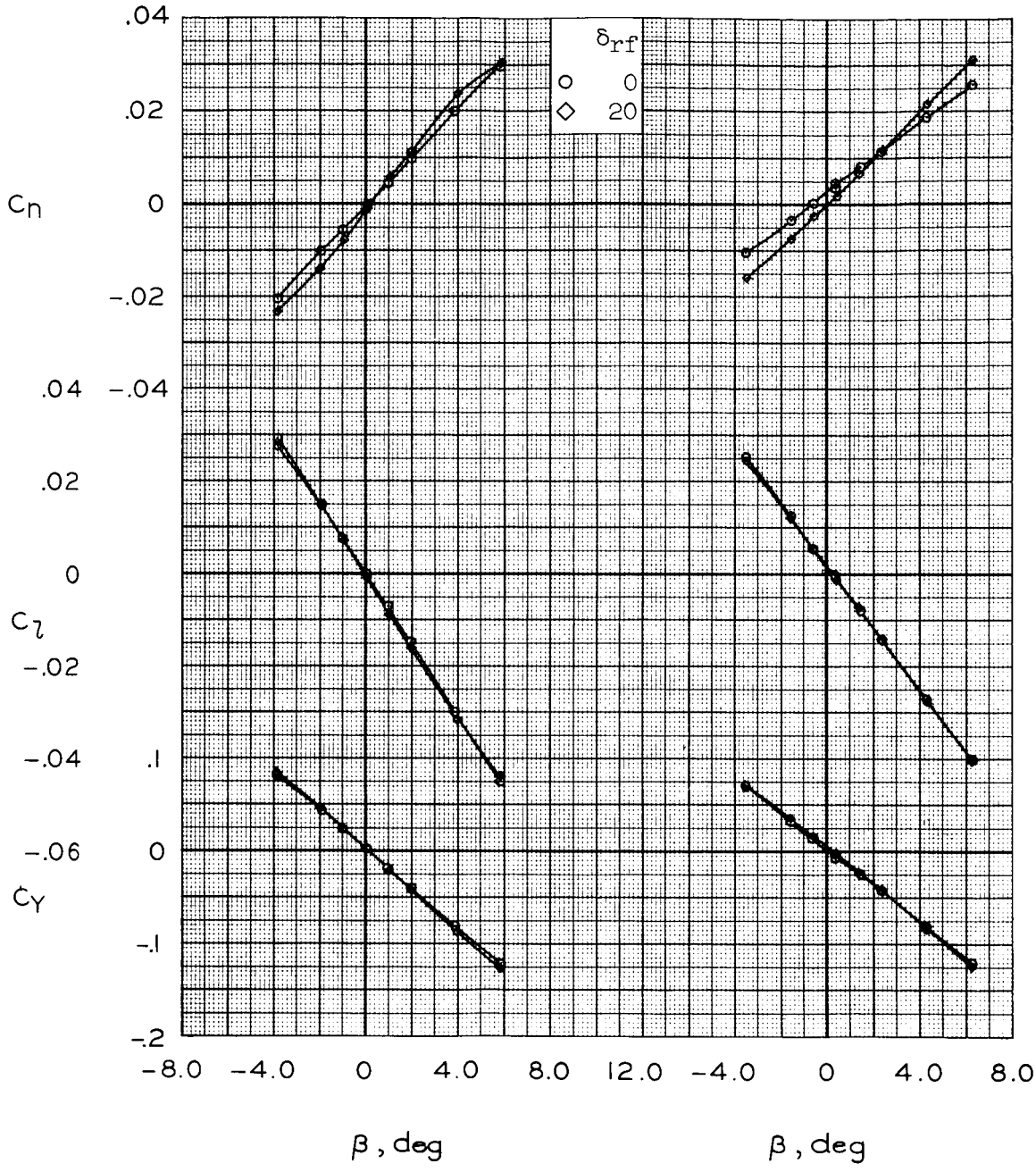

(c) M = 0.90, R = 6.5×10^6 (d) M = 1.10, R = 4.2×10^6

Figure 27.- Continued.

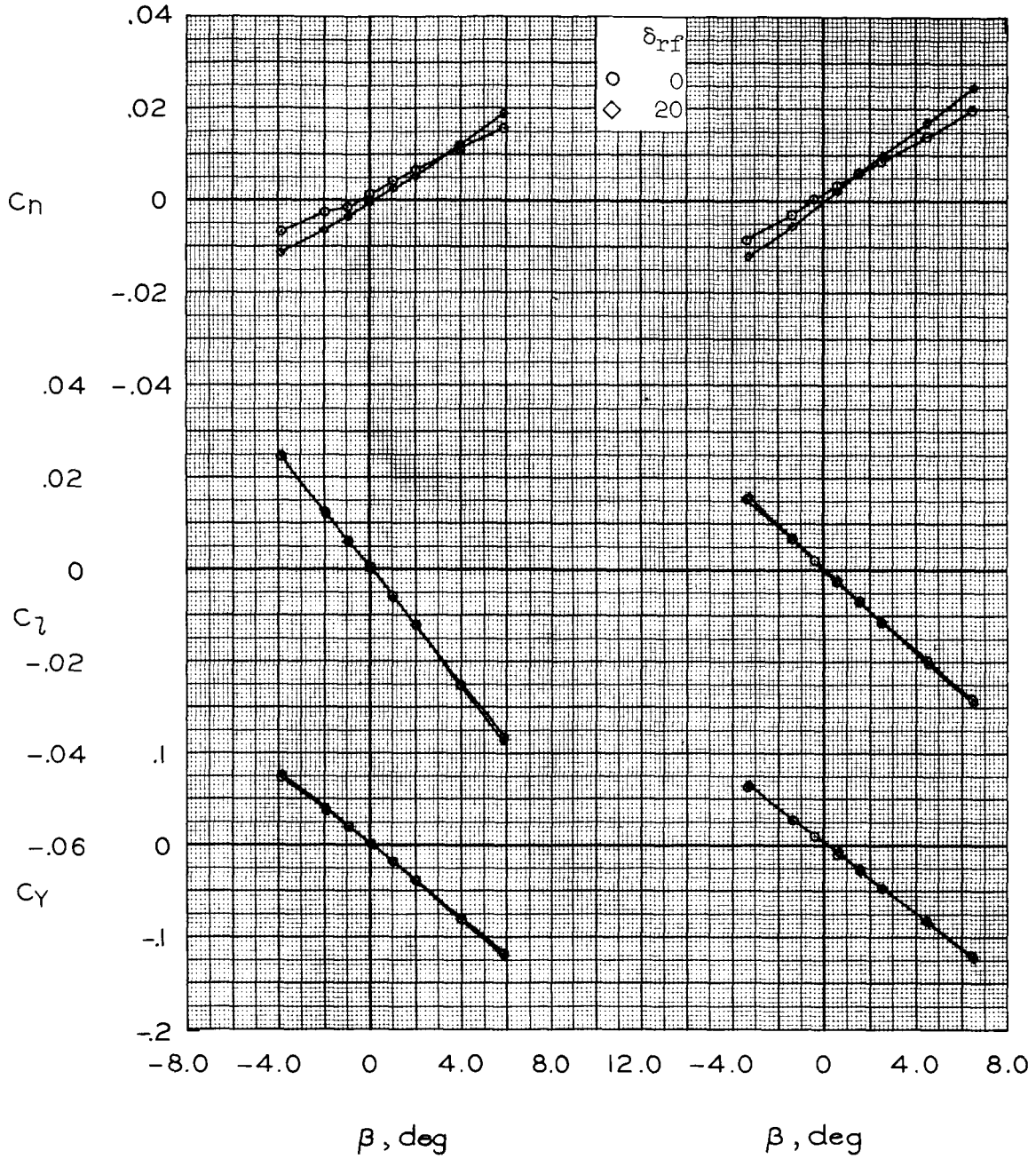

(e) M = 1.30, R = 4.2×10^6 (f) M = 2.00, R = 4.2×10^6

Figure 27.- Concluded.

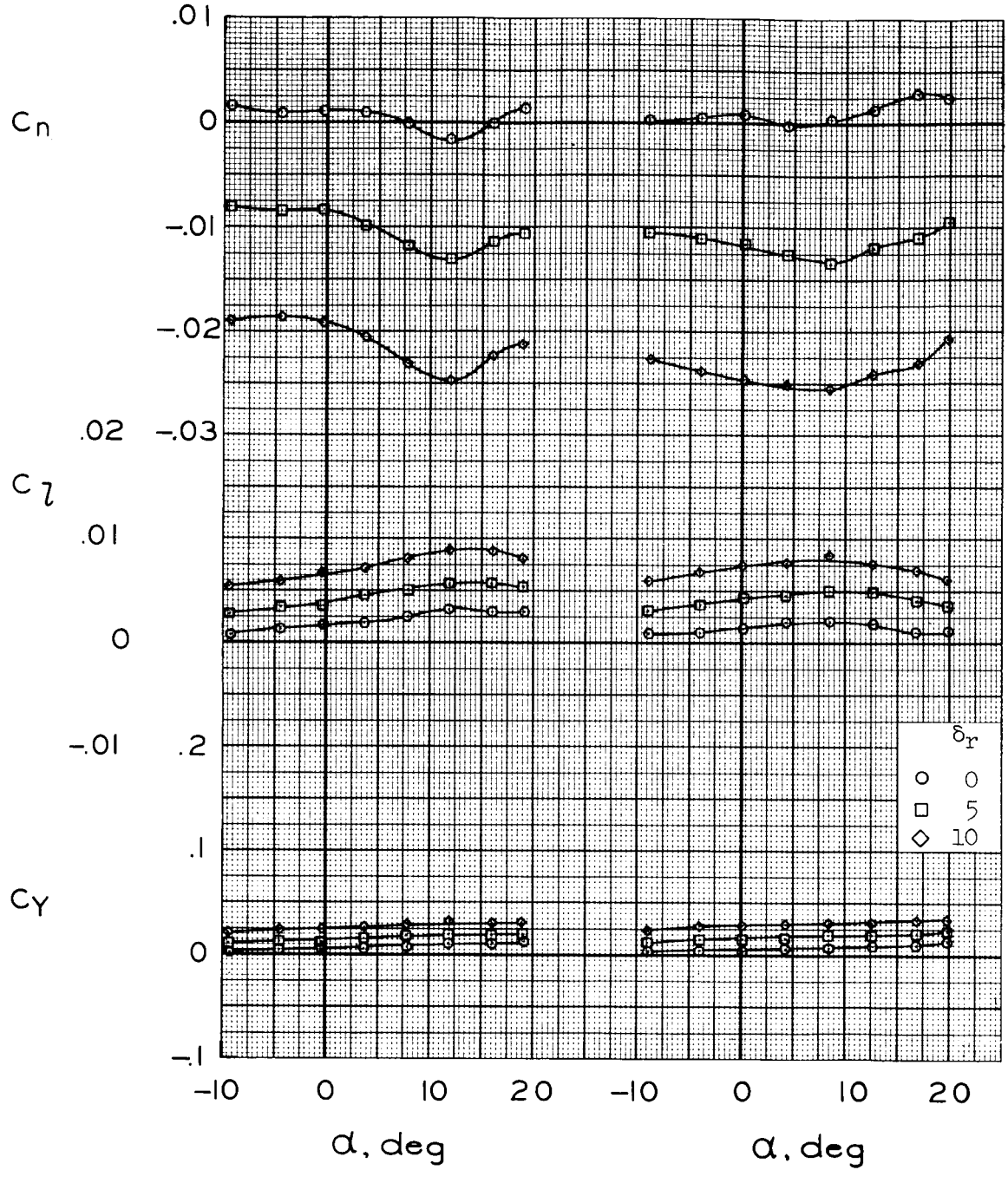

(a) M = 0.60, R = 5.8×10^6 (b) M = 0.80, R = 6.6×10^6

Figure 28.- Effect of rudder deflection on lateral-directional control; $\beta = 0°$, $\delta_u = -20°$, $\delta_l = 35°$, $\delta_{rf} = 0°$.

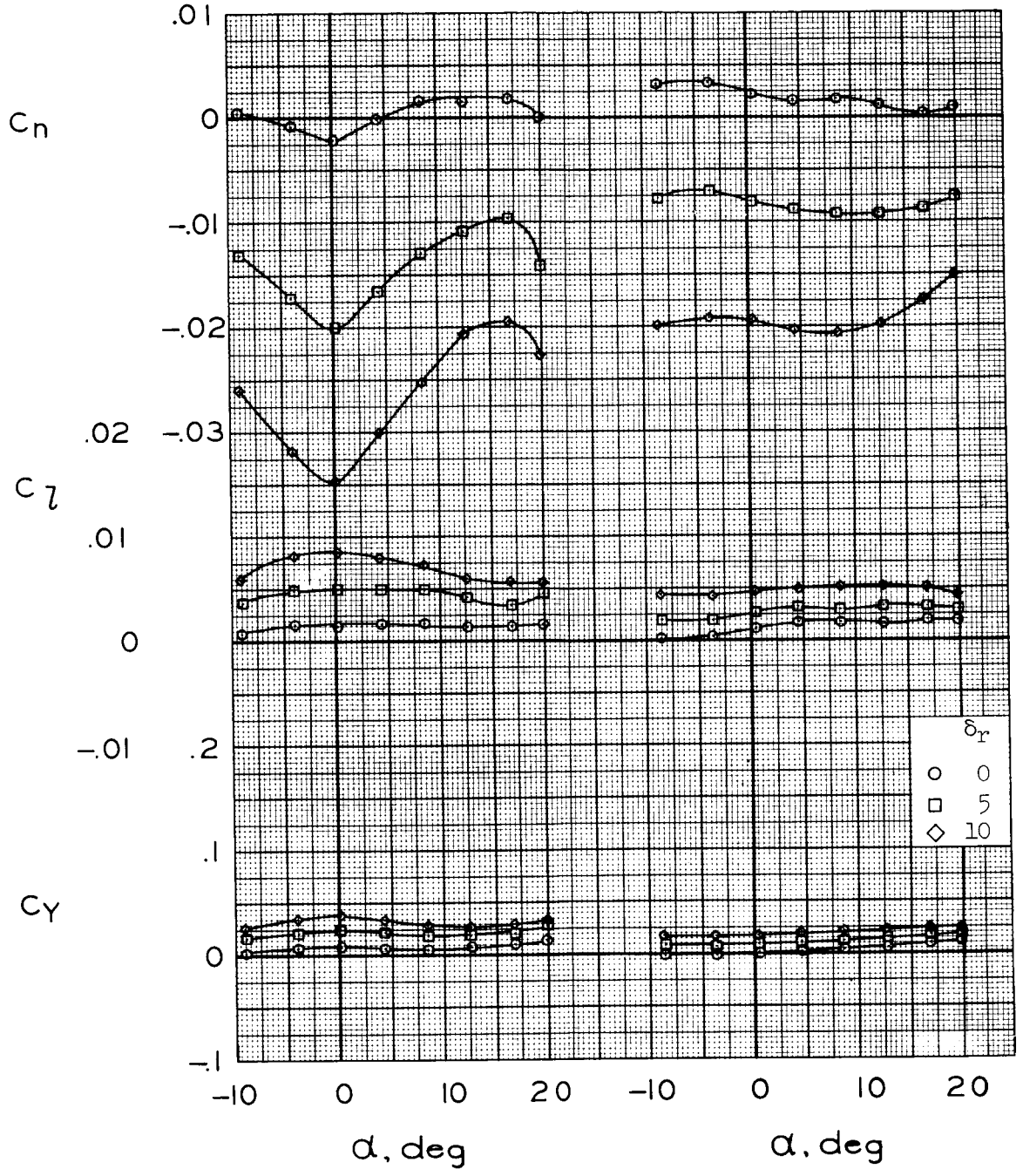

(c) M = 0.90, R = 6.5×10^6 (d) M = 1.10, R = 4.2×10^6

Figure 28.- Continued.

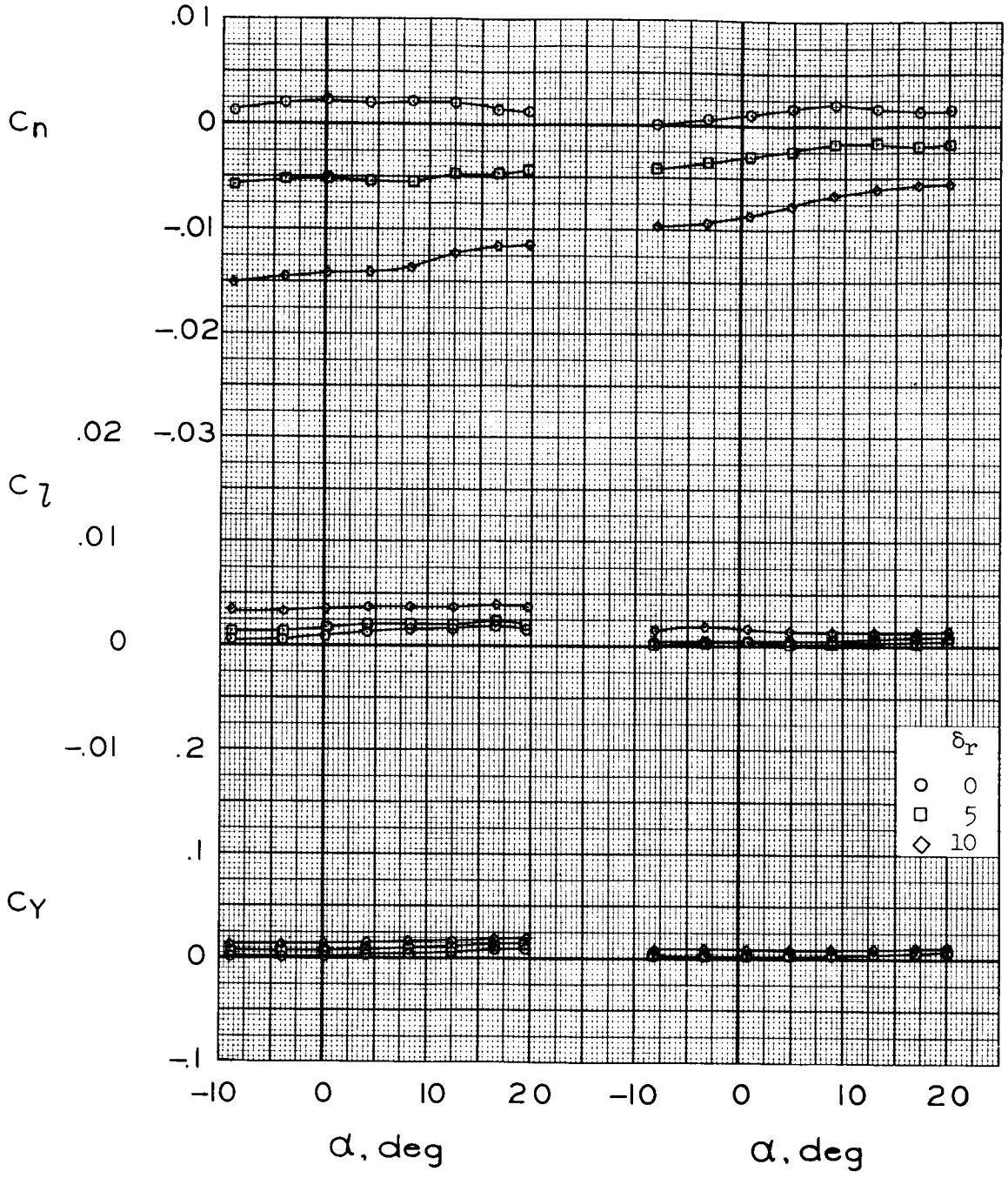

(e) M = 1.30, R = 4.2×10^6 (f) M = 2.00, R = 4.2×10^6

Figure 28.- Concluded.

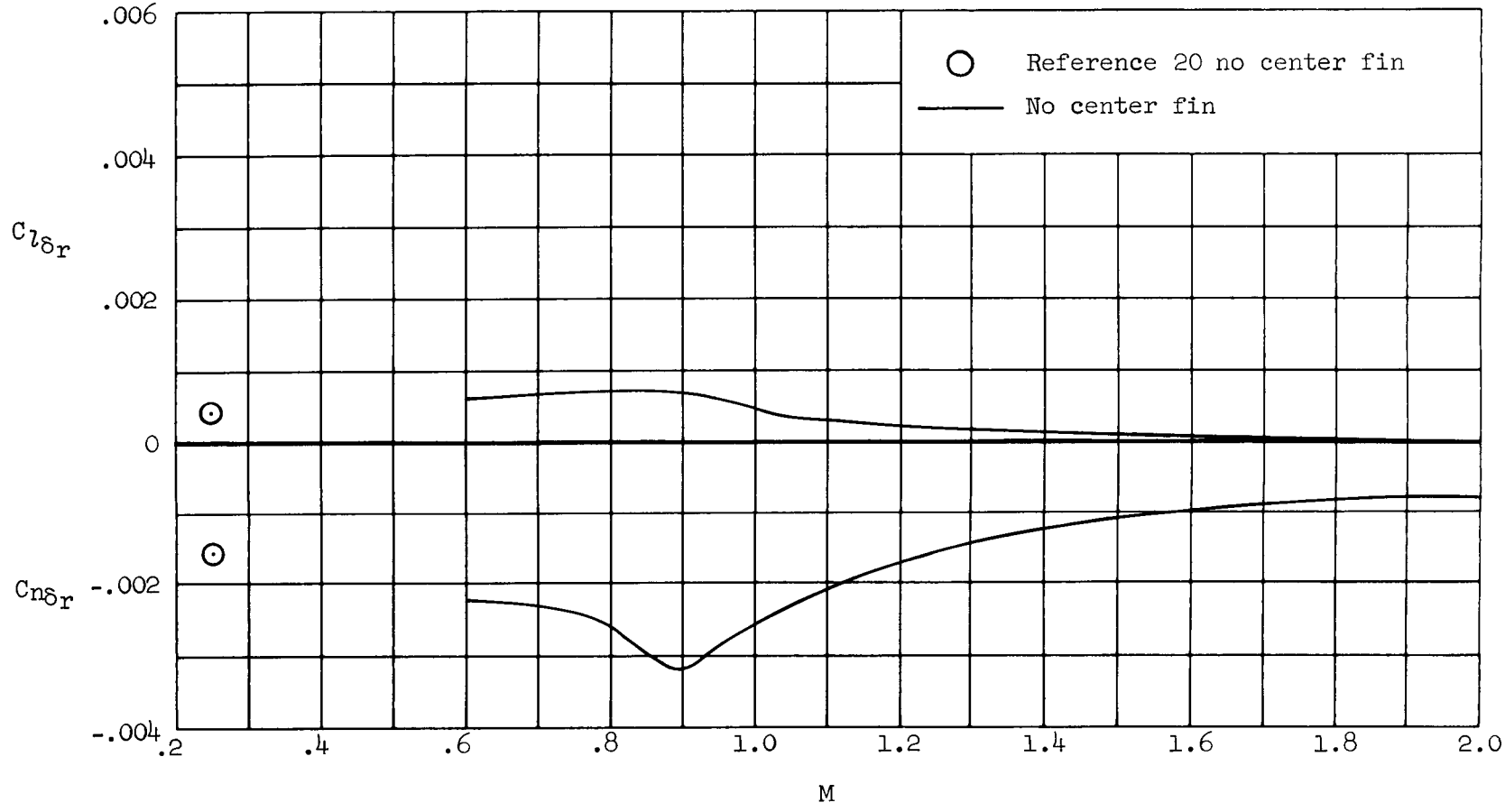

Figure 29.- Variation of rudder effectiveness with Mach number; $\alpha = 0.6°$, $\beta = 0°$, $\delta_u = -20°$, $\delta_l = 35°$, $\delta_{rf} = 0°$.

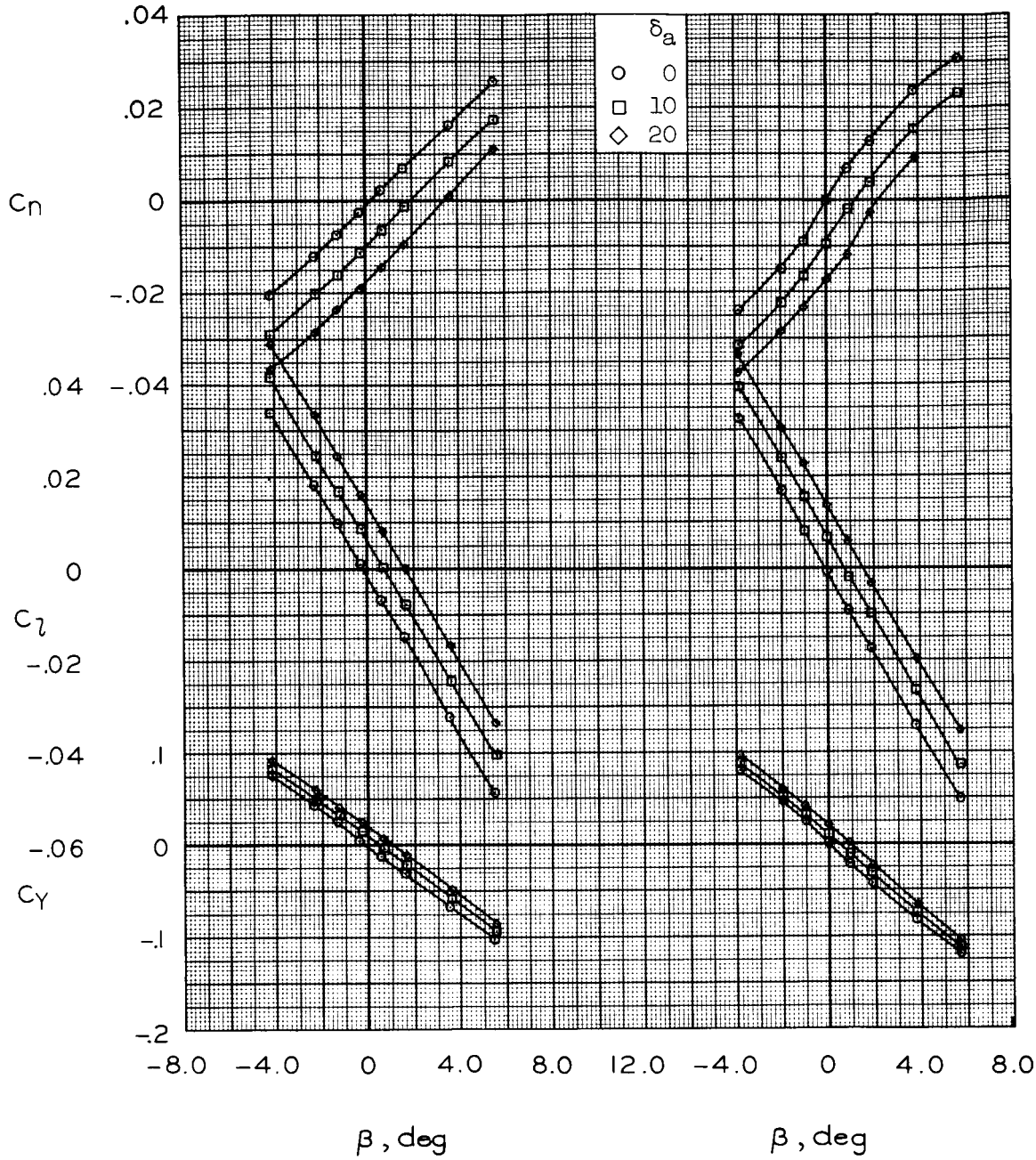

(a) M = 0.60, R = 5.8×10^6 (b) M = 0.80, R = 6.6×10^6

Figure 30.- Lateral-directional characteristics at selected aileron deflections without center fin; $\alpha = 6°$, $\delta_u = -20°$, $\delta_l = 35°$, $\delta_{rf} = 0°$.

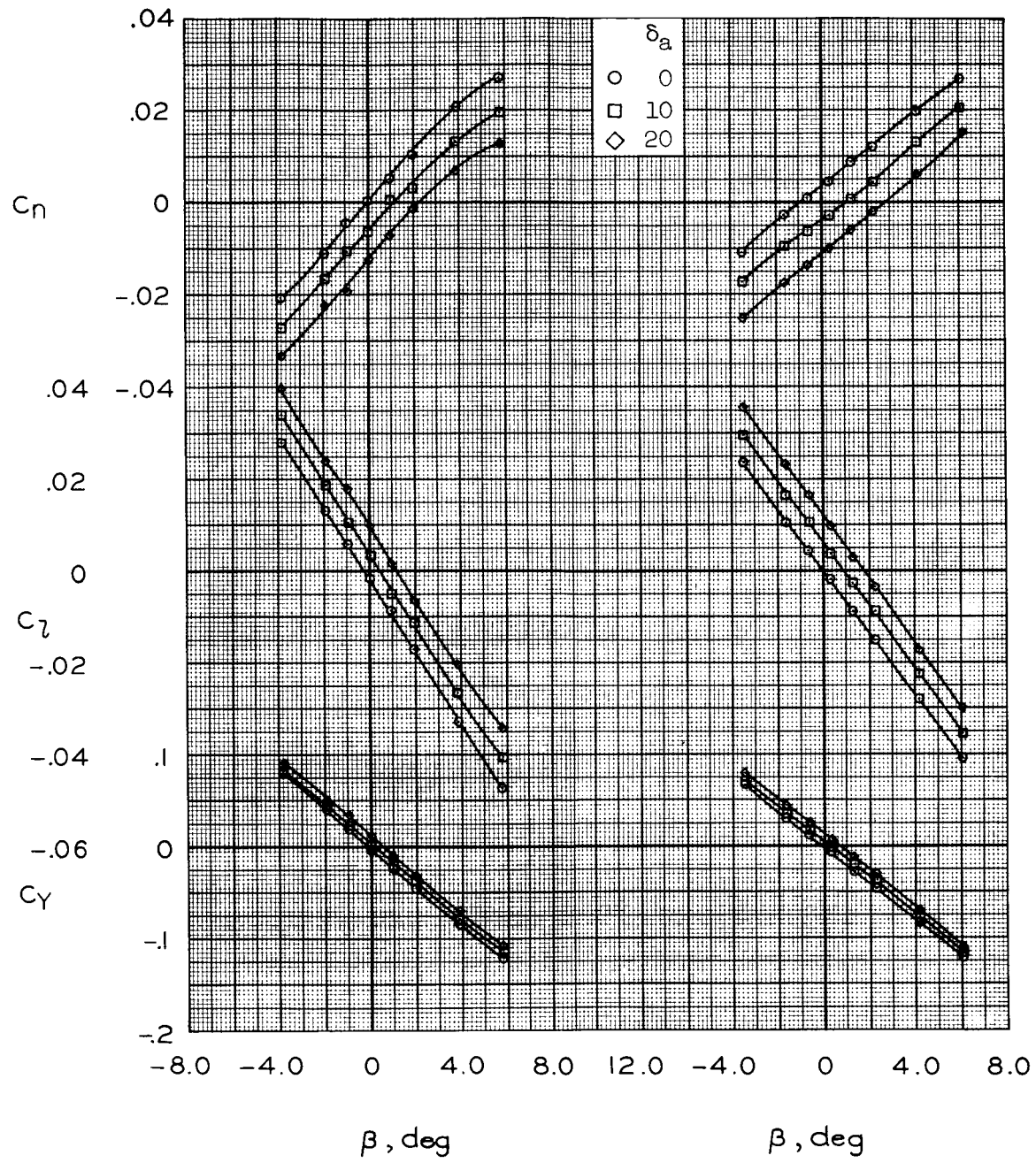

(c) M = 0.90, R = 6.5×10^6 (d) M = 1.10, R = 4.2×10^6

Figure 30.- Continued.

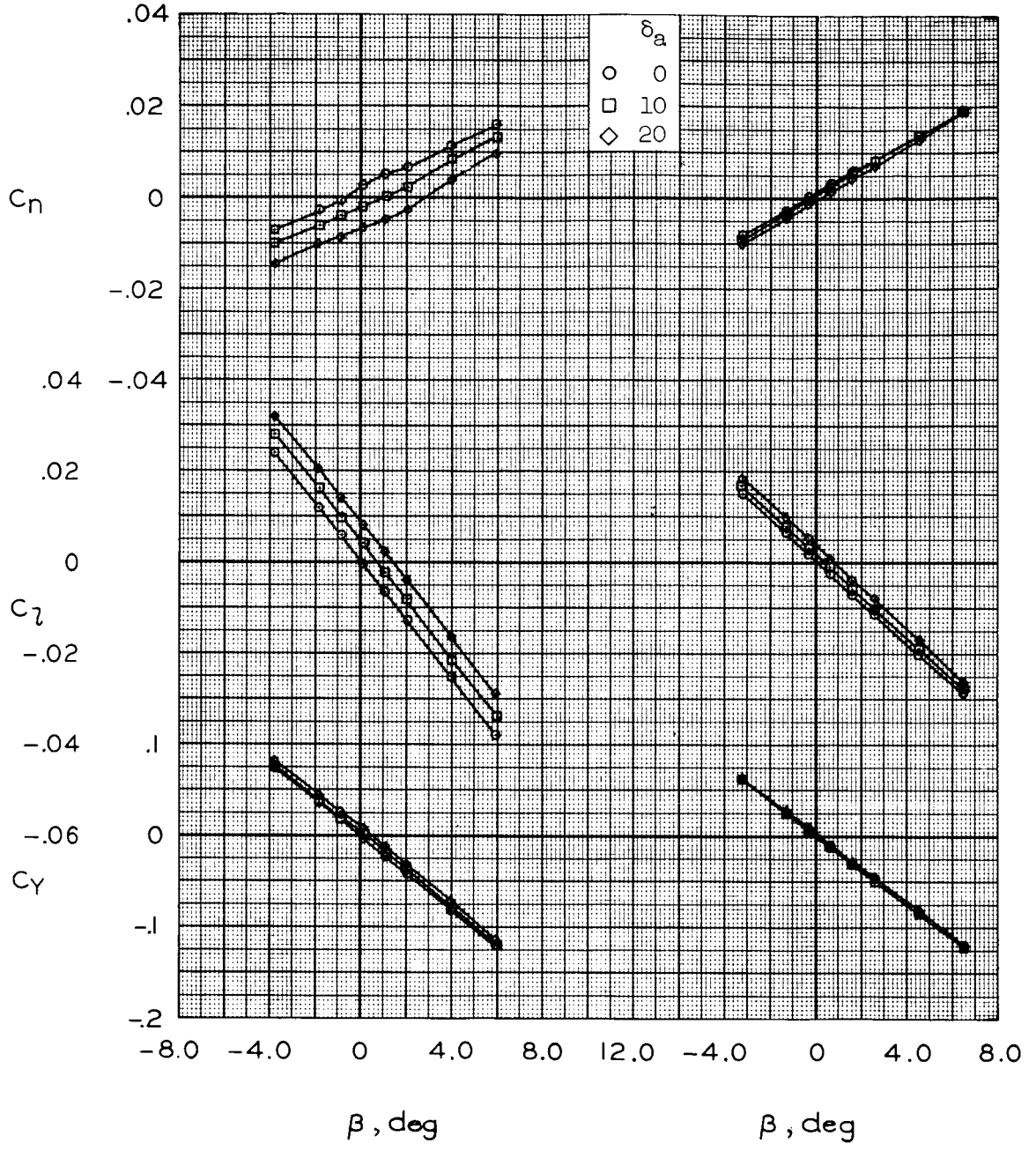

(e) M = 1.30, R = 4.2×10^6 (f) M = 2.00, R = 4.2×10^6

Figure 30.- Concluded.

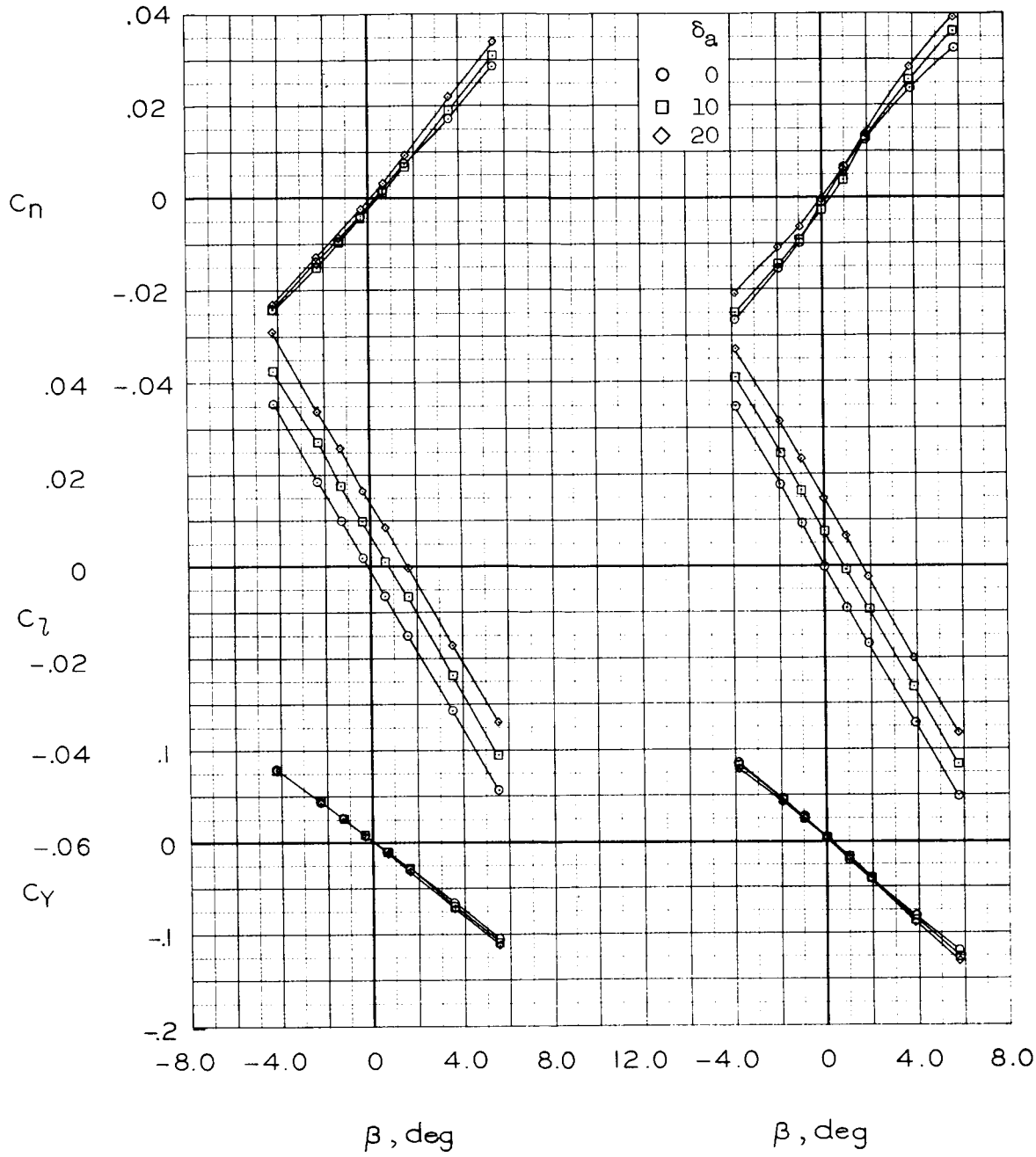

(a) M = 0.60, R = 5.8×10^6 (b) M = 0.80, R = 6.6×10^6

Figure 31.- Lateral-directional characteristics at selected aileron deflections with center fin; $\alpha = 6°$, $\delta_u = -20°$, $\delta_l = 35°$, $\delta_{rf} = 0°$.

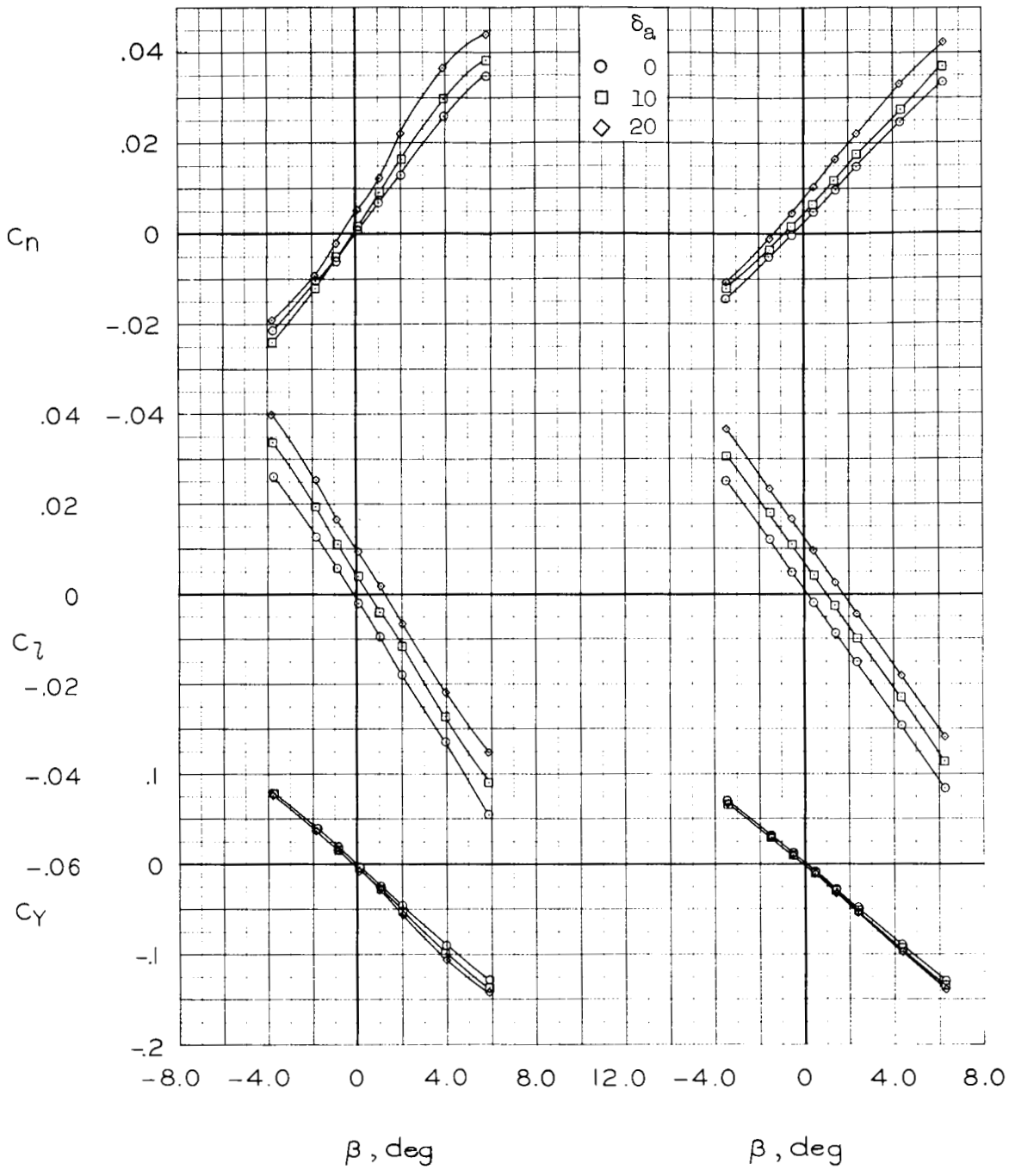

(c) M = 0.90, R = 6.5×10^6 (d) M = 1.10, R = 4.2×10^6

Figure 31.- Continued.

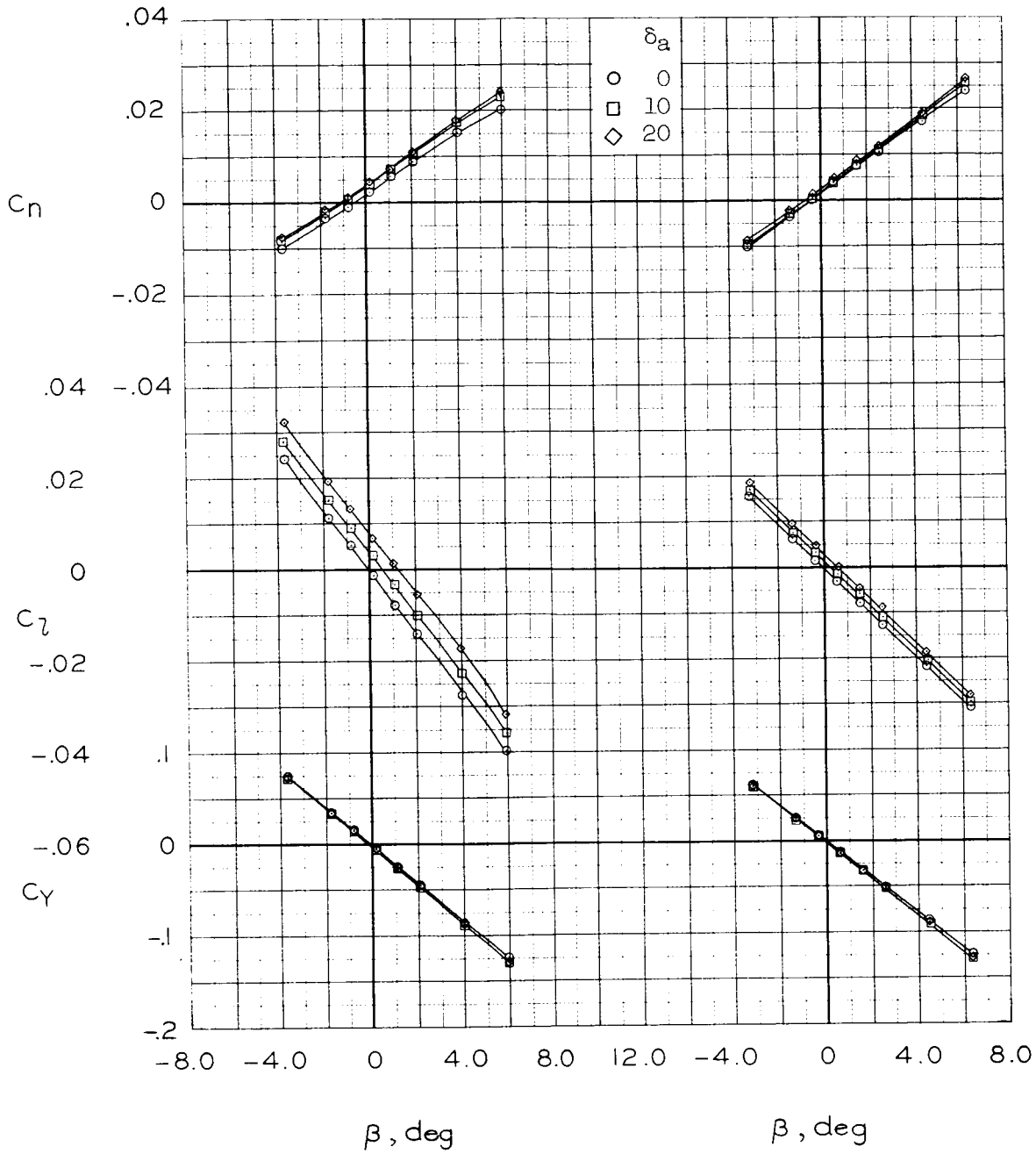

(e) M = 1.30, R = 4.2×10^6 (f) M = 2.00, R = 4.2×10^6

Figure 31.- Concluded.

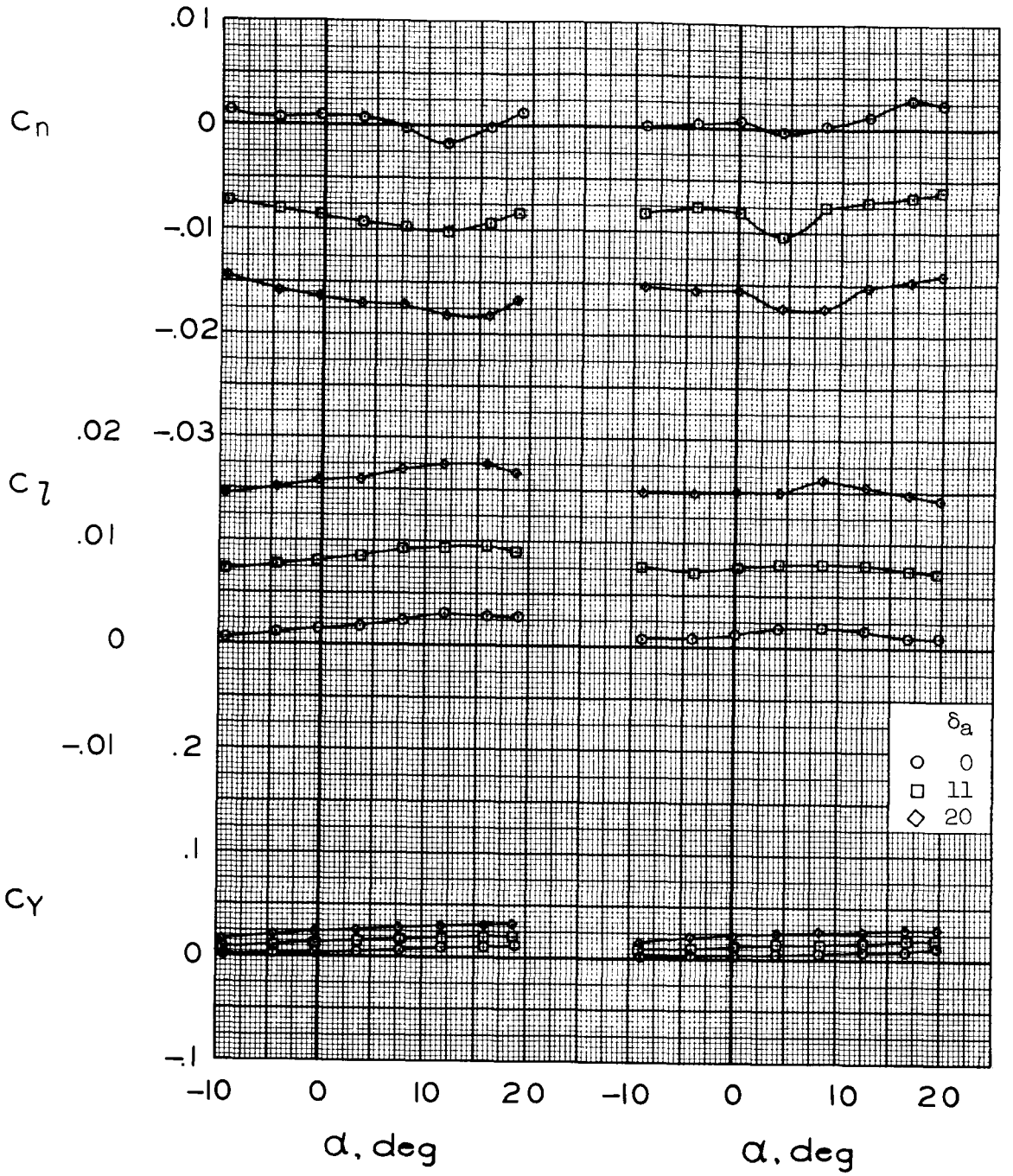

(a) M = 0.60, R = 5.8×10^6 (b) M = 0.80, R = 6.6×10^6

Figure 32.- Effect of aileron deflection on lateral-directional control without center fin; $\beta = 0°$, $\delta_u = -20°$, $\delta_l = 35°$, $\delta_{rf} = 0°$.

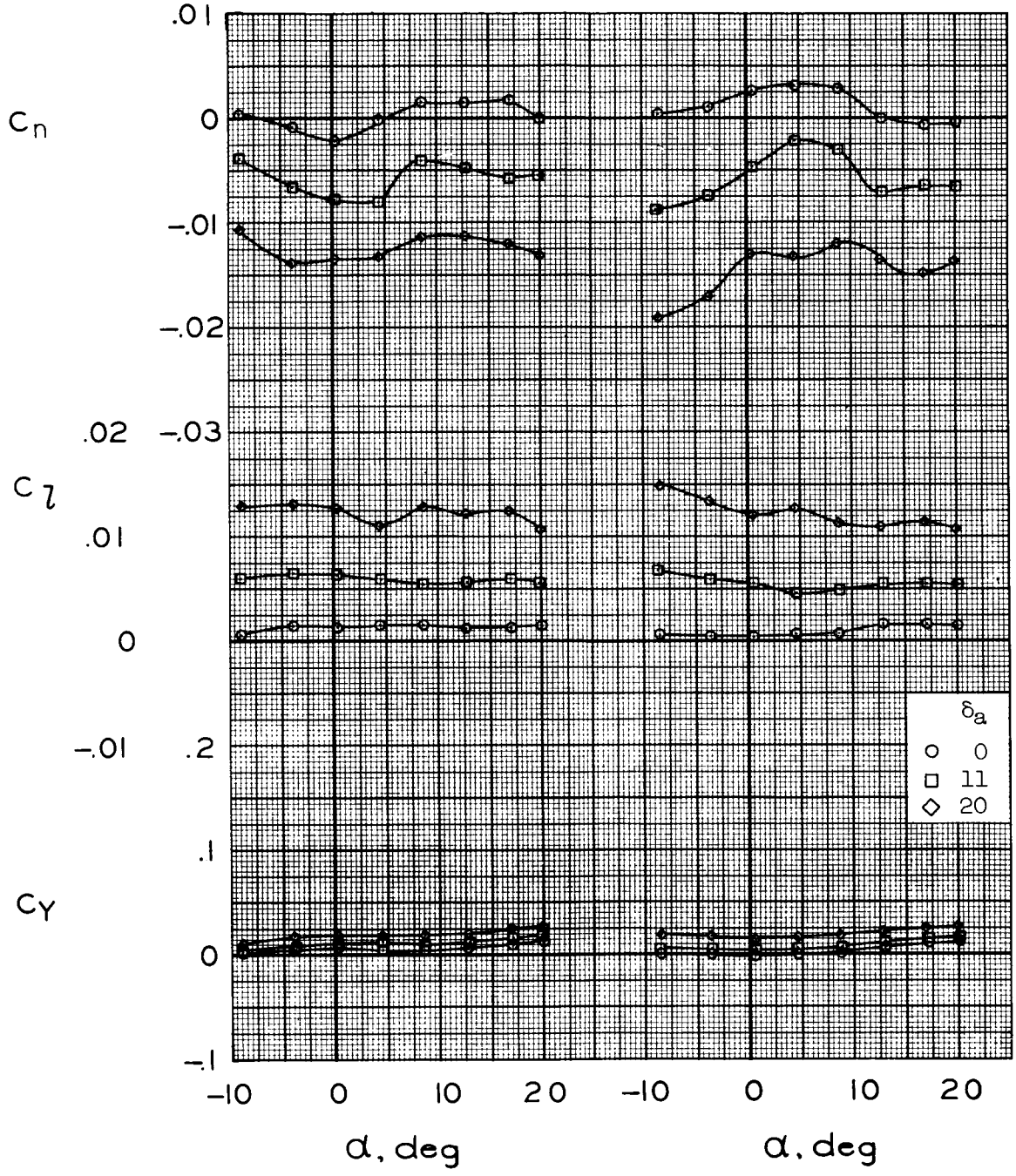

(c) M = 0.90, R = 6.5×10^6 (d) M = 0.95, R = 5.7×10^6

Figure 32.- Continued.

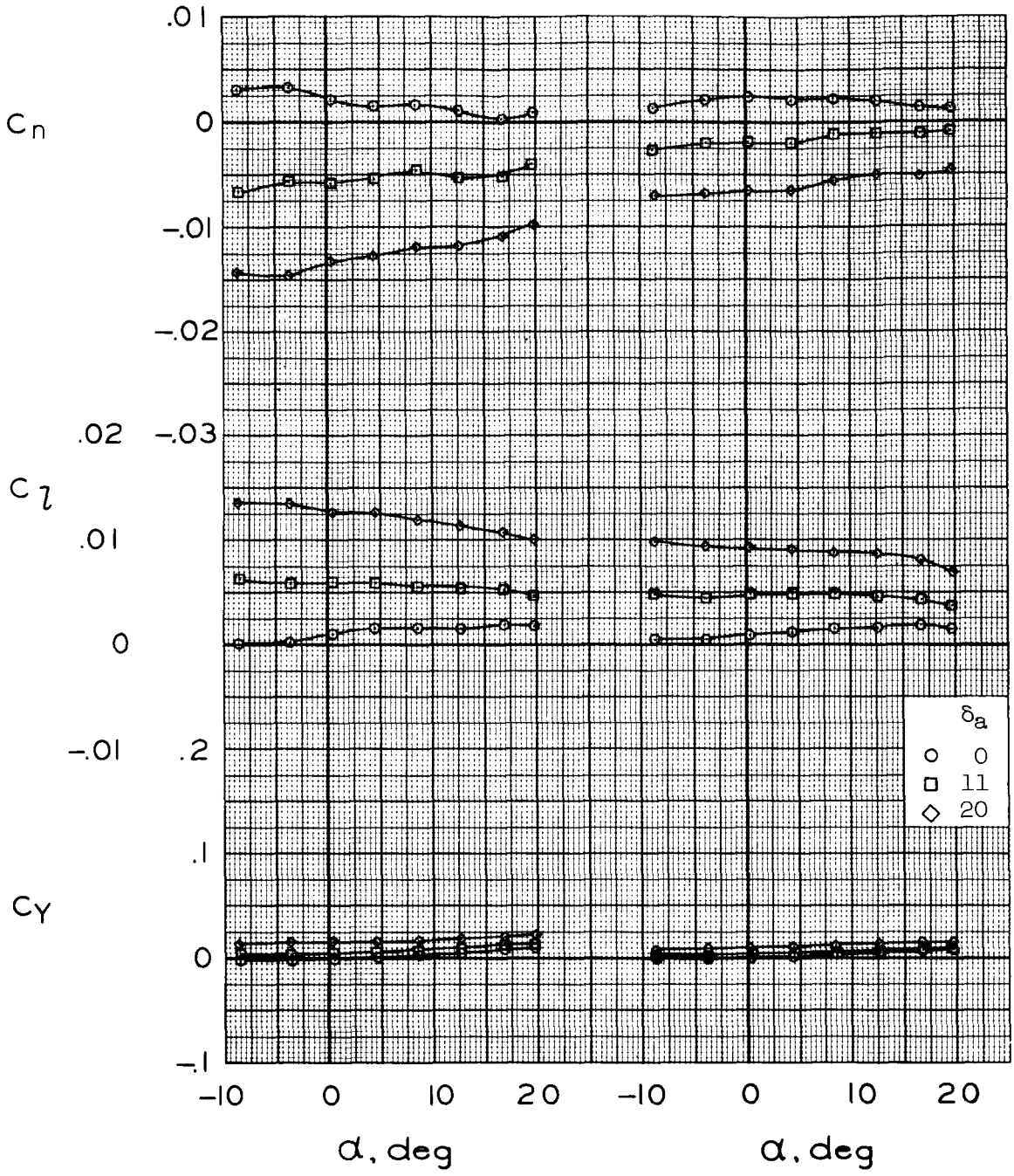

(e) M = 1.10, R = 4.2×10^6 (f) M = 1.30, R = 4.2×10^6

Figure 32.- Continued.

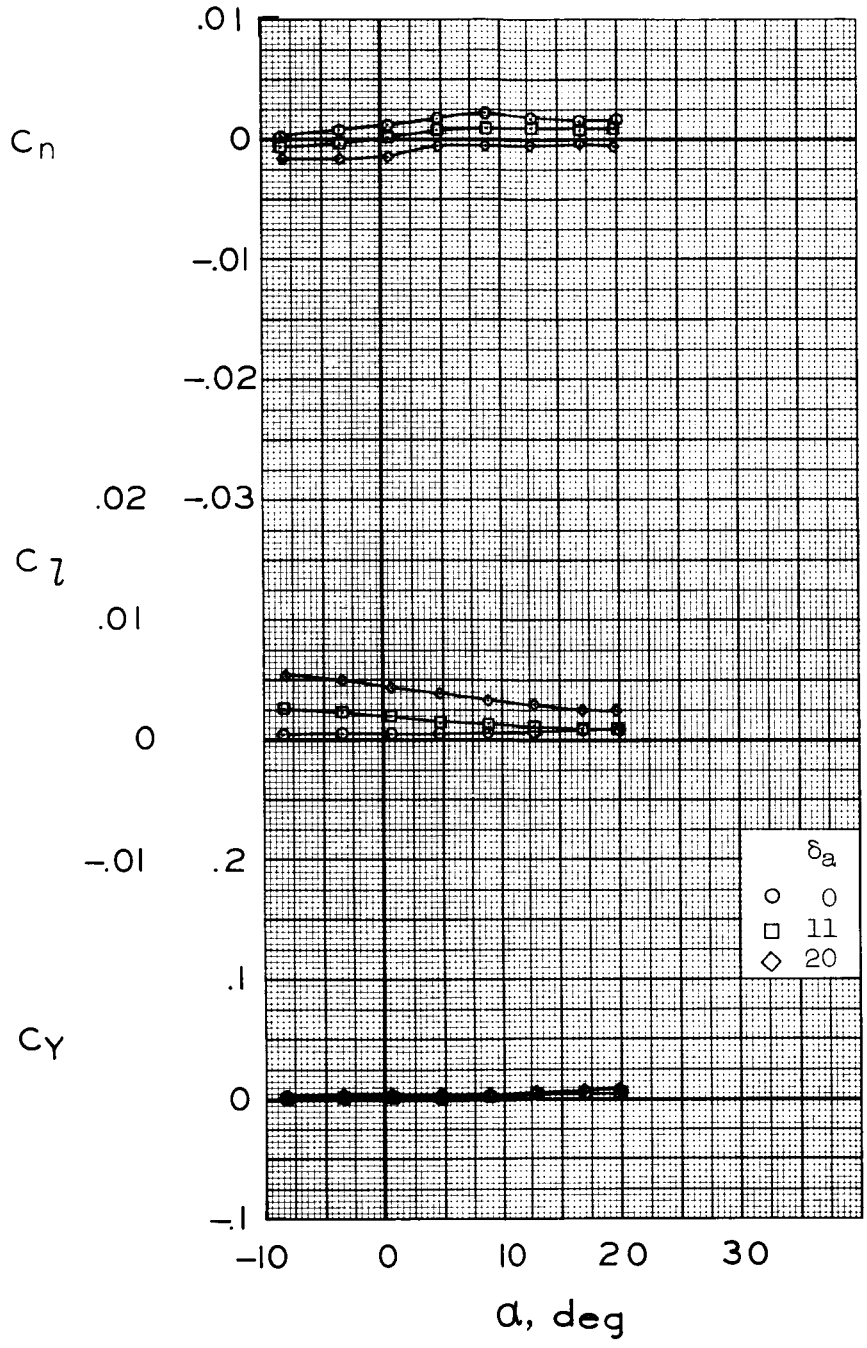

(g) M = 2.00, R = 4.2×10^6

Figure 32.- Concluded.

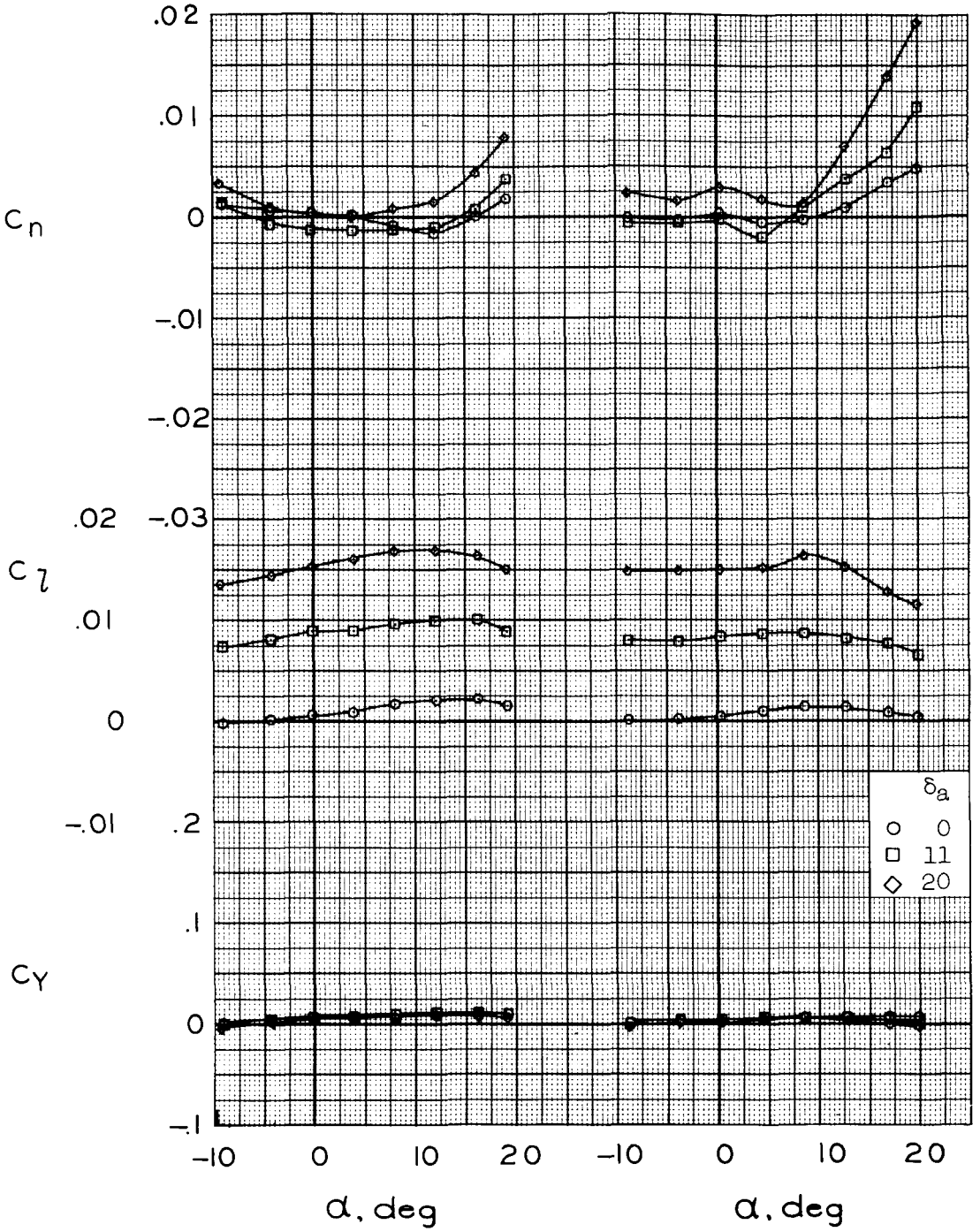

Figure 33.- Effect of aileron deflection on lateral-directional control with center fin; $\beta = 0°$, $\delta_u = -20°$, $\delta_l = 35°$, $\delta_{rf} = 0°$.

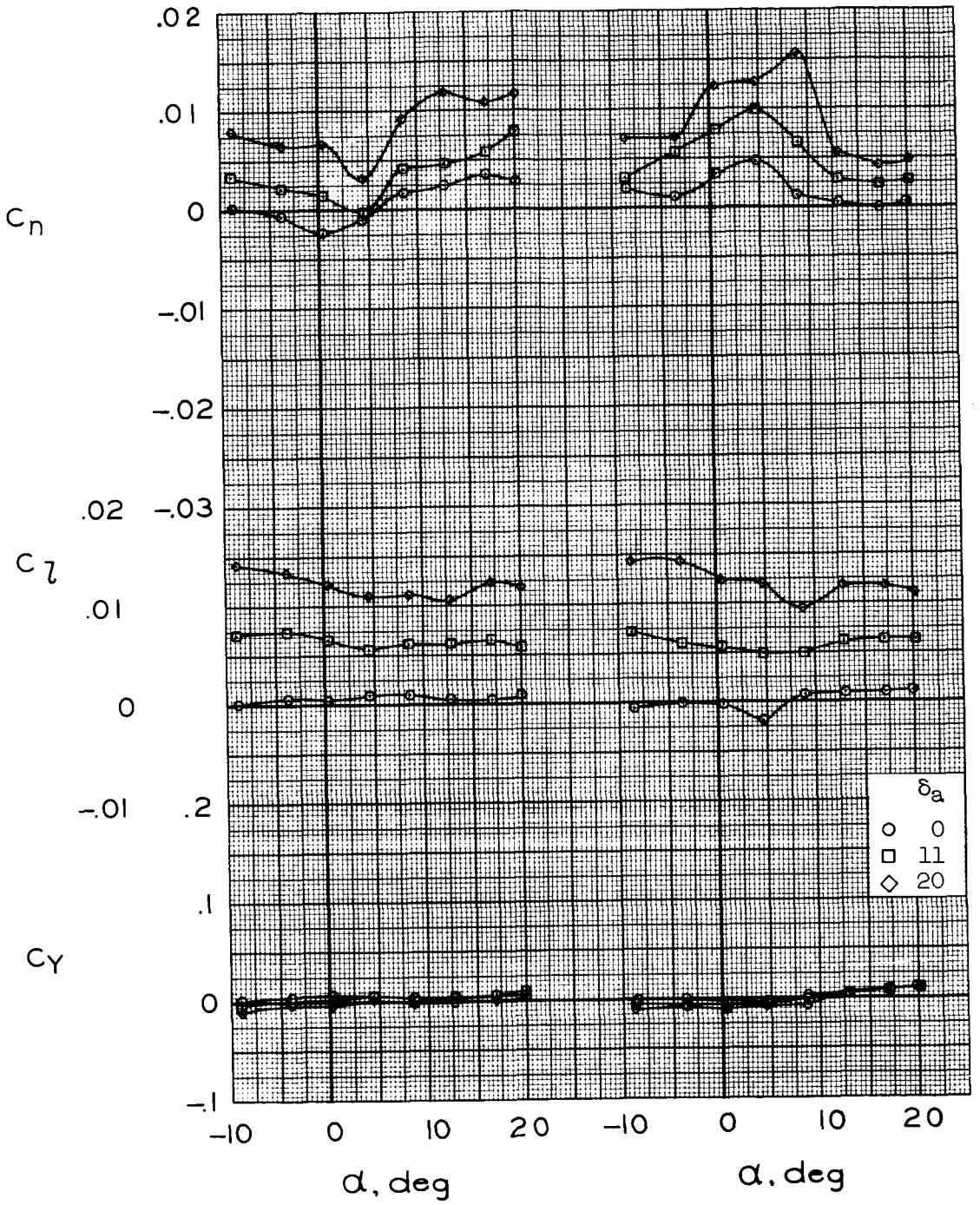

(c) M = 0.90, R = 6.5×10^6 (d) M = 0.95, R = 5.7×10^6

Figure 33.- Continued.

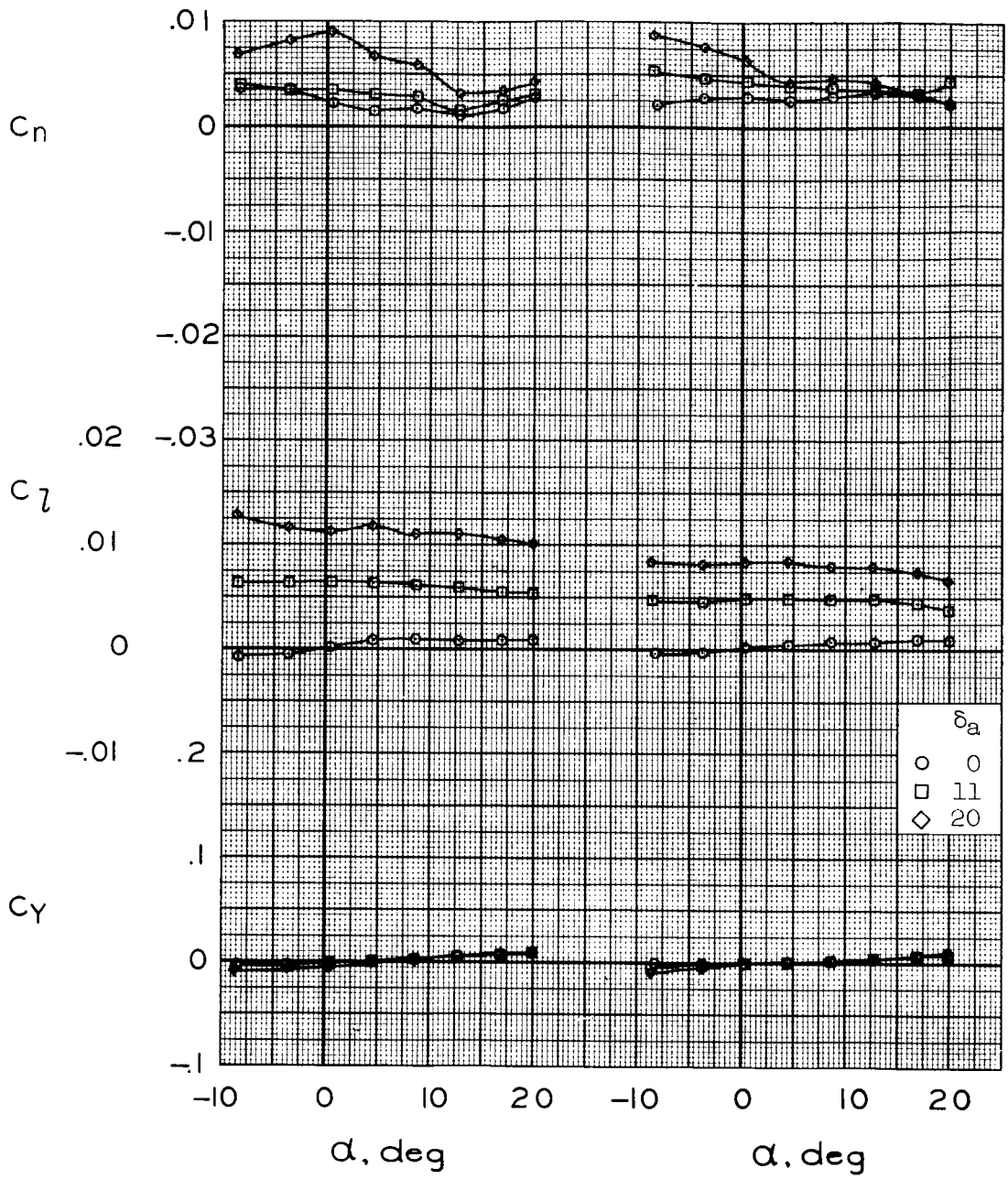

(e) M = 1.10, R = 4.2×10^6 (f) M = 1.30, R = 4.2×10^6

Figure 33.- Continued.

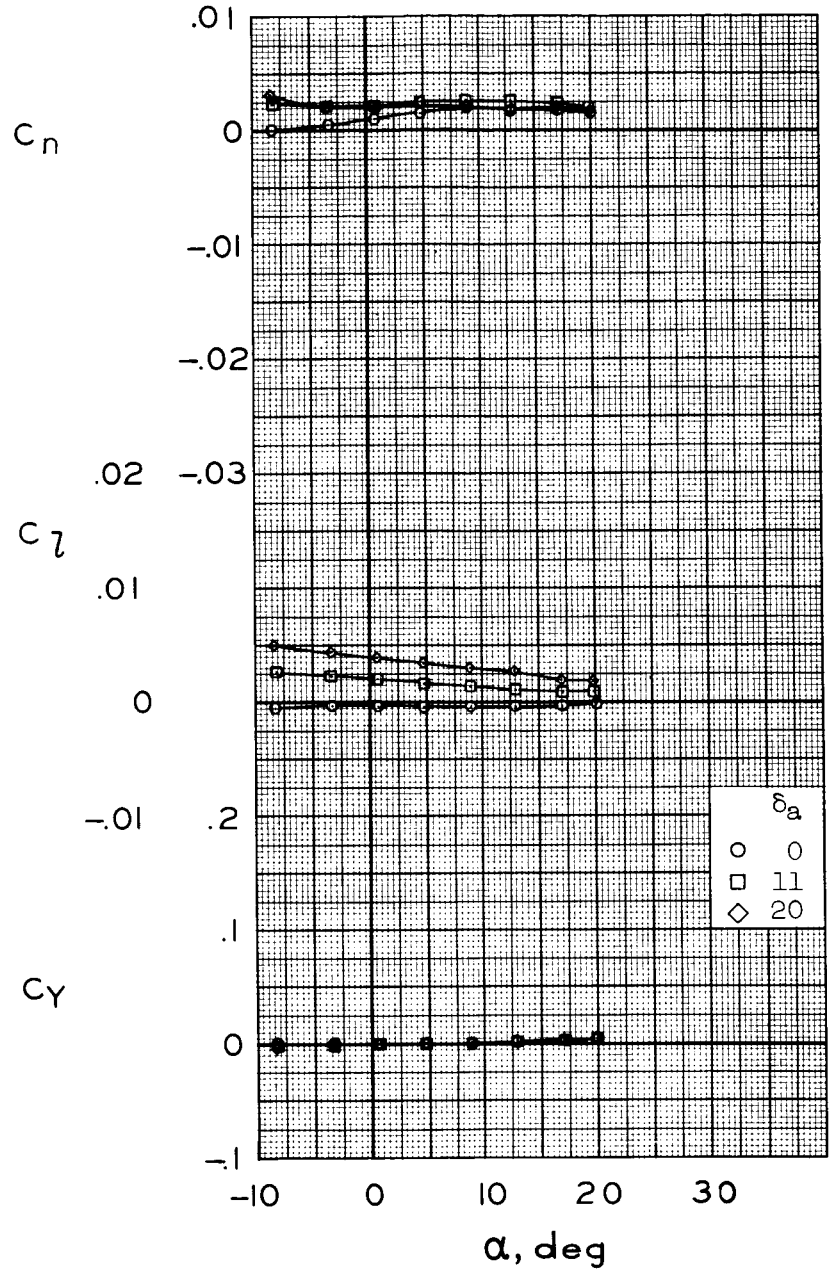

(g) M = 2.00, R = 4.2×10^6

Figure 33.- Concluded.

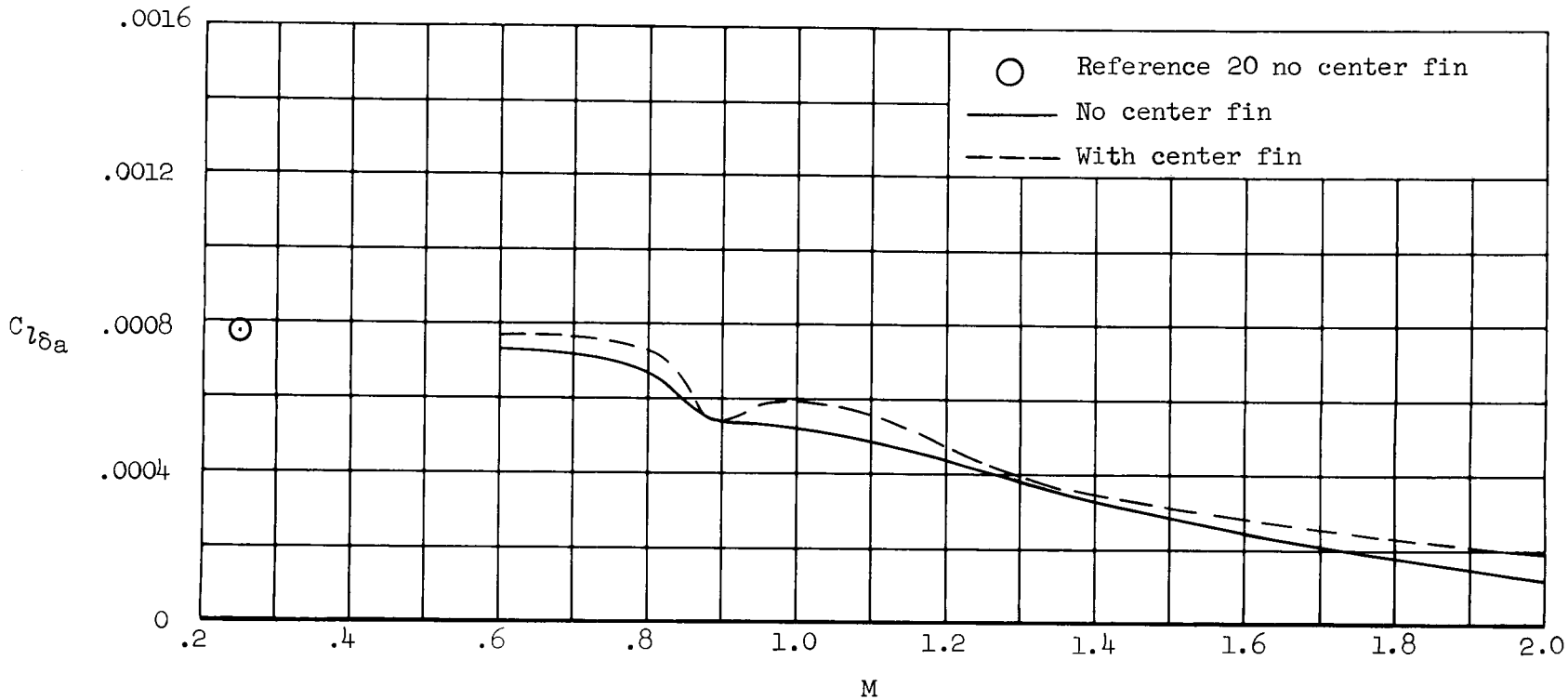

(a) $C_{l_{\delta a}}$ vs M

Figure 34.- Variation of aileron effectiveness with Mach number; $\alpha = 0.6°$, $\beta = 0°$, $\delta_u = -20°$, $\delta_l = 35°$, $\delta_{rf} = 0°$.

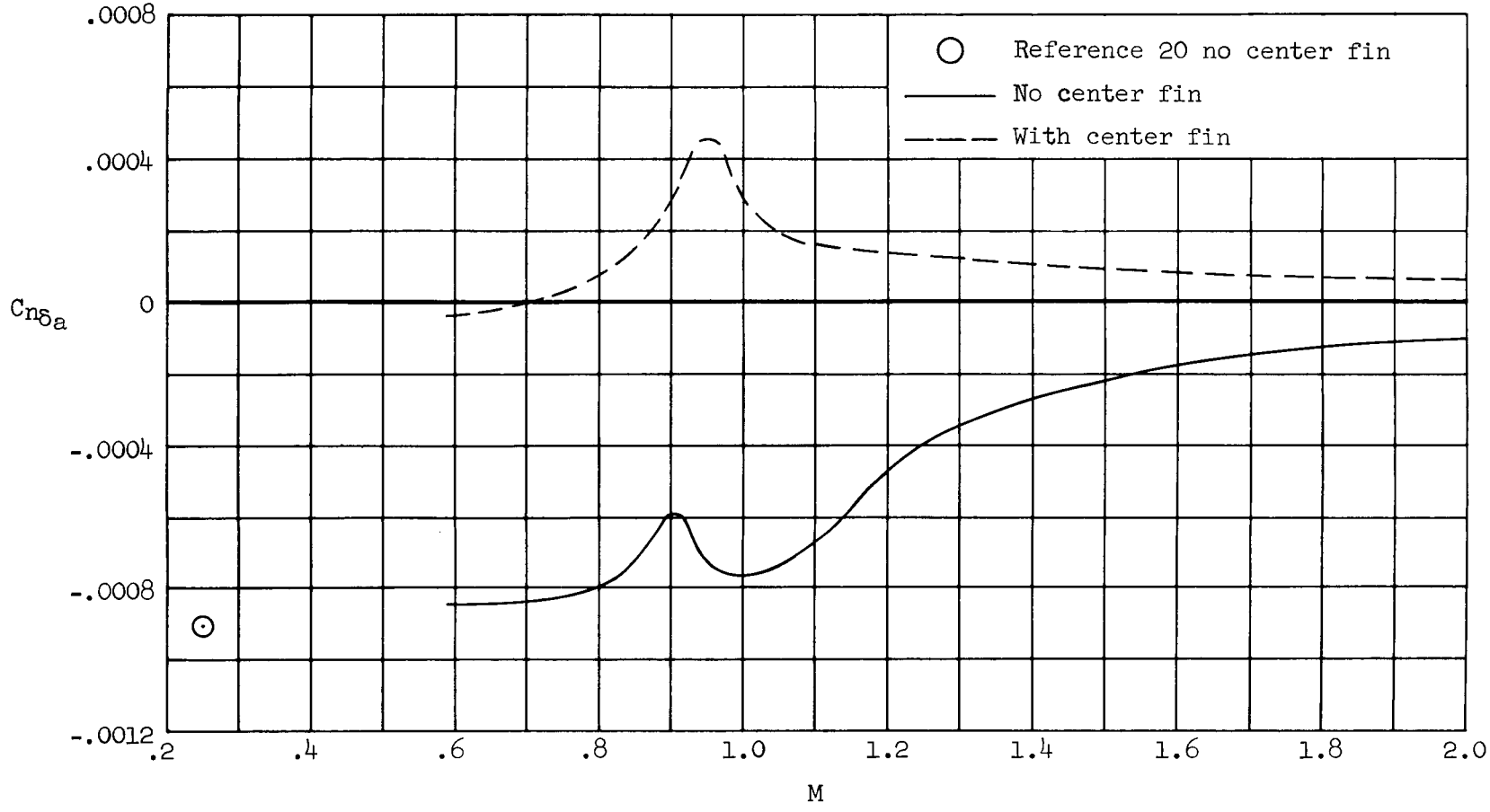

(b) $C_{n\delta_a}$ vs M

Figure 34.- Concluded.

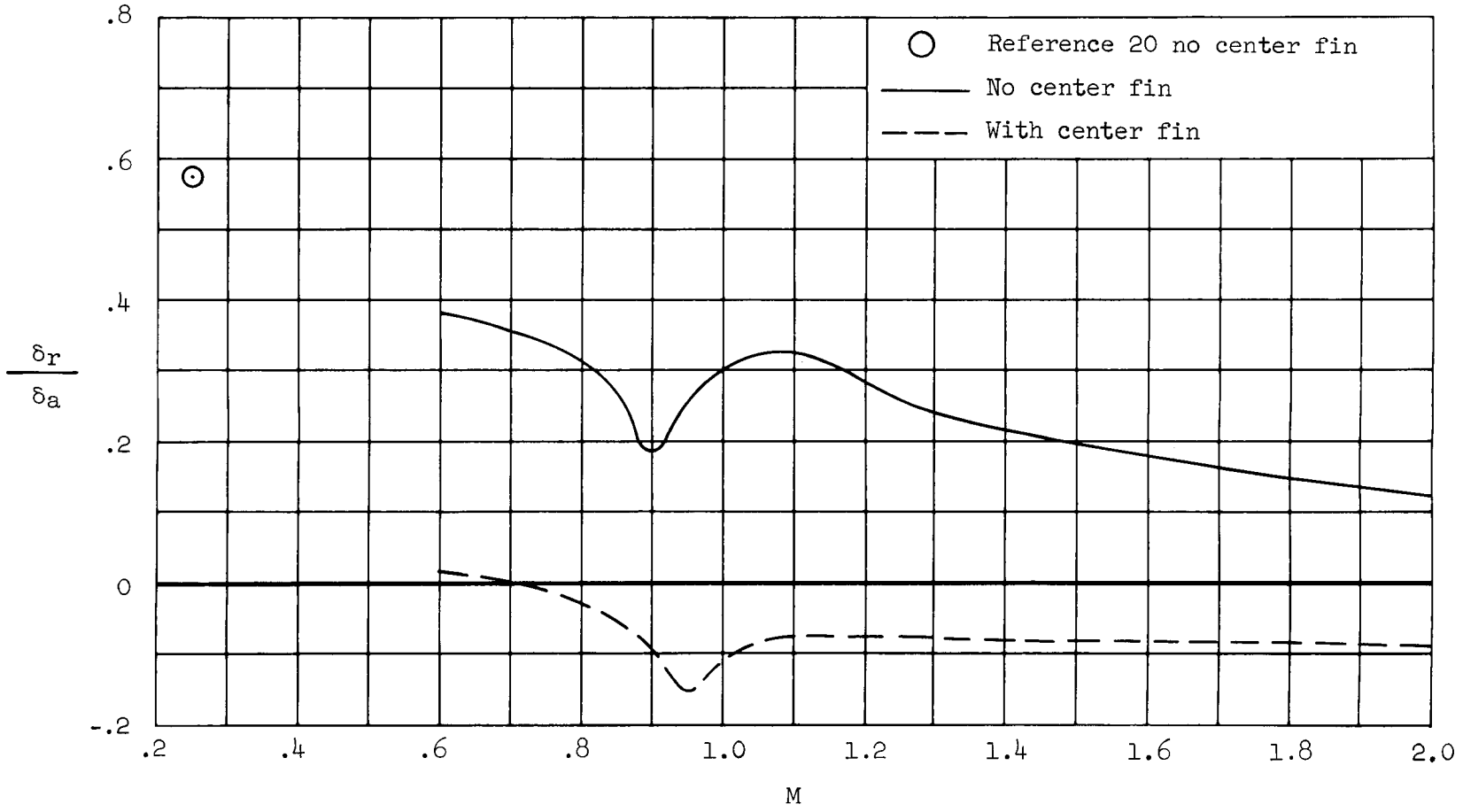

Figure 35.- Aileron-rudder interconnect ratio required for $C_{n_{\delta_a}} = 0$, $\alpha = 0.6°$, $\beta = 0°$, $\delta_u = -20°$, $\delta_l = 35°$, $\delta_{rf} = 0°$.

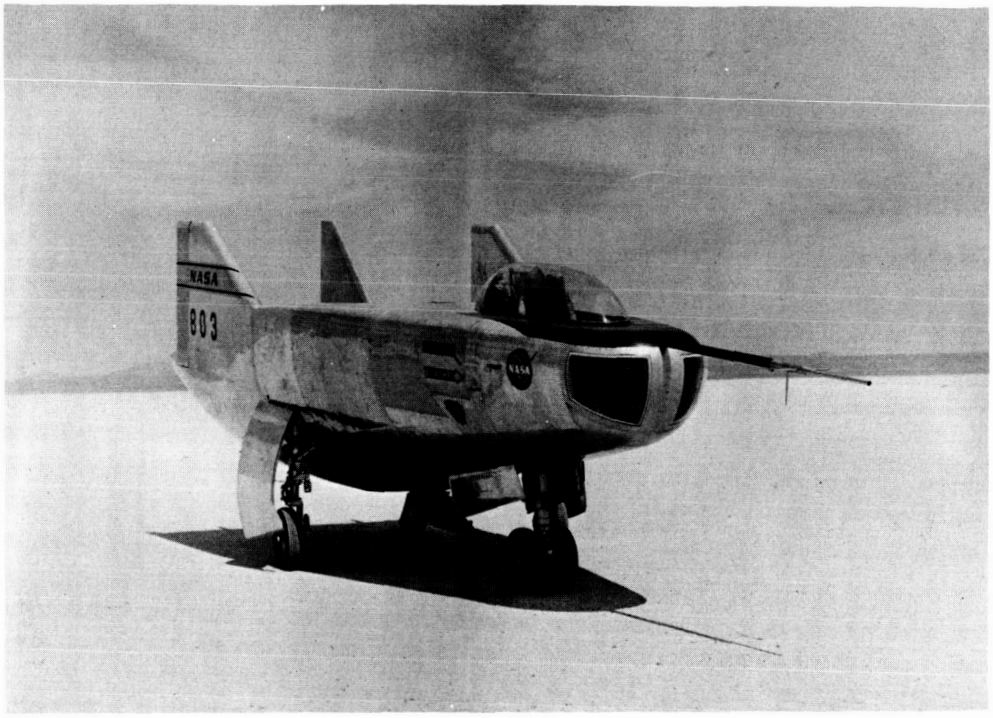

Figure 36.- M2-F3 flight research vehicle.

☆ U. S. GOVERNMENT PRINTING OFFICE : 1972 735-026/1053